July 2018

Motor Protein Regulation in Mammalian Mitosis

Barbara Mann

MOTOR PROTEIN REGULATION IN MAMMALIAN MITOSIS

A Dissertation Presented

by

BARBARA JENKINS MANN

Submitted to the Graduate School of the
University of Massachusetts Amherst in partial fulfillment
of the requirements for the degree of

DOCTOR OF PHILOSOPHY

May 2018

Molecular & Cellular Biology

MOTOR PROTEIN REGULATION IN MAMMALIAN MITOSIS

A Dissertation Presented

by

BARBARA JENKINS MANN

Approved as to style and content by:

_____
Patricia Wadsworth, Chair

_____
Thomas J. Maresca, Member

_____
Wei-Lih Lee, Member

_____
Michelle E. Farkas, Member

_____
Scott C. Garman, Director
Molecular & Cellular Biology Program

DEDICATION

To Dianne and Kimberly for teaching me that I could be anything I wanted, while loving and supporting me every step of the way.

To all of my little brothers, both human and canine, for making sure I don't take life too seriously.

To my Papaw for showing me what hard work and dedication looks like.

ACKNOWLEDGEMENTS

First and foremost, I would like to thank my advisor Patricia Wadsworth. You've offered me just the right amount of guidance while still allowing me to try new things. Your excitement for science is contagious.

I also want to thank the other members of my committee, Tom Maresca, Wei-Lih Lee, and Michelle Farkas for offering helpful suggestions and insight.

I credit a lot of where I am today to two former science teachers of mine, Robin Scarrell and Christine Guillette (Abbott). They showed me that being a woman in science is cool and ultimately started me on my career path.

I thank the current and former members of the Wadsworth lab. When I was a rotation student, Janel, Liz, and Sasha welcomed me into lab and made it feel like home. Sai was a great collaborator and person to bounce ideas off. Brett and Heather were great masters students who started as mentees but became long lasting friends. I also have had a great group of undergrads who have helped me with everything especially data analysis. There are too many names to list but all of your hard work is greatly appreciated.

I also need to thank everyone on the fourth floor of Morrill, both past and present. My tenure at UMASS has provided me a great atmosphere in which to work and I always felt like even though we weren't in the same labs there was always someone around.

There are several resources on campus that need to be thanked as well. Amy Burnside in the Flow cytometry facility, Jim Chambers in the imaging facility and Phuson from Nikon. Amy really helped speed up my last year or so by sorting my cells and Jim and Phuson have been instrumental in helping me with imaging and ensuring that everything was just the way I wanted.

I could not imaging getting through grad school without the support of my friends. The longer I've been at UMASS the more my friend group has grown. I was lucky to not only have a family in MCB but also in Chemistry and these friends will be with me for life.

There are few words to express my appreciation and gratitude for Jake Pawlowski. You always look on the bright side of life and never take things too seriously. You definitely keep my feet grounded. I look forward to what the future brings for us and that I'll get to experience it all with you.

Last but not least, I thank my family. My brother is someone I have come to realize I can totally rely on no matter what. Sometimes you drive me crazy but I know you'll always be there for me. I don't even know where to start to thank my parents, Dianne and Kim. Education was a high priority in our house growing up and we were always expected to do our best, no matter what that was. You always encouraged and supported me and I like to think that you aren't just my parents but also my friends. You are my rocks and I dedicate this accomplishment to you.

ABSTRACT

MOTOR PROTEIN REGULATION IN MAMMALIAN MITOSIS

MAY 2018

BARBARA JENKINS MANN, B.S. ROGER WILLIAMS UNIVERSITY

PhD., UNIVERSITY OF MASSACHUSETTS AMHERST

Directed by: Professor Patricia Wadsworth

Developing and maintaining a multicellular organism relies on the fundamental biological process of cell division, which ensures that genetic material is equally segregated between daughter cells. During mitosis, cells completely rearrange their cytoskeleton into a bipolar spindle through the concerted efforts of microtubules, motor proteins, and microtubule-associated proteins, which cells must regulate spatially and temporally to prevent errors such as chromosomal missegregation: a major cause of cancer. Although the mitotic spindle is a validated target for chemotherapy drug resistance and redundant pathways have highlighted the need for new targets. It is therefore important to understand how proteins that help build and/or maintain the spindle are regulated. Consequently, this dissertation focuses on the regulation of two separate but somewhat redundant mitotic kinesin motor proteins, Eg5 and Kif15, *in vitro* and *in vivo*.

In general, proteins are regulated several ways, including protein-protein interactions and post-translational modifications. My data show that the C-terminal 37 amino acids of the microtubule-associated protein, TPX2, which were known to regulate Eg5 localization, are also responsible for Kif15 localization. TPX2 inhibits Eg5 walking on single microtubules by acting as both a brake and a roadblock but only inhibits Kif15

as a brake. *In vivo*, dynamic microtubules are also involved in Kif15 behavior. These results highlight the differences in the mechanisms that govern the regulation of these motors. To further demonstrate this, I found that Eg5 activity is also regulated motor domain phosphorylation by Src kinase. Eg5 phosphomimic mutations produce monopolar spindles due to reduced Eg5 activity while non-phosphorylatable mutants result in disorganized spindles. Together, these data suggest that phosphorylation of Eg5 must be temporally regulated. Finally, using CRISPR/Cas9, I endogenously tagged Eg5 and TPX2 with EGFP in HeLa cells and quantified protein distribution. My results differed from reports using non-endogenous tags and reveal that Eg5 and TPX2 have distinct spindle localization throughout mitosis with TPX2 absent in areas where Eg5 activity is required. Additionally, I correlated fluorescence to protein concentration both locally and globally in mammalian cells, which is the first step in developing models to understand this complex biological process.

TABLE OF CONTENTS

LIST OF TABLES

LIST OF FIGURES

CHAPTER 1

FUNCTION AND REGULATION OF KINESIN-5

1.1 Introduction

The main structural elements of the mitotic spindle are microtubules, hollow polar filaments built from dimers of α/β tubulin. Spindle formation and function requires numerous motor and non-motor microtubule-associated proteins (MAPs) that regulate the nucleation, dynamics, and crosslinking of microtubules. In nearly every organism that has been studied, a member of the Kinesin-5 family of motor proteins localizes to the spindle (Fig. 1.1 A, B) and is required for spindle assembly (Blangy et al., 1995; Enos and Morris, 1990; Ferenz et al., 2010; Goshima and Vale, 2003; Hagan and Yanagida, 1990; Hoyt et al., 1992). Kinesin-5s function as bipolar homotetramers (Acar et al., 2013; Gordon and Roof, 1999; Hildebrandt et al., 2006; Kashina et al., 1997; Sharp et al., 1999a), and this structural organization allows the motor to crosslink and slide antiparallel microtubules. Inhibition of kinesin-5 activity by genetic or chemical perturbations results in monopolar spindles that fail to establish bipolarity, demonstrating the critical role that this protein plays in cell division (Kapoor et al., 2000; Mayer et al., 1999).

In many cell types, Kinesin-5 also contributes to spindle elongation in anaphase. Anaphase is typically divided into two temporally overlapping sub-phases, anaphase A and B (Fig. 1.1 E). In anaphase A, the distance between the kinetochores and the spindle pole decreases as kinetochore fiber microtubules shorten by microtubule disassembly at

kinetochores and/or spindle poles (McIntosh et al., 2012; Roostalu et al., 2010). During anaphase B the distance between the two spindle poles increases as the spindle elongates (Roostalu et al., 2010; Scholey et al., 2016). In many cells, spindle elongation occurs when antiparallel microtubules slide relative to each other driven by kinesin-5. In some cases, this sliding is accompanied by microtubule polymerization. In other cells, kinesin-5 motors oppose outward pulling forces, acting as frictional brakes (Hu et al., 2011; McIntosh et al., 2012; Scholey et al., 2016) (see section 1.4.4). Thus, despite variation among different cells, kinesin-5 force production plays a key role.

Although Kinesin-5 has been studied for decades, new features of motor behavior and regulation continue to be discovered. These studies provide insight into how the motor is spatially and temporally regulated during mitosis, and how various properties of the motor contribute to mitosis in diverse cells.

1.2 Kinesin-5 motile behavior

1.2.1 Kinesin-5 Motility

Kinesins with the motor domain located at the N-terminus of the protein, like Kinesin-5, were originally shown to move toward microtubule plus-ends (Miki et al., 2005; Sawin et al., 1992). Consistent with this, purified vertebrate Kinesin-5s walk processively toward the plus-ends of microtubules with relatively short run lengths (~8 steps) (Fig. 1.1 C) (Kapitein et al., 2005; Valentine et al., 2006; Valentine and Gilbert, 2007). Additionally, because they are bipolar homotetramers, Kinesin-5s use both their motor domains and non-motor tail domains to crosslink and simultaneous walk on two microtubules, showing a preference for microtubules in the antiparallel configuration

(Kapitein et al., 2008; Kapitein et al., 2005; van den Wildenberg et al., 2008; Weinger et al., 2011) resulting in microtubules sliding. The ability to move microtubules relative to each other is thought to be the key feature of kinesin-5 motors that enables bipolar spindle formation and elongation. This feature also distinguishes kinesin-5 from other kinesins, which typically transport vesicular cargos along the microtubule lattice. For kinesin-5, the microtubule is both the cargo and track.

Despite the evidence that kinesin-5 is a plus-end directed motor, several groups recently made the surprising discovery that kinesin-5s from budding and fission yeast (Cin8, Kip1, Cut7) can move toward microtubule plus or minus ends using the same motility mechanism; differences in motor concentration or ionic strength dictate their directionality on microtubules (Britto et al., 2016; Edamatsu, 2014; Fallesen et al., 2017; Fridman et al., 2013; Gerson-Gurwitz et al., 2011; Roostalu et al., 2011; Shapira and Gheber, 2016; Shapira et al., 2017). For example, *in vitro* assays show that when individual Cin8, Kip1, and/or Cut7 motors are observed either walking on or gliding individual microtubules *in vitro*, they move in a fast (up to 360 nm/s), processive, minus-end directed manner (Britto et al., 2016; Edamatsu, 2014; Fridman et al., 2013; Gerson-Gurwitz et al., 2011; Roostalu et al., 2011; Thiede et al., 2012). As the concentration of motors is increased, motor direction changes to the more canonical plus-end directed (Figure 1.2 B). This result suggests that kinesin-5s work in mechanically coupled teams (Fallesen et al., 2017; Roostalu et al., 2011; Shimamoto et al., 2015), although the mechanism by which this behavior is controlled is not yet established.

In addition to motor number, ionic strength also affects directionality of Cin8, Kip1 and Cut7. Minus end directed motility is observed under relatively high, close to

physiological, ionic conditions (~200-300mM NaCl) (Thiede et al., 2012). As ionic strength is lowered, plus-end directed motility is observed. Further, when engaged by two antiparallel microtubules, motors switch direction and become less processive but the net overall movement is plus-end directed, regardless of ionic strength. These data show that when kinesin-5 is engaged between two antiparallel microtubules plus-end directed motility is triggered (Thiede et al., 2012).

The *Saccharomyces cerevisiae* kinesin-5, Cin8, is unique because it has an extra loop (Loop 8, 99 amino acids long) that is lacking in other kinesin-5 motors. When Loop 8 is deleted, Cin8 becomes unidirectional towards the minus end and can no longer switch direction as ionic strength is lowered (Gerson-Gurwitz et al., 2011). Expression of this mutant construct in yeast reduces both motility toward the spindle midzone, where microtubule plus-ends are located and spindle elongation suggesting a role for directional switching in anaphase (Gerson-Gurwitz et al., 2011). Further, this loop facilitates unique binding of the motor to microtubules, which promotes clustering (Bell et al., 2017). Sequence comparisons of kinesin-5 proteins from diverse organisms have identified several domains unique to the yeast bi-directional kinesin-5 motors (Singh et al., 2018). Future studies will likely reveal how these domains contribute to motor bi-directionality and function *in vivo* and *in vitro* (Singh et al., 2018).

1.2.2 Tip-Tracking

The association of molecules with the plus-ends of microtubules is called tip tracking; some proteins track microtubule tips autonomously while others bind to other tip tracking proteins (e.g. EB family members) for tracking activity (Akhmanova and

Steinmetz, 2008; Akhmanova and Steinmetz, 2010). Kinesins from several different families can tip track including members of the kinesin-13, -8 and -14 families (Akhmanova and Steinmetz, 2008; Honnappa et al., 2009). *In vitro* vertebrate kinesin-5s are observed to move toward the plus-ends where they can remain attached (Fig. 1.1 C), although these microtubules are non dynamic and are not thought to have the same structural features as dynamic MTs (Balchand et al., 2015; Kapitein et al., 2005). The *Saccharomyces cerevisiae* kinesin-5, Kip1, is one of the only kinesin-5 proteins that has been shown to autonomously tip track (Fridman et al., 2013). Kip1 localizes to the midzone in anaphase where it remains associated with the plus-ends of depolymerizing microtubules eventually translocating to the spindle poles.

Kinesin-5 tip tracking has also been demonstrated using a dimeric Eg5-Kinesin-1 chimera composed of the kinesin-5 motor fused to the Kinesin-1 tail (Chen and Hancock, 2015). In *in vitro* assays, this chimeric motor protein was shown to both prevent microtubule catastrophes and track growing ends. This result is in contrast to prior work showing that in cells the yeast kinesin-5, Cin8, promotes catastrophes at plus-ends (Gardner et al., 2008). Thus, kinesin-5 may act at microtubule plus-ends, but additional work is needed to define this activity.

1.3 Kinesin-5 Phosphoregulation

Like many mitotic proteins, kinesin-5 localization and activation are controlled by cell cycle regulated phosphorylation. Although kinesin-5 phospho-regulation is common across organisms, the kinases and phosphatases, the phosphorylation sites, timing and consequences of phosphorylation vary (**Table 1.1**).

1.3.1. Tail Domain Phosphorylation

As mentioned, kinesin-5s are important for establishing spindle bipolarity and therefore must localize to the spindle microtubules and spindle poles early in mitosis. Kinesin-5s are generally not found on interphase microtubules (Blangy et al., 1995; Sawin and Mitchison, 1995) except in certain specialized cell types such as neurons where they contribute to microtubule organization (Falnikar et al., 2011; Kahn et al., 2015; Myers and Baas, 2007). Kinesin-5 also localizes to interphase microtubules in plants, but the function is unknown (Bannigan et al., 2007).

In dividing cells, kinesin-5s bind to mitotic microtubules for spindle formation and this is regulated by phosphorylation within the tail domain. A conserved region within the C-terminal tail, known as the 'BimC box', originally identified kinesin-5 family members (Ferenz et al., 2010). This BimC box contains a consensus Cdk1 phosphorylation site (Blangy et al., 1995) (Table 1.1). In *H. sapiens*, *X. laevis* and *D. melanogaster*, phosphorylation of kinesin-5s tail domain by Cdk1 is required to localize the motors to centrosomes and spindle microtubules early in mitosis (Blangy et al., 1997; Blangy et al., 1995; Cahu et al., 2008; Goshima and Vale, 2005; Heck et al., 1993; Sawin and Mitchison, 1995; Sharp et al., 1999a). Not only does Cdk1 phosphorylation regulate microtubule interaction of kinesin-5s, but also facilitates interactions with other proteins. For example, when Cdk1 phosphorylates HsEg5 early in mitosis it localizes to centrosomes where it co-localizes and associates with the dynactin subunit p150 (Blangy et al., 1997; Blangy et al., 1995). In *C. elegans*, Aurora B (AIR-2) kinase, not Cdk1, is

responsible for phosphorylating the BMK-1 tail resulting in its localization to both the mitotic and meiotic spindle microtubules (Bishop et al., 2005).

Interestingly, in fission yeast, the kinesin-5 Cut7 also contains the Cdk1 consensus site (T1011), however it is not required for spindle localization suggesting divergent regulation (Drummond and Hagan, 1998). Neither of the budding yeast kinesin-5s (Kip1, Cin8) contain the conserved Cdk1 site (Chee and Haase, 2010) that is required for localization in other organisms; however, mass spectrometry analysis of *in vivo* phosphorylation by Cdk1 identified alternate sites within the tail domain of Kip1 and Cin8 (Table 1.1) (Chee and Haase, 2010). These sites do not affect protein localization; however, phosphorylation is essential for protein function as corresponding non-phosphorylatable alanine mutations result in defects in spindle pole body (SPB) separation (Chee and Haase, 2010).

The tail domain of HsEg5 is also phosphorylated by Nek6/Nek7 (Table 1.1) and this is necessary for HsEg5 motor function and to establish spindle bipolarity (Bertran et al., 2011; Rapley et al., 2008). Plk1 phosphorylates Nek9, which then activates Nek6/Nek7, ultimately resulting in phosphorylation of kinesin-5 at S1033 specifically at centrosomes (Bertran et al., 2011; Fry et al., 2017). Unlike the Cdk1 site, Nek6/Nek7 phosphorylation does not affect the ability of HsEg5 to bind microtubules, but regulates spindle pole localization where phosphorylation is needed for motor activity specifically to separate centrosomes (Rapley et al., 2008). The proposed model is that in prophase, Cdk1 phosphorylation first localizes HsEg5 to the centrosome microtubules where it accumulates. Then, Nek6/Nek7 can then phosphorylate the motor initiating centrosome separation and ultimately spindle bipolarity (Bertran et al., 2011; Fry et al., 2017). Not

only does Nek6/Nek7 phosphorylation regulate HsEg5 activity at poles but was also recently found to facilitate interaction with the microtubule associated protein, TPX2, (Eibes et al., 2017). Although TPX2 is predominantly nuclear in prophase, a centrosomal pool is required for Eg5 localization and centrosome separation.

1.3.2. Motor Domain Phosphorylation

Once motors have been localized to the mitotic spindle, their activity must be regulated and several studies have shown that phosphorylation of the motor head, near the ATP binding pocket contributes to this regulation.

Motor domain phosphorylation was first demonstrated in *D. melanogaster* kinesin-5, KLP61F, in which three tyrosine residues within the motor head are phosphorylated by Wee1 (dWee1) Kinase (**Table 1.1**) (Garcia et al., 2009). Phosphorylation at these sites is required for motor function and normal spindle morphology. Embryos expressing a homozygous loss of function allele (*klp61f*^{3}) have spindle defects including monopolar spindles that could only be rescued by expressing wild-type KLP61F (KLP61F^{WT}), not a non-phosphorylatable (KLP61F^{3YF}) mutant. These embryos also showed dominant effects including extra microtubule organizing centers (MTOCs) and abnormal microtubules.

One of the three tyrosine residues phosphorylated in *D. melanogaster*, Y207, is conserved in mammalian cells (Y211) where it is also essential for normal spindle formation (Bickel et al., 2017) (Chapter IV). However, *in vitro* kinase reactions show that Src, not Wee1, is the kinase responsible for this phosphorylation (**Table 1.1**) (Bickel et al., 2017) (Chapter IV). Although phosphorylation of these sites does not affect the

motors ability to bind to microtubules, motor activity is altered. When phosphorylation is mimicked at Y211 (Y211E), ATP hydrolysis and motor driven microtubule gliding both significantly decrease. In cells, the same mutation results in monopolar spindles. Taken together, this suggests phosphorylation renders the motor less active and thus unable to produce sufficient outward force necessary for bipolarity. Conversely, a non-phosphorylatable mutation (Y211F) increases the prevalence of disorganized spindles similar to those seen when Src specific inhibitors are used (Bickel et al., 2017) (Chapter IV). These results suggest that motor activity is regulated by temporally specific phosphorylation and dephosphorylation at this site.

In yeast, a different set of sites in the motor domain regulates activity and spindle localization. Cdk1 phosphorylates Cin8 and Kip1 at several sites within the motor head (**Table 1.1**) (Avunie-Masala et al., 2011; Chee and Haase, 2010; Gerson-Gurwitz et al., 2011; Goldstein et al., 2017). One of these sites is a conserved consensus site between Cin8 and Kip1 (S455 and S388 respectively) and is essential for proper spindle pole body separation and cell proliferation. In Cin8, phosphorylation of S455 in combination with two other sites in the motor head specific to Loop 8, regulate localization to the spindle midzone in anaphase (Avunie-Masala et al., 2011). Non-phosphorylatable mutants fail to localize to the midzone due to a weakened intereraction of Cin8 with the microtubule resulting in faster minus-end directed motion (Gerson-Gurwitz et al., 2011).

Differential timing of Cdk1 phosphorylation at 3 different sites within the motor head (**Table 1.1**) also regulates Cin8 localization to the anaphase spindle (Goldstein et al., 2017). In early anaphase, phosphorylation of S277 causes Cin8 to detach from the spindle pole bodies (SPBs) and move to the midzone. As anaphase progresses, S493 also

becomes phosphorylated and further moves Cin8 from the SPBs to the midzone where it helps regulate the rate of spindle elongation. Finally, as the cell enters late anaphase, T285 phosphorylation occurs detaching Cin8 from the spindle because all 3 sites are phosphorylated. This detachment was also observed *in vitro*, where a phosphomimic (3D) mutant motor increased minus end directed motility, increased velocity and had a weaker interaction with the microtubule (Shapira and Gheber, 2016). This is the only evidence of phosphorylation regulating localization of a Kinesin-5 late in mitosis but further investigations are needed in other systems to see if there is conservation.

1.3.3. Stalk Domain Phosphorylation

Aurora Kinase has been shown to phosphorylate *Xenopus laevis* Eg5 (XlEg5) in the Stalk region (Giet et al., 1999) at S543 (Cahu et al., 2008). Though it was initially suggested that this phosphorylation was essential, when the site was mutated to a non-phosphorylatable alanine, spindles were normal suggesting the opposite (Cahu et al., 2008). There is a (putative) Aurora kinase consensus site in HsEg5 (S511) but no studies have been done to investigate a potential role in mammalian mitosis.

1.3.4. Kinesin-5 De-Phosphorylation

Although phosphorylation sites and the kinases involved have been well studied in kinesin-5s, less is known about the corresponding phosphatases. Two recent studies looked at the phosphatase responsible for removing the phosphate at the HsEg5 Cdk1 tail domain consensus site (T926) (He et al., 2016; Liu et al., 2017). The first identified was PTEN phosphatase which interacts with HsEg5 in mitosis and regulates its

dephosphorylation at T926 (He et al., 2016). Alternately, PP2A is also implicated in removing the phosphate from T926, which then removes HsEg5 from the spindle later in mitosis (Liu et al., 2017). In either case, cells fail to progress through mitosis when a phosphomimic is expressed or when either phosphatase is depleted. Investigators have just started looking into phosphatases and their role in kinesin-5 regulation.

1.3.5. Other Post-Translational Modifications

While the role of phosphorylation in localization and activity of kinesin-5 has been well studied, other post-translational modifications are beginning to be explored. Of note, a recent study found an acetylation site in the motor domain of Eg5 (L146) (Muretta et al., 2018). This site forms a salt bridge with D91 which when disrupted using an acetylation mimic (L146Q) results in coupling of the neck-linker with the catalytic domain and causes Eg5 to act as a brake. Instead of the short run lengths seen under low load (Valentine et al., 2006), the motor becomes dissociation resistant with an increase in stalling. *In vivo*, this modification results in slower spindle pole separation due to this braking ability. Further investigations might establish other post-translational modifications that also result in changes to the motor behavior.

1.4 Physiological Roles

1.4.1. Bipolar Spindle Formation

As noted in section 1.1, perhaps the most conserved role of kinesin-5 family members is to establish spindle bipolarity in early mitosis (Fig. 1.1 D). Although some organisms do not require kinesin-5s for building a bipolar spindle (i.e. *C. elegans*,

Dictyostelium), mitotic spindles fail to form when kinesin-5 is mutated or inhibited across most organisms that have been studied (Bishop et al., 2005; Kapoor et al., 2000; Mayer et al., 1999; Sawin and Mitchison, 1995; Tikhonenko et al., 2008). Accumulating evidence suggests that regulation of kinesin-5 localization and activity as described above, is responsible for this key function.

For example, although the discovery of minus end directed motility in yeast kinesin-5 was surprising at first, several studies suggest that this behavior contributes to spindle formation. Motor accumulation at spindle poles may increase the probability that antiparallel microtubules from the opposite pole are captured, initiating sliding and generation of the outward forces required for bipolarity (Saunders et al., 1997). Motor clustering, like that seen by Cin8 (Bell et al., 2017), at minus ends could also contribute to plus-end directed motility, allowing Cin8 to redistribute along the microtubules, further indicating that motor directionality and reversal is important for establishing bipolarity (Blackwell et al., 2017; Shapira et al., 2017).

Bi-directional motility has only been described for yeast kinesin-5 motors, but kinesin-5 is enriched at spindle poles in other cells (Cheerambathur et al., 2008; Gable et al., 2012; Sawin et al., 1992; Sawin and Mitchison, 1995; Uteng et al., 2008) (Chapter V). Previous work showed that both *X. laevis* and Human Eg5 are transported toward spindle poles (microtubule minus-ends) in a dynein/dynactin dependent manner (Gable et al., 2012; Uteng et al., 2008), although the mechanism is not fully understood. In mammalian cells, the microtubule associated protein, TPX2, regulates HsEg5 motor stepping and localization to the spindle, and potentially couples Eg5 to dynein/dynactin for minus end directed transport (Balchand et al., 2015; Eckerdt et al., 2008; Gable et al.,

2012; Ma et al., 2011) (Chapter II). A link between Eg5 and dynein/dynactin was previously shown (Blangy et al., 1997) and an interaction between Dynein and TPX2 as was previously suggested (Gable et al., 2012; Wittmann et al., 1998) but more work is needed to establish a relationship and/or mechanism between these oppositely directed motors. Recently, it was shown that TPX2 plays a role in localizing HsEg5 to centrosomes in prophase (Eibes et al., 2017) via an importin-independent cytoplasmic pool of TPX2 that localizes HsEg5 in a Nek6/Nek7 dependent manner (Table 1.1). Thus in mammalian cells both transport and interactions with specific binding partners contribute to kinesin-5 enrichment toward microtubule minus ends. Despite differences in the mechanism of localization, we speculate that poleward accumulation in prophase may serve to initiate microtubule sliding when antiparallel microtubules are encountered (Fig. 1.1 D, D'), as in yeast spindles (Blackwell et al., 2017; Shapira et al., 2017).

A recent computation model has achieved bipolar spindle formation from an initially monopolar configuration, using parameters from fission yeast (Blackwell et al., 2017). In the model, bidirectional behavior of kinesin-5 motors was required for bipolar spindle formation. Removing minus end motion entirely or including it for only single heads bound to a microtubule prevented bipolar spindle formation (Blackwell et al., 2017). These results support the idea that motor bidirectionality plays an essential physiological role in spindle formation in this organism and potentially highlights the need for a mechanism for pole localization/minus-end directed movement during bipolar establishment in diverse cells (Fig. 2 A, B).

1.4.2. Maintenance of Spindle Bipolarity

Although much of the work on kinesin-5 has focused on its essential role in spindle formation, kinesin-5 is also needed to maintain spindle bipolarity in some organisms (Hoyt, 1994; Kapoor et al., 2000; Saunders and Hoyt, 1992; Sharp et al., 2000b; Sharp et al., 1999b). In vertebrate cells, spindles remain bipolar following treatment with Eg5 inhibitors (Cameron et al., 2006; Ferenz et al., 2009b; Kapoor et al., 2000) due to the action of kinesin-12 (Sturgill et al., 2016; Sturgill and Ohi, 2013; Tanenbaum et al., 2009; Vanneste et al., 2009). In cells depleted of kinesin-12, a short spindle phenotype is observed, demonstrating that the motor also contributes to outward force production. Additionally, overexpression of kinesin-12 (Kif15) can drive spindle formation in the absence of kinesin-5, although an alternate pathway for spindle formation is used (Sturgill et al., 2016; Sturgill and Ohi, 2013). Interestingly, both kinesin-12 and kinesin-5 are regulated by TPX2 suggesting redundancy in motor regulation (Balchand et al., 2015; Drechsler et al., 2014; Ma et al., 2011; Mann et al., 2017; Vanneste et al., 2009) (Chapters II &III). Kinesin-12 has been reported to exist as a tetramer, although a dimeric form may also be functional (Drechsler and McAinsh, 2016; Drechsler et al., 2014; Mann et al., 2017; Sturgill et al., 2014) (Chapter III). However, kinesin-12 tetramers crosslink only parallel microtubules, aligning them into bundles (Drechsler and McAinsh, 2016). Consistent with a conserved role for kinesin-12 in establishment and maintenance of spindle bipolarity, kinesin-12 contributes to meiotic spindle formation in *C. elegans* by sorting microtubules into an acentrosomal spindle (Wolff et al., 2016).

1.4.3. Kinesin-5s on Parallel Microtubules

As noted in section 1.2.1, although kinesin-5s act on antiparallel microtubules, they can also crosslink parallel microtubules (Kapitein et al., 2005; Shimamoto et al., 2015). Recent *in vitro* experiments showed that Eg5 can crosslink parallel microtubules and generate braking forces that scale with motor number and microtubule overlap length (Shimamoto et al., 2015). This idea of crosslinking parallel microtubules was also suggested to be important for ensuring proper chromosome segregation in budding yeast. Cin8 and Kip1 localize to kinetochore microtubules (kMTs) where they cluster the kinetochores (Tytell and Sorger, 2006). Cin8 specifically crosslinks these parallel microtubules creating bundles that help establish and maintain normal metaphase spindles. Though kinesin-5 is enriched at the spindle poles in metaphase, where parallel microtubules are located, (Mastronarde et al., 1993; Sharp et al., 1999a) evidence for a specific role on these microtubules is lacking.

1.4.4. Kinesin-5s in Anaphase

Kinesin-5 motors also contribute to spindle elongation in anaphase in a cell type specific manner. Anaphase cells are characterized by an array of overlapping antiparallel microtubules in the interpolar region between the separating chromosomes (Ding et al., 1993; Mastronarde et al., 1993; McIntosh and Landis, 1971; Winey et al., 1995) which is established by antiparallel crosslinking microtubule associated proteins (i.e. Ase1/PRC1) (Scholey et al., 2016). These antiparallel microtubules serve as a scaffold on which kinesin-5s can act (Fig. 1.1 E).

In some cells, kinesin-5 motors generate the force for spindle elongation. For example, in budding yeast, Cin8 and Kip1 drive antiparallel microtubule sliding and the contribution of each to anaphase is distinct. Kip1 plays a greater role in later anaphase events than Cin8 ultimately allowing the spindle to increase up to 5 times its initial length (Straight et al., 1998). Similarly, in *D. melanogaster,* KLP61F is required to generate the sliding forces for anaphase B and spindle pole separation (Brust-Mascher et al., 2009; Scholey et al., 2016).

In other cells, kinesin-5 activity is dispensable for anaphase B and in some cases contributes antagonistic braking forces. In *C. elegans,* cells lacking the kinesin-5 homolog, BMK1, show faster elongation than wild type cells (Saunders et al., 2007). This is also observed in pig epithelial cells, where acute treatment with kinesin-5 inhibitors at anaphase onset results in faster spindle elongation (Collins et al., 2014). Finally, in *Dictyostelium discoideum,* deletion of the kinesin-5 homolog, Kif13, causes premature spindle pole separation and more extensive elongation (Tikhonenko et al., 2008). Thus kinesin-5 in these systems is thought to act as a frictional brake, limiting the rate and extent of spindle elongation (Shimamoto et al., 2015).

In some spindles, forces external to the midzone generate pulling forces to elongate the spindle; in these cases, braking forces may be required to limit the extent of elongation (Saunders et al., 2007; Tikhonenko et al., 2008). This is also the case in yeast, where the Chromosome Passenger Complex (CPC) causes Kip1 and Cin8 to switch from sliding to braking forces on the spindle countering pulling forces from astral microtubules (Rozelle et al., 2011). Conversely, astral microtubules are not present or play only a minor role in elongation and in these cells, active pushing forces from the midzone may

be critical to achieve chromosome segregation (Brust-Mascher et al., 2009; Scholey et al., 2016).

Thus, the contribution of kinesin-5 to spindle elongation varies with cell type. There are several established roles for kinesin-5s in anaphase; however, in almost all cells that have been examined, redundant mechanisms contribute to spindle elongation. This redundancy is most evident in anaphase B where different motors, different mechanisms and different regulation by maps have been described (reviewed (Scholey et al., 2016)).

1.5 Future Directions

Prior work has shown that outward forces generated by kinesin-5 are opposed by inward forces generated by minus end directed motors (Saunders et al., 1997; She and Yang, 2017). Disrupting the balance of forces by eliminating the activity of Eg5 leads to dynein dependent spindle collapse (Ferenz et al., 2009b; Tanenbaum et al., 2008; van Heesbeen et al., 2014). Interestingly, when both inward and outward motor dependent forces are eliminated, bipolar spindles form (Mitchison et al., 2005; Sharp et al., 1999b). Recent work demonstrated that in fission yeast this required the microtubule crosslinker Ase1 (PRC1) suggesting that forces from crosslinked and growing microtubules are sufficient for bipolar spindle formation in the absence of motors (Rincon et al., 2017). However, precisely how the balance of inward and outward forces is achieved is not clear in any system. Recent work, which directly measured force production by multiple kinesin-5s, showed that both sliding and braking forces scale with motor number and overlap length (Fallesen et al., 2017; Shimamoto et al., 2015). Further investigations are required to understand how these parameters are regulated *in vivo*.

Table 1.1 Phosphorylation of Kinesin-5

Region	Organism	Kinesin-5	Kinase	Site(s)	Function	Reference(s)
Tail	*Homo sapiens*	*Kif11/HsEg5*	Cdk1	T926	Localization to Spindle MTs	(Blangy et al., 1997; Blangy et al., 1995)
	Homo sapiens	*Kif11/HsEg5*	Nek6/Nek7	S1033	Interaction with TPX2, Localization to Centrosomes & Motor Activity	(Bertran et al., 2011; Eibes et al., 2017; Rapley et al., 2008)
	Xenopus laevis	*XlEg5*	Cdk1	T937	Localization to Spindle MTs	(Cahu et al., 2008; Sawin and Mitchison, 1995)
	Drosophila melanogaster	*KLP61F*	Cdk1	T933	Localization to Spindle MTs	(Goshima and Vale, 2005; Heck et al., 1993; Sharp et al., 1999a)
	Caenorhabditis elegans	*BMK-1*	Aurora B	T921, T922 & T928	Localization to Spindle MTs	(Bishop et al., 2005)
	Saccharomyces cerevisiae	*Cin8*	Cdk1	S972	SPB separation defects	(Chee and Haase, 2010)
	Saccharomyces cerevisiae	*Kip1*	Cdk1	S1037 & T1040	SPB separation defects	(Chee and Haase, 2010)
Motor	*Homo sapiens*	*Kif11/HsEg5*	Src	Y125, Y211, Y231	Phosphorylation results in loss of MT gliding, reduced ATPase activity, monopolar spindles; No phosphorylation results in disorganized spindles	(Bickel et al., 2017)
	Drosophila melanogaster	*KLP61F*	dWee1	Y23, Y152, Y207	Monopolar Spindles	(Garcia et al., 2009)
	Saccharomyces cerevisiae	*Cin8*	Cdk1	S277, T285, S493	Re-Localization from SPBs to Midzone of Anaphase Spindle followed by detachment	(Goldstein et al., 2017)
	Saccharomyces cerevisiae	*Cin8*	Cdk1	S239, S247	Located in Loop 8, Localization in anaphase, pole-directed movements	(Avunie-Masala et al., 2011; Gerson-Gurwitz et al., 2011)
	Saccharomyces cerevisiae	*Cin8*	Cdk1	S455	SPB separation defects, failure to divide, cell death	(Avunie-Masala et al., 2011; Chee and Haase, 2010)
	Saccharomyces cerevisiae	*Kip1*	Cdk1	S388	SPB separation defects, failure to divide, cell death	(Chee and Haase, 2010)
Stalk	*Xenopus laevis*	*XlEg5*	Aurora A	S543	Direct interaction but spindles appear normal when not phosphorylated	(Cahu et al., 2008; Giet et al., 1999)

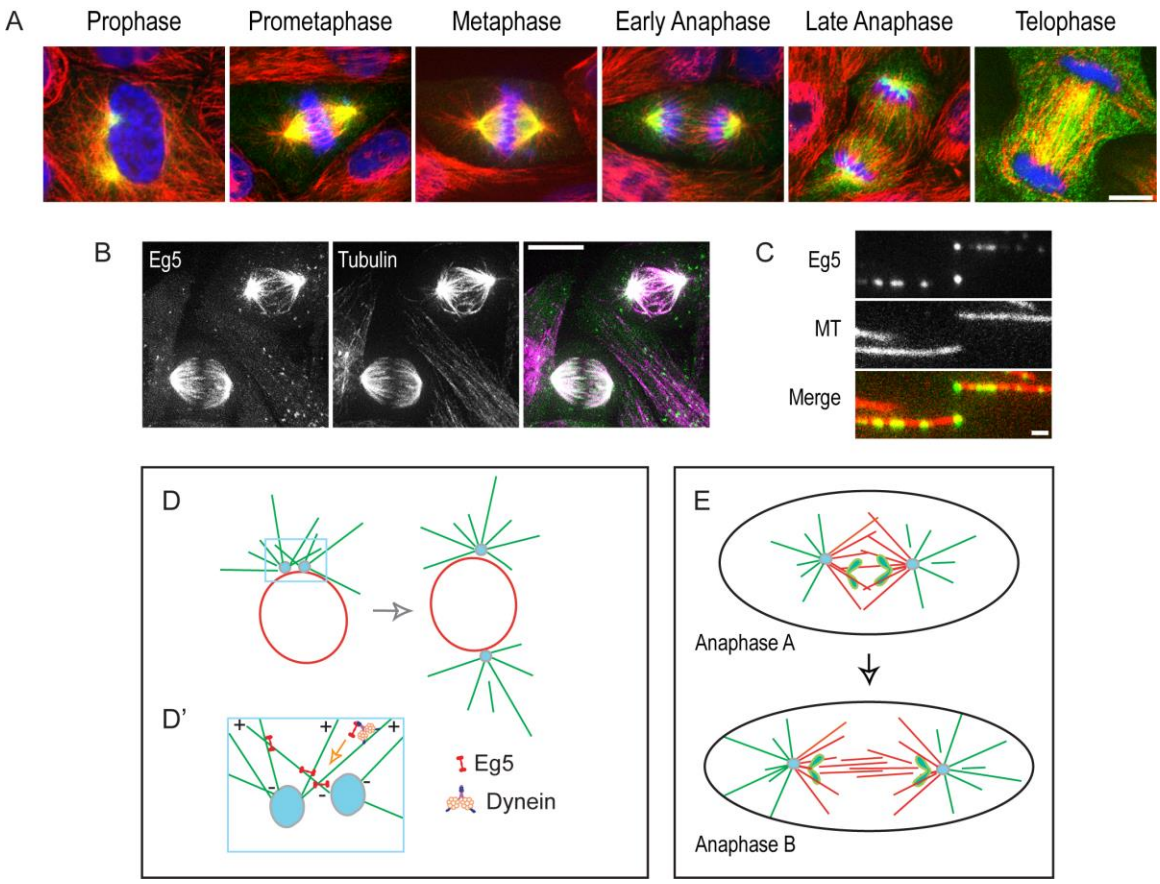

Figure 1.1 Kinesin-5 Localization and where it is acting. (A) Max projected images of LLC-Pk1 cells immunostained for Eg5 (green) and MTs (red) through the stages of mitosis. (B) Max projected images of live, HeLa cells stably expressing endogenously tagged Eg5-EGFP (green) and labeled MTs (SiR Tubulin; magenta). (C) TIRF images of Eg5-EGFP accumulating at microtubule plus ends. (D) Schematic of centrosome separation in prophase. (D') Zoom of Eg5 accumulation at spindle poles during prophase; transported by Dynein/dynactin to microtubule minus ends at the pole. (E) Schematic of anaphase. Scale bars in A and B = 10 μm. Scale bar in C = 1 μm.

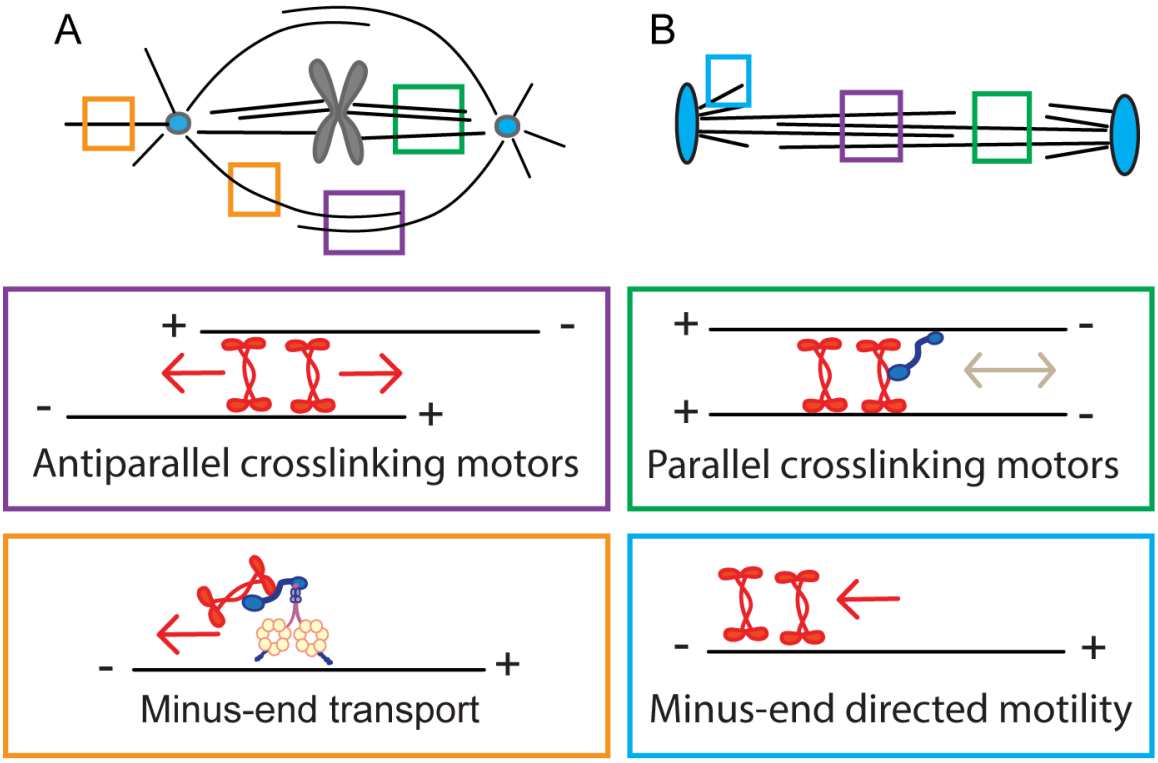

Figure 1.2 Kinesin-5 Motility and Engagement. Mammalian (A) and yeast spindle (B) diagrams. Boxes highlight areas where Kinesin-5 motors are engaged and/or moving within each respective spindle.

1.6 References

Acar, S., D.B. Carlson, M.S. Budamagunta, V. Yarov-Yarovoy, J.J. Correia, M.R. Ninonuevo, W. Jia, L. Tao, J.A. Leary, J.C. Voss, J.E. Evans, and J.M. Scholey. 2013. The bipolar assembly domain of the mitotic motor kinesin-5. *Nature communications*. 4:1343.

Akhmanova, A., and M.O. Steinmetz. 2008. Tracking the ends: a dynamic protein network controls the fate of microtubule tips. *Nature reviews. Molecular cell biology*. 9:309-322.

Akhmanova, A., and M.O. Steinmetz. 2010. Microtubule +TIPs at a glance. *Journal of cell science*. 123:3415-3419.

Avunie-Masala, R., N. Movshovich, Y. Nissenkorn, A. Gerson-Gurwitz, V. Fridman, M. Koivomagi, M. Loog, M.A. Hoyt, A. Zaritsky, and L. Gheber. 2011. Phospho-regulation of kinesin-5 during anaphase spindle elongation. *Journal of cell science*. 124:873-878.

Balchand, S.K., B.J. Mann, J. Titus, J.L. Ross, and P. Wadsworth. 2015. TPX2 Inhibits Eg5 by Interactions with Both Motor and Microtubule. *The Journal of biological chemistry*. 290:17367-17379.

Bannigan, A., W.R. Scheible, W. Lukowitz, C. Fagerstrom, P. Wadsworth, C. Somerville, and T.I. Baskin. 2007. A conserved role for kinesin-5 in plant mitosis. *Journal of cell science*. 120:2819-2827.

Bell, K.M., H.K. Cha, C.V. Sindelar, and J.C. Cochran. 2017. The yeast kinesin-5 Cin8 interacts with the microtubule in a noncanonical manner. *The Journal of biological chemistry*. 292:14680-14694.

Bertran, M.T., S. Sdelci, L. Regue, J. Avruch, C. Caelles, and J. Roig. 2011. Nek9 is a Plk1-activated kinase that controls early centrosome separation through Nek6/7 and Eg5. *The EMBO journal*. 30:2634-2647.

Bickel, K.G., B.J. Mann, J.S. Waitzman, T.A. Poor, S.E. Rice, and P. Wadsworth. 2017. Src family kinase phosphorylation of the motor domain of the human kinesin-5, Eg5. *Cytoskeleton (Hoboken, N.J.)*.

Bishop, J.D., Z. Han, and J.M. Schumacher. 2005. The Caenorhabditis elegans Aurora B kinase AIR-2 phosphorylates and is required for the localization of a BimC kinesin to meiotic and mitotic spindles. *Molecular biology of the cell*. 16:742-756.

Blackwell, R., C. Edelmaier, O. Sweezy-Schindler, A. Lamson, Z.R. Gergely, E. O'Toole, A. Crapo, L.E. Hough, J.R. McIntosh, M.A. Glaser, and M.D. Betterton. 2017. Physical determinants of bipolar mitotic spindle assembly and stability in fission yeast. *Science advances*. 3:e1601603.

Blangy, A., L. Arnaud, and E.A. Nigg. 1997. Phosphorylation by p34cdc2 protein kinase regulates binding of the kinesin-related motor HsEg5 to the dynactin subunit p150. *The Journal of biological chemistry*. 272:19418-19424.

Blangy, A., H.A. Lane, P. d'Herin, M. Harper, M. Kress, and E.A. Nigg. 1995. Phosphorylation by p34cdc2 regulates spindle association of human Eg5, a kinesin-related motor essential for bipolar spindle formation in vivo. *Cell*. 83:1159-1169.

Britto, M., A. Goulet, S. Rizvi, O. von Loeffelholz, C.A. Moores, and R.A. Cross. 2016. Schizosaccharomyces pombe kinesin-5 switches direction using a steric blocking

mechanism. *Proceedings of the National Academy of Sciences of the United States of America*. 113:E7483-e7489.
Brust-Mascher, I., P. Sommi, D.K. Cheerambathur, and J.M. Scholey. 2009. Kinesin-5-dependent poleward flux and spindle length control in Drosophila embryo mitosis. *Molecular biology of the cell*. 20:1749-1762.
Cahu, J., A. Olichon, C. Hentrich, H. Schek, J. Drinjakovic, C. Zhang, A. Doherty-Kirby, G. Lajoie, and T. Surrey. 2008. Phosphorylation by Cdk1 increases the binding of Eg5 to microtubules in vitro and in Xenopus egg extract spindles. *PloS one*. 3:e3936.
Cameron, L.A., G. Yang, D. Cimini, J.C. Canman, O. Kisurina-Evgenieva, A. Khodjakov, G. Danuser, and E.D. Salmon. 2006. Kinesin 5-independent poleward flux of kinetochore microtubules in PtK1 cells. *The Journal of cell biology*. 173:173-179.
Chee, M.K., and S.B. Haase. 2010. B-cyclin/CDKs regulate mitotic spindle assembly by phosphorylating kinesins-5 in budding yeast. *PLoS genetics*. 6:e1000935.
Cheerambathur, D.K., I. Brust-Mascher, G. Civelekoglu-Scholey, and J.M. Scholey. 2008. Dynamic partitioning of mitotic kinesin-5 cross-linkers between microtubule-bound and freely diffusing states. *The Journal of cell biology*. 182:429-436.
Chen, Y., and W.O. Hancock. 2015. Kinesin-5 is a microtubule polymerase. *Nature communications*. 6:8160.
Collins, E., B.J. Mann, and P. Wadsworth. 2014. Eg5 restricts anaphase B spindle elongation in mammalian cells. *Cytoskeleton (Hoboken, N.J.)*. 71:136-144.
Ding, R., K.L. McDonald, and J.R. McIntosh. 1993. Three-dimensional reconstruction and analysis of mitotic spindles from the yeast, Schizosaccharomyces pombe. *The Journal of cell biology*. 120:141-151.
Drechsler, H., and A.D. McAinsh. 2016. Kinesin-12 motors cooperate to suppress microtubule catastrophes and drive the formation of parallel microtubule bundles. *Proceedings of the National Academy of Sciences of the United States of America*. 113:E1635-1644.
Drechsler, H., T. McHugh, M.R. Singleton, N.J. Carter, and A.D. McAinsh. 2014. The Kinesin-12 Kif15 is a processive track-switching tetramer. *eLife*. 3:e01724.
Drummond, D.R., and I.M. Hagan. 1998. Mutations in the bimC box of Cut7 indicate divergence of regulation within the bimC family of kinesin related proteins. *Journal of cell science*. 111 (Pt 7):853-865.
Eckerdt, F., P.A. Eyers, A.L. Lewellyn, C. Prigent, and J.L. Maller. 2008. Spindle pole regulation by a discrete Eg5-interacting domain in TPX2. *Current biology : CB*. 18:519-525.
Edamatsu, M. 2014. Bidirectional motility of the fission yeast kinesin-5, Cut7. *Biochemical and biophysical research communications*. 446:231-234.
Eibes, S., N. Gallisa-Sune, M. Rosas-Salvans, P. Martinez-Delgado, I. Vernos, and J. Roig. 2017. Nek9 Phosphorylation Defines a New Role for TPX2 in Eg5-Dependent Centrosome Separation before Nuclear Envelope Breakdown. *Current biology : CB*.
Enos, A.P., and N.R. Morris. 1990. Mutation of a gene that encodes a kinesin-like protein blocks nuclear division in A. nidulans. *Cell*. 60:1019-1027.

Fallesen, T., J. Roostalu, C. Duellberg, G. Pruessner, and T. Surrey. 2017. Ensembles of Bidirectional Kinesin Cin8 Produce Additive Forces in Both Directions of Movement. *Biophysical journal*. 113:2055-2067.

Falnikar, A., S. Tole, and P.W. Baas. 2011. Kinesin-5, a mitotic microtubule-associated motor protein, modulates neuronal migration. *Molecular biology of the cell*. 22:1561-1574.

Ferenz, N.P., A. Gable, and P. Wadsworth. 2010. Mitotic functions of kinesin-5. *Seminars in cell & developmental biology*. 21:255-259.

Ferenz, N.P., R. Paul, C. Fagerstrom, A. Mogilner, and P. Wadsworth. 2009. Dynein antagonizes eg5 by crosslinking and sliding antiparallel microtubules. *Current biology : CB*. 19:1833-1838.

Fridman, V., A. Gerson-Gurwitz, O. Shapira, N. Movshovich, S. Lakamper, C.F. Schmidt, and L. Gheber. 2013. Kinesin-5 Kip1 is a bi-directional motor that stabilizes microtubules and tracks their plus-ends in vivo. *Journal of cell science*. 126:4147-4159.

Fry, A.M., R. Bayliss, and J. Roig. 2017. Mitotic Regulation by NEK Kinase Networks. *Frontiers in cell and developmental biology*. 5:102.

Gable, A., M. Qiu, J. Titus, S. Balchand, N.P. Ferenz, N. Ma, E.S. Collins, C. Fagerstrom, J.L. Ross, G. Yang, and P. Wadsworth. 2012. Dynamic reorganization of Eg5 in the mammalian spindle throughout mitosis requires dynein and TPX2. *Molecular biology of the cell*. 23:1254-1266.

Garcia, K., J. Stumpff, T. Duncan, and T.T. Su. 2009. Tyrosines in the kinesin-5 head domain are necessary for phosphorylation by Wee1 and for mitotic spindle integrity. *Current biology : CB*. 19:1670-1676.

Gardner, M.K., D.C. Bouck, L.V. Paliulis, J.B. Meehl, E.T. O'Toole, J. Haase, A. Soubry, A.P. Joglekar, M. Winey, E.D. Salmon, K. Bloom, and D.J. Odde. 2008. Chromosome congression by Kinesin-5 motor-mediated disassembly of longer kinetochore microtubules. *Cell*. 135:894-906.

Gerson-Gurwitz, A., C. Thiede, N. Movshovich, V. Fridman, M. Podolskaya, T. Danieli, S. Lakamper, D.R. Klopfenstein, C.F. Schmidt, and L. Gheber. 2011. Directionality of individual kinesin-5 Cin8 motors is modulated by loop 8, ionic strength and microtubule geometry. *The EMBO journal*. 30:4942-4954.

Giet, R., R. Uzbekov, F. Cubizolles, K. Le Guellec, and C. Prigent. 1999. The Xenopus laevis aurora-related protein kinase pEg2 associates with and phosphorylates the kinesin-related protein XlEg5. *The Journal of biological chemistry*. 274:15005-15013.

Goldstein, A., N. Siegler, D. Goldman, H. Judah, E. Valk, M. Koivomagi, M. Loog, and L. Gheber. 2017. Three Cdk1 sites in the kinesin-5 Cin8 catalytic domain coordinate motor localization and activity during anaphase. *Cellular and molecular life sciences : CMLS*.

Gordon, D.M., and D.M. Roof. 1999. The kinesin-related protein Kip1p of Saccharomyces cerevisiae is bipolar. *The Journal of biological chemistry*. 274:28779-28786.

Goshima, G., and R.D. Vale. 2003. The roles of microtubule-based motor proteins in mitosis: comprehensive RNAi analysis in the Drosophila S2 cell line. *The Journal of cell biology*. 162:1003-1016.

Goshima, G., and R.D. Vale. 2005. Cell cycle-dependent dynamics and regulation of mitotic kinesins in Drosophila S2 cells. *Molecular biology of the cell*. 16:3896-3907.

Hagan, I., and M. Yanagida. 1990. Novel potential mitotic motor protein encoded by the fission yeast cut7+ gene. *Nature*. 347:563-566.

He, J., Z. Zhang, M. Ouyang, F. Yang, H. Hao, K.L. Lamb, J. Yang, Y. Yin, and W.H. Shen. 2016. PTEN regulates EG5 to control spindle architecture and chromosome congression during mitosis. *Nature communications*. 7:12355.

Heck, M.M., A. Pereira, P. Pesavento, Y. Yannoni, A.C. Spradling, and L.S. Goldstein. 1993. The kinesin-like protein KLP61F is essential for mitosis in Drosophila. *The Journal of cell biology*. 123:665-679.

Hildebrandt, E.R., L. Gheber, T. Kingsbury, and M.A. Hoyt. 2006. Homotetrameric form of Cin8p, a Saccharomyces cerevisiae kinesin-5 motor, is essential for its in vivo function. *The Journal of biological chemistry*. 281:26004-26013.

Honnappa, S., S.M. Gouveia, A. Weisbrich, F.F. Damberger, N.S. Bhavesh, H. Jawhari, I. Grigoriev, F.J. van Rijssel, R.M. Buey, A. Lawera, I. Jelesarov, F.K. Winkler, K. Wuthrich, A. Akhmanova, and M.O. Steinmetz. 2009. An EB1-binding motif acts as a microtubule tip localization signal. *Cell*. 138:366-376.

Hoyt, M.A. 1994. Cellular roles of kinesin and related proteins. *Current opinion in cell biology*. 6:63-68.

Hoyt, M.A., L. He, K.K. Loo, and W.S. Saunders. 1992. Two Saccharomyces cerevisiae kinesin-related gene products required for mitotic spindle assembly. *The Journal of cell biology*. 118:109-120.

Hu, C.K., M. Coughlin, C.M. Field, and T.J. Mitchison. 2011. KIF4 regulates midzone length during cytokinesis. *Current biology : CB*. 21:815-824.

Kahn, O.I., V. Sharma, C. Gonzalez-Billault, and P.W. Baas. 2015. Effects of kinesin-5 inhibition on dendritic architecture and microtubule organization. *Molecular biology of the cell*. 26:66-77.

Kapitein, L.C., B.H. Kwok, J.S. Weinger, C.F. Schmidt, T.M. Kapoor, and E.J. Peterman. 2008. Microtubule cross-linking triggers the directional motility of kinesin-5. *The Journal of cell biology*. 182:421-428.

Kapitein, L.C., E.J. Peterman, B.H. Kwok, J.H. Kim, T.M. Kapoor, and C.F. Schmidt. 2005. The bipolar mitotic kinesin Eg5 moves on both microtubules that it crosslinks. *Nature*. 435:114-118.

Kapoor, T.M., T.U. Mayer, M.L. Coughlin, and T.J. Mitchison. 2000. Probing spindle assembly mechanisms with monastrol, a small molecule inhibitor of the mitotic kinesin, Eg5. *The Journal of cell biology*. 150:975-988.

Kashina, A.S., G.C. Rogers, and J.M. Scholey. 1997. The bimC family of kinesins: essential bipolar mitotic motors driving centrosome separation. *Biochimica et biophysica acta*. 1357:257-271.

Liu, Y., Z. Zhang, H. Liang, X. Zhao, L. Liang, G. Wang, J. Yang, Y. Jin, M.A. McNutt, and Y. Yin. 2017. Protein Phosphatase 2A (PP2A) Regulates EG5 to Control Mitotic Progression. *Scientific reports*. 7:1630.

Ma, N., J. Titus, A. Gable, J.L. Ross, and P. Wadsworth. 2011. TPX2 regulates the localization and activity of Eg5 in the mammalian mitotic spindle. *The Journal of cell biology*. 195:87-98.

Mann, B.J., S.K. Balchand, and P. Wadsworth. 2017. Regulation of Kif15 localization and motility by the C-terminus of TPX2 and microtubule dynamics. *Molecular biology of the cell*. 28:65-75.

Mastronarde, D.N., K.L. McDonald, R. Ding, and J.R. McIntosh. 1993. Interpolar spindle microtubules in PTK cells. *The Journal of cell biology*. 123:1475-1489.

Mayer, T.U., T.M. Kapoor, S.J. Haggarty, R.W. King, S.L. Schreiber, and T.J. Mitchison. 1999. Small molecule inhibitor of mitotic spindle bipolarity identified in a phenotype-based screen. *Science (New York, N.Y.)*. 286:971-974.

McIntosh, J.R., and S.C. Landis. 1971. The distribution of spindle microtubules during mitosis in cultured human cells. *The Journal of cell biology*. 49:468-497.

McIntosh, J.R., M.I. Molodtsov, and F.I. Ataullakhanov. 2012. Biophysics of mitosis. *Quarterly reviews of biophysics*. 45:147-207.

Miki, H., Y. Okada, and N. Hirokawa. 2005. Analysis of the kinesin superfamily: insights into structure and function. *Trends in cell biology*. 15:467-476.

Mitchison, T.J., P. Maddox, J. Gaetz, A. Groen, M. Shirasu, A. Desai, E.D. Salmon, and T.M. Kapoor. 2005. Roles of polymerization dynamics, opposed motors, and a tensile element in governing the length of Xenopus extract meiotic spindles. *Molecular biology of the cell*. 16:3064-3076.

Muretta, J.M., B.J.N. Reddy, G. Scarabelli, A.F. Thompson, S. Jariwala, J. Major, M. Venere, J.N. Rich, B. Willard, D.D. Thomas, J. Stumpff, B.J. Grant, S.P. Gross, and S.S. Rosenfeld. 2018. A posttranslational modification of the mitotic kinesin Eg5 that enhances its mechanochemical coupling and alters its mitotic function. *Proceedings of the National Academy of Sciences of the United States of America*. 115:E1779-e1788.

Myers, K.A., and P.W. Baas. 2007. Kinesin-5 regulates the growth of the axon by acting as a brake on its microtubule array. *The Journal of cell biology*. 178:1081-1091.

Rapley, J., M. Nicolas, A. Groen, L. Regue, M.T. Bertran, C. Caelles, J. Avruch, and J. Roig. 2008. The NIMA-family kinase Nek6 phosphorylates the kinesin Eg5 at a novel site necessary for mitotic spindle formation. *Journal of cell science*. 121:3912-3921.

Rincon, S.A., A. Lamson, R. Blackwell, V. Syrovatkina, V. Fraisier, A. Paoletti, M.D. Betterton, and P.T. Tran. 2017. Kinesin-5-independent mitotic spindle assembly requires the antiparallel microtubule crosslinker Ase1 in fission yeast. *Nature communications*. 8:15286.

Roostalu, J., C. Hentrich, P. Bieling, I.A. Telley, E. Schiebel, and T. Surrey. 2011. Directional switching of the kinesin Cin8 through motor coupling. *Science (New York, N.Y.)*. 332:94-99.

Roostalu, J., E. Schiebel, and A. Khmelinskii. 2010. Cell cycle control of spindle elongation. *Cell cycle (Georgetown, Tex.)*. 9:1084-1090.

Rozelle, D.K., S.D. Hansen, and K.B. Kaplan. 2011. Chromosome passenger complexes control anaphase duration and spindle elongation via a kinesin-5 brake. *The Journal of cell biology*. 193:285-294.

Saunders, A.M., J. Powers, S. Strome, and W.M. Saxton. 2007. Kinesin-5 acts as a brake in anaphase spindle elongation. *Current biology : CB*. 17:R453-454.

Saunders, W., V. Lengyel, and M.A. Hoyt. 1997. Mitotic spindle function in Saccharomyces cerevisiae requires a balance between different types of kinesin-related motors. *Molecular biology of the cell*. 8:1025-1033.

Saunders, W.S., and M.A. Hoyt. 1992. Kinesin-related proteins required for structural integrity of the mitotic spindle. *Cell*. 70:451-458.

Sawin, K.E., K. LeGuellec, M. Philippe, and T.J. Mitchison. 1992. Mitotic spindle organization by a plus-end-directed microtubule motor. *Nature*. 359:540-543.

Sawin, K.E., and T.J. Mitchison. 1995. Mutations in the kinesin-like protein Eg5 disrupting localization to the mitotic spindle. *Proceedings of the National Academy of Sciences of the United States of America*. 92:4289-4293.

Scholey, J.M., G. Civelekoglu-Scholey, and I. Brust-Mascher. 2016. Anaphase B. *Biology*. 5.

Shapira, O., and L. Gheber. 2016. Motile properties of the bi-directional kinesin-5 Cin8 are affected by phosphorylation in its motor domain. *Scientific reports*. 6:25597.

Shapira, O., A. Goldstein, J. Al-Bassam, and L. Gheber. 2017. A potential physiological role for bi-directional motility and motor clustering of mitotic kinesin-5 Cin8 in yeast mitosis. *Journal of cell science*. 130:725-734.

Sharp, D.J., K.L. McDonald, H.M. Brown, H.J. Matthies, C. Walczak, R.D. Vale, T.J. Mitchison, and J.M. Scholey. 1999a. The bipolar kinesin, KLP61F, cross-links microtubules within interpolar microtubule bundles of Drosophila embryonic mitotic spindles. *The Journal of cell biology*. 144:125-138.

Sharp, D.J., G.C. Rogers, and J.M. Scholey. 2000. Microtubule motors in mitosis. *Nature*. 407:41-47.

Sharp, D.J., K.R. Yu, J.C. Sisson, W. Sullivan, and J.M. Scholey. 1999b. Antagonistic microtubule-sliding motors position mitotic centrosomes in Drosophila early embryos. *Nature cell biology*. 1:51-54.

She, Z.Y., and W.X. Yang. 2017. Molecular mechanisms of kinesin-14 motors in spindle assembly and chromosome segregation. *Journal of cell science*. 130:2097-2110.

Shimamoto, Y., S. Forth, and T.M. Kapoor. 2015. Measuring Pushing and Braking Forces Generated by Ensembles of Kinesin-5 Crosslinking Two Microtubules. *Developmental cell*. 34:669-681.

Singh, S.K., H. Pandey, J. Al-Bassam, and L. Gheber. 2018. Bidirectional motility of kinesin-5 motor proteins: structural determinants, cumulative functions and physiological roles. *Cellular and molecular life sciences : CMLS*.

Straight, A.F., J.W. Sedat, and A.W. Murray. 1998. Time-lapse microscopy reveals unique roles for kinesins during anaphase in budding yeast. *The Journal of cell biology*. 143:687-694.

Sturgill, E.G., D.K. Das, Y. Takizawa, Y. Shin, S.E. Collier, M.D. Ohi, W. Hwang, M.J. Lang, and R. Ohi. 2014. Kinesin-12 Kif15 targets kinetochore fibers through an intrinsic two-step mechanism. *Current biology : CB*. 24:2307-2313.

Sturgill, E.G., S.R. Norris, Y. Guo, and R. Ohi. 2016. Kinesin-5 inhibitor resistance is driven by kinesin-12. *The Journal of cell biology*. 213:213-227.

Sturgill, E.G., and R. Ohi. 2013. Kinesin-12 differentially affects spindle assembly depending on its microtubule substrate. *Current biology : CB*. 23:1280-1290.

Tanenbaum, M.E., L. Macurek, N. Galjart, and R.H. Medema. 2008. Dynein, Lis1 and CLIP-170 counteract Eg5-dependent centrosome separation during bipolar spindle assembly. *The EMBO journal*. 27:3235-3245.

Tanenbaum, M.E., L. Macurek, A. Janssen, E.F. Geers, M. Alvarez-Fernandez, and R.H. Medema. 2009. Kif15 cooperates with eg5 to promote bipolar spindle assembly. *Current biology : CB*. 19:1703-1711.

Thiede, C., V. Fridman, A. Gerson-Gurwitz, L. Gheber, and C.F. Schmidt. 2012. Regulation of bi-directional movement of single kinesin-5 Cin8 molecules. *Bioarchitecture*. 2:70-74.

Tikhonenko, I., D.K. Nag, N. Martin, and M.P. Koonce. 2008. Kinesin-5 is not essential for mitotic spindle elongation in Dictyostelium. *Cell motility and the cytoskeleton*. 65:853-862.

Tytell, J.D., and P.K. Sorger. 2006. Analysis of kinesin motor function at budding yeast kinetochores. *The Journal of cell biology*. 172:861-874.

Uteng, M., C. Hentrich, K. Miura, P. Bieling, and T. Surrey. 2008. Poleward transport of Eg5 by dynein-dynactin in Xenopus laevis egg extract spindles. *The Journal of cell biology*. 182:715-726.

Valentine, M.T., P.M. Fordyce, T.C. Krzysiak, S.P. Gilbert, and S.M. Block. 2006. Individual dimers of the mitotic kinesin motor Eg5 step processively and support substantial loads in vitro. *Nature cell biology*. 8:470-476.

Valentine, M.T., and S.P. Gilbert. 2007. To step or not to step? How biochemistry and mechanics influence processivity in Kinesin and Eg5. *Current opinion in cell biology*. 19:75-81.

van den Wildenberg, S.M., L. Tao, L.C. Kapitein, C.F. Schmidt, J.M. Scholey, and E.J. Peterman. 2008. The homotetrameric kinesin-5 KLP61F preferentially crosslinks microtubules into antiparallel orientations. *Current biology : CB*. 18:1860-1864.

van Heesbeen, R.G., M.E. Tanenbaum, and R.H. Medema. 2014. Balanced activity of three mitotic motors is required for bipolar spindle assembly and chromosome segregation. *Cell reports*. 8:948-956.

Vanneste, D., M. Takagi, N. Imamoto, and I. Vernos. 2009. The role of Hklp2 in the stabilization and maintenance of spindle bipolarity. *Current biology : CB*. 19:1712-1717.

Weinger, J.S., M. Qiu, G. Yang, and T.M. Kapoor. 2011. A nonmotor microtubule binding site in kinesin-5 is required for filament crosslinking and sliding. *Current biology : CB*. 21:154-160.

Winey, M., C.L. Mamay, E.T. O'Toole, D.N. Mastronarde, T.H. Giddings, Jr., K.L. McDonald, and J.R. McIntosh. 1995. Three-dimensional ultrastructural analysis of the Saccharomyces cerevisiae mitotic spindle. *The Journal of cell biology*. 129:1601-1615.

Wittmann, T., H. Boleti, C. Antony, E. Karsenti, and I. Vernos. 1998. Localization of the kinesin-like protein Xklp2 to spindle poles requires a leucine zipper, a microtubule-associated protein, and dynein. *The Journal of cell biology*. 143:673-685.

Wolff, I.D., M.V. Tran, T.J. Mullen, A.M. Villeneuve, and S.M. Wignall. 2016. Assembly of Caenorhabditis elegans acentrosomal spindles occurs without

evident microtubule-organizing centers and requires microtubule sorting by KLP-18/kinesin-12 and MESP-1. *Molecular biology of the cell*. 27:3122-3131.

CHAPTER 2

TPX2 INHIBITS EG5 BY INTERACTIONS WITH BOTH MOTOR AND MICROTUBULE

This chapter is adapted from Balchand et al. 2015 and was completed with the guidance of Patricia Wadsworth in collaboration with Sai K. Balchand, Janel Titus and Jennifer L. Ross. JT cloned the TPX2 constructs expressed in Sf9 cells. Microtubule gliding, microtubule-microtubule sliding assays, pelleting assays, and Mean Squared Displacement (MSD) experiments were performed by SKB. Single-molecule TIRF experiments and data analysis were performed in collaboration with SKB and JLR.

2.1 Introduction

Accurate chromosome segregation during cell division requires the assembly and function of the mitotic spindle. The spindle is composed of a bipolar array of dynamic microtubules that are required for chromosome alignment and segregation. Mitotic motor proteins play important roles in regulating microtubule organization and dynamics and in generating the forces required for spindle formation and chromosome motion. Despite the characterization of many mitotic motor proteins, how their activity is regulated both spatially and temporally in the spindle remains incompletely understood (Walczak and Heald, 2008).

TPX2 is a conserved mitotic microtubule-associated protein (MAP) that was originally identified as a protein required for the dynein-dependent targeting of the

Xenopus kinesin Xklp2 to mitotic spindle poles (Wittmann et al., 1998). In mammalian cells, TPX2 localizes to the nucleus in interphase and to the spindle in mitosis with an enrichment near spindle poles (Garrett et al., 2002; Gruss et al., 2002). Depletion of TPX2 using siRNA results in short bipolar or multipolar spindles that fail to progress through mitosis (Garrett et al., 2002; Gruss et al., 2002). The N-terminus of TPX2 binds and activates the mitotic kinase Aurora A, and is required to localize the kinase to spindle microtubules (Bayliss et al., 2003; Eyers and Maller, 2004; Kufer et al., 2002). During spindle formation, TPX2 is required for microtubule formation near kinetochores, an activity that requires GTP bound Ran, which relieves the inhibitory action of importin □□□ on TPX2 (Tulu et al., 2006). In addition, it has been demonstrated that the C-terminus of TPX2 binds to the bipolar kinesin Eg5 and targets the motor to spindle microtubules (Eckerdt et al., 2008; Ma et al., 2010). Expression of TPX2 lacking the C-terminal 35 amino acids, which contribute to Eg5 binding, results in defective spindles with greatly reduced Eg5 on spindle microtubules, unfocussed spindle poles and bent and buckled microtubules (Ma et al., 2011).

Because Eg5 plays a critical and conserved function in establishing spindle bipolarity, it is important to understand how this motor is regulated in the spindle. Previous *in vitro* experiments have shown that purified TPX2 reduces the velocity of Eg5-dependent microtubule gliding and microtubule-microtubule dependent sliding (Ma et al., 2011). Eg5 accumulation on microtubules is enhanced in the presence of full length TPX2, but less in the presence of TPX2 lacking the Eg5 binding domain (Ma et al., 2011). These results directly demonstrate that TPX2 inhibits the ability of Eg5 to translocate microtubules, but the mechanism of inhibition is not established. Here we use

in vitro assays and single molecule TIRF microscopy to characterize the interaction of TPX2 with microtubules and to examine the behavior of Eg5 in the presence of TPX2. Our results demonstrate that TPX2 blocks Eg5 motility by both a direct interaction with Eg5 and by binding to microtubules and acting as a roadblock. Using microtubule gliding assays, we further show that dimeric, but not monomeric, Eg5 is differentially inhibited by full-length and truncated TPX2. Our experiments provide new insight into the microtubule-associated protein TPX2 and its regulation of the mitotic kinesin Eg5.

2.2 Results

2.2.1 TPX2 binding to microtubules

To examine the regulation of mammalian Eg5 by TPX2, we expressed and purified full-length TPX2 and a truncated version lacking the C-terminal 35 amino acids (referred to as TPX2-710) that mediate the interaction with Eg5 (Eckerdt et al., 2008; Ma et al., 2011) (Fig. 2.1A). To characterize the microtubule binding of these proteins, we performed microtubule co-sedimentation experiments. Both full-length TPX2 and TPX2-710 co-sedimented with microtubules with apparent dissociation constants of 125 and 240 nM, respectively (Fig. 2.1B,C). Both full length and truncated TPX2 could be released from the microtubule lattice by adding KCl to the buffer, with negligible binding at 250 mM KCl. This demonstrates that, like other microtubule-associated proteins, TPX2 makes ionic interactions with the microtubule lattice (Fig. 2.2A).

Microtubule-associated proteins are thought to make electrostatic interactions specifically with the negatively-charged C-terminal E-hooks of tubulin, named for the abundance of glutamic acid residues (Paschal et al., 1989). To determine whether the E-

hooks are either a requirement for or facilitate TPX2 binding to microtubules, polymerized microtubules were digested with the enzyme Subtilisin A to cleave off the E-hooks and binding of TPX2 and TPX2-710 to control and digested microtubules was measured. The results show that binding of full length or truncated TPX2 to microtubules was not different for untreated, compared to Subtilisin digested, microtubules (Fig. 2.2B).

To examine the interaction of individual molecules of TPX2 with the microtubule we performed single molecule TIRF microscopy of Halo-tagged TPX2 full length and TPX2-710. Individual molecules were stationary on the microtubule lattice and, at the concentration examined, no enrichment at either end of the microtubule was observed. The average dwell time of full length TPX2-Halo, measured from image sequences acquired at 2 s intervals for 15 min, was 60.1 sec (Fig. 2.2C). The average dwell time of Halo tagged TPX2-710 was 46.6 sec and was not statistically different from the Halo tagged full length TPX2.

Together these results demonstrate that TPX2 binds to the microtubule lattice with high affinity, and that the C-terminal 35 amino acids do not contribute significantly to this interaction. Additionally, TPX2 does not require the tubulin E-hook for microtubule binding, suggesting that other tubulin residues are responsible for the interaction.

2.2.2 Functional Eg5 from mammalian cell extracts

We prepared cytoplasmic extracts (Cai et al., 2009) from a mammalian cell line stably expressing full length, localization and affinity purification (LAP)-tagged Eg5 (hereafter Eg5-EGFP) expressed from a bacterial artificial chromosome under control of

the native promoter (Cheeseman and Desai, 2005; Gable et al., 2012) (see Methods). The concentration of Eg5-EGFP in the cell extracts was determined using Western blotting; values of 20-60 nM were obtained depending on the extract (Fig. 2.3A). The concentration of TPX2 in these cytoplasmic extracts was less than ~1 nM, consistent with the localization of TPX2 to the nucleus during interphase (data not shown).

To analyze Eg5-EGFP motors in cell extracts, the extract was diluted into motility buffer (Methods) to achieve a final motor concentration of ~ 1 nM. Diluted extract was added to flow chambers containing rhodamine-labeled, taxol-stabilized microtubules immobilized to the surface using anti-tubulin antibodies (Methods). Using TIRF microscopy, bright puncta were observed to bind to the microtubules in the absence of ATP. Upon addition of ATP, robust motility of nearly all puncta was observed (Fig. 2.3B). We observed an accumulation of motors at one end of most microtubules in the field of view (Fig. 2.3B) indicating that motors remain associated with the microtubule plus-end after motion. This is consistent with the previously observed tethering of microtubules near the microtubule end in sliding assays using *Xenopus* Eg5 (see below) (Kapitein et al., 2005). At higher motor concentration, microtubules were uniformly coated with fluorescence, and individual puncta could not be resolved. The average velocity of individual puncta was 14.7 ± 0.9 nm/s, (SEM, N = 205) similar to the velocity of purified *Xenopus* and *Drosophila* Eg5 motors (Kapitein et al., 2008; Kwok et al., 2006; van den Wildenberg et al., 2008) (Fig. 2.3D). The average association time of Eg5 with the microtubules was not determined because motors rarely dissociated over the course of a 10 min movie and longer movies resulted in photobleaching of individual puncta. Finally, motor behavior was not altered following storage in liquid nitrogen for several

weeks, so a single extract could be used for multiple experiments, making this a robust and versatile method for studying motor behavior (see Discussion).

To determine the directionality of motor motion, Kinesin-1-EGFP, a plus-end directed motor, was added to the chamber and the direction of motion observed. Next, the chamber was washed with 5 chamber volumes of ATP containing motility buffer, to remove the Kinesin-1-EGFP, and Eg5-EGFP was added to the same chamber and motor behavior was followed in the same field of view. In all cases, both Kinesin-1-EGFP and Eg5-EGFP moved to the same end of the microtubule (Fig. 2.3C) demonstrating that the motile puncta in the mammalian extract walk to the microtubule plus-end.

Next, we wished to determine if the Eg5-EGFP motors in the extract were present as tetramers. Because the cells expressing Eg5-EGFP also express endogenous Eg5, the motile motors could be composed of between 1 and 4 EGFP molecules. In this cell line, the Eg5-EGFP is not resistant to the siRNA designed to deplete endogenous Eg5 (Gable et al., 2012). Therefore, to estimate the number of labeled Eg5 motors in the motile puncta, we depleted endogenous Eg5 from parental cells co-transfected with siRNA resistant Eg5-mEmerald, and prepared cell extracts. The average fluorescence intensity of Eg5-mEmerald puncta was measured and compared with the fluorescence intensity of bacterially expressed Kinesin-1-EGFP dimers imaged under identical conditions (Fig. 2.3E). On average, the Eg5-mEmerald puncta were twice as bright as the Kinesin-1-EGFP dimers indicating that Eg5 was predominately tetrameric. The increase in quantum fluorescence yield of mEmerald alone is not sufficient to explain the nearly two-fold increase in fluorescence intensity (Day and Davidson, 2009). Additionally, the siRNA

may not deplete 100% of the endogenous Eg5, which could form tetramers with the Eg5-mEmerald, resulting in decreased fluorescence of some puncta.

To determine if the Eg5-EGFP molecules function as tetramers, we examined the ability of Eg5-EGFP from extracts to crosslink two microtubules. To do this we added Eg5-EGFP to immobilized microtubules in a flow chamber and then added additional microtubules. The added microtubules bound to the immobilized microtubules and were translocated upon addition of ATP demonstrating that Eg5-EGFP was capable of crosslinking and sliding microtubules (Fig. 2.3F). In addition, the moving microtubule remained associated with the tip of the track microtubule, consistent with previous observations (Kapitein et al., 2005). Together, these experiments demonstrate that Eg5-EGFP from extracts is tetrameric (Fig. 2.3 E,F).

Next, we performed size exclusion chromatography on the extracts from LLC-Pk1 cells. Owing to the low abundance of Eg5-EGFP in our extracts, we used cells overexpressing Eg5-mEmerald to aid in the detection. The western blots of the fractions obtained show that Eg5-mEmerald elutes around the same fractions as the Eg5-EGFP molecules, which are purified from SF9 insect cells, suggesting that the Eg5 molecules obtained from cell extracts are tetramers (Fig. 2.3G)

To demonstrate that the bright motile puncta derived from the cell extract are Eg5 molecules, we added S-trityl-L-cysteine (STLC) or 2-[1-(4-fluorophenyl)cyclopropyl]-4-(pyridin-4-yl)thiazole (FCPT) which specifically inhibit Eg5 (Groen et al., 2008; Skoufias et al., 2006b). Each inhibitor completely stopped the motion of motile puncta (Fig. 2.3H); in the presence of FCPT, motors remained bound to the microtubule lattice,

whereas in the presence of STLC, motors stopped walking and in many cases were released from the microtubule (Kwok et al., 2006) (Fig. 2.3H).

Eg5 has been shown to exhibit diffusive behavior on microtubules at physiological salt concentration (Kwok et al., 2006; Weinger et al., 2011). To determine if mammalian Eg5 present in diluted cell extracts showed similar diffusive behavior, we added increasing concentrations of KCl to the motility buffer, and examined motor behavior. At 20 mM KCl, the velocity of Eg5 was 12.1 nm/s, similar to that observed in 0 mM KCl, and the diffusion coefficient, D, obtained from plots of MSD over time, was 1588 nm^2/s. At 50 mM KCl, motor velocity dropped to 3 nm/s and the value of D was 4556 nm^2/s (Fig. 2.3I). These results demonstrate that motor processivity is dependent on the ionic conditions, consistent with previous results using *Xenopus* Eg5 (Kapitein et al., 2008; Weinger et al., 2011).

Together, our results show that Eg5-EGFP motors in mammalian cell extracts behave in a manner similar to purified *Xenopus* and *Drosophila* Eg5 tetramers. Specifically, the velocity, directionality, sensitivity to STLC and FCPT and diffusive behavior in higher ionic strength buffer are all consistent with previously reported properties of purified *Xenopus* and *Drosophila* Kinesin-5 motors. Somewhat surprisingly, the behavior of mammalian Eg5 motors has not been previously examined. Our data show that these motors are similar to insect and other vertebrate Eg5 motors and distinct from kinesin-5 motors from yeast that show directional switching (Gerson-Gurwitz et al., 2011; Roostalu et al., 2011). Importantly, the similar properties of the mammalian motors strongly suggests that components that are present in the cell extract do not have a major effect on motor behavior.

2.2.3 Interactions of TPX2 with the microtubule and with Eg5 both contribute to inhibition of motility

Previous work demonstrated that the gliding of microtubules by surface attached Eg5 dimers is inhibited by TPX2 full length and to a lesser extent by TPX2-710 (Ma et al., 2011). Full length TPX2 also inhibits Eg5 mediated microtubule-microtubule sliding (Ma et al., 2011). In both of these assays, however, the behavior of populations of motors is examined, so how individual Eg5 molecules are regulated by TPX2 was not revealed. To gain a better understanding of the mechanism of inhibition of Eg5 by TPX2, we performed single molecule experiments.

To determine the effect of TPX2 on Eg5 behavior, the cytoplasmic extract containing Eg5-EGFP was diluted in motility buffer, added to chambers of immobilized microtubules, and motors were imaged. Next, TPX2 was added to the chamber during image acquisition (Fig. 2.4A). For these experiments, the velocity of motors following addition of TPX2 is expressed as a percentage of the velocity prior to addition of TPX2. The data show that full-length TPX2 is a potent inhibitor of the velocity of individual Eg5 motors: at 250 nM, TPX2 reduced Eg5 velocity by 83% and at 50 nM Eg5 velocity was reduced by 32% (Fig. 2.4B). To understand how the interaction of TPX2 with Eg5 contributes to motor inhibition, we repeated the experiment using TPX2-710. Addition of TPX2-710 also substantially reduced the velocity of Eg5-EGFP indicating that microtubule binding by TPX2 contributes to the reduction in motor velocity. At low concentrations (50 nM) both TPX2 and TPX2-710 showed similar inhibition of Eg5 (32% and 24% respectively. However, at higher concentrations (250 nM) TPX2-710 was

a less effective inhibitor of Eg5-EGFP than TPX2 full length (inhibition of 53% and 83%, respectively) (Fig. 2.4B).

The results further show that TPX2 reduces the velocity of Eg5-EGFP motors without inducing dissociation of most motors from the microtubule (Fig. 2.4A) consistent with the established role of TPX2 in targeting Eg5 to spindle microtubules (Ma et al., 2011). In the presence of TPX2-710, more motors appeared to dissociate from the microtubule, although photobleaching precluded accurate quantification. In some cases, we saw that following addition of TPX2 to the motility chamber, motors from solution associated with the microtubule, and these motors also moved with reduced velocity (Fig. 2.4A).

To confirm the specificity of the Eg5-TPX2 interaction, we added full length TPX2-Halo covalently tagged with an Alexa 660 ligand to Kinesin-1-EGFP dimers in a single molecule assay (Fig. 2.4C). Consistent with prior results from microtubule gliding assays, TPX2 addition did not alter the motility of Kinesin-1-EGFP (11).

To visualize the interaction between Eg5 and TPX2 in the single molecule experiments, we used TPX2-Halo covalently tagged with an Alexa 660 ligand (Fig. 2.4D). In this experiment, addition of TPX2-Halo (at 20 nM**)** reduced the velocity of Eg5-EGFP. Analysis of kymographs showed that individual motors that encountered TPX2-Halo walked at reduced velocity. In some cases a motor that has reduced velocity can resume motion when it encounters an area of the microtubule that is relatively free of TPX2 (Fig. 2.4D, right panels). Note that in this experiment, a lower concentration of TPX2 was used because at higher concentration, fluorescent TPX2 coated the entire microtubule surface.

We also performed experiments in which 50 nM TPX2 or TPX2-710 was pre-mixed with the motor in motility buffer before addition to the chamber. This method allows Eg5 and TPX2 to potentially interact, and both molecules are introduced to the chamber simultaneously (Fig. 2.4E,F). This experiment also showed greater inhibition of Eg5-EGFP by the full-length compared to the truncated TPX2 (Fig. 2.4E,F). Interestingly, pre-mixing full-length TPX2 with Eg5-EGFP resulted in greater inhibition than when the same concentration of TPX2 was added to motors pre-bound to microtubules (60% vs. 32% inhibition, Fig. 2.4B, F). This result indicates that when the motor and TPX2 bind to the microtubule at the same time, stronger inhibition results. In contrast, when TPX2 is added to motors already bound to microtubules, TPX2 can bind to the microtubule at sites distant from the motors, and thus not immediately impact motor velocity. Interestingly, in the case of TPX2-710, inhibition of Eg5-EGFP was similar regardless of whether the motors were premixed or added sequentially (Fig. 2.4B, F).

Finally, to exclude the possibility that adding a Halo tag to TPX2 affected the TPX2-Eg5 interaction, we compared inhibition of Eg5 by untagged and Halo tagged TPX2. As seen in Fig. 2.4F, inhibition of Eg5-EGFP by TPX2 was not changed by the presence of the Halo tag demonstrating that the Halo tag was not detectably affecting TPX2-Eg5 interaction (Fig. 2.4F).

Together, the results of these experiments demonstrate that Eg5 in cytoplasmic extracts is inhibited by TPX2. Full length TPX2, which can interact with Eg5 and with the microtubule, is a more potent inhibitor than TPX2-710, which lacks the Eg5

interaction domain. However, by binding to the microtubule lattice, TPX2-710 also substantially reduces the velocity of individual Eg5 puncta.

2.2.4 TPX2 differentially inhibits Microtubule gliding by Eg5 dimers, but not monomers

To determine how Eg5-EGFP motors are inhibited by TPX2, we performed microtubule gliding assays using Eg5 dimers and Eg5 monomers (Methods). Dimers supported microtubule gliding at an average rate of ~20 nm/s. The velocity of gliding was reduced to ~6 nm/s by 250 nM full length TPX2; addition of the same concentration of TPX2-710 reduced the velocity of gliding to ~15 nm/s, demonstrating that TPX2-710 was a less effective inhibitor than the full length protein (Fig. 2.5A). This result demonstrates that dimeric Eg5 retains the ability to interact with TPX2, consistent with previous *in vitro* binding assays (Ma et al., 2011). In contrast, the velocity of microtubule gliding driven by monomeric Eg5 was inhibited to a similar extent by either full length or truncated TPX2 (Fig. 2.5B). It should be noted that the velocity of microtubule gliding driven by monomeric Eg5 is approximately half the rate of the dimeric construct, presumably due to the uncoordinated action of monomers. Further, our results also show that monomer-driven microtubule gliding is inhibited at lower concentrations of TPX2 or TPX2-710 (Fig. 2.5B). For example, addition of 25 nM TPX2 or TPX2-710 nearly completely halted microtubule gliding by monomeric Eg5 whereas a 20-fold greater concentration of TPX2 is required to result in a similar reduction in the velocity of microtubule gliding by Eg5 dimers. The reason for this increased sensitivity is not known, but may relate to the presence of a single motor head. These results

suggest that the stalk region in the dimeric construct, or the dimer conformation, is required for differential inhibition by TPX2 and TPX2-710.

2.3 Discussion

2.3.1 TPX2 binding to microtubules

The results of our experiments provide insight into the interaction of TPX2 with the microtubule lattice. Our data show that TPX2 and TPX2-710 bind with relatively high apparent affinity to microtubules; these results are similar to the previously reported K_D of 0.5 □M for full length *Xenopus* TPX2 (Wittmann et al., 2000). The similar binding of TPX2 and TPX2-710 suggests that the C-terminal region is not a major contributor to microtubule binding, and instead interacts with the motor. The apparent affinity of TPX2 for microtubules is similar to other MAPs, including the dynein regulator, She1, MAP2 and Cep170 (Illenberger et al., 1996; Markus et al., 2012; Welburn and Cheeseman, 2012). The relatively strong interaction of TPX2 with the microtubule lattice is also reflected in the long dwell time measured for individual TPX2 puncta using microscopy (~60 s). Our experiments did not reveal a diffusive component to TPX2 behavior under the conditions used. Under physiological ionic conditions, however, we expect that TPX2 would bind less strongly to the microtubule lattice and could exhibit 1-D diffusive behavior that is characteristic of many MAPs.

Somewhat surprisingly, our results show that the C-terminal tails of tubulin, the E-hooks, do not contribute to TPX2 interaction with the microtubule. Other MAPs, including Tau, She1, and XMAP215 require the tubulin E-hooks for microtubule binding (Brouhard et al., 2008; Hinrichs et al., 2012; Markus et al., 2012). Additionally, the

processivity of Kinesin-1 and dynein motors, and the diffusive end targeting of MCAK, are enhanced by the E-hooks (Helenius et al., 2006; Thorn et al., 2000; Wang and Sheetz, 2000). The observation that the interaction of TPX2 with microtubules does not require the E-hooks indicates that TPX2 binds to tubulin residues that are located between protofilaments, as opposed to along the ridge where the E-hooks are located. This is consistent with the observation that TPX2 does not inhibit single molecule motion of Kinesin-1-EGFP dimers on microtubules (Fig. 2.4C) and previous work demonstrating that TPX2 does not inhibit Kinesin-1 in a gliding assay (Ma et al., 2011). In contrast, Tau, which binds along the outer ridge and requires the E-hook for lattice diffusion (Hinrichs et al., 2012), induces the release of kinesin motors, including both Kinesin-1 and Eg5, from the microtubule. This suggests that the location of MAP binding to the microtubule lattice results in differential effects on motor behavior (e.g. inhibition of motility vs. release) (Ma et al., 2011).

The high affinity interaction of TPX2 with microtubules is consistent with its established role in promoting microtubule assembly near kinetochores (Tulu et al., 2006) and branched microtubules in the spindle (Petry et al., 2013). However, the interaction of TPX2 with microtubules in cells is dynamic, as evidenced by its poleward motion in the spindle (Ma et al., 2010). One possibility that can account for these differences is that modifications, such as phosphorylation, or interactions with other binding partners, such as dynein, regulate TPX2 dynamic behavior in cells.

2.3.2 Functional Eg5 from mammalian cell extracts

Previous work showed that the behavior of motors present in extracts of cultured mammalian or budding yeast cells is comparable to the behavior of the purified motor (Cai et al., 2007; Gerson-Gurwitz et al., 2011). We found that the rate of Eg5-EGFP stepping along the microtubule was ~14 nm/s in the plus-end direction, which is similar to the values obtained for purified *Xenopus* or *Drosophila* Eg5. To our knowledge, our results are the first report of single molecule data on the behavior of Eg5-EGFP tetramers from a mammalian source, although the behavior of human Eg5 dimers has been previously measured (Valentine et al., 2006). Mammalian Eg5-EGFP showed exclusively plus-end directed motion at low salt and diffusive behavior at higher salt concentrations. At the highest salt concentration that we examined, no processive minus-end directed motion was detected, indicating that mammalian Eg5 does not show directional switching like the yeast homolog, Cin8 (Gerson-Gurwitz et al., 2011; Roostalu et al., 2011).

There are several potential advantages to using motors present in mammalian extracts for biophysical experiments. For example, the contribution of specific domains or potential phosphorylation sites can be determined using extracts prepared from cells transfected with fluorescent constructs encoding mutant versions of the protein of interest. Similarly, to eliminate binding partners, or accessory subunits implicated in motor regulation or function, cells can be treated with siRNA prior to preparation of the extract. In addition, cells can be arrested at particular stages of the cell cycle prior to preparation of the extract to determine how cell cycle-dependent modifications may impact motor function. Finally, the ease of preparation and robust motile behavior

demonstrate that biophysical measurements of motors from cell extracts is a powerful tool for future experiments.

2.3.3 TPX2 inhibits Eg5 by interactions with both the motor and microtubule

The single molecule data presented here demonstrate that TPX2 has two modes of inhibition for Eg5. Truncated TPX2 that cannot interact directly with Eg5, still bound to the microtubule lattice and substantially reduced the velocity of Eg5. Full-length TPX2, which binds to both the microtubule and the motor, was an even more potent inhibitor of Eg5. These results show that both binding to the microtubule and to Eg5 contribute to inhibition of the motor.

Our work is consistent with previous work demonstrating that MAPs can regulate motor behavior. For example, Tau results in differential regulation of Kinesin-1 and dynein; upon encountering a Tau patch, Kinesin-1 motors frequently detach from the microtubule, whereas dynein motors are likely to reverse direction or pause (Dixit et al., 2008). However, a direct interaction of either Kinesin-1 or dynein with Tau has not been reported. Other MAPs function to target motors to microtubules. For example, Cep170, is important for targeting the kinesin-13, Kif2b, to the spindle (Welburn and Cheeseman, 2012) and the yeast microtubule associated protein She-1 prolongs the attachment of dynein to the microtubule in a stalled state in addition to inhibiting dynein motility (Markus et al., 2012). In contrast, the MAP ensconsin recruits and activates Kinesin-1 (Sung et al., 2008) independent of microtubule binding by ensconsin (Barlan et al., 2013).

Recent *in vitro* experiments show that TPX2 inhibits the stepping behavior of the kinesin-12, Kif15, the human homolog of Xklp2 (Drechsler et al., 2014). TPX2 enhances

the binding of Kif15 to microtubules in pelleting assays and increases motor binding to the microtubule under load in optical trapping experiments (Drechsler et al., 2014). Purified Eg5 has been shown to detach from the microtubule before stalling (Korneev et al., 2007), suggesting that TPX2 may function to increase Eg5 binding to the microtubule under load, as is the case for Kif15. In mitotic cells, Eg5 and Kif15 act redundantly to establish and maintain spindle bipolarity. Furthermore, minus-end directed forces generated by cytoplasmic dynein antagonize force generated by these plus-end directed motors. Though TPX2 slows Eg5 and Kif15 motion on microtubules, by increasing the force generating capacity of these motors, it may play a key role in regulating forces needed for spindle bipolarity.

2.3.4 Model for Regulation of Eg5 by TPX2

The data presented here are consistent with the following model for the regulation of Eg5 by TPX2 (Fig. 2.5C): Eg5 motors step along the microtubule protofilament and encounter TPX2, resulting in reduced velocity without inducing motor detachment from the microtubule. Our data showing that TPX2 does not require the E-hooks for microtubule binding suggest that TPX2 and Eg5 do not compete with each other for microtubule binding. The differential slowing of the motor by full length and truncated TPX2 demonstrates that binding of TPX2-710 to the microtubule is sufficient to reduce motor velocity but that the C-terminus of TPX2, which interacts with Eg5, results in stronger inhibition (Fig. 2.5C). This suggests that TPX2-710 acts as a slowing agent, reducing velocity when encountered by Eg5 motors. Additionally, our data suggest that the C-terminal domain may contribute to the retention of the motor on the microtubule

(Ma et al., 2011). Although our experiments, and those of others (Drechsler et al., 2014), clearly demonstrate that TPX2 greatly reduces motor stepping on the microtubule, the TPX2-motor interaction must be regulated in live cells so that the motor can generate sliding forces to establish and maintain spindle bipolarity. Discovering precisely how this MAP-motor interaction is regulated spatially and temporally will provide important insight into spindle function *in vivo*.

2.4 Materials and Methods

2.4.1 Materials

All chemicals, unless otherwise specified, were purchased from Sigma-Aldrich.

2.4.2 Cell culture

LLC-Pk1 cells were cultured in a 1:1 mixture of F10 Hams and Opti-MEM (Life Technologies, Grand Island, N.Y.) containing 7.5% fetal bovine serum and antibiotics at 1X and 5% CO_2. Cell extracts were made from LLC-Pk1 cells stably expressing LAP-tagged Eg5 from a bacterial artificial chromosome (Gable et al., 2012). To prepare the extract, a confluent 100 mm diameter cell culture dish was washed twice with 5 ml of room temperature PBS. Then, 300 µl of extraction buffer containing 40 mM HEPES/KOH pH 7.6, 100 mM NaCl, 1 mM EDTA, 1 mM PMSF, 10 µg/ml Leupeptin, 1 mg/ml pepstatin, 0.5% Triton X 100 and 1 mM ATP (Cai et al., 2007) was added dropwise to the dish and incubated for approximately 2 min, without disrupting the monolayer. The cell extract was transferred to a microcentrifuge tube and centrifuged at 14,500 RPM at 4°C for 10 min in a tabletop centrifuge. The supernatant was recovered

and aliquoted into small tubes, flash frozen and stored in liquid nitrogen. Protein concentration was determined using the method of Lowry (Lowry et al., 1951). For fluorescent intensity measurement experiments with Eg5-mEmerald, an siRNA resistant Eg5-mEmerald construct was transiently co-transfected into LLC-Pk1 cells with siRNA directed against endogenous Eg5 (target sequence CUGAAGACCUGAAGACAAU). The extract was made 48 hours post transfection as described. For the extracts used in size exclusion chromatography, siRNA treatment against endogenous Eg5 was omitted.

2.4.3 Construction of plasmids

For bacterial expression, desired nucleotide sequences of human TPX2 constructs (full length or truncated at amino acid 710) were cloned into a pGEX vector following an N-terminal GST tag and a ULP1 protease cleavage site (Markus et al., 2012). At the C-terminus of TPX2, the stop codon was removed and the Halo tag sequence was introduced. Constructs were verified by sequencing. For expression in SF9 insect cells, nucleotides coding for full length or the first 710 amino acids of human TPX2 were cloned into the pFast Bac A vector after an N terminal 6X His tag and the constructs were verified by sequencing. The virus for infecting the cells was obtained following the Bac-to-Bac protocol (Invitrogen, Grand Island, NY). The plasmid for monomeric Eg5-367 containing the first 367 amino acids of human Eg5 was a kind gift from the laboratory of Dr. Sarah Rice. The plasmid for the expression of dimeric Eg5-513 containing the first 513 amino acids of Eg5 was the kind gift from the laboratory of Dr. Susan Gilbert.

2.4.4 Protein purification

Full length TPX2 and TPX2-710 were expressed and purified from Sf9 cells using the Bac-to-Bac expression system (Invitrogen, Grand Island, NY). Infected cells were harvested, washed with ice-cold water and resuspended in lysis buffer (50 mM potassium phosphate pH 8, 250 mM KCl, 40 mM imidazole, 1% NP-40, 10 mM beta mercaptoethanol, and a protease inhibitor tablet (Roche, Indianapolis, IN) on ice. The lysate was spun at 125,000 x g for 45 min at 4°C. The supernatant was loaded onto pre-equilibrated Ni NTA agarose beads (Qiagen, Valencia, CA) and incubated for 90 min at 4°C with end-over-end shaking. The flow through was removed and beads were washed with wash buffer (same as lysis buffer with 10% glycerol and 0.01% NP-40). The protein was eluted with elution buffer (50 mM potassium phosphate pH 7, 150 mM KCl, 250 mM imidazole, 10% Glycerol, 10 mM beta mercaptoethanol, and 0.01% NP-40) and dialyzed in a buffer containing 25 mM HEPES, pH 7.6, 10 mM KCl, 2 mM MgCl2, 10% Glycerol, 0.01% NP-40 and 1 mM DTT for 4 hours at 4°C. Aliquots were flash frozen in liquid nitrogen and stored at -80°C.

Full length TPX2-Halo and TPX2-710-Halo were expressed and purified from *E.coli* Rosetta DE3 pLysS cells. In short, 500 ml of culture was grown to an optical density of 0.5-0.8, induced with 0.1 mM IPTG at 18°C for 16 hours. The bacteria were harvested and washed with ice-cold distilled water. The cell pellet was resuspended in 2X lysis buffer (60 mM HEPES pH 7.4, 0.4 mM EGTA, 2 mM DTT, 1.4 μg/ml pepstatin, 1.0 mM Pefabloc, 4 μg/ml leupeptin, and 2 μg/ml Aprotinin), diluted to 1X with cold dH_2O, sonicated on ice (3X 30 s at maximum setting), and clarified at 15,000 x g for 20 min at 4°C. The supernatant was incubated for 1 hour at 4°C with Glutathione sepharose beads

that were pre-equilibrated in lysis buffer. The beads were then washed 3X in wash buffer (10% glycerol, 300 mM KCl, 0.1% Triton X-100, 1 mM DTT, 0.7 μg/ml pepstatin and 0.5 mM Pefabloc) and twice in TEV buffer (5 mM Tris pH 8.0, 150 mM KCl, 10% glycerol, 0.1% Triton X-100, 1 mM DTT and 0.5 mM Pefabloc). The beads were resuspended in TEV buffer and incubated with 23 μM Halo tag Alexa fluor 660 (Promega, Madison, WI) for 15-20 min at room temperature and then washed to remove unbound ligand. The beads were then resuspended in TEV buffer containing Ulp1 protease and incubated at 16°C for 1 hr to cleave protein off the beads. The supernatant containing the protein was collected by centrifugation and aliquots were flash frozen and stored in liquid nitrogen.

Monomeric Eg5-367 was purified from *E.coli* as described in (Larson et al., 2010). Briefly, 500 ml of bacteria was grown and induced at an OD of 0.5-0.8 with 0.1 mM IPTG and incubated at 16°C for 16 hours. The bacteria were pelleted and washed with ice-cold water. The pellet was resuspended in lysis buffer (10 mM sodium phosphate buffer pH 7.2, 20 mM NaCl, 2 mM $MgCl_2$, 1 mM EGTA, 1 mM DTT, and 0.1 mM ATP with protease inhibitor tablet) and lysed by sonication. The lysate was clarified by centrifuging at 15,000 x g for 30 min at 4°C. The supernatant was incubated with pre-equilibrated Ni NTA agarose beads for 90 min at 4°C. The beads were then washed in wash buffer (same as lysis buffer containing 20 mM imidazole) and eluted in elution buffer (same as lysis buffer with 300 mM imidazole). The eluate was then dialyzed against buffer containing 20 mM HEPES pH 7.2, 5 mM magnesium acetate, 0.1 mM EDTA, 0.1mM EGTA, 50 mM potassium acetate, 1 mM DTT, and 5% sucrose for 4

hours at 4°C. Aliquots were flash frozen in liquid nitrogen and stored at -80°C. Dimeric Eg5-513 was expressed and purified from *E.coli* exactly as described (Ma et al., 2011).

2.4.5 TPX2 co-sedimentation with microtubules

Unlabeled tubulin prepared from porcine brains (Hyman et al., 1991b) was polymerized and resuspended in PEM 100 buffer containing 50 μM Taxol. 500 nM full length TPX2 or TPX2-710 was incubated with indicated concentration of unlabeled polymerized microtubules at room temperature for 10 min. The mixture was centrifuged for 10 min at room temperature in a tabletop centrifuge at maximum speed. The supernatant and pellet fractions were carefully separated. Samples for SDS electrophoresis were prepared by boiling the samples with SDS protein sample buffer and run on an 8% polyacrylamide gel. The proteins were then transferred to a PVDF membrane and probed using antibodies against TPX2 (Novus Biologicals, Littleton, CO) and tubulin (DM1A, Sigma-Aldrich). The blots were developed by chemiluminescence and captured on a Biorad (Hercules, CA) imaging station. Analysis of band intensities were performed using ImageJ. Data were plotted using KaleidaGraph and fit with a quadratic equation (Markus et al., 2012). Subtilisin A treated microtubules were prepared as described (Markus et al., 2012).

2.4.6 TPX2-Halo Microtubule Binding Assays

For TPX2-Halo binding experiments, first 10 μL of 10% Rat YL ½ (0.1 mg/ml) anti-tubulin antibody (Accurate Chemical, Westbury, N.Y.) was added to the flow chamber and incubated for 2 min. Second, 0.1 mg/ml Rhodamine-microtubules

(untreated or treated with Subtilisin A) were flowed in and incubated for 2 min. Third, the surface was blocked by adding 5 % Pluronic F-127 and incubated for 2 min. For assays done in epifluorescence, the chamber was incubated with the indicated concentration of TPX2-Halo for 2 min in PEM 100, [100 mM K-Pipes, pH 6.8, 2 mM MgSO4, and 2 mM EGTA] plus 0.5% Pluronic F-127, 50 μM taxol, 5 mM DTT, 15 mg/ml glucose, 1.23 mg/ml glucose oxidase and 0.375 mg/ml catalase). Salt (KCl) from a 10 X stock of the working concentration was added directly to the buffer. Wide field images were acquired with a constant exposure time. To measure dwell times of TPX2-Halo and TPX2-710-Halo, experiments were performed using TIRF microscopy.

2.4.7 Eg5 single molecule experiments

The concentrations of Eg5 in the extracts were measured by quantitative Western blots. For the single molecule experiments, the perfusion chambers were made from glass slides, silanized coverslips and double stick tape. 10 μL of 10% Rat YL ½ anti-tubulin antibody (Accurate Chemical, Westbury, N.Y.) was flowed into the chamber and incubated for 3 min. Then, the chamber was blocked by flowing in 5% Pluronic F127 for 3 min. Diluted Cy5 labeled microtubules (composed of a mixture of Cy5 tubulin (Cytoskeleton, Inc, Denver, CO) and unlabeled brain tubulin) were flowed into the chamber and incubated for 3 min followed by a second block of 5% pluronic F127. Eg5 was diluted to 1 or 1.5 nM in motility buffer containing PEM 50 (50 mM Pipes pH 6.9, 2 mM EGTA, 2 mM MgSO4), 0.5% F127, 5 mM ATP, 1 mM DTT, 25 μM Taxol supplemented with oxygen scavenging system (15 mg/ml glucose, 1.23 mg/ml glucose oxidase and 0.375 mg/ml catalase) and flowed into the chamber and imaged. For pre-

incubation experiments with TPX2, the indicated concentrations of TPX2 were added to the motility buffer along with Eg5 in extract and incubated on ice for 2 min before flowing into the chamber.

2.4.8 Kinesin-1 single molecule experiments

Perfusion chambers were made as described above. 10 μL of 10% Rat YL ½ anti-tubulin antibody, 5% pluronic F127, and diluted Cy5 labeled microtubules were added sequentially and incubated for 5 min each. The chamber was washed with PEM 100 plus Taxol. Kinesin-1 was diluted in PEM 100 with 10 mM DTT. This was then added to the motility buffer (PEM100, 25 μM Taxol, 0.5% F127, 0.5 mg/mL BSA, oxygen scavenging system, and 0.5 mM ATP) and flowed into the chamber and imaged. For experiments with TPX2 addition, TPX2-Halo was diluted into the motility buffer (without Kinesin-1) and flowed into the chamber during image acquisition.

2.4.9 Microtubule-microtubule gliding assays

Biotinylated, Cy5 labelled microtubules were immobilized on silanized coverslips using anti-Biotin antibody (Sigma-Aldrich). The chamber was blocked using 5% F127. Eg5-EGFP from extracts was preincubated with rhodamine labelled microtubules for 3 min and the mixture was flowed into the chamber. Finally, motility buffer was added followed by acquisition on a TIRF microscope.

2.4.10 Size Exclusion Chromatography

Eg5-EGFP was purified from SF9 insect cells as per manufacturer's instructions (Bac to Bac, Invitrogen, Grand Island, NY). The extract from LLC-Pk1 cells was prepared as mentioned before. The Superose 6 10/300 GL column (GE Healthcare, Pittsburgh, PA) was pre equilibrated with 10mM HEPES, pH7.6, 0.05% triton X100, 100mM NaCl, 1mM ATP before use. 100μL of the purified protein was loaded onto the column and run at a constant flow rate of 0.2ml/min. The Elution profile of Eg5-EGFP was directly followed by measuring absorbance at 488nm. For the size exclusion of LLC-Pk1 cell extracts, 175μL of cell extract was loaded on the column and run under identical conditions. The collected fractions were separated by SDS PAGE, transferred to a PVDF membrane and were probed for the presence of Eg5 using western blot.

2.4.11 Microtubule surface gliding assays

Perfusion chambers of approximately 10 μL volume were made using glass slides and coverslips with a double stick tape spacer. For gliding assays with the Eg5-367 monomer, the chamber was incubated with anti-His antibody and 2 mg/ml BSA for 3 min followed by two washes with motility buffer (80 mM PIPES pH 6.8, 2 mM MgCl2, 1 mM EGTA, 0.2 mg/ml BSA, and 150 mM sucrose). Then, the chamber was incubated with Eg5-367 for 3 min and washed again with motility buffer. Finally, the activation mix, consisting of motility buffer containing oxygen scavenging system, ATP, Taxol and diluted Cy5 labeled microtubules was added and imaged on a Nikon TiE microscope using epifluorescence. Surface gliding experiments with the dimeric Eg5-513 were performed exactly as described in Ma et al (2011). For TPX2 addition experiments, the

TPX2 constructs were added to the activation mix, incubated for 2 min on ice and the flowed into the chamber.

2.4.12 Microscope Imaging and Analysis

TIRF microscopy was performed using a microscope (Ti-E; Nikon Instruments, Melville, N.Y.) equipped with a 60X 1.4 NA objective lens. The system was run by Elements software (Nikon Instruments, Melville, N.Y.). Images were acquired using a 512 x 512–pixel camera (Cascade II; Photometrics, Tuscon, AZ). A 4X image expansion telescope in front of the camera was used. The micron-to-pixel ratio was 68.5 nm/px. A blue diode laser (488 nm, 50 mW) was used. Images were acquired every 2 or 3 seconds for 10 min. For two color TIRF, a 488 nm argon laser and a 647 nm diode laser were used on a custom built TIRF system on a Nikon TiE stand, run by Elements software. A 60X objective lens was used; exposure times for both red and green illumination were 50-100 ms. Wide field Imaging for Eg5-513 gliding assays, and for binding of TPX2-Halo to microtubules, was performed using epifluorescence illumination.

2.4.13 Quantification of gliding velocity, single molecule velocity and MSD

The velocity of Eg5-513- and Eg5-367-dependent microtubule gliding movement was calculated using the MTrackJ plugin in ImageJ. To calculate the velocity of Eg5-EGFP single molecules from TIRF images, ImageJ was used to generate a kymograph of moving molecules. Velocities were calculated by manually tracking individual puncta. The data were ported to excel and a polynomial 2 trendline was added to the MSD vs time plot to determine D.

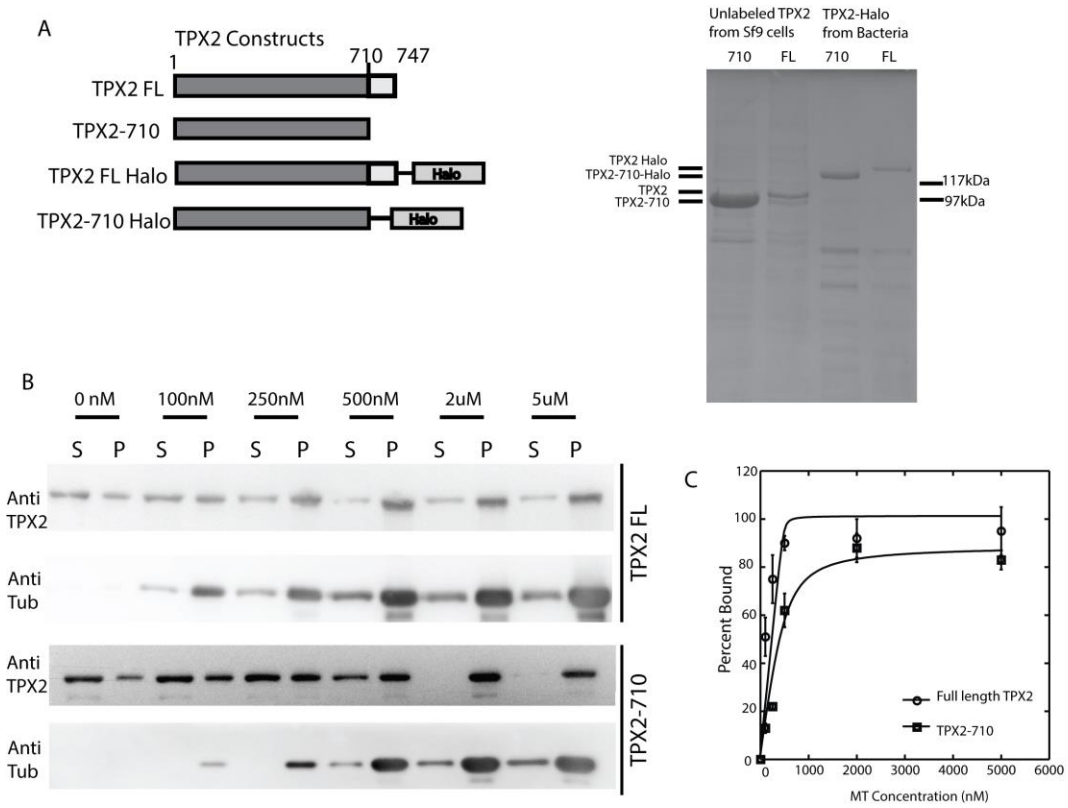

Figure 2.1 Binding of TPX2 and TPX2-710 to microtubules. (A) Schematic diagram of the TPX2 constructs (left) and Commassie Brilliant Blue stained gel of the purified proteins (right). (B) Co-sedimentation of TPX2 with microtubules; S-supernatant; P-pellet. Concentration of microtubules in each pair of lanes is noted above. Western blots stained for TPX2 or tubulin. (C) Quantification of apparent affinity was performed using a quadratic fit. Experiment was performed twice and the values averaged; Error Bars = standard deviation.

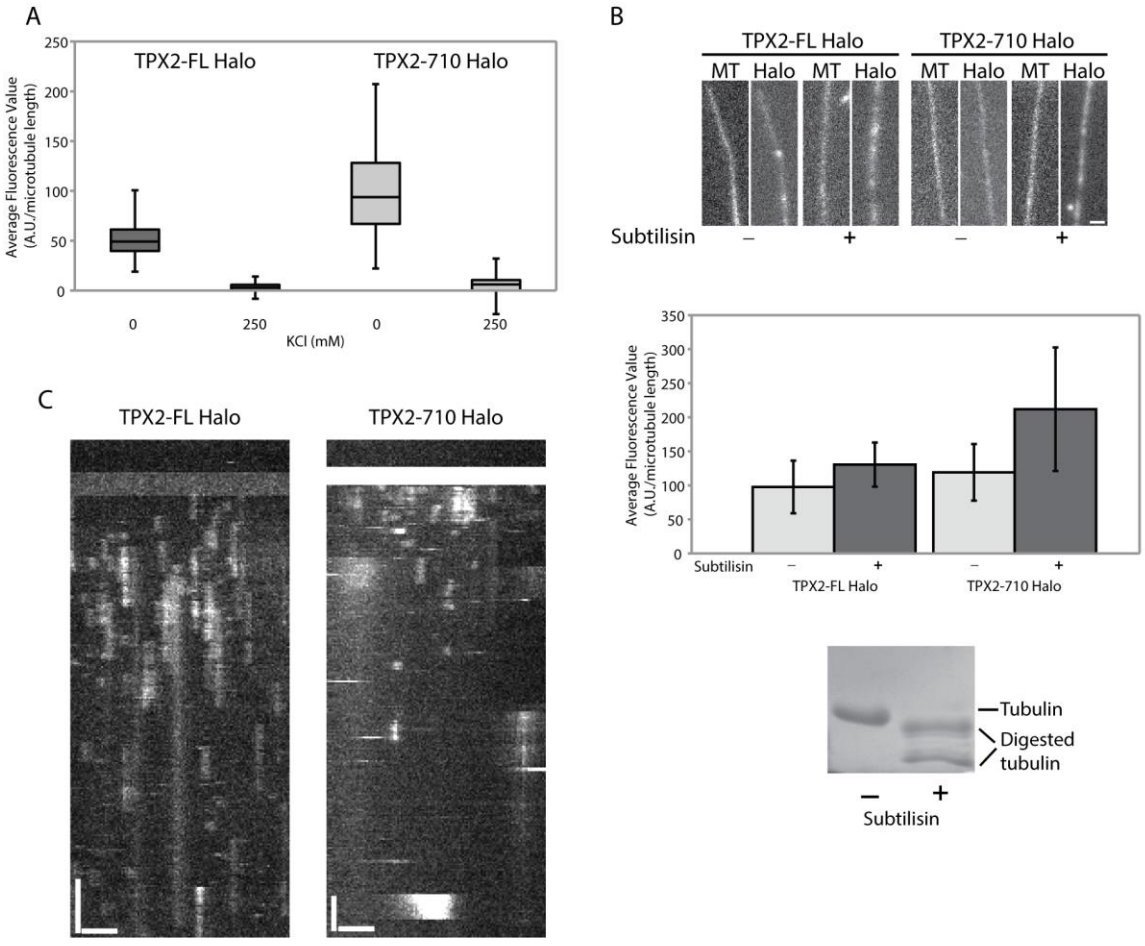

Figure 2.2 Binding Dynamics of TPX2 and TPX2-710. (A) Box plot showing release of TPX2 and TPX2-710 from microtubules in the presence of the indicated concentration of KCl added to the buffer. TPX2 fluorescence reported as AU = arbitrary units. Whiskers define the range, boxes encompass 25th to 75th quartiles, lines depict the medians. (B) TPX2 and TPX2-710 binding to untreated and Subtilisin A digested microtubules; (upper panels) fluorescence images of TPX2-Halo or TPX2-710-Halo bound to untreated and Subtilisin A digested microtubules; (middle) quantification of TPX2 fluorescence; (lower) polyacrylamide gel showing digested and control microtubules. TPX2 fluorescence measured for at least 60 microtubules for each of two independent experiments; error bars = SD. (C) Kymograph of TPX2-Halo and TPX2-710-Halo on microtubules. Vertical scale (time) is 60 s; horizontal scale bar is 2 μm.

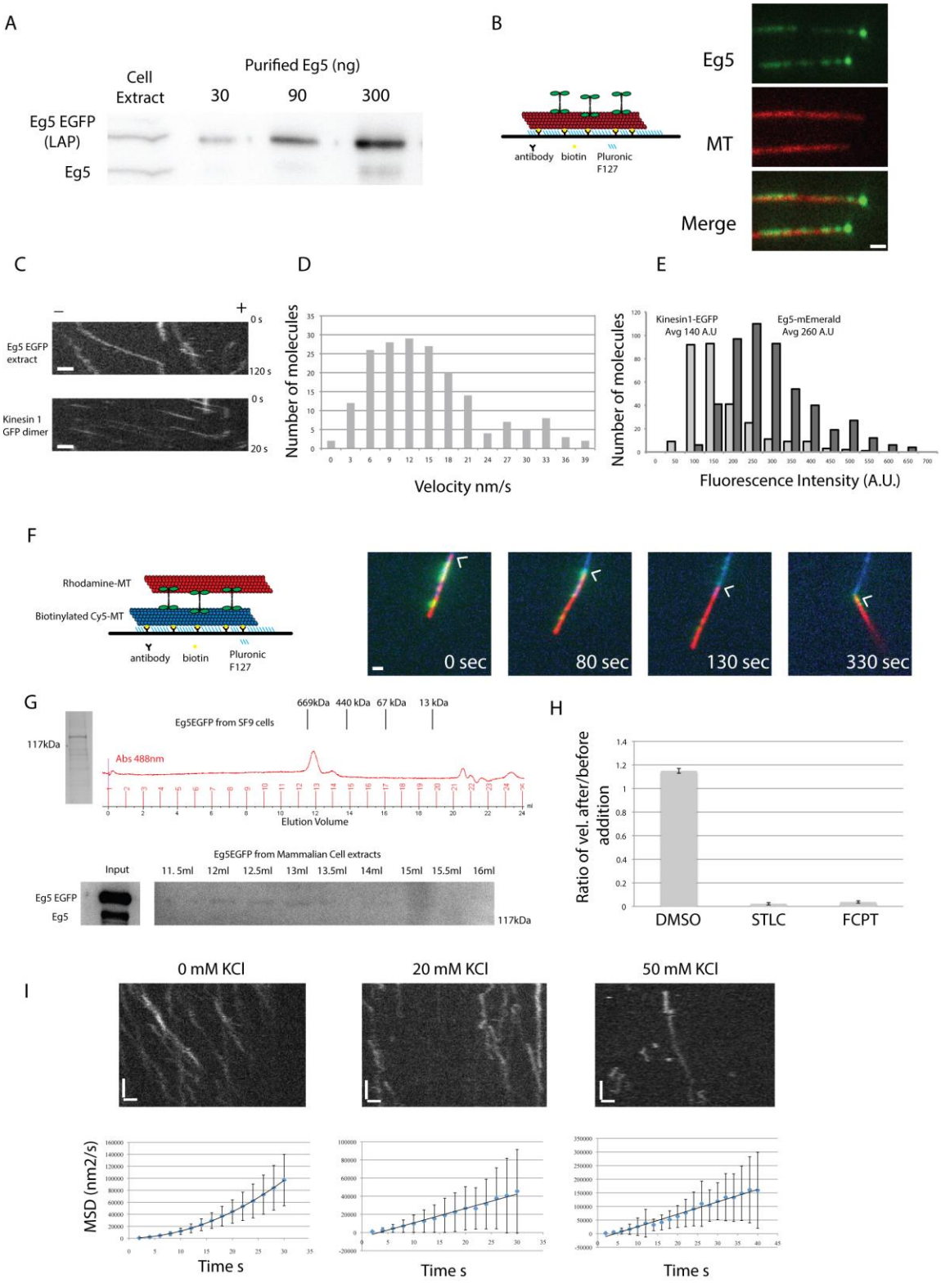
A
Purified Eg5 (ng)
Cell Extract
30
90
300
Eg5 EGFP (LAP)
Eg5
B
antibody
biotin
Pluronic F127
Eg5
MT
Merge
C
Eg5 EGFP extract
0 s
120 s
Kinesin 1 GFP dimer
0 s
20 s
D
Number of molecules
Velocity nm/s
E
Kinesin1-EGFP Avg 140 A.U
Eg5-mEmerald Avg 260 A.U
Number of molecules
Fluorescence Intensity (A.U.)
F
Rhodamine-MT
Biotinylated Cy5-MT
antibody
biotin
Pluronic F127
0 sec
80 sec
130 sec
330 sec
G
669kDa
440 kDa
67 kDa
13 kDa
Eg5EGFP from SF9 cells
117kDa
Abs 488nm
Elution Volume
Eg5EGFP from Mammalian Cell extracts
Input
11. 5ml
12ml
12.5ml
13ml
13.5ml
14ml
15ml
15.5ml
16ml
Eg5 EGFP
Eg5
117kDa
H
Ratio of vel. after/before addition
DMSO
STLC
FCPT
I
0 mM KCl
20 mM KCl
50 mM KCl
MSD (nm2/s)
Time s
Time s
Time s

Figure 2.3 Characterization of Eg5 in mammalian cell extracts. (A) Western blot of cell extract and purified Eg5. (B) Schematic diagram of the single molecule TIRF experiments (left) and TIRF images of Eg5-EGFP accumulating at the microtubule plus-end (right). (C) Kymographs of Kinesin-1 EGFP dimers and Eg5-EGFP from extracts on the same microtubule. Note the different time scale. Plus and minus ends of the microtubules are indicated. (D) Histogram of Eg5-EGFP motor velocity. (E) Histogram of the fluorescence of Kinesin-1 dimers (light gray) and Eg5 molecules (dark gray) in the extract. (F) Schematic diagram (left) and fluorescence images (right) showing microtubule-microtubule sliding by Eg5. Arrowhead marks the end of the sliding microtubule. (G) Coomassie Brilliant Blue stained gel of Eg5-EGFP purified from insect cells and the trace of absorbance at 488nm on the size exclusion column for the purified protein. The western blot shown is for the fractions obtained from size exclusion chromatography of Eg5-mEmerald from LLC-Pk1 extract probed for Eg5. (H) Quantification of the velocity of Eg5-EGFP after addition of DMSO, STLC or FCPT (right). Error bars = SEM. (I) Directional and diffusive motility of Eg5-EGFP in the presence of 0, 20 or 50 mM KCl added to the motility buffer. Kymographs (upper) and mean squared displacement (lower). Horizontal scale bar in B, C, F, I is 1 μm; vertical scale bar in I is 60 s. Vertical scale in C is provided on the image.

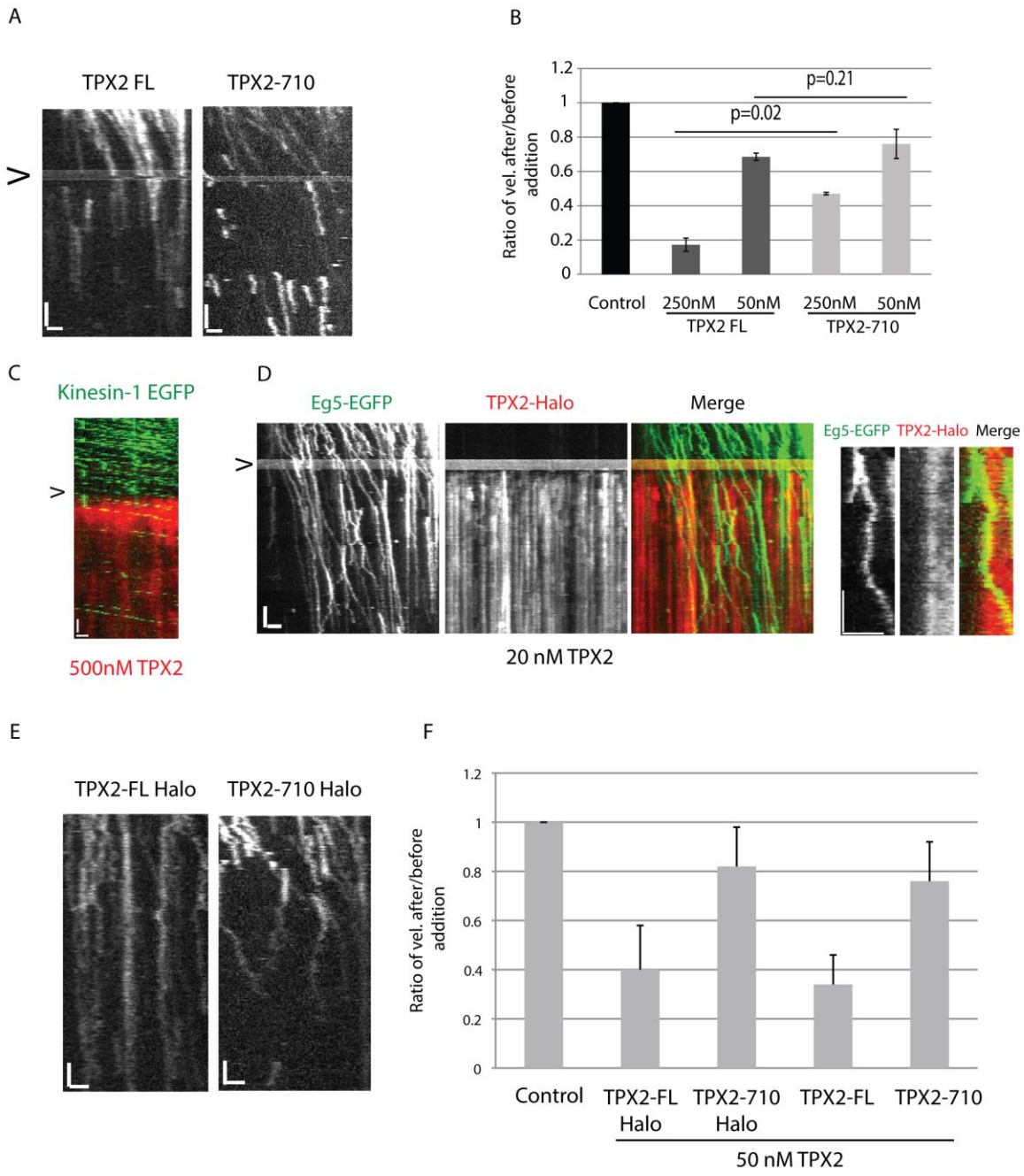

Figure 2.4 Inhibition of Eg5 by TPX2 requires both binding to the microtubule and an interaction between TPX2 and Eg5. (A) Kymographs of Eg5-EGFP before and following addition of TPX2 or TPX2-710; arrowhead marks time of TPX2 addition. (B) Quantification of Eg5-EGFP velocity; error bars = SD. (C) Kymograph of Kinesin-1 EGFP dimers walking on microtubules before and after addition of TPX2 (arrowhead). 1 nM Kinesin-1 EGFP (green) and 500 nM TPX2-Halo (red) were used. (D) Kymographs of Eg5-EGFP (green) before and following addition of 20 nM TPX2-Halo (red). Right panels show enlarged view. (E) Kymographs of Eg5-EGFP that was pre-mixed with TPX2-Halo or TPX2-710-Halo. (F) Quantification of Eg5-EGFP velocity in the presence

of 50 nM TPX2 that was Halo tagged (left) or untagged (right). Error bars = SEM. Horizontal scale bars in A, C, E are 1 μm; horizontal scale bar in D is 2 μm; vertical scale bar in A,D,E is 60 s and is 5 s in C.

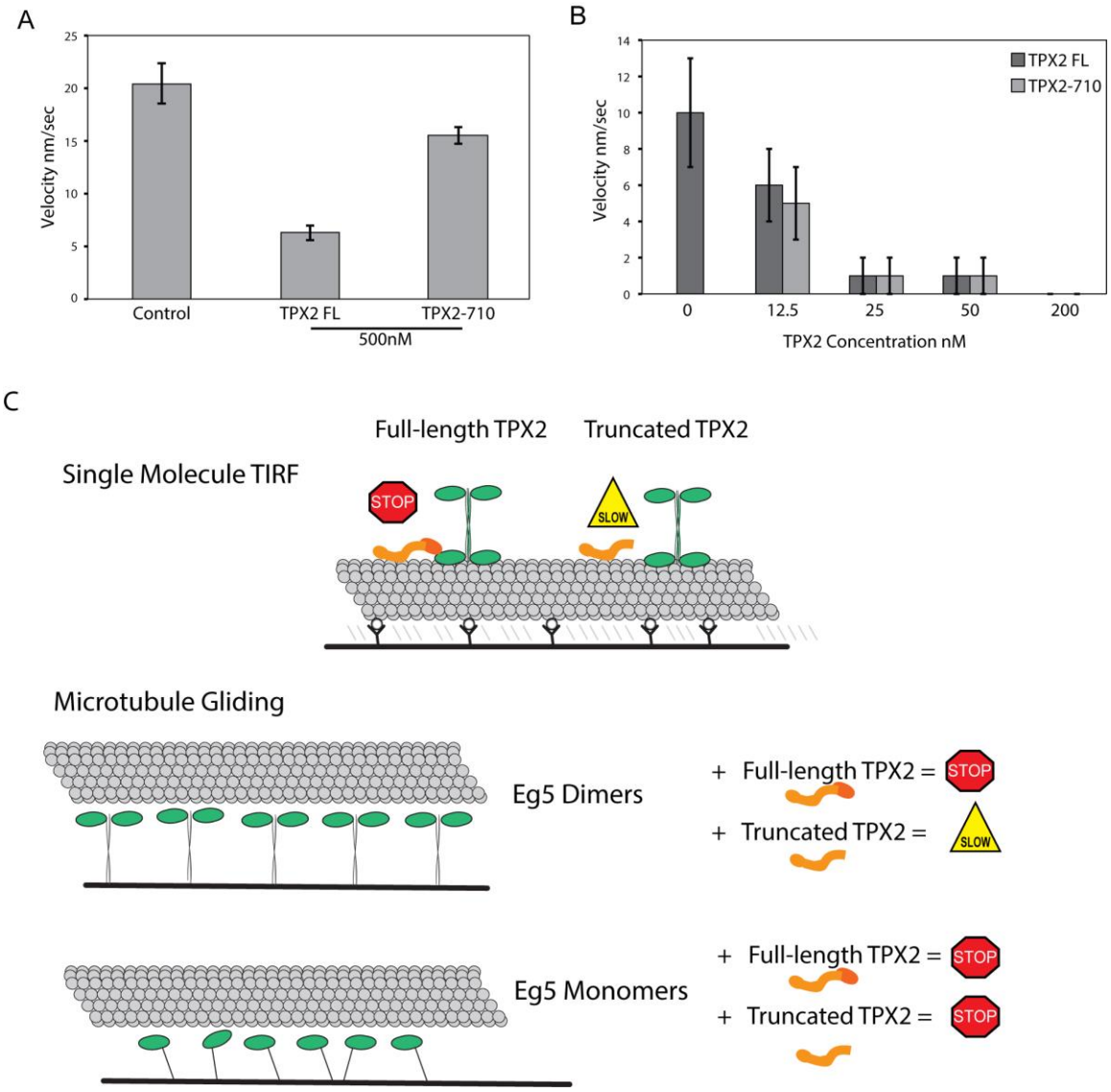

Figure 2.5 Differential regulation of Eg5 dimers, but not monomers, by full length and truncated TPX2. Velocity of microtubule gliding driven by (A) Eg5 dimers or (B) Eg5 monomers. Error bars show SEM. (C). Model for inhibition of Eg5 by TPX2. Top shows inhibition of motor stepping by full length (left, stop symbol) and truncated TPX2 (right, slow symbol) in single molecule assays. Lower panels show inhibition of microtubule gliding by Eg5 dimers (top) and Eg5 monomers (bottom). Eg5 - green; TPX2 - orange.

2.5 References

Barlan, K., W. Lu, and V.I. Gelfand. 2013. The microtubule-binding protein ensconsin is an essential cofactor of kinesin-1. *Curr. Biol.* 23:317-322.

Bayliss, R., T. Sardon, I. Vernos, and E. Conti. 2003. Structural basis of Aurora A activation by TPX2 at the mitotic spindle. *Mol. Cell*. 12:851-862.

Brouhard, G.J., J.H. Stear, T.L. Noetzel, J. Al-Bassam, K. Kinoshita, S.C. Harrison, J. Howard, and A.A. Hyman. 2008. XMAP215 is a processive microtubule polymerase. *Cell*. 132:79-88.

Cai, D., D.P. McEwen, J.R. Martens, E. Meyhofer, and K.J. Verhey. 2009. Single molecule imaging reveals differences in microtubule track selection between kinesin motors. *PLOS Bio*. 7:e1000216.

Cai, D., K.J. Verhey, and E. Meyhofer. 2007. Tracking single kinesin molecules in the cytoplasm of mammalian cells. *Biophysical journal*. 92:4137-4144.

Cheeseman, I.M., and A. Desai. 2005. A combined approach for the localization and tandem affinity purification of protein complexes from metazoans. *Sci. STKE*:p11.

Day, R.N., and M.W. Davidson. 2009. The fluorescent protein palette: tools for cellular imaging. *Chem Soc Rev*. 38:2887-2921.

Dixit, R., J.L. Ross, Y.E. Goldman, and E.L. Holzbaur. 2008. Differential regulation of dynein and kinesin motor proteins by Tau. *Science (New York, N.Y.)*. 319:1086-1089.

Drechsler, H., T. McHugh, M.R. Singleton, N.J. Carter, and A.D. McAinsh. 2014. The Kinesin-12 Kif15 is a processive track-switching tetramer. *eLife*. 3:e01724.

Eckerdt, F., P.A. Eyers, A.L. Lewellyn, C. Prigent, and J.L. Maller. 2008. Spindle pole regulation by a discrete Eg5-interacting domain in TPX2. *Current biology : CB*. 18:519-525.

Eyers, P.A., and J.L. Maller. 2004. Regulation of Xenopus Aurora A activation by TPX2. *J. Biol. Chem.* 279:9008-9015.

Gable, A., M. Qiu, J. Titus, S. Balchand, N.P. Ferenz, N. Ma, E.S. Collins, C. Fagerstrom, J.L. Ross, G. Yang, and P. Wadsworth. 2012. Dynamic reorganization of Eg5 in the mammalian spindle throughout mitosis requires dynein and TPX2. *Molecular biology of the cell*. 23:1254-1266.

Garrett, S., K. Auer, D.A. Compton, and T. Kapoor. 2002. hTPX2 is required for normal spindle morphology and centrosome integrity during vertebrate cell division. *Curr. Biol.* 12:2055-2059.

Gerson-Gurwitz, A., C. Thiede, N. Movshovich, V. Fridman, M. Podolskaya, T. Danieli, S. Lakamper, D.R. Klopfenstein, C.F. Schmidt, and L. Gheber. 2011. Directionality of individual kinesin-5 Cin8 motors is modulated by loop 8, ionic strength and microtubule geometry. *The EMBO journal*. 30:4942-4954.

Groen, A.C., D. Needleman, C. Brangwynne, C. Gradinaru, B. Fowler, R. Mazitschek, and T.J. Mitchison. 2008. A novel small-molecule inhibitor reveals a possible role of kinesin-5 in anastral spindle-pole assembly. *J. Cell Sci.* 121:2293-2300.

Gruss, O.J., M. Wittmann, H. Yokoyama, R. Pepperkok, T. Kufer, H. Sillje, E. Karsenti, I.W. Mattaj, and I. Vernos. 2002. Chromosome-induced microtubule assembly mediated by TPX2 is required for spindle formation in HeLa cells. *Nature cell biology*. 4:871-879.

Helenius, J., G.J. Brouhard, Y. Kalaidzidis, S. Diez, and J. Howard. 2006. The depolymerizing kinesin MCAK uses lattice diffusion to rapidly target microtubule ends. *Nature*. 441:115-119.

Hinrichs, M.H., A. Jalal, B. Brenner, E. Mandelkow, S. Kumar, and T. Scholz. 2012. Tau protein diffuses along the microtubule lattice. *J. Biol. Chem.* 287:38559-38568.

Hyman, A., D. Drechsel, D. Kellogg, S. Salser, K. Sawin, L. Wordeman, and T. Mitchison. 1991. Preparation of modified tubulins. *Meth. Enzymol.* 196:478-485.

Illenberger, S., G. Drewes, B. Trinczek, J. Biernat, H.E. Meyer, J.B. Olmsted, E.-M. Mandelkow, and E. Mandelkow. 1996. Phosphorylation of microtubule-associated proteins MAP2 and MAP4 by the protein kinase p110mark. *J. Biol. Chem.* 271:10834-10843.

Kapitein, L.C., B.H. Kwok, J.S. Weinger, C.F. Schmidt, T.M. Kapoor, and E.J. Peterman. 2008. Microtubule cross-linking triggers the directional motility of kinesin-5. *The Journal of cell biology*. 182:421-428.

Kapitein, L.C., E.J. Peterman, B.H. Kwok, J.H. Kim, T.M. Kapoor, and C.F. Schmidt. 2005. The bipolar mitotic kinesin Eg5 moves on both microtubules that it crosslinks. *Nature*. 435:114-118.

Korneev, M.J., S. Lakamper, and C.F. Schmidt. 2007. Load-dependent release limits the processive stepping fo the tetrameric Eg5 motor. *Eur. Biophys. J.* 36:675-681.

Kufer, T.A., H.H.W. Sillje, R. Korner, O.J. Gruss, P. Meraldi, and E.A. Nigg. 2002. Human TPX2 is required for targeting Aurora-A kinase to the spindle. *J. Cell Bio.* 158:617-623.

Kwok, B.H., L.C. Kapitein, J.H. Kim, E.J. Peterman, C.F. Schmidt, and T.M. Kapoor. 2006. Allosteric inhibition of kinesin-5 modulates its processive directional motility. *Nature chemical biology*. 2:480-485.

Larson, A.G., N. Naber, R. Cooke, E. Pate, and S.E. Rice. 2010. The conserved L5 loop establishes the pre-powerstroke conformation of the kinesin-5 motor, Eg5. *Biophysical journal*. 98:2619-2627.

Lowry, O.H., N.J. Rosenbrough, A.L. Farr, and R.J. Randall. 1951. Protein measurement with the Folin phenol reagent. *J. Biol. Chem.* 193:265-275.

Ma, N., J. Titus, A. Gable, J.L. Ross, and P. Wadsworth. 2011. TPX2 regulates the localization and activity of Eg5 in the mammalian mitotic spindle. *The Journal of cell biology*. 195:87-98.

Ma, N., S. Tulu, N. Ferenz, C. Fagerstrom, A. Wilde, and P. Wadsworth. 2010. Poleward Transport of TPX2 in mammalian spindles requires Eg5, dynein and microtubule flux. *Mol. Bio. Cell*. 21:979-988.

Markus, S.M., K.A. Kalutkiewicz, and W.-L. Lee. 2012. She1-mediated inhibition of dynein motility along astral microtubules promotes polarized spindle movements. *Current biology : CB*. 22:1-10.

Paschal, B.M., R.A. Obar, and R.B. Vallee. 1989. Interaction of brain cytoplasmic dynein and MAP2 with a common sequence at the C terminus of tubulin. *Nature*. 342:569-572.

Petry, S., A.C. Groen, K. Ishihara, T.J. Mitchison, and R.D. Vale. 2013. Branching microtubule nucleation in Xenopus egg extracts mediated by augmin and TPX2. *Cell*. 152:768-777.

Roostalu, J., C. Hentrich, P. Bieling, I.A. Telley, E. Schiebel, and T. Surrey. 2011. Directional switching of the kinesin Cin8 through motor coupling. *Science (New York, N.Y.)*. 332:94-99.

Skoufias, D.A., S. DeBonis, Y. Saoudi, L. Lebeau, I. Crevel, R. Cross, R.H. Wade, D. Hackney, and F. Kozielski. 2006. S-trityl-L-cysteine is a reversible, tight binding inhibitor of the human kinesin Eg5 that specifically blocks mitotic progression. *J. Biol. Chem.* 281:17559-17569.

Sung, H.-H., I.A. Telley, P. Papadaki, A. Ephrussi, T. Surrey, and P. Rorth. 2008. Drosophila Ensconsin promotes productive recruitment of kinesin-1 to microtubules. *Devel. Cell*. 15:866-876.

Thorn, K.S., J.A. Ubersax, and R.D. Vale. 2000. Engineering the processive run length of the kinesin motor. *The Journal of cell biology*. 151:1093-1100.

Tulu, U.S., C. Fagerstrom, N.P. Ferenz, and P. Wadsworth. 2006. Molecular requirements for kinetochore-associated microtubule formation in mammalian cells. *Curr. Biol.* 16:536-541.

Valentine, M.T., P.M. Fordyce, T.C. Krzysiak, S.P. Gilbert, and S.M. Block. 2006. Individual dimers of the mitotic kinesin motor Eg5 step processively and support substantial loads in vitro. *Nature cell biology*. 8:470-476.

van den Wildenberg, S.M., L. Tao, L.C. Kapitein, C.F. Schmidt, J.M. Scholey, and E.J. Peterman. 2008. The homotetrameric kinesin-5 KLP61F preferentially crosslinks microtubules into antiparallel orientations. *Current biology : CB*. 18:1860-1864.

Walczak, C.E., and R. Heald. 2008. Mechanisms of mitotic spindle assembly and function. *Int. Rev. Cytol.* 265:111-158.

Wang, Z., and M.P. Sheetz. 2000. The C-terminus of tubulin increases cytoplasmic dynein and kinesin processivity. *Biophys. J.* 78:1955-1964.

Weinger, J.S., M. Qiu, G. Yang, and T.M. Kapoor. 2011. A nonmotor microtubule binding site in kinesin-5 is required for filament crosslinking and sliding. *Current biology : CB*. 21:154-160.

Welburn, J.P.I., and I.M. Cheeseman. 2012. The microtubule-binding protein Cep170 promotes the targeting of the kinesin-13 depolymerase Kif2b to the mitotic spindle. *Molecular biology of the cell*. 23:4786-4796.

Wittmann, T., H. Boleti, C. Antony, E. Karsenti, and I. Vernos. 1998. Localization of the kinesin-like protein Xklp2 to spindle poles requires a leucine zipper, a microtubule-associated protein, and dynein. *The Journal of cell biology*. 143:673-685.

Wittmann, T., M. Wilm, E. Karsenti, and I. Vernos. 2000. TPX2, a novel Xenopus MAP involved in spindle pole organization. *J. Cell Biol.* 149:1405-1418.

CHAPTER 3

REGULATION OF KIF15 LOCALIZATION AND MOTILITY BY THE C-TERMINUS OF TPX2 AND MICROTUBULE DYNAMICS

This chapter is adapted from Mann et al. 2017 and was completed with the guidance of Patricia Wadsworth and in collaboration with Sai K. Balchand. PW generated the GFP-Kif15 LLC-Pk1 cell line used for live cell experiments and extracts for single-molecule TIRF microscopy. Live cell imaging and analysis were performed in collaboration with SKB and PW.

3.1 Introduction

During mitosis, microtubules are nucleated and organized into a dynamic structure called the mitotic spindle, which mediates chromosome segregation into two daughter cells. In mammalian cells, microtubule nucleation at centrosomes, near chromatin and from pre-existing microtubules all contribute to spindle formation (Meunier and Vernos, 2016). Microtubule formation near chromatin and at kinetochores is regulated by nuclear localization sequence containing spindle assembly factors that are inactive when bound to importins α/β (Gruss and Vernos, 2004). The small GTPase Ran, which is locally activated near chromatin (Kalab et al., 2006), binds to importin β and relieves this inhibitory effect, thus promoting microtubule formation. A well-studied Ran-regulated spindle assembly factor is TPX2, which stimulates microtubule formation

at kinetochores and in the chromatin region and is required for spindle assembly and completion of mitosis (O'Connell et al., 2009; Tulu et al., 2006).

During spindle formation the duplicated centrosomes separate to establish spindle bipolarity. Centrosome separation is driven by the Kinesin-5, Eg5, a bipolar, tetrameric motor which crosslinks and slides antiparallel microtubules (Ferenz et al., 2010; Kapitein et al., 2005). More recently it has been shown that following bipolar spindle formation the action of Eg5 is dispensable and spindle bipolarity is maintained by a Kinesin-12, Kif15 (Tanenbaum et al., 2009; Vanneste et al., 2009). Spindles in cells depleted of Kif15 are shorter than spindles in control cells, consistent with a model in which Kif15, like Eg5, generates outward force in the spindle (Sturgill and Ohi, 2013). However, in contrast to Eg5, Kif15 preferentially associates with kinetochore fiber microtubules. Cells overexpressing Kif15 can form a bipolar spindle in the absence of Eg5 activity (Raaijmakers et al., 2012; Sturgill and Ohi, 2013; Tanenbaum et al., 2009). The existence of two mitotic motors that can each power bipolar spindle formation may contribute to the lack of efficacy of Eg5 inhibitors in clinical trials and understanding how these motors are regulated may therefore be of clinical significance (Waitzman and Rice, 2014).

Localization of Kinesin-12 and Kinesin-5 motors to spindle microtubules requires TPX2 (Ma et al., 2011; Tanenbaum et al., 2009; Vanneste et al., 2009). In fact, TPX2 was initially discovered as a factor required for the dynein-dependent targeting of the *Xenopus* Kinesin-12, Xklp2 to spindle poles (Wittmann et al., 1998). The C-terminal 37 amino acids of TPX2 are required to target Eg5 to the spindle; targeting of Kif15 requires the C-terminal leucine zipper of the motor (Wittmann et al., 1998). The C-terminal half

of TPX2 is required to localize Kif15 to the spindle (Brunet et al., 2004) but if a specific domain of the protein is necessary is not yet known.

These initial studies on TPX2 and Kif15 were consistent with the idea that dimers of Kif15 walked along one microtubule while tethered to a second microtubule via TPX2, thus generating force for spindle formation (Vanneste et al., 2009). Subsequently, Sturgill *et al.* provided biochemical data showing that the motor was an autoinhibited dimer and identified a second, non-motor microtubule binding site in the coil 1 region of Kif15 (Sturgill et al., 2014). These data led to a model in which autoinhibited Kif15 dimers were first unmasked and then bound to microtubule bundles via motor and non-motor binding sites (Sturgill et al., 2014). More recent work, however, has shown that Kif15 exists as a tetramer which displays processive motility along individual microtubules *in vitro* (Drechsler et al., 2014; Dreschler and McAinsh, 2016). Thus, the oligomeric state of Kif15, and how it contributes to mitotic spindle formation remain unresolved. Finally, experiments using dynamic microtubules *in vitro* show that Kif15 accumulates at microtubule plus-ends and suppresses catastrophe events, can crosslink microtubules and move them relative to one another, promoting the formation of parallel microtubule arrays (Dreschler and McAinsh, 2016). Thus, both Eg5 and Kif15 contribute to spindle bipolarity and are regulated by TPX2, but their mechanism of action is distinct.

To gain insight into the cellular function and regulation of the Kinesin-12, Kif15, we investigated the behavior of the motor and its regulation by TPX2 *in vitro* and *in vivo*. Our data show that Kif15 motors, present in diluted mammalian cell extracts, are processive, track-switching tetramers and that the C-terminal region of TPX2 is required to inhibit Kif15 motor stepping. Using a knockdown rescue approach in mammalian

cells, we further demonstrate that the C-terminal region of TPX2 contributes to targeting the motor to the mitotic spindle and that Eg5-independent bipolar spindle formation by overexpressed Kif15 requires the TPX2 C-terminal region. In live cells, GFP-Kif15 displays robust, plus-end directed motility at a rate similar to that of microtubule growth, and this behavior is suppressed by Paclitaxel. Together these results document the behavior of Kif15 in cells and demonstrate the importance of TPX2 and its C-terminal region for motor localization and activity.

3.2 Results

3.2.1 TPX2 C-terminus is required for Kif15 targeting to spindle microtubules

The C-terminal 37 amino acids of TPX2 contribute to the targeting of the Kinesin-5, Eg5, to spindle microtubules (Ma et al., 2011), but if this domain contributes to the targeting of the Kinesin-12, Kif15, to the spindle is not known (Brunet et al., 2004; Tanenbaum et al., 2009; Vanneste et al., 2009; Wittmann et al., 1998). To address this, we first examined the distribution of endogenous Kif15 in LLC-Pk1 cells expressing full-length TPX2 or TPX2-710, which lacks the C-terminal 37 amino acids, from bacterial artificial chromosomes (BAC), and depleted of the endogenous protein using siRNA (Ma et al., 2011). Cells were fixed and stained for microtubules and Kif15 at 40 hours following nucleofection with TPX2 siRNA, a time when the majority of TPX2 is depleted (Fig. 3.5A) (Ma et al., 2011). Kif15 was present along spindle microtubules in parental LLC-Pk1 cells, but not in parental cells depleted of TPX2 (Fig. 3.1A). In LLC-Pk1 cells expressing full-length TPX2 or TPX2-710 from a BAC, and depleted of endogenous TPX2, Kif15 was detected on spindle microtubules when full-length TPX2

was present and was reduced when TPX2-710 was expressed (Fig. 3.1A). Quantification of the ratio of Kif15 to microtubules at the spindle pole and in the spindle, midway between the chromosomes and pole, shows a statistically significant reduction at both locations in cells expressing TPX2-710, as compared with cells expressing full-length TPX2 (Fig. 3.1C). As previously reported (Ma et al., 2011), expression of TPX2-710 in cells depleted of TPX2 resulted in aberrant spindle morphology (Fig. 3.1B). These results demonstrate that for both Eg5 and Kif15, the C-terminal domain of TPX2 contributes to spindle targeting.

3.2.2 Full-length TPX2 inhibits Kif15 motor velocity

Next, we wished to determine if the C-terminal domain of TPX2 was required to regulate Kif15 motor stepping *in vitro*. To do this, we transfected LLC-Pk1 cells with full-length Kif15 tagged with EGFP (hereafter GFP-Kif15) (Vanneste et al., 2009) and used these cells to prepare cytoplasmic extracts for use in single molecule total internal reflection fluorescence (TIRF) microscopy experiments (Fig. 3.2A) (Balchand et al., 2015; Cai et al., 2007). Rhodamine-labeled, Paclitaxel stabilized microtubules were attached to the surface of a microscope flow chamber and cell extract, diluted in motility buffer, was added (Methods). Fluorescent puncta were observed to bind to microtubules and processively move upon addition of ATP (Fig. 3.2B, C, G). Notably, nearly every GFP-Kif15 puncta that bound a microtubule was motile, demonstrating that Kif15 from mammalian cells is not autoinhibited (Sturgill et al., 2014), but displays robust motility. TPX2 is undetectable in these cytoplasmic extracts because they are prepared from

asynchronous cells, >95% of which are in interphase, a time when TPX2 is located in the nucleus (Balchand et al., 2015).

GFP-Kif15 was observed to move predominantly in a plus-end directed manner (86% of events) with a smaller percentage of events toward the minus-end (see Methods) (14% of events) (Drechsler et al., 2014) (Fig. 3.2B). The average velocity of plus-end directed motion was 128.7 nm/sec while the velocity of minus-end directed motion was slower, 86.6 nm/sec. Motility was processive with average run lengths of 1.9 and 0.9 microns in the plus- and minus-end directions, respectively (Fig. 3.2B). In addition to directional reversals, Kif15 motors moving on one microtubule could switch to a neighboring microtubule and continue processive motility (Fig. 3.2C). In extracts prepared from LLC-Pk1 cells arrested in mitosis with a low concentration of nocodazole (Methods), motor velocity (151 nm/sec, n = 54, 53 plus- and 1 minus-end directed) was not different from that measured in interphase, with the caveat that TPX2 is present in these extracts. Interestingly, minus-end directed motility was reduced in the mitotic compared with interphase extract. This data suggests that in *in vitro* assays motor microtubule affinity is sufficiently strong to overcome any potential mitotic regulation (vanHeesbeen et al., 2016). This possibility is consistent with the observation that Eg5 prepared from interphase extracts, and thus lacking the mitosis specific phosphorylation that is required for spindle microtubule binding (Blangy et al., 1995) shows robust motility *in vitro* (Balchand et al., 2015).

Kif15 has been previously reported to exist as a tetramer or dimer using purified motors (Drechsler et al., 2014; Sturgill et al., 2014), or motors in mammalian cell extracts (Dreschler and McAinsh, 2016; Sturgill et al., 2016). Understanding the quaternary

structure of the molecule is significant because tetramers can potentially interact with more than one microtubule simultaneously, and because formation of tetramers could potentially alter the availability of a second microtubule binding site in the motor tail (Sturgill et al., 2014). To determine the oligomeric state of GFP-Kif15 in our experiments, we acquired images of purified Kinesin-1-GFP, which is known to be a dimer, and GFP-Kif15 using identical imaging conditions and using only motors that bound to microtubules. For this experiment, endogenous Kif15 was depleted from the cells prior to preparation of the extract, so that the motors would be composed predominantly of the expressed GFP-tagged protein (Fig. 3.5B). As shown in the histogram in Fig. 3.2D, bottom), Kif15 puncta showed a range of fluorescence intensities with an average intensity that was 1.6X the average fluorescence intensity of Kinesin-1-GFP (Fig. 3.2D, top) (average fluorescence of 220.5 and 141.0 A.U.). The reason that the average value was not twice the intensity of Kinesin-1-GFP may result from incomplete depletion of endogenous Kif15 by siRNA (Fig. 3.5B), resulting in a mixture of motors containing two, three or four GFP-tagged motors. Additionally, some motors may dissociate into dimers during preparation (Drechsler et al., 2014; Sturgill et al., 2014; Sturgill et al., 2016). We also imaged GFP-Kif15 in the absence of ATP and counted bleach steps. We observed at least three discreet bleach events for approximately half of the particles (Fig. 3.2E) consistent with at least some of the GFP-Kif15 existing as a tetramer under these conditions. To determine if Kif15 exists as a tetramer in mitosis, mitotic extract was added to microtubules in chambers without ATP and the number of bleach steps counted. In this experiment, we observed particles with greater than three

bleach steps for more than half of the particles (Fig. 3.2E) demonstrating that in both interphase and mitotic extracts some of the Kif15 motors exist as tetramers.

In summary, these data show that GFP-Kif15, prepared from mammalian cells, moves rapidly and processively toward microtubule plus-ends and can both switch microtubule tracks and reverse direction. The motile parameters of Kif15 prepared from mammalian cells are strikingly similar to motors prepared from Sf9 cells and indicate that the native state of Kif15 in interphase and mitotic mammalian cells is likely a tetramer (Drechsler et al., 2014) that can dissociate into dimers depending on the experimental conditions (Drechsler et al., 2014; Dreschler and McAinsh, 2016; Sturgill et al., 2014; Sturgill et al., 2016).

To identify the region, or regions, of TPX2 that regulate Kif15 motility *in vitro*, TPX2 was incubated with diluted extract containing GFP-Kif15, and then introduced into the motility chamber. When full-length TPX2 was present in the reaction, motor velocity was reduced to ~65% of controls (Fig. 3.2F and G). Next, we added TPX2-710 which binds microtubules (Balchand et al., 2015) and contributes to motor targeting (Figure 1) to determine if it also regulates motility *in vitro*. Incubation of TPX2-710 with GFP-Kif15 prior to addition to the motility chamber did not result in a statistically significant reduction in motor velocity (Fig. 3.2F and G) demonstrating that full-length TPX2 is required for motor inhibition. Two additional constructs, one lacking a larger C-terminal region (TPX2-657) and one containing a deletion of a conserved PFAM domain near the C-terminus (TPX2□ΔPFAM) (Fig. 3.5C) also failed to inhibit Kif15 (Fig. 3.2F and G). The lack of inhibition with the ΔPFAM construct, which is missing only part of the region deleted in TPX2-710, indicates that these nine amino acids may play a role in

motor inhibition. Both TPX2-657 and TPX2□ΔPFAM bound microtubules following expression in mammalian cells that were depleted of endogenous TPX2 (Fig. 3.5D) demonstrating that failure to inhibit Kif15 did not result from failure of these proteins to bind microtubules. In summary, these experiments show that full-length TPX2 is required to inhibit Kif15 motor stepping *in vitro*.

3.2.3 TPX2 is required for bipolar spindle formation in cells overexpressing Kif15

Previous work has shown that bipolar spindle formation can proceed in cells lacking Eg5 activity and overexpressing Kif15, demonstrating that Kif15 can generate force for spindle formation *in vivo* (Sturgill and Ohi, 2013; Tanenbaum et al., 2009). To understand how TPX2 contributes to Kif15-dependent spindle formation *in vivo*, we examined spindle formation in LLC-Pk1 cells overexpressing GFP-Kif15. In these cells, the distribution of GFP-Kif15 on spindle microtubules was similar to the distribution of Kif15 in the parental cells, showing a punctate staining pattern with enrichment along kinetochore fiber microtubules and near spindle poles (Fig. 3.3A). This distribution is equivalent to that observed in *Xenopus* cultured cell spindles (Wittmann et al., 2000) and similar to the distribution in other cultured mammalian cells (Sturgill and Ohi, 2013; Tanenbaum et al., 2009; Vanneste et al., 2009). Western blots of an extract of GFP-Kif15 cells show that GFP-Kif15 is present at approximately 10X the level of endogenous Kif15 in the parental cells (Methods) (Fig. 3.3B).

First, we asked if TPX2 is required for Kif15 localization in the overexpressing cells. Treatment with siRNA targeting TPX2 resulted in a dramatic reduction in GFP-Kif15 on spindle microtubules and an ensuing increase in the level of cytoplasmic

fluorescence (Fig. 3.3C). In some cells, residual GFP-Kif15 was detected near spindle poles (Fig. 3.3C). These results demonstrate that TPX2 contributes to the localization of GFP-Kif15 to spindle microtubules, even when high levels of the motor are present.

In control cells, Kif15 is enriched on kinetochore fiber microtubules (Sturgill and Ohi, 2013) and when overexpressed Kif15 binds and stabilizes non-kinetochore microtubules as well, where it is thought to play a key role in Eg5-independent spindle formation (Sturgill and Ohi, 2013). We asked if kinetochore fiber microtubules are needed for Kif15 localization in LLC-Pk1 GFP-Kif15 cells. In cells depleted of Nuf2, a treatment that prevents kinetochore fiber formation (Fig. 3.6), GFP-Kif15 remained associated with the spindle (Fig. 3.3C, left) despite the loss of kinetochore fibers and concomitant failure of chromosome congression (Fig. 3.3C, right). We also tested the requirement for kinetochore fibers for Kif15 localization in parental cells by depleting Nuf2 and staining for Kif15; in these cells the spindle localization of Kif15 is reduced, but not completely abolished, consistent with previous observations (Vanneste et al., 2009). Together these results show that overexpressed GFP-Kif15 is distributed in a manner similar to that of the endogenous protein and that TPX2, but not kinetochore fibers, is required for spindle localization.

To examine Kif15-dependent spindle formation in LLC-Pk1 GFP-Kif15 cells we first treated parental and GFP-Kif15 cells with 1 □M STLC (DeBonis et al., 2004) for 18 hours and quantified spindle morphology (Fig. 3.3D). In parental cells treated with STLC, 96% of spindles were monopolar. In STLC treated GFP-Kif15 cells, the majority of spindles were bipolar (87%), demonstrating that GFP-Kif15 can support bipolar spindle formation in these cells, consistent with results in other mammalian cells either

overexpressing Kif15 or treated to develop resistance to STLC (Raaijmakers et al., 2012; Sturgill et al., 2016; Sturgill and Ohi, 2013; Vanneste et al., 2009). Next, we assessed the ability of STLC treated GFP-Kif15 expressing cells to form bipolar spindles following siRNA mediated depletion of TPX2. As shown in Figure 3D, 97% of spindles were monopolar, indicating that TPX2 is required for Kif15 dependent bipolar spindle formation (Tanenbaum et al., 2009). It should be noted, however, that depletion of TPX2 in control cells also leads to defects in spindle formation, resulting in short bipolar spindles, multipolar spindles and monopolar spindles (Gruss and Vernos, 2004) Because our data showed that the C-terminal 37 amino acids of TPX2 are important for spindle localization of Kif15 and inhibition of Kif15 motility *in vitro,* we next used cell lines expressing full-length or truncated TPX2 from a BAC to determine if the C-terminal region is important for force generation by Kif15 *in vivo*. Cells were co-nucleofected with siRNA to deplete endogenous TPX2 and with a plasmid encoding mCherry-Kif15. 40 hours post nucleofection cells were treated with STLC and spindle morphology scored. As shown in Figure 3D, bipolar spindles were present in the majority of cells expressing full-length TPX2, but not in cells expressing TPX2-710. This result demonstrates that the C-terminal region of TPX2 is necessary for Eg5-independent bipolar spindle formation in cells overexpressing Kif15.

The mechanism by which Kif15 promotes spindle bipolarity in the absence of Eg5 activity is not known, but has been proposed to result from Kif15 action on parallel, bundled microtubules (Sturgill and Ohi, 2013). Consistent with this, recent work shows that some Kinesin-5 inhibitor-resistant cell lines express low levels of a rigor mutant of Eg5 that promotes microtubule bundle formation (Sturgill et al., 2016). To determine if

microtubule bundles are sufficient for Kif15 localization in the absence of TPX2, we depleted cells of TPX2 and added FCPT, which induces microtubule bundle formation by promoting rigor binding of Eg5 to microtubules (Groen et al., 2008). Treatment of parental cells with FCPT alone promoted microtubule bundle formation as expected; however, very few bundles were observed in the absence of TPX2 (Fig. 3.3E). Immunostaining showed that Eg5 bound to microtubule bundles in FCPT treated cells, was reduced in siTPX2 treated cells, and bound to residual bundles in cells treated with both FCPT and siRNA to TPX2 (Fig. 3.3E). Although Kif15 was detected on bundles in FCPT treated cells, it was not detected in cells treated with siRNA targeting TPX2, even when FCPT was added to promote bundle formation (Fig. 3.3E). These results show that Eg5 can bind to spindle microtubules in the absence of TPX2 when rigor binding of Eg5 to microtubules is promoted by FCPT treatment. However, in cells lacking TPX2, the formation of microtubule bundles using FCPT treatment alone may not be sufficient to localize Kif15 properly to the spindle.

3.2.4 Dynamic microtubules contribute to Kif15 behavior *in vivo*

Although Kif15 motility *in vitro* has been characterized (Drechsler et al., 2014; Sturgill et al., 2014), the motile behavior of Kif15 *in vivo* has not been reported. To investigate this, we performed time-lapse confocal microscopy of GFP-Kif15 expressing LLC-Pk1 cells, which facilitate imaging due to their flat morphology throughout mitosis remain relatively flattened during mitosis, facilitating imaging. We observed rapid motion of fluorescent particles of GFP-Kif15 toward the spindle equator, where microtubule plus-ends are located (Fig. 3.4A). Close inspection of the confocal image

sequences revealed some variation in the fluorescence intensity and morphology of the motile particles (Fig. 3.4A,D). The larger or brighter particles may represent clusters of Kif15 tetramers, a possibility that is consistent with recent *in vitro* experiments that show accumulation of Kif15 at intersections of dynamic microtubules and at microtubule plus-ends (Dreschler and McAinsh, 2016). However, the fluorescent puncta move rapidly, and photobleach quickly, so variation in morphology of individual puncta could not be quantified. When cells progressed into anaphase, GFP-Kif15 was enriched along kinetochore fibers and in some cases showed an accumulation near kinetochore fiber plus-ends (Fig. 3.4B, Fig. 3.7B).

We also performed TIRF microscopy of live cells to visualize motors on microtubules that extended to the peripheral regions of the cell (Gable et al., 2012). In accord with results from confocal microscopy, GFP-Kif15 motors appeared to move in a directed manner, away from the centrosome, consistent with predominantly plus-end directed motion (Fig. 3.7A).

To determine if the fluorescent particles of GFP-Kif15 are walking along the lattice of spindle microtubules or moving with the tips of growing microtubules, we measured the velocity of GFP-Kif15 *in vivo,* from kymographs (Fig. 3.4C) of fluorescent particles in the image sequences taken of metaphase and anaphase cells (Methods). We also imaged LLC-Pk1 cells expressing GFP-EB1, using identical imaging parameters, to determine the rate of microtubule growth (Piehl et al., 2004). This analysis showed that particles of GFP-Kif15 moved in a processive manner at a velocity of 133 ± 43 nm/sec This value was not different from the rate of microtubule growth determined from the GFP-EB1 movies, 119 ± 26 nm/sec ($P = 0.09$) suggesting that Kif15 motility results from

association with growing microtubule ends. We also imaged both GFP-Kif15 and GFP-EB1 at room temperature, which reduced photobleaching, and again found that the velocities were not different (data not shown). The relatively wide distribution in the velocities of GFP-Kif15 puncta could reflect different rates for single or multiple motors, for motors walking on one microtubule with a second microtubule as cargo, or because some motors are moving on microtubule growing ends and others are walking along the microtubule lattice (Dreschler and McAinsh, 2016). To determine if this motile behavior is unique to GFP-Kif15, we overexpressed Eg5-Emerald from a plasmid, and imaged the cells. In this case, plus-end directed motile behavior was not observed (data not shown), consistent with previous work demonstrating that Eg5, expressed from a BAC, bound and unbound rapidly from mitotic microtubules and showed dynein-dependent minus-end motion (Gable et al., 2012; Uteng et al., 2008).

To determine if GFP-Kif15 motility results from motors associating with dynamic microtubule plus-ends (Dreschler and McAinsh, 2016), we treated GFP-Kif15 cells with nanomolar concentrations of Paclitaxel, to suppress microtubule dynamics (Yvon et al., 1999). Under these conditions (Methods), the velocity and number of growing microtubule plus-ends, measured in GFP-EB1 expressing LLC-Pk1 cells was reduced, confirming a suppression of microtubule dynamics (Fig. 3.7C,D). Time-lapse movies of Paclitaxel treated GFP-Kif15 cells showed a dramatic reduction of Kif15 motility on the spindle, which precluded tracking. This result shows that microtubule dynamics contribute to GFP-Kif15 behavior *in vivo* (Fig. 3.4D). Because of the high density of microtubules in the spindle, and the fact that the Kif15 antibody is only compatible with methanol fixed cells, we were not able to document co-localization of Kif15 and GFP-

EB1 in fixed cells, and in live cells expression of both GFP-Kif15 and mCherry-EB1 resulted in aberrant spindle morphology.

To determine if the distribution of Kif15 and TPX2 was altered in Paclitaxel treated cells, as might be expected if the motors preferentially associate with dynamic microtubules, parental cells were fixed and stained for microtubules and TPX2 or Kif15. The results show that suppression of dynamics with Paclitaxel resulted in an increase in TPX2 and Kif15 near the spindle poles and a reduction along spindle microtubules (Fig. 3.4E). To quantify this, TPX2 and Kif15 levels were normalized to tubulin, and the ratio of each protein in the half-spindle and at the pole was determined; the results show that Paclitaxel treatment reduced this ratio for both Kif15 and TPX2 (Fig. 3.4E'). This result shows that the distribution of TPX2 and Kif15 is impacted by microtubule dynamics, consistent with the enrichment of TPX2 and Kif15 at plus-ends of dynamic microtubules *in vitro* (Dreschler and McAinsh, 2016; Reid et al., 2016; Roostalu et al., 2015). Kif15 and TPX2 lack a short amino acid motif, composed of Serine, any amino acid, Isoleucine and Proline and abbreviated SxIP, that is commonly found in proteins that localize to microtubule plus-ends in a EB-1–dependent manner (Honnappa et al., 2009). This suggests that the association of TPX2 and Kif15 with microtubules is direct rather than mediated by EB1. TPX2 has been reported to associate with dynamic microtubule ends *in vitro* at low concentrations (Reid et al., 2016; Roostalu et al., 2015) but has not been reported to tip track *in vivo*, where it is present at higher concentrations (~20 nM in a mitotic cell extract). One possibility is that TPX2 is required to load Kif15 onto microtubules but not required for it to remain at the growing plus-end (Fig. 3.4Fa); alternatively TPX2 may remain at the plus-end with Kif15 (Fig. 3.4Fb), but may not be

detectable *in vivo* (Dreschler and McAinsh, 2016; Reid et al., 2016; Roostalu et al., 2015).

3.3 Discussion

The results of these experiments demonstrate that the C-terminal region of TPX2, which was shown previously to contribute to the regulation of the Kinesin-5, Eg5, also contributes to the regulation of the Kinesin-12, Kif15. Specifically, the C-terminal 37 amino acids of TPX2 contribute to the spindle localization of each motor and inhibition of motor walking *in vitro*. In the case of Eg5, both TPX2-710 and full length TPX2 had an inhibitory effect on motor stepping *in vitro*, although full-length TPX2 was a more effective inhibitor (Balchand et al., 2015). This is in contrast to Kif15, which was only inhibited when the full-length protein was added. The reason for these differences is not clear; one possibility is that Eg5 is more susceptible to inhibition because of differences in the neck linker and stalk which are unique to Eg5 (Waitzman and Rice, 2014).

Our results showing that the C-terminal region of TPX2 contributes to the spindle localization of both Eg5 and Kif15, two kinesins that contribute to spindle bipolarity, raises the question of how bipolarity is achieved in cells expressing truncated TPX2. First, for both motors, spindle localization is reduced but not eliminated when TPX2-710 is expressed, which is consistent with the observation that the Eg5-TPX2 interaction is not completely abolished when the C-terminal region is removed from the protein (Eckerdt et al., 2008; Ma et al., 2011); the residual binding may be sufficient to generate bipolar spindles. In addition, incomplete knockdown of TPX2 may contribute to motor binding to spindle microtubules. Second, in LLC-Pk1 cells centrosome separation

typically occurs during prophase when most of TPX2 is in the nucleus and thus before complete inhibition of Eg5 by TPX2 can occur (Raaijmakers et al., 2012). Finally, it is possible that TPX2 also impacts minus-end directed motility (Wittmann et al., 1998), and that the reduction of both inward and outward force generators enables spindle bipolarization via microtubule pushing forces (Ferenz et al., 2009b; Toso et al., 2009; Wittmann et al., 1998).

In Kif15 overexpressing cells treated with STLC, spindle formation is thought to occur when a monopolar spindle breaks symmetry, driven by Kif15 acting on parallel, bundled microtubules (Sturgill et al., 2014; Sturgill and Ohi, 2013). When TPX2 is depleted from these cells, bipolar spindles are not observed (this report and (Tanenbaum et al., 2009)). One possibility is that TPX2 is needed to generate microtubule bundles to which Kif15 binds (Sturgill et al., 2014); alternatively, TPX2 may play a more direct role in promoting force generation by Kif15 (Drechsler et al., 2014). It should be noted that depletion of TPX2 results in a dramatic alteration of spindle morphology resulting in short spindles with extensive astral arrays and few or no spindle microtubules (Gruss et al., 2002), and these changes impact spindle formation. However, in Kif15 overexpressing cells expressing TPX2-710, microtubule formation in the chromosome pathway can proceed (Ma et al., 2011), and these cells also fail to generate bipolar spindles. This suggests that TPX2 is needed not only to promote microtubule formation but to also regulate motor activity, which is consistent with *in vitro* experiments showing that the C-terminus of TPX2 is required for motor regulation on individual, unbundled, microtubules (this report) and experiments showing that Kif15 can generate greater force in the presence of TPX2 (Drechsler et al., 2014).

Our analysis is the first report of the motile behavior of GFP-Kif15 on spindle microtubules *in vivo*. We observed plus-end directed motion of Kif15 puncta in prometaphase, metaphase and anaphase cells. In live cells, Kif15 puncta moved at a rate (133 nm/sec) that was indistinguishable from microtubule plus-end growth in these cells (119 nm/sec) and was suppressed in cells treated with Paclitaxel to reduce microtubule dynamics. These observations support the idea that motion of Kif15 is due, at least in part, to tracking with microtubule plus-ends. This possibility is also consistent with *in vitro* experiments showing that Kif15 tracks, and accumulates at the plus-ends of dynamic microtubules, in the absence of other microtubule-associated proteins (Dreschler and McAinsh, 2016). The velocity of GFP-Kif15 puncta in live cells overlaps with the velocity of GFP-Kif15 measured *in vitro* on stable microtubules (~130 nm/sec) but is slower than the velocity on dynamic microtubules (~500 nm/sec) (Dreschler and McAinsh, 2016). Because microtubules *in vivo* are highly dynamic, the velocity of Kif15 *in vivo* would be predicted to be ~500 nm/sec (Verhey et al., 2011). The similarity of the velocities of microtubule growth and Kif15 puncta motility is thus consistent with motors tracking plus-ends, but we cannot eliminate the possibility that Kif15 walking on spindle microtubules *in vivo* also contributes to the observed motility. Because puncta composed of multiple tetramers of GFP-Kif15 are easier to detect in live cells, our imaging experiments may preferentially capture the brighter puncta at microtubule ends and individual motors on the microtubule lattice may be insufficiently bright to track. It should be noted that measuring the rate that a mitotic motor walks *in vivo* is challenging. In the case of Eg5, prior work showed that motors bound and unbound rapidly to spindle microtubules (Gable et al., 2012). In the interzonal region, short excursions were

measured with a rate of ~6.5 nm/sec, similar to the rate that Eg5 walks *in vitro* (Balchand et al., 2015; Weinger et al., 2011). In contrast, in the half-spindle, Eg5 moved toward the spindle poles in a dynein dependent manner (Gable et al., 2012; Uteng et al., 2008). To our knowledge, the *in vivo* motile behavior of individual molecules of other mammalian mitotic motors has not been reported. Therefore, additional experiments will be required to establish if Kif15 walks on the microtubule lattice, tracks the microtubule plus-end, or both, *in vivo* (Dreschler and McAinsh, 2016).

We observed Kif15 puncta on kinetochore fibers, in fixed and live cells, consistent with the fact that Kif15 can crosslink parallel microtubules *in vitro* (Drechsler et al., 2014; Sturgill et al., 2014). One appealing possibility is that Kif15 can aid in the formation of parallel microtubule bundles in the spindle by walking along a kinetochore microtubule while associated with a dynamic growing microtubule. In late anaphase and telophase cells, Kif15 was not detected on interzonal microtubules, consistent with preferential binding to parallel microtubules.

Mitotic motors, including Eg5 and Kif15, and TPX2 are all subject to mitotic regulation (Blangy et al., 1997; Fu et al., 2015a; Nousiainen et al., 2006; vanHeesbeen et al., 2016), but how these modifications impact motor behavior *in vitro* and *in vivo* remains incompletely understood. For example, modifications of mitotic motors regulate their binding to spindle microtubules as cells enter mitosis, but if these modifications also impact their interaction with TPX2 is not known. Additionally, if there is competition between these motors for interaction with TPX2 has not been determined. Enrichment of GFP-Kif15 on kinetochore fibers was observed as cells progressed into anaphase

suggesting that Kif15 distribution and function may change not only as cells enter mitosis, but also as cells progress into anaphase.

In conclusion, the results of these *in vitro* experiments show that Kif15 is a processive, track-switching motor and that a fraction of the motors exist as tetramers in both interphase and mitotic extracts, supporting the view that Kif15, like Eg5, functions as a tetramer. The results presented here demonstrate that the C-terminal 37 amino acids of TPX2 regulates *in vitro* motility of Kif15, contributes to the spindle localization of Kif15 and to Eg5-independent force generation *in vivo*. Our live cell imaging shows that Kif15 moves in a manner consistent with tracking microtubule plus-ends *in vivo*, a property that likely aids the motor aligning microtubules into kinetochore fibers and generating force for bipolarization. Together with other recent work, our results highlight the essential role of microtubule-associated proteins in regulating of the cellular activity of kinesin motors (Barlan et al., 2013; Dixit et al., 2008; Li et al., 2016; Wignall and Villeneuve, 2009).

3.4 Materials and Methods

3.4.1 Materials

All chemicals, unless otherwise specified, were purchased from Sigma-Aldrich.

3.4.2 Cell Culture, nucleofection and inhibitor treatments

LLC-Pk1 cells were cultured in a 1:1 mixture of F10 Hams and Opti-MEM containing 7.5% fetal bovine serum and antibiotics and maintained at 37□C and 5% CO_2. LLC-Pk1 cells were nucleofected using an Amaxa nucleofector (Lonza) using program

X-001 and Mirus nucleofection reagent (Mirus Bio LLC, Madison, WI) according to the manufacturers recommendations. The following siRNAs were used: TPX2, GGACAAAACUCCUCUGAGA; Nuf2, AAGCAUGCCGUGAAACGUAUA; Kif15, UGACAUCACUUGCAAAUAC. siRNAs were purchased from Dharmacon (GE Healthcare Life Sciences, Pittsburgh, PA).

LLC-Pk1 cells expressing full-length TPX2 or TPX2-710 from a bacterial artificial chromosome (BAC) were grown as previously described (Ma et al., 2011). To generate cells expressing GFP-Kif15, parental cells were nucleofected with GFP-Kif15 and selected using the appropriate antibiotic; cells were subcloned to enrich for GFP-Kif15 expressing cells. For some experiments, GFP-Kif15 cells that had been further selected for fluorescence using cell sorting were used. mCherry-Kif15 was prepared by subcloning of GFP-Kif15 into the appropriate vector.

Paclitaxol, FCPT and STLC were prepared as stock solutions in DMSO, stored at -20 °C and diluted with culture medium prior to use. FCPT was used at 200 □M, Paclitaxol at 330 nM and STLC at 1 □M.

3.4.3 Preparation of cell extracts

Cell extracts for TIRF experiments were prepared from LLC-Pk1 cells expressing GFP-Kif15. A confluent 100 mm diameter cell culture dish was washed twice with calcium and magnesium free PBS and then 300 □l extraction buffer (40 mM HEPES/KOH pH 7.6, 100 mM NaCl, 1 mM EDTA, 1 mM PMSF, 10 µg/ml Leupeptin, 1 mg/ml pepstatin, 0.5% Triton X 100 and 1 mM ATP) was added drop wise to the dish and incubated with gentle rotation for approximately 2 min (Balchand et al., 2015; Cai et

al., 2007). The extract was transferred to a microcentrifuge tube on ice and centrifuged at 15,000 RPM at 4□C for 10 min in a tabletop centrifuge. The supernatant was recovered and used immediately or stored in aliquots in liquid nitrogen; protein concentration was determined using the method of Lowry (Lowry et al., 1951). For quantification of the fluorescence intensity of individual puncta using TIRF microscopy, the cells were treated with siRNA targeting endogenous Kif15 72 hours prior to preparation of the extract.

To prepare mitotic extracts, GFP-Kif15 cells were treated with siRNA targeting endogenous Kif15, and were synchronized using 330nM Nocodazole for the final 18 hours of the 72 hr siRNA treatment. Extracts were prepared as described above with the addition of Simple Stop 1 Phosphatase Inhibitor Cocktail (1X)(Gold Biotechnology Inc., St. Louis, MO) to the extract buffer.

3.4.4 Protein purification

Full-length and truncated TPX2 were expressed and purified from bacteria as previously described (Balchand et al., 2015). Kinesin-1-GFP was prepared using the dimeric construct as previously described (Balchand et al., 2015). To generate TPX2-657, a stop codon was introduced at amino acid 657 in the bacterially expressed Full-length TPX2 construct. To generate TPX2 Δ PFAM, PCR was used to remove amino acids 662 to 719 from full-length TPX2. Proteins were run on 8% polyacrylamide gels using appropriate MW standards, and stained with Commassie brilliant blue.

3.4.5 Single molecule experiments

For the single molecule experiments, perfusion chambers (~10 □l volume) were made from glass slides, silanized coverslips and double stick tape (Balchand et al., 2015). First, 10 □l of 10% Rat YL ½ anti-tubulin antibody (Accurate Chemical and Scientific, Corp) was flowed into the chamber and incubated for 3 min. Next, the chamber was blocked by flowing in 5% pluronic F127 for 3 min. Diluted rhodamine labeled microtubules, composed of 10% rhodamine tubulin (Cytoskeleton, Inc.) and unlabeled porcine brain tubulin, were flowed into the chamber and incubated for 3 min followed by a second block of 5% pluronic F127. Cell extract containing GFP-Kif15 was diluted in PEM 20 motility buffer (20 mM Pipes pH 6.9, 2 mM EGTA, 2 mM MgSO4), containing 0.25% F127, 100 μM ATP, 1 mM DTT, 25 μM Paclitaxel and supplemented with oxygen scavenging system (15 mg/ml glucose, 1.23 mg/ml glucose oxidase and 0.375 mg/ml catalase), flowed into the chamber and imaged. To determine the directionality of Kif15, polarity marked microtubules were used and confirmed that Kif15 walked toward the plus-end for the majority of excursions. For pre-incubation experiments with TPX2, the indicated concentrations of TPX2 were added to the motility buffer containing GFP-Kif15 and incubated on ice for 2 min before flowing into the chamber. Single molecule imaging of Kinesin-1-GFP was performed as described previously (Balchand et al., 2015).

3.4.6 Microscope Imaging and Analysis

TIRF microscopy was performed using a Nikon Ti-E microscope with a 100X 1.49 NA objective lens, and an Andor Zyla sCMOS camera; the system was run by

Nikon Elements software. TIRF imaging was performed at room temperature; images were collected at 1 frame per second for a total of 300 seconds. To measure motor velocity, individual puncta were tracked using the Particle Tracking function of Nikon Elements software and exported to Excel for analysis. For the experiment with mitotic extract, a Nikon Ti-E microscope run by Metamorph software and with a Hammamatsu Flash 4.0 camera was used.

Live and fixed cells were imaged using either spinning disc confocal microscopy or point scanning confocal microscopy. For spinning disc confocal, two different systems were used, either a Nikon Ti-E microscope with a CSU-X1 Yokogawa spinning disc confocal scan head (PerkinElmer, Wellesley, MA), and an Andor iXon+ EMCCD camera (Andor, Belfast, Northern Ireland), and a 100X 1.4 NA objective lens or a CSU-10 Yokogawa spinning disc confocal on a Nikon TE300 as previously described (Tulu et al., 2003). For live cell imaging, exposures were adjusted without saturating the camera's pixels; typical exposures were 50 - 800 msec. For point scanning confocal, a Nikon A1R system with a 60X 1.4 N.A. objective lens was used. Images of live cells were acquired every 2 sec at room temperature or every 3 sec at ~34 □C; images were typically collected for 2-5 min. For both fixed and live cell imaging, a laser power of 1-2 % was used. For heating the cells during imaging, a Nicholson Precision Instruments (Bethesda, MD) Air Stream Stage Incubator was used; temperature was measured using a thermistor probe taped to the microscope stage outside of the cell chamber. When the thermistor temperature is 37□C, the temperature inside the chamber is ~34□C.

To quantify the fluorescence intensity of tubulin and Kif15, a 1 X 1 micron box was placed midway between the spindle pole and the chromosomes, or at the spindle

pole, and the ratio of Kif15 to tubulin fluorescence was measured, after background subtraction. Statistical analysis was performed in Excel. Velocity of GFP-EB1 dashes and Kif15 puncta were tracked in ImageJ using the M Track J plug-in.

3.4.7 Immunofluorescence

LLC-Pk1 cells were plated on #1.5 glass coverslips approximately 48 hours prior to experiments. For Kif15 staining, cells were rinsed twice with room temperature PBS lacking calcium and magnesium, and fixed in -20 □C methanol for 5-10 minutes, and rehydrated in PBS containing 0.1 %Tween and 0.02 % sodium azide (PBS-Tw-Az). Kif15 primary antibodies (Cytoskeleton, Inc.) were used following the manufacturers' recommendation and subsequently stained with fluorescent secondary anti-rabbit antibodies (Ma et al., 2011). For TPX2 staining, cells were fixed in 2% paraformaldehyde, 0.25% glutaraldehype, 0.5% Triton X 100, made fresh daily in PBS lacking calcium and magnesium. TPX2 antibodies were obtained from Novus Biologicals; Hec1 antibodies (Abcam) were the kind gift of T. Maresca. Microtubules were stained with either DM1a mouse anti-tubulin (Sigma Chemical Co.) or YL1/2 rat anti-tubulin (Accurate Chemical and Scientific Corporation) and appropriate secondary antibodies as previously described (Ma et al., 2011). Stained cells were mounted on glass slides using Fluomount G (Southern Biotech) to which DAPI was added to stain DNA.

3.4.8 Western blotting and detection

Whole cell extracts of control or siRNA treated cells were prepared by adding SDS sample buffer to 35mm dishes of cells, followed by sonication. Extracts were run

on 8% SDS polyacrylamide gels using the formulation of Laemmli (Laemmli, 1970). Gels were transferred onto Amersham Hybond-P membrane (GE Healthcare, Waukesha, WI). Blots were probed with Kif15 or TPX2 antibodies used at 1:1,000 for 1 h at room temperature in 5% non-fat dry milk dissolved in Tris buffered saline containing 0.02% Tween-20 (TBS-Tween). The blots were then probed with goat anti-rabbit HRP conjugated secondary antibody (Jackson Immunoresearch Laboratories, Inc.) (1:5,000) for 1 hr at room temperature in 5% non-fat dry milk dissolved in TBS-Tween and were detected using chemiluminescence.

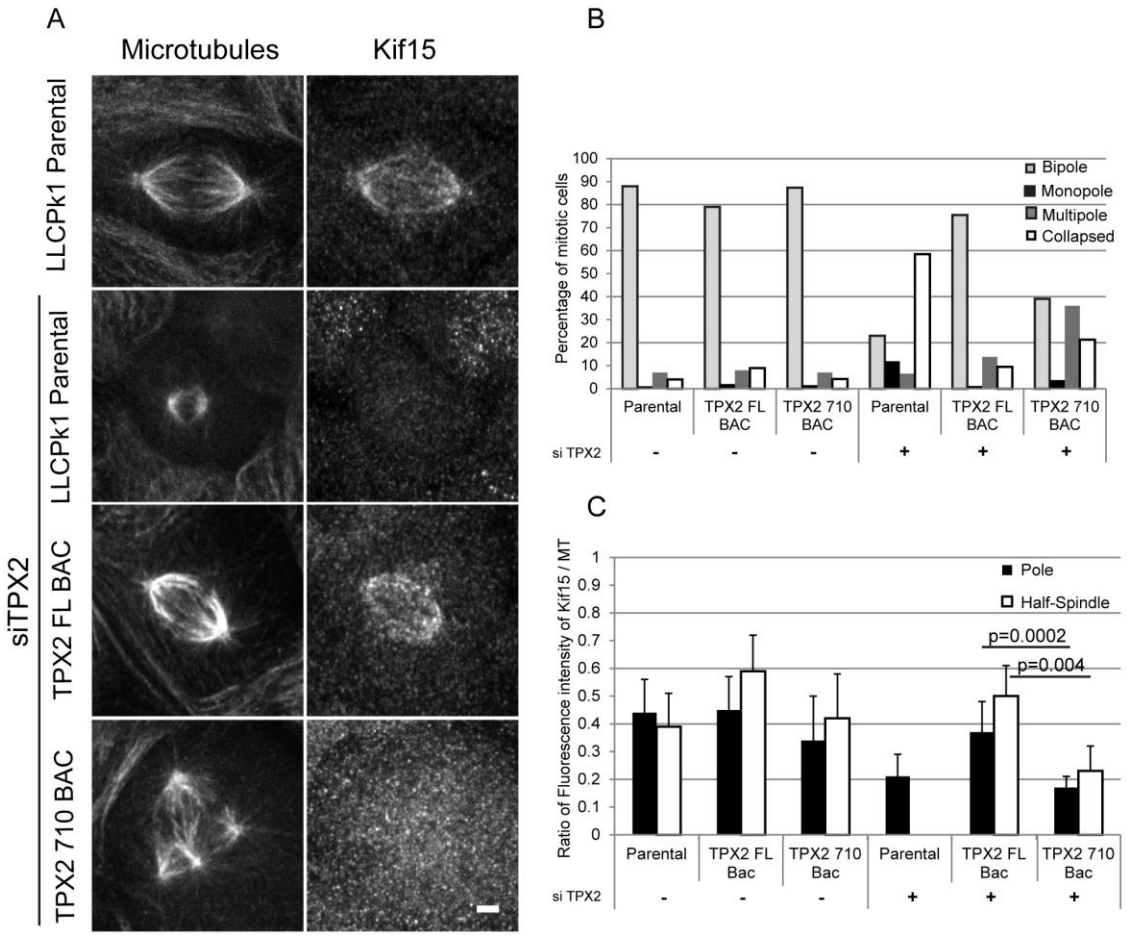

Figure 3.1 The C-terminal region of TPX2 contributes to spindle localization of Kif15. (A). Immunofluorescence staining for microtubules (left) and Kif15 (right). Top row, parental cells; bottom three rows show cells depleted of TPX2 and expressing: no transgene (parental); transgene encoding full length TPX2 (middle) or TPX2-710 (bottom). (B). Spindle morphology for parental cells and cells expressing full-length or truncated TPX2; cells on the right were additionally treated with siRNA targeting TPX2. (C). Quantification of fluorescence ratio of Kif15 to tubulin at pole and in the half spindle. Error bars are standard deviation. Parental cells depleted of TPX2 were only measured at spindle pole due to loss of spindle microtubules. Scale bar in (A) is 2 μm.

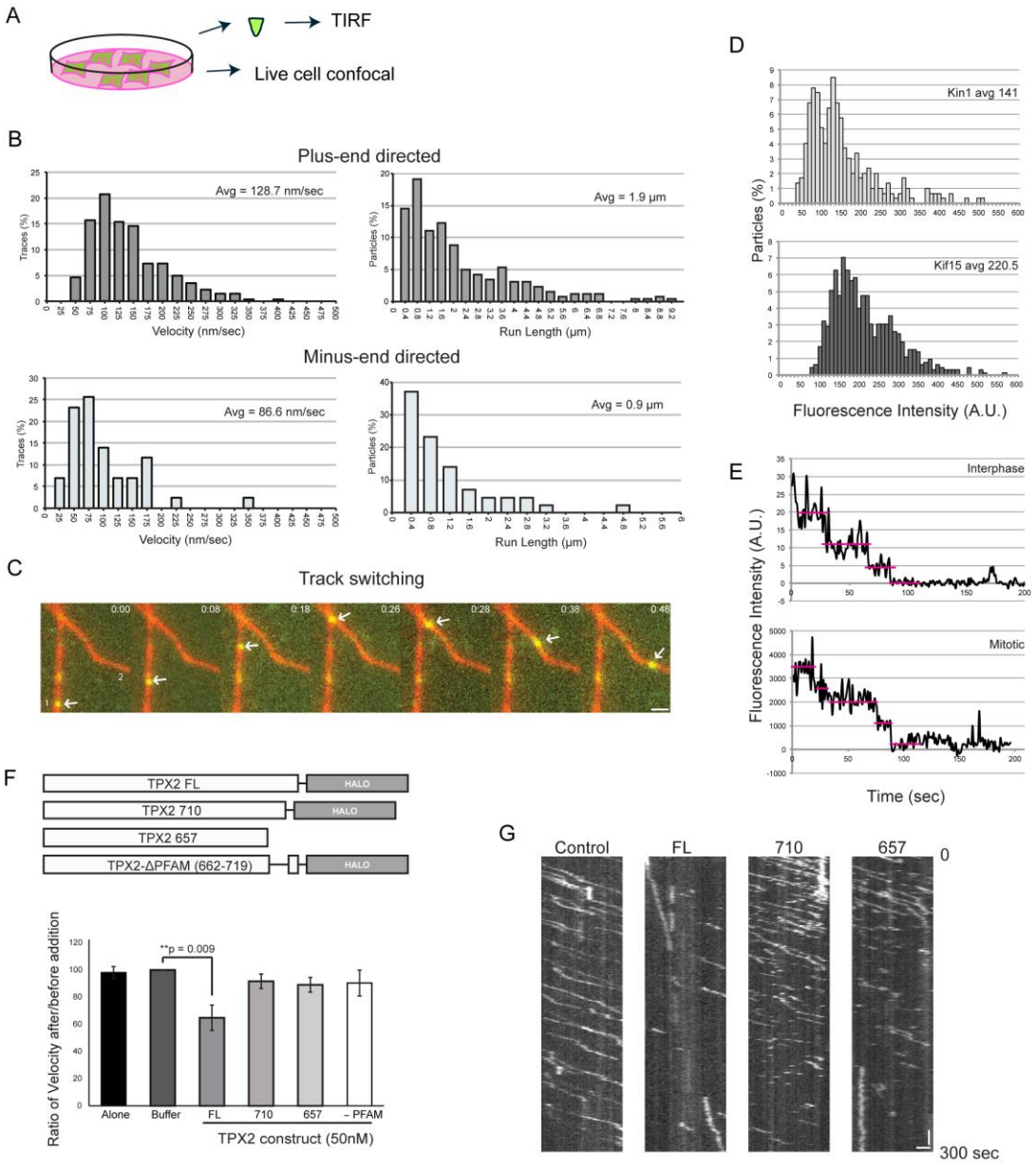

Figure 3.2 Inhibition of Kif15 motor stepping requires full-length TPX2. (A) Schematic diagram of experiment. (B) Histograms of GFP-Kif15 velocity (left) and run length (right) for plus-end and minus-end directed motion, n = 261 and 43 motors, respectively. Data from 2 independent experiments. (C) GFP-Kif15 switches microtubule tracks; arrow marks moving GFP-Kif15 puncta. Time in min:sec. (D) Histogram of fluorescence intensity of Kinesin-1-GFP (top) and GFP-Kif15 (bottom); fluorescence in arbitrary units (AU). For Kinesin-1-GFP, n = 295 and for GFP-Kif15, n = 652, from 2 independent experiments. (E) Photobleaching of microtubule bound GFP-Kif15 from interphase and mitotic extracts. Horizontal pink lines show bleach steps. For interphase, n = 11 particles, 5 >3 steps and 6 <3 steps; data from 2 independent experiments; for mitotic extracts n = 15 particles, 10 > 3 steps and 5 < 3 steps. (F) Schematic diagram of

constructs used for inhibition experiments (top) and bar graph (lower) showing ratio of velocity without and with added proteins; error bars SEM. (G) Kymographs showing motility of GFP-Kif15; added TPX2 construct indicated at top; vertical axis marker bar = 15 sec; horizontal axis marker bar = 1 μm. Bar in C = 1 μm.

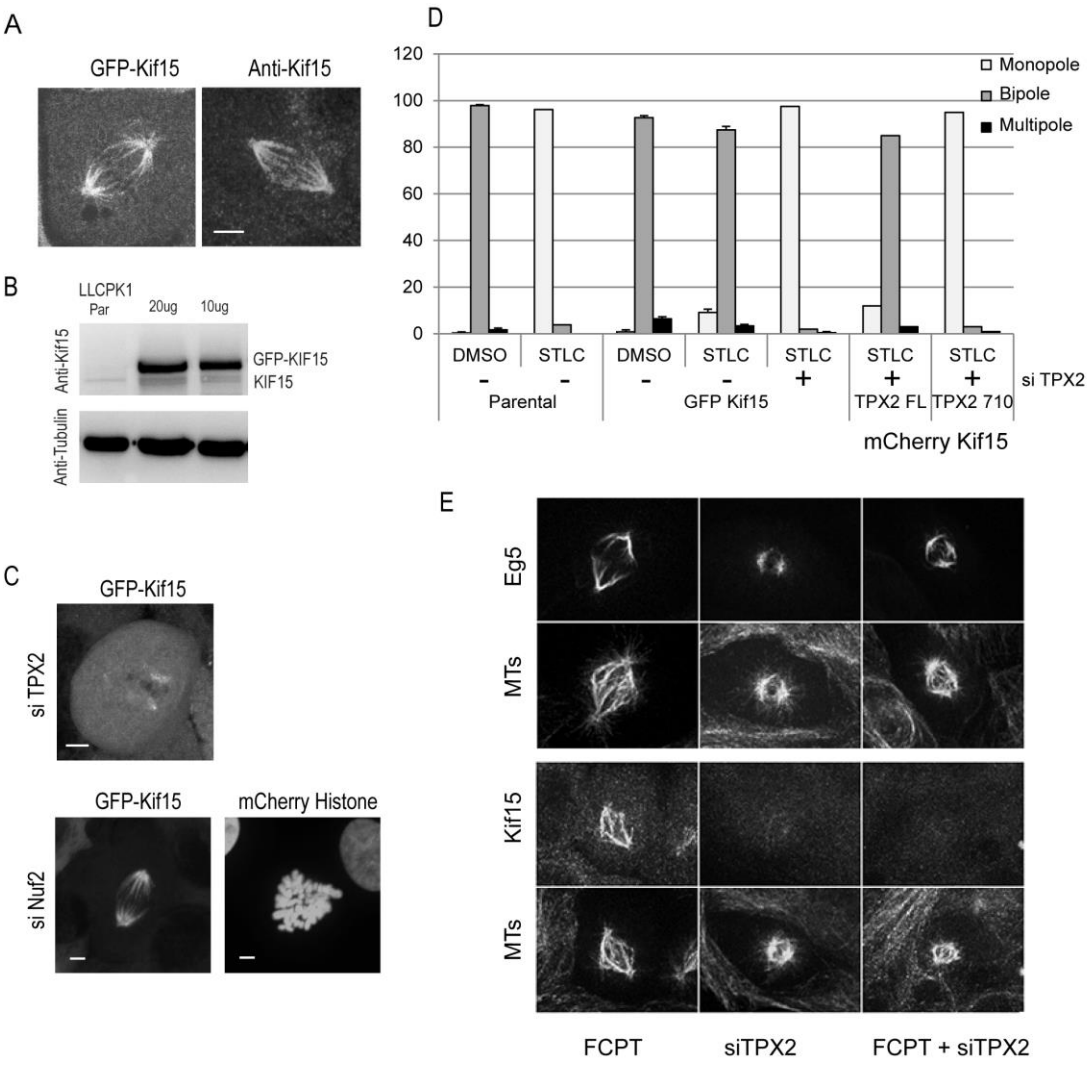

Figure 3.3 TPX2 is required for bipolar spindle formation in cells overexpressing Kif15. (A) LLC-Pk1 cells expressing GFP-Kif15 (left) and parental cells fixed and stained for Kif15 (right). (B) Western blot of extracts from parental and GFP-Kif15 expressing cells; blot stained for Kif15 (top) and tubulin as loading control (bottom). (C) Images of GFP-Kif15 expressing cells treated with siRNA targeting TPX2 (top) or Nuf2 (bottom); GFP-Kif15 (left) and co-nucleofected mCherry-H2B to label chromosomes (right). (D) Bar graphs showing percent of bipolar, monopolar and multipolar spindles for each treatment condition. Error bars show standard deviation. (E) Parental cells treated with FCPT, with siRNA targeting TPX2, or with both. Cells were stained for microtubules (lower panels) and either Kif15 or Eg5 (upper panels). Marker bar, A, C, E = 2 μm.

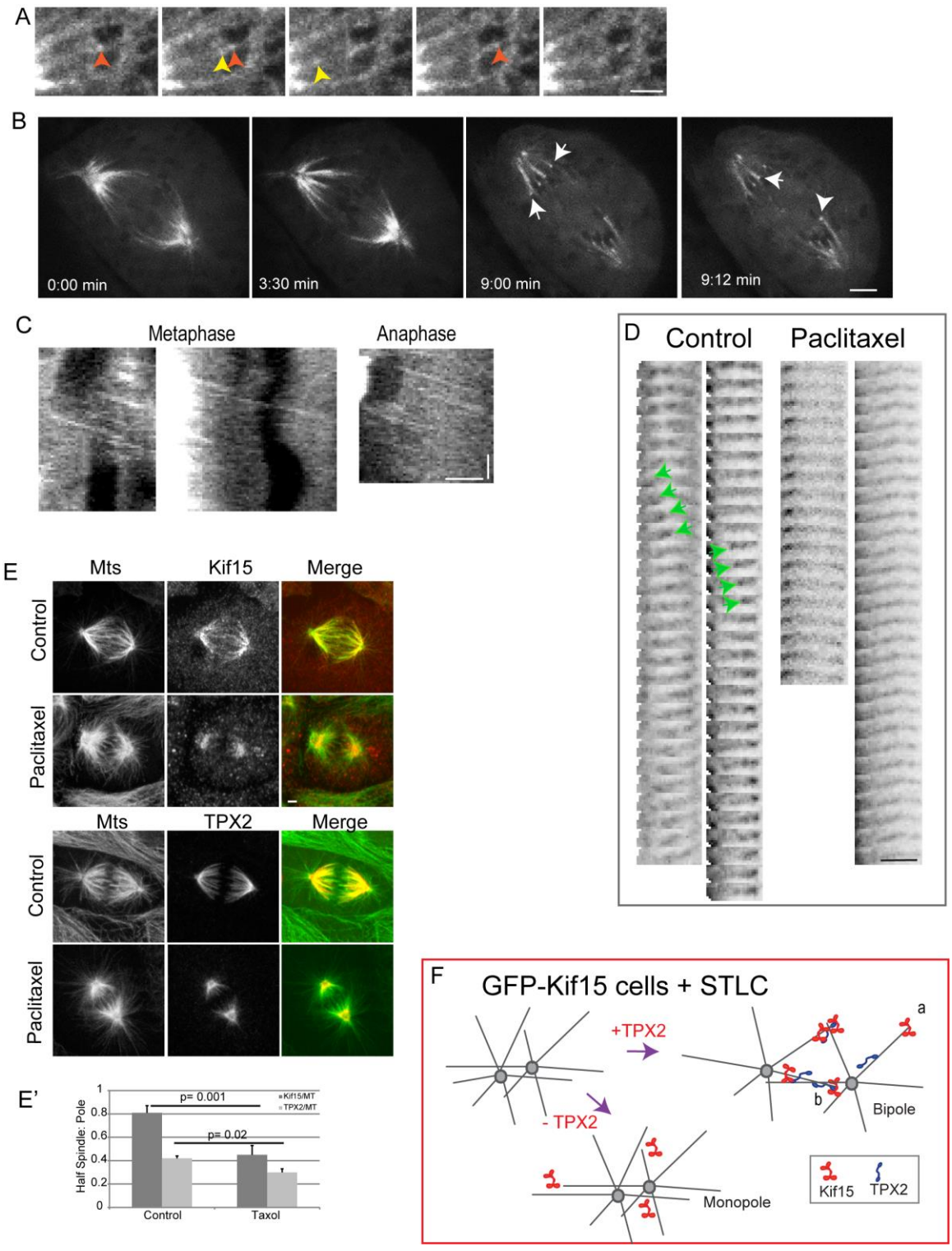

Figure 3.4 Dynamics of GFP-Kif15 *in vivo.* (A) Selected frames from a movie of GFP-Kif15 expressing cells; red and yellow arrowheads mark fluorescent particles traveling toward the chromosome region (spindle equator to right; dark ovals are chromosomes). (B) Live cell expressing GFP-Kif15 progressing from prometaphase (0:00) to metaphase

(3:30) and anaphase (9:00); arrows show accumulation of fluorescence near the kinetochores. (C) Kymographs from movie sequences of GFP-Kif15 expressing metaphase and anaphase cells; distance, horizontal axis; time, vertical axis; dark regions are chromosomes; spindle midzone to right. (D) Sequential frames (2 sec interval) from movies of GFP-Kif15 expressing control and Paclitaxel treated cells (inverted contrast); motion of fluorescent particles toward the kinetochore region (right in all panels) in control but not Paclitaxel treated cells. Green arrowheads mark moving puncta. (E) LLC-Pk1 parental cells fixed and stained for microtubules and Kif15 (top) or TPX2 (bottom); control and Paclitaxel as indicated; merged images to the right. (E') Bar graph showing quantification of images in E. (F) Cartoon showing GFP-Kif15 cells in the presence of STLC; bipolar spindle formation requires TPX2. TPX2 could load Kif15 onto the microtubule, followed by motor motion to the microtubule + end (a) or TPX2 and Kif15 could both localize to microtubule ends (b). Marker bars in A,B,C,D,E_ = 2 μm; time scale in C, 30sec.

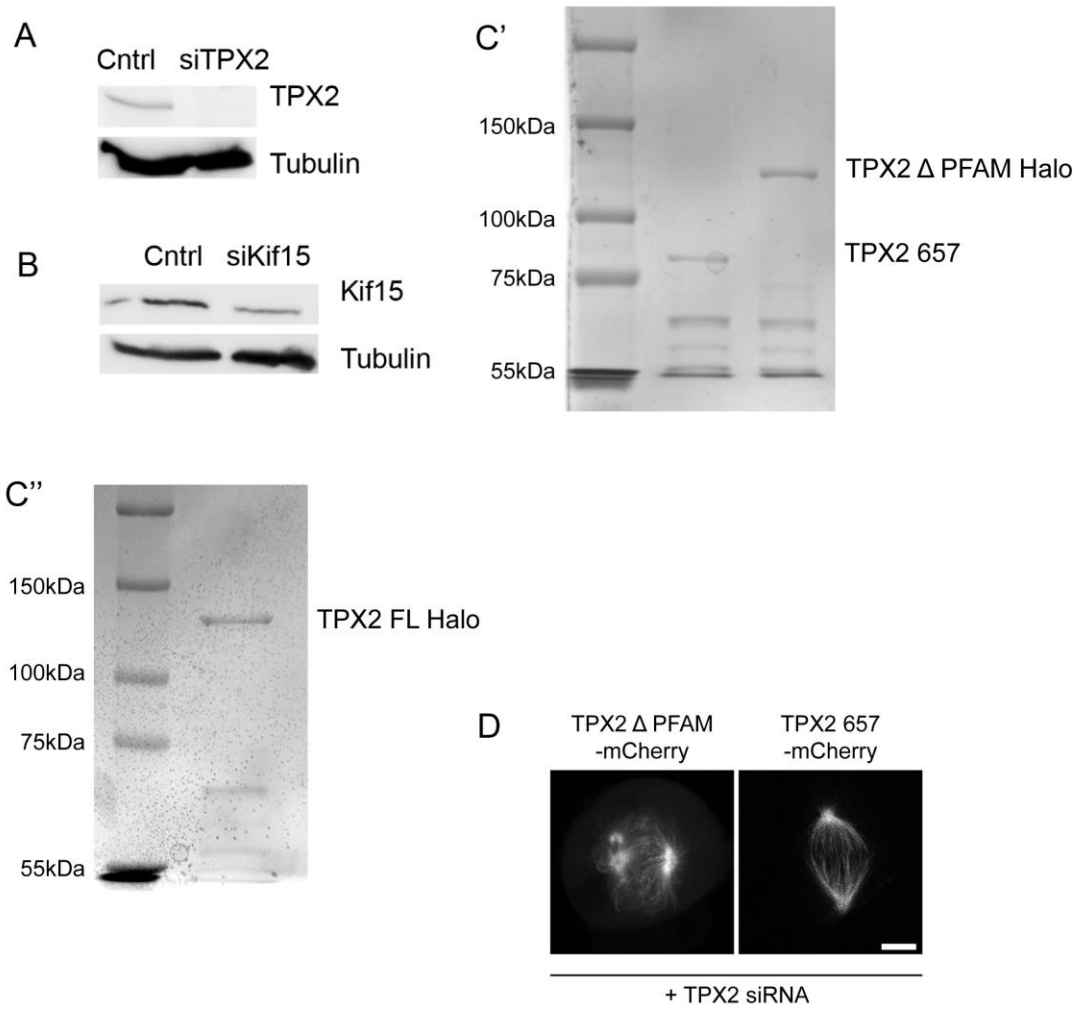

Figure 3.5 TPX2 constructs purified from bacteria and binding to microtubules *in vivo*. Western blot showing protein depletion following siRNA treatment. (A) TPX2, (B) Kif15. Tubulin was used as a loading control (lower). For the blots shown, TPX2 was depleted 95% and Kif15 75.5%. (C', C'') Polyacrylamide gel showing the truncated and full length TPX2 proteins used in *in vitro* experiments. (D) Images of truncated TPX2-mCherry constructs bound to microtubules in LLC-Pk1 cells depleted of full length TPX2 using siRNA. Molecular weight of markers in kilodaltons. Marker bar = 5 μm.

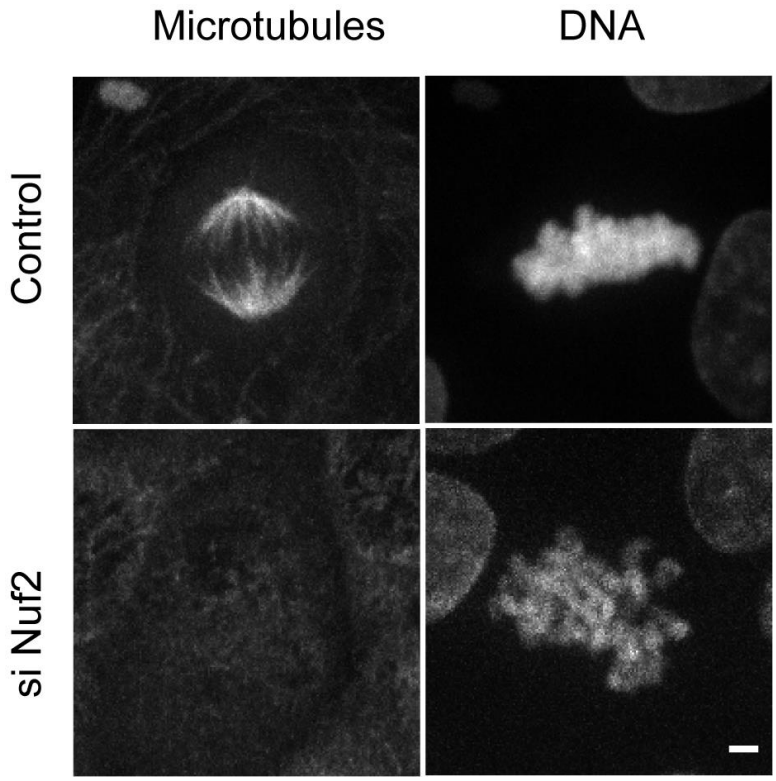

Figure 3.6 Depletion of Nuf2 reduces cold-stable kinetochore fibers. LLC-Pk1 cells were treated with siRNA targeting Nuf2, treated with 5 □M MG132 to arrest cells in metaphase, and then in ice-cold medium for 10 min, fixed and stained for microtubules and DNA. Bar = 2 μm.

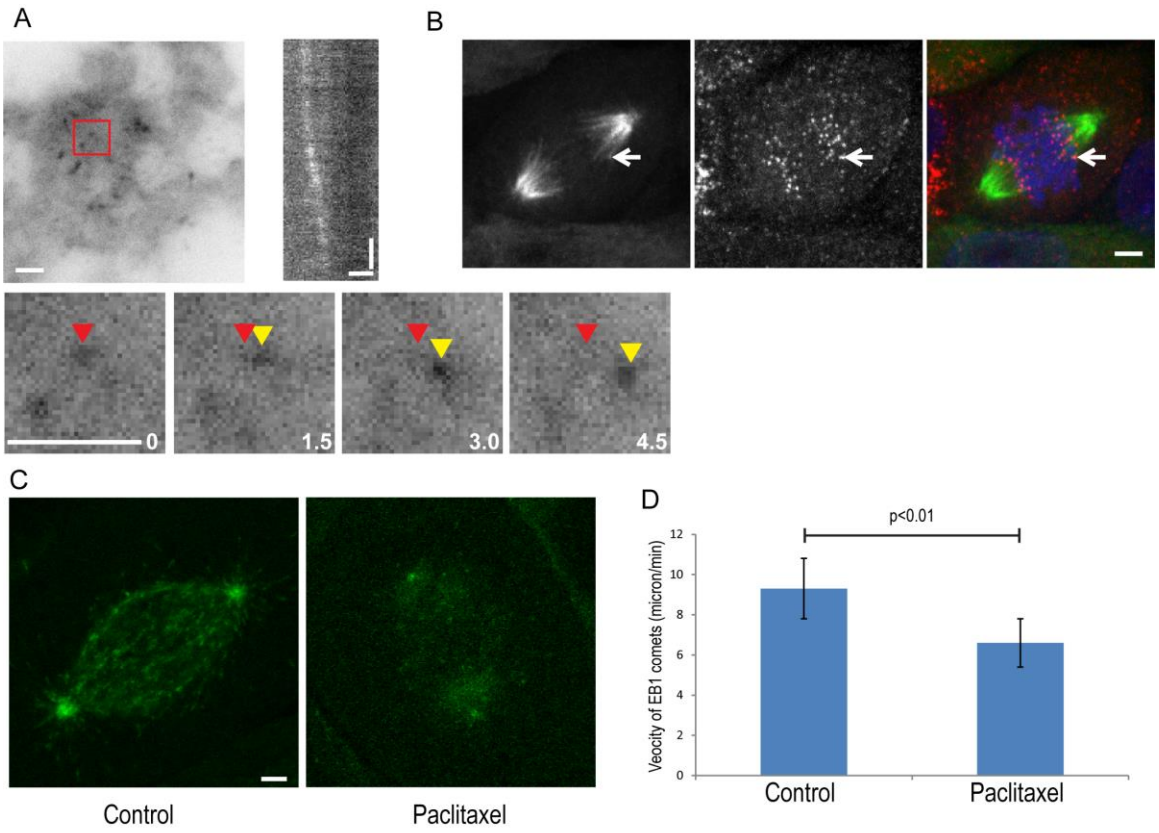

Figure 3.7 Tracking GFP-Kif15 and EB1 puncta *in vivo*. (A) TIRF microscopy of GFP-Kif15 expressing cells; region marked with red box is shown enlarged in lower panels; red arrowhead shows initial position of puncta (contrast inverted); yellow arrow marks puncta. Time in seconds. Kymograph of an individual puncta of GFP-Kif15 (upper right); time: vertical axis; distance: horizontal axis. (B) GFP-Kif15 associates with kinetochore fibers in anaphase. Image of GFP-Kif15 expressing cell fixed and stained with antibodies to Hec1 to mark kinetochores. GFP-Kif15 (left) associates with fibers that end at Hec1 positive dots (middle). (C,D) Microtubule dynamics in LLC-Pk1 cells treated with Paclitaxel. (C) Live cells expressing GFP-EB1; control (left) and Paclitaxel treated (right). (D) Velocity of GFP-EB1 dashes in control and Paclitaxel treated. Bar = 2 μm; error bars show Std. Dev.

3.5 References

Balchand, S.K., B.J. Mann, J. Titus, J.L. Ross, and P. Wadsworth. 2015. TPX2 Inhibits Eg5 by Interactions with Both Motor and Microtubule. *The Journal of biological chemistry*. 290:17367-17379.

Barlan, K., W. Lu, and V.I. Gelfand. 2013. The microtubule-binding protein ensconsin is an essential cofactor of kinesin-1. *Curr. Biol.* 23:317-322.

Blangy, A., L. Arnaud, and E.A. Nigg. 1997. Phosphorylation by p34cdc2 protein kinase regulates binding of the kinesin-related motor HsEg5 to the dynactin subunit p150. *The Journal of biological chemistry*. 272:19418-19424.

Blangy, A., H.A. Lane, P. d'Herin, M. Harper, M. Kress, and E.A. Nigg. 1995. Phosphorylation by p34cdc2 regulates spindle association of human Eg5, a kinesin-related motor essential for bipolar spindle formation in vivo. *Cell*. 83:1159-1169.

Brunet, S., T. Sardon, T. Zimmerman, T. Wittman, R. Pepperkok, E. Karsenti, and I. Vernos. 2004. Characterization of the TPX2 domains involved in microtubule nucleation and spindle assembly in Xenopus egg extracts. *Mol. Biol. Cell*. 15:5318-5328.

Cai, D., K.J. Verhey, and E. Meyhofer. 2007. Tracking single kinesin molecules in the cytoplasm of mammalian cells. *Biophysical journal*. 92:4137-4144.

DeBonis, S., D.A. Skoufias, L. Lebeau, R. Lopez, G. Robin, R.L. Margolis, R.H. Wade, and F. Kozielski. 2004. In vitro screening for inhibitors of the human mitotic kinesin Eg5 with antimitotic and antitumor activities. *Mol. Cancer Ther.* 3:1079-1090.

Dixit, R., J.L. Ross, Y.E. Goldman, and E.L. Holzbaur. 2008. Differential regulation of dynein and kinesin motor proteins by Tau. *Science (New York, N.Y.)*. 319:1086-1089.

Drechsler, H., T. McHugh, M.R. Singleton, N.J. Carter, and A.D. McAinsh. 2014. The Kinesin-12 Kif15 is a processive track-switching tetramer. *eLife*. 3:e01724.

Dreschler, H., and A.D. McAinsh. 2016. Kinesin-12 motors cooperate to suppress microtubule catastrophes and drive the formation of parallel microtubule bundles. *Proc. Nat'l. Acad. Sci. USA*. 113:E1635-E1644.

Eckerdt, F., P.A. Eyers, A.L. Lewellyn, C. Prigent, and J.L. Maller. 2008. Spindle pole regulation by a discrete Eg5-interacting domain in TPX2. *Current biology : CB*. 18:519-525.

Ferenz, N.P., A. Gable, and P. Wadsworth. 2010. Mitotic functions of kinesin-5. *Seminars in cell & developmental biology*. 21:255-259.

Ferenz, N.P., R. Paul, C. Fagerstrom, A. Mogilner, and P. Wadsworth. 2009. Dynein antagonizes eg5 by crosslinking and sliding antiparallel microtubules. *Current biology : CB*. 19:1833-1838.

Fu, J., M. Bian, G. Xin, Z. Deng, J. Luo, X. Guo, H. Chen, Y. Wang, Q. Jiang, and C. Zhang. 2015. TPX2 phosphorylation maintains metaphase spindle length by regulating microtubule flux. *J. Cell Biol.* 210:373-383.

Gable, A., M. Qiu, J. Titus, S. Balchand, N.P. Ferenz, N. Ma, E.S. Collins, C. Fagerstrom, J.L. Ross, G. Yang, and P. Wadsworth. 2012. Dynamic

reorganization of Eg5 in the mammalian spindle throughout mitosis requires dynein and TPX2. *Molecular biology of the cell*. 23:1254-1266.
Groen, A.C., D. Needleman, C. Brangwynne, C. Gradinaru, B. Fowler, R. Mazitschek, and T.J. Mitchison. 2008. A novel small-molecule inhibitor reveals a possible role of kinesin-5 in anastral spindle-pole assembly. *J. Cell Sci.* 121:2293-2300.
Gruss, O.J., and I. Vernos. 2004. The mechanism of spindle assembly: functions of Ran and its target TPX2. *J. Cell Biol.* 166:949-955.
Gruss, O.J., M. Wittmann, H. Yokoyama, R. Pepperkok, T. Kufer, H. Sillje, E. Karsenti, I.W. Mattaj, and I. Vernos. 2002. Chromosome-induced microtubule assembly mediated by TPX2 is required for spindle formation in HeLa cells. *Nature cell biology*. 4:871-879.
Honnappa, S., S.M. Gouveia, A. Weisbrich, F.F. Damberger, N.S. Bhavesh, H. Jawhari, I. Grigoriev, F.J. van Rijssel, R.M. Buey, A. Lawera, I. Jelesarov, F.K. Winkler, K. Wuthrich, A. Akhmanova, and M.O. Steinmetz. 2009. An EB1-binding motif acts as a microtubule tip localization signal. *Cell*. 138:366-376.
Kalab, P., A. Pralle, E.Y. Isacoff, and K. Weis. 2006. Analysis of a RanGTP-regulated gradient in mitotic somatic cells. *Nature*. 440:697-701.
Kapitein, L.C., E.J. Peterman, B.H. Kwok, J.H. Kim, T.M. Kapoor, and C.F. Schmidt. 2005. The bipolar mitotic kinesin Eg5 moves on both microtubules that it crosslinks. *Nature*. 435:114-118.
Laemmli, U.K. 1970. Cleavage of structural proteins during the assembly of the head of bacteriophase T4. *Nature*. 227:680-685.
Li, C., Y. Zhang, Q. Yang, F. Ye, S.Y. Sun, E.S. Chen, and Y.C. Liou. 2016. NuSAP modulates the dynamics of kinetochore microtubules by attenuating MCAK depolymerization activity. *Scientific reports*. 6.
Lowry, O.H., N.J. Rosenbrough, A.L. Farr, and R.J. Randall. 1951. Protein measurement with the Folin phenol reagent. *J. Biol. Chem.* 193:265-275.
Ma, N., J. Titus, A. Gable, J.L. Ross, and P. Wadsworth. 2011. TPX2 regulates the localization and activity of Eg5 in the mammalian mitotic spindle. *The Journal of cell biology*. 195:87-98.
Meunier, S., and I. Vernos. 2016. Acentrosomal microtubule assembly in mitosis: the where, when and how. *Trends in Cell Biol.* 26:80-87.
Nousiainen, M., H.H.W. Sillje, G. Sauer, E.A. Nigg, and R. Korner. 2006. Phosphoproteome analysis of the human mitotic spindle. *Proc. Nat'l. Acad. Sci. USA.* 103:5391-5396.
O'Connell, C.B., J. Loncarek, P. Kalab, and A. Khodjakov. 2009. Relative contributions of chromatin and kinetochores to mitotic spindle assembly. *J. Cell Biol.* 187:43-51.
Piehl, M., U.S. Tulu, P. Wadsworth, and L. Cassimeris. 2004. Centrosome maturation: measurement of microtubule nucleation throughout the cell cycle using GFP tagged EB1. *Proc. Natl. Acad. Sci. USA.* 101:1584-1588.
Raaijmakers, J.A., R.G. van Heesbeen, J.L. Meaders, E.F. Geers, B. Fernandez-Garcia, R.H. Medema, and M.E. Tanenbaum. 2012. Nuclear envelope-associated dynein drives prophase centrosome separation and enables Eg5-independent bipolar spindle formation. *EMBO J.*

Reid, T.A., B.M. Schuster, B.J. Mann, S.K. Balchand, M. Plooster, M. McClellan, C.E. Coombes, P. Wadsworth, and M.K. Gardner. 2016. Suppression of microtubule assembly kinetics by the mitotic protein TPX2. *J. Cell Sci.* 129:1319-1328.

Roostalu, J., N.I. Cade, and T. Surrey. 2015. Complementary activities of TPX2 and chTOG constitute an efficient importin-rregulated microtubule nucleation module. *Nat. Cell Biol.* 17:1422-1437.

Sturgill, E.G., D.K. Das, Y. Takizawa, Y. Shin, S.E. Collier, M.D. Ohi, W. Hwang, M.J. Lang, and R. Ohi. 2014. Kinesin-12 Kif15 targets kinetochore fibers through an intrinsic two-step mechanism. *Current biology : CB.* 24:2307-2313.

Sturgill, E.G., S.R. Norris, Y. Guo, and R. Ohi. 2016. Kinesin-5 inhibitor resistance is driven by kinesin-12. *The Journal of cell biology*. 213:213-227.

Sturgill, E.G., and R. Ohi. 2013. Kinesin-12 differentially affects spindle assembly depending on its microtubule substrate. *Current biology : CB.* 23:1280-1290.

Tanenbaum, M.E., L. Macurek, A. Janssen, E.F. Geers, M. Alvarez-Fernandez, and R.H. Medema. 2009. Kif15 cooperates with eg5 to promote bipolar spindle assembly. *Current biology : CB.* 19:1703-1711.

Toso, A., J.R. Winter, A.J. Garrod, A.C. Amaro, P. Meraldi, and A.D. McAinsh. 2009. Kinetochore-generated pushing forces separate centrosomes during bipolar spindle assembly. *J. Cell Biol.* 184:365-372.

Tulu, U.S., C. Fagerstrom, N.P. Ferenz, and P. Wadsworth. 2006. Molecular requirements for kinetochore-associated microtubule formation in mammalian cells. *Curr. Biol.* 16:536-541.

Tulu, U.S., N. Rusan, and P. Wadsworth. 2003. Peripheral, non-centrosome-associated microtubules contribute to spindle formation in centrosome containing cells. *Curr. Biol.* 13:1894-1899.

Uteng, M., C. Hentrich, K. Miura, P. Bieling, and T. Surrey. 2008. Poleward transport of Eg5 by dynein-dynactin in Xenopus laevis egg extract spindles. *The Journal of cell biology*. 182:715-726.

vanHeesbeen, R.G., J.A. Raaijmakers, M.E. Tanenbaum, V.A. Halim, D. Lelieveld, C. Lieftink, A.J. Heck, D.A. Egan, and R.H. Medema. 2016. Aurora A, MCAK, and Kif18b promote Eg5-independent spindle formation. *Chromosoma*. 125:1-14.

Vanneste, D., M. Takagi, N. Imamoto, and I. Vernos. 2009. The role of Hklp2 in the stabilization and maintenance of spindle bipolarity. *Current biology : CB.* 19:1712-1717.

Verhey, K.J., N. Kaul, and V. Soppina. 2011. Kinesin assembly and movement in cells. *Annu. Rev. Biophys.* 40:267-288.

Waitzman, J.S., and S.E. Rice. 2014. Mechanism and regulation of kinesin-5, an essential motor for the mitotic spindle. *Biology of the cell*. 106:1-12.

Weinger, J.S., M. Qiu, G. Yang, and T.M. Kapoor. 2011. A nonmotor microtubule binding site in kinesin-5 is required for filament crosslinking and sliding. *Current biology : CB.* 21:154-160.

Wignall, S.M., and A.M. Villeneuve. 2009. Lateral microtubule bundles promote chromosome alignment during acentrosomal oocyte meiosis. *Nat Cell Bio*. 11:839-844.

Wittmann, T., H. Boleti, C. Antony, E. Karsenti, and I. Vernos. 1998. Localization of the kinesin-like protein Xklp2 to spindle poles requires a leucine zipper, a

microtubule-associated protein, and dynein. *The Journal of cell biology*. 143:673-685.

Wittmann, T., M. Wilm, E. Karsenti, and I. Vernos. 2000. TPX2, a novel Xenopus MAP involved in spindle pole organization. *J. Cell Biol.* 149:1405-1418.

Yvon, A.C., P. Wadsworth, and M.A. Jordan. 1999. Taxol suppresses dynamics of individual microtubules in living human tumor cells. *Molec. Biol. Cell*. 10:947-959.

CHAPTER 4

SRC FAMILY KINASE PHOSPHORYLATION OF THE MOTOR DOMAIN OF THE HUMAN KINESIN-5, EG5

This chapter is adapted from Bickel et al. 2017 and was completed with the guidance of Patricia Wadsworth. This project was performed in collaboration with Kathleen G. Bickel (Northwestern Medical School), Joshua S. Waitzman (Northwestern Medical School) and Taylor A. Poor (Northwestern Medical School) under the guidance of Dr. Sarah E. Rice (Northwestern Medical School). KGB performed *in vitro* phosphorylation assays, immunoprecipitations, and bacterial protein purifications. JSW performed initial *in silico* and *in vitro* work, ITC experiments and assisted KGB with microtubule gliding assays. JSW and TAP performed Mass Spectrometry and analysis (data not shown).

4.1 Introduction

Chromosome segregation during mitosis requires the mitotic spindle, a dynamic structure composed of microtubules (MTs), motor proteins, and non-motor MT-associated proteins. All spindles are bipolar and in most cell types, spindle bipolarity relies on the activity of kinesin-5 motor proteins (Blangy et al., 1995; Enos and Morris, 1990; Goshima and Vale, 2003; Hagan and Yanagida, 1990; Hoyt et al., 1992; Kapitein et al., 2005; Scholey et al., 2014). The bipolar arrangement of tetrameric kinesin-5 family members allows them to crosslink and slide MTs originating from each of the two centrosomes, thus establishing the bipolar spindle (Kapitein et al., 2005). Inhibition of the mammalian kinesin-5, Eg5, early in mitosis induces the formation of monopolar

spindles that are incapable of proper chromosome segregation (Goshima and Vale, 2003; Maliga et al., 2002).

During spindle formation, outward forces generated by kinesin-5 and other motors are opposed by motor-dependent inward forces. How these forces are balanced and regulated remains incompletely understood (Brust-Mascher et al., 2009; Ferenz et al., 2010; Saunders et al., 1997; Tanenbaum et al., 2008). Past studies have shown that phosphorylation of the kinesin-5 tail domain and interaction with binding partners such as TPX2 are important for motor localization to the spindle (Blangy et al., 1997; Blangy et al., 1995; Ma et al., 2011; Ma et al., 2010). Phosphatase and tensin homolog (PTEN) activity has also been shown to contribute to Eg5 localization (He et al., 2016). Other work demonstrated that phosphorylation of the motor domain contributes to kinesin-5 regulation in yeast and *Drosophila* (Avunie-Masala et al., 2011; Garcia et al., 2009; Shapira and Gheber, 2016; Shapira et al., 2017); whether similar modifications affect Eg5 is not yet established.

Although Eg5 is mostly degraded as cells exit mitosis (Uzbekov et al., 1999; Venere et al., 2015), some studies show an interphase function for the motor in neurons, where it contributes to neuronal migration and growth cone behavior (Falnikar et al., 2011; Myers and Baas, 2007; Nadar et al., 2008; Venere et al., 2015). Eg5 fails to undergo cell-cycle regulated degradation in patient-derived glioblastoma cells and contributes to the invasive behavior of these cells (Venere et al., 2015). These data suggest that Eg5 function is precisely regulated by a variety of mechanisms, and that dysregulation of Eg5 function can contribute to human disease.

Here we present evidence that Eg5 is phosphorylated at three sites in its motor domain by Src family kinases (SFKs) in mammalian cells. This phosphorylation modulates Eg5 activity *in vitro* and spindle morphology *in vivo*. Several SFKs, particularly those that are activated and upregulated in mitosis (c-Src, Fyn, c-Yes, and Lyn; (Kuga et al., 2007) overlap in substrate and inhibitor specificity (Thomas and Brugge, 1997). Therefore, in this work we refer to the SFKs as kinases collectively acting on Eg5, except when discussing experiments that specifically use c-Src. SFKs are best known for activating cell proliferation, migration, and cytoskeletal reorganization (Sen and Johnson, 2011). Their dysregulation also contributes to oncogenesis (Kim et al., 2009) and recent data points to a new role for SFKs in regulating spindle establishment and orientation (Nakayama et al., 2012). Other recent work suggests that phosphotyrosine (pTyr) modifications are more prevalent than previously appreciated, particularly in the kinetochore/spindle region and particularly by SFKs (Caron et al., 2016). To date, however, few mitotic SFK targets have been identified and none of them are known to regulate the MT cytoskeleton (Bhatt et al., 2005; Fumagalli et al., 1994; Wang et al., 2008). SFK phosphorylation of the Eg5 motor domain is potentially a novel regulatory mode that links SFK activity to the MT cytoskeleton during spindle establishment and may provide insight into how Eg5 becomes dysregulated in the context of cancer.

4.2 Results and Discussion

4.2.1 Endogenous Eg5 is phosphorylated on motor domain tyrosines in mammalian cells

To test whether Eg5 is phosphorylated on tyrosine residues, we immunoprecipitated Eg5 from HEK293T cells and used a two-color Western blot to probe for tyrosine phosphorylation (Fig. 4.1 A; signals from red (Eg5) and green (pTyr) channels are displayed separately). We observed co-localization of pTyr and Eg5 signals, suggesting that human Eg5 is phosphorylated on tyrosines. Additionally, we observed tyrosine phosphorylation of Eg5 immunoprecipitated from pig-derived LLC-Pk1 cells (Fig. 4.1 A). Treatment of immunoprecipitated Eg5 with lambda phosphatase diminished pTyr signal (Fig. 4.4 A), confirming that the anti-pTyr antibody binds specifically to phosphorylated protein. These data and previous work showing that Eg5 is phosphorylated at multiple tyrosines in the motor domain (Fig. 4.1 B, 4.4 B; (Han et al., 2010; Hornbeck et al., 2015; Iliuk et al., 2010; Kim et al., 2010; Li et al., 2009; Luo et al., 2008) establish that mammalian Eg5 is phosphorylated on tyrosines.

4.2.2 Src kinase phosphorylates Eg5 more efficiently than Wee1 *in vitro*

Previous data reported that the mitotic kinase Wee1 phosphorylates the *Drosophila* kinesin-5, KLP61F, at three tyrosines in the motor head, including the tyrosine homologous to mammalian Y211 (Garcia et al., 2009). However, querying the complete Eg5 peptide sequence in the Scansite 3 kinase predictor site (Methods; (Obenauer et al., 2003) suggested SFKs as potential kinases targeting Y211. In addition, a Src homology domain 3 (SH3) targeting sequence (–PXXP–) is located in the MT

binding face of several kinesin-5s, including Eg5 (Fig. 4.1 B, inset, Fig. 4.1 C and Fig. 4.4 C-D; (Kim et al., 2010). Furthermore, post-translational modification databases recorded Y125, Y211, and Y231 as phosphorylation sites in the motor domain (Fig. 4.4 B; (Hornbeck et al., 2015; Li et al., 2009). We performed *in vitro* kinase assays to test whether Eg5 motor heads could be phosphorylated on these residues and to compare the ability of c-Src and Wee1 to phosphorylate Eg5 motor heads *in vitro* (Fig. 4.2 A, B).

For all *in vitro* kinase assays we used a previously well-characterized 367-amino acid monomeric Eg5 motor head construct (Eg5-367; (Cochran and Gilbert, 2005; Cochran et al., 2004; Maliga et al., 2002) that additionally harbored an E270A mutation in the active site (termed Eg5-367 E270A; in KLP61F-364, E266A was mutated, Fig. 4.4 E, F). This mutation served to abolish the basal ATPase activity of Eg5 and thus to prevent motor heads from depleting the kinase's supply of ATP during the assay (Methods; (Kull et al., 1996). We incubated either human c-Src or human Wee1 (Fig. 4.2 A, B) with the indicated kinesin-5 substrates and radiolabeled ATP. In addition to Eg5-367 E270A and KLP61F E266A, we also tested a non-phosphorylatable Eg5 mutant with phenylalanines at the three putative sites (Eg5-367-3Y->F E270A), and a -PXXP-null mutant (Eg5-367-GSTY E270A) as kinase substrates (Methods; Fig. 4.4 E). c-Src robustly phosphorylated Eg5-367 E270A and KLP61F E266A motor heads under these conditions (Fig. 4.2 A). c-Src phosphorylated the -PXXP-null construct Eg5-367-GSTY E270A *in vitro*, albeit markedly less efficiently than wild-type (Fig. 4.2 A), suggesting a role for the –PXXP- targeting motif in Eg5 phosphorylation. In contrast to c-Src, Wee1 showed minimal phosphorylation of all motor head constructs, including *Drosophila* KLP61F E266A, despite robust autophosphorylation (Fig. 4.2 B).

To identify the residues phosphorylated by c-Src, we performed an *in vitro* phosphorylation assay with purified Eg5 motor heads and c-Src kinase, and performed liquid chromatography-mass spectrometry (LC-MS) on the trypsinized protein products. The LC-MS data confirmed that c-Src phosphorylated Y211 and Y231 (data not shown; provided by KGB). We generated a construct harboring Y211F and Y231F mutations as well as the E270A mutation and showed that it was still robustly phosphorylated by c-Src. However, an additional Y125F mutation diminished c-Src phosphorylation of Eg5 to near background levels (data not shown). Notably, c-Src showed no phosphorylation of Eg5-367-3Y->F E270A (Fig. 4.2 A), despite the presence of 7 other tyrosines in the motor head, confirming c-Src phosphorylates Y125. These data show that c-Src phosphorylates Eg5 on Y125, Y211, and Y231, and that this effect is aided by the presence of the SH3-targeting –PXXP- motif in the Eg5 MT binding domain.

4.2.3 SFKs phosphorylate Eg5 in mammalian cells

To examine the ability of c-Src to phosphorylate Eg5 motor heads on Y125, Y211, and Y231 in the cellular environment, we transfected HEK293T cells with either a constitutively active human c-Src construct (c-Src-Active, Fig. 4.4 F), a C-terminal myc-tagged Eg5 motor head construct (Eg5-367myc), or both. We then immunoprecipitated Eg5-367myc from the cells and analyzed the motor heads for phosphorylation by two-color Western blot (Fig. 4.2 C, Methods). In cells co-transfected with c-Src-Active and either Eg5-367myc-WT or Eg5-367myc-GSTY, robust phosphorylation was observed. However, c-Src-Active did not phosphorylate Eg5-367myc-3Y->F. This result shows that c-Src is capable of phosphorylating Eg5 motor heads in a cellular environment and

that it likely phosphorylates Eg5 on the Y125, Y211, and Y231 residues. We did not detect phosphorylation of transfected Eg5-367myc by endogenous SFKs in cells lacking a transfected c-Src-Active construct, as we did for endogenous Eg5. This apparent difference may be because the expressed motor heads lack the tail domain, which is required for localization of Eg5 to spindles (Blangy et al., 1995; Rapley et al., 2008), where a subset of SFKs is known to localize during mitosis (David-Pfeuty et al., 1993; Levi et al., 2010; Ley et al., 1994). Phosphorylation was not observed in cells co-transfected with c-Src-Active and Eg5 motor heads and treated with the SFK-specific inhibitor, A-419259 (Fig. 4.2C; (Calderwood et al., 2002). This confirms that phosphorylation of Eg5-WT and Eg5-GSTY motor heads was due to c-Src-Active.

Finally, we used a chemical genetics approach to determine whether SFKs phosphorylated endogenous Eg5 in cells. We transfected HEK293Ts with either an empty vector control, cSrc-Active, or a constitutively active point mutant of c-Src that is resistant to A-419259 (cSrc-IR, Fig. 4.4 F), with or without treatment with A-419259, and measured endogenous Eg5 phosphorylation (Fig. 4.2 D). Phosphorylation of endogenous Eg5 was detected even in the absence of transfected c-Src but was significantly enhanced following transfection of cSrc-Active. In both cases treatment with A-419259 abrogated Eg5 phosphorylation. In contrast, Eg5 from cells transfected with the resistant cSrc-IR showed robust phosphorylation regardless of whether they were treated with A-419259. These results strongly suggest that Eg5 tyrosine phosphorylation in cells is dependent on SFK activity.

In summary, these data show Eg5 is phosphorylated in an SFK-dependent manner at the same three residues both *in vitro* and in cells. Also, since the A-419259 inhibitor

that blocked Eg5 phosphorylation in cells is relatively specific for SFKs (Calderwood et al., 2002; Wilson et al., 2002), these results give us confidence that SFKs phosphorylate Eg5.

4.2.4 Tyrosine phosphomimetic mutants alter Eg5 activity *in vitro*

Since Eg5 motor domains are phosphorylated in an SFK-dependent manner, we tested how phosphomimetic mutations at Y125, Y211, and Y231 affect Eg5 motor activity. For these experiments we generated phosphomimetic (E) and non-phosphorylatable (F) mutants of Eg5-367, as well as the -PXXP-null mutant, Eg5-367-GSTY (Fig. 4.4 E). We measured both the MT-stimulated ATPase rate and MT-sliding motility velocities (Methods) for each mutant and compared these rates to both wild-type monomeric Eg5 motor heads and an Eg5-367 construct lacking the eight residues ^{125}YTWEEDPL$_{132}$ from loop L5 (Eg5-367-DL5, Fig. 4.4 E; (Maliga et al., 2002). L5 includes Y125 and lies near Y211. The Eg5-Y211E phosphomimetic mutant exhibited the greatest changes in activity, with an ATPase rate and sliding velocity that were two-fold and three-fold decreased compared to wild-type, respectively (Table 4.1). In fact, Eg5-367-Y211E motor properties were quite similar to those of Eg5-367-DL5 (Table 4.1), consistent with the idea that SFK-dependent phosphorylation may regulate Eg5 by directly altering its motor characteristics, although other mechanisms are possible.

L5 is the binding site for many small molecule inhibitors of Eg5 (Maliga et al., 2002) some of which are in clinical trials for use as cancer therapy (Sarli and Giannis, 2008). One could speculate based on our results that Eg5 phosphorylation may affect inhibitor efficacy, and vice-versa (Smith et al., 2015). As a preliminary test of this, we

conducted isothermal calorimetry (ITC) experiments (methods and data provided by KGB) to measure the binding affinity of the Eg5-367 phosphomimetic and non-phosphorylatable mutants for the inhibitor s-trityl-L-cysteine (STLC), which binds near L5 in human Eg5 (Kim et al., 2010; Skoufias et al., 2006a). The ITC data showed that each of the phosphomimetic mutations significantly diminished STLC binding to Eg-367, and the largest effect was observed for the Y211 E mutant (Table 4.1). Binding of STLC to the non-phosphorylatable mutants was similar to wild-type (Table 4.1).

Phosphomimetic mutations give only a first approximation of the effects of a uniformly phosphorylated protein sample, but the latter is nearly impossible to generate. Corroborating our results, L5 is a major conformational regulator of the Eg5 mechanochemical cycle, and several mutations and deletions in this region diminish motor activity (Behnke-Parks et al., 2011; Kaan et al., 2009; Maliga and Mitchison, 2006; Maliga et al., 2006; Muretta et al., 2013; Waitzman et al., 2011). Furthermore, key structural transitions during the Eg5 mechanochemical cycle require pi-stacking and hydrophobic interactions between Y211 and residues in L5, specifically W127; L5 inhibitors bind through similar interactions (Muretta et al., 2015). By introducing a negatively-charged glutamate residue at position 211 we are most likely abolishing those interactions. It is worth noting that phosphate groups have double the negative charge and increased bulk relative to glutamate (Waksman et al., 1992). In summary, the available structural data suggest that any substantial modification in the L5 region, including phosphomimetic mutation or phosphorylation, is likely to affect Eg5 motor properties, and that phosphorylating Y211 would be at least as disruptive to the mechanochemical

cycle as a glutamate phosphomimetic mutation. Based on these results and our ITC data, we would expect that phosphorylation would similarly disrupt L5 inhibitor binding.

4.2.5 SFK phosphorylation of Eg5 regulates spindle morphology

Because Eg5 plays a critical role in mitotic spindle assembly and maintenance, we next assessed the effects of SFK phosphorylation of Eg5 on mitotic spindle morphology. LLC-Pk1 cells were used for these studies because they remain relatively flat during mitosis, facilitating imaging. In initial experiments, we transfected cells with plasmids encoding Emerald-tagged Eg5 with mutations at Y125, Y211, and Y231, to generate stable cell lines for use in experiments. Despite multiple attempts, we were unable to achieve this, suggesting that these mutants have deleterious effects on cell division. Next we adapted and optimized a previously described protein replacement strategy (Gable et al., 2012; Zaytsev et al., 2014), in which we expressed Emerald-tagged Eg5 wild-type, phosphomimetic, and non-phosphorylatable mutants, while simultaneously inhibiting endogenous Eg5 expression using siRNA (Methods). For these experiments, we targeted Y211, which has been shown to alter mitosis in *Drosophila* (Garcia et al., 2009) and resulted in the most pronounced defects in Eg5 motor behavior *in vitro* (Table 4.1). Using this protocol, endogenous Eg5 protein levels decreased to approximately 50% of wild-type (Fig. 4.5) which caused cells to exhibit a large percentage of monopolar spindles (56% of cells), consistent with previous work (Goshima and Vale, 2003; Ma et al., 2010; Mayer et al., 1999; Skoufias et al., 2006a). Spindle bipolarity was rescued (81%) when LLC-Pk1 cells were co-transfected with Eg5 siRNA and an siRNA-resistant Eg5-WT-Emerald construct (Eg5-WT-Em, Fig. 4.3 A). In contrast, co-transfection of

cells with siRNA and siRNA-resistant phosphomimetic Eg5-Y211E-Em resulted in a significant increase in monopolar spindles as compared to the wild-type rescue construct ($p < 0.01$), suggesting that modification of this site inhibits Eg5 activity in mitosis (Fig. 4.3 A). When this site was made non-phosphorylatable (Y211F) there was also a significant increase in spindle defects, specifically disorganized spindles ($p<0.01$). Aberrant spindles that could not be designated as monopoles or multipoles and included spindles with extra foci, fragmented poles, shorter length, and bent morphology were classified as disorganized (Fig. 4.3 A). In addition to these phosphomimetic and non-phosphorylatable mutants, we also tested the -PXXP-null mutant (GSTY) which alters the MT binding site. As expected, since the GSTY mutation weakens MT binding by Eg5 (Table 4.1), there was a significant increase in monopolar spindles as compared to the wild-type rescue construct ($p<0.01$).

To determine whether the monopolar spindle phenotype resulted from spindle collapse or from failure of centrosome separation we performed live cell imaging of mCherry-tubulin-expressing LLC-Pk1 cells. Cells co-transfected with siRNA targeting Eg5 and rescued with Eg5-WT-Em progressed through mitosis (Fig. 4.3 B). In contrast, cells rescued with Eg5-Y211E-Em initially formed a bipolar spindle that eventually collapsed into a monopolar spindle. Residual endogenous Eg5 in the siRNA treated cells, or the presence of Kif15, which functions redundantly with Eg5, could support the initial bipolarization in these cells (Tanenbaum et al., 2009; Vanneste et al., 2009). Distinct from the monopolar spindles observed in cells rescued with Eg5-Y211E-Em, cells rescued with Eg5-Y211F-Em formed disorganized spindles, consistent with the disorganized phenotype observed in fixed cells (Fig. 4.3 B).

While phosphomimetic Eg5 is an imperfect substitution for phosphorylated protein, generating cells with hyper-phosphorylated Eg5 is not trivial. Mitosis involves a complicated and inter-connected network of kinase signaling that is highly regulated (Caron et al., 2016). Simply over-expressing c-Src kinase would not guarantee that Eg5 is hyper-phosphorylated at Y211 and the interpretation of spindle phenotypes would be complicated by the effect of c-Src overactivation on other mitotic targets, potentially including other mitotic kinases. Thus, the use of phosphomimetics allows us to examine the effects in cells of introducing a negative charge at position 211 directly.

In addition to evaluating spindle phenotypes using cells expressing non-phosphorylatable and phosphomimetic mutants of Eg5, we treated non-synchronized LLC-Pk1 cells with the SFK inhibitor SU6656. Similar to our observations in LLC-Pk1 cells expressing the non-phosphorylatable Eg5-Y211F-Em, we observed that LLC-Pk1 cells treated with SU6656 (Methods) displayed high percentages of disorganized mitotic spindles (Fig. 4.3 C, D). Consistent with this, Nakayama et al. observed mis-oriented spindles in HeLa cells treated with the SFK inhibitor PP2 (Nakayama et al., 2012). The SU6656 inhibitor we used has been reported to have some activity on other kinases that contribute to spindle formation, for example, Aurora kinases (Bain et al., 2007). To determine if treatment with SU6656 inhibits Aurora A, we stained LLC-Pk1 cells for phosphorylated Aurora A after treatment with SU6656 (Fig. 4.3 E). Phosphorylated Aurora A was detected at spindle poles/centrosomes, similar to controls. Additionally, cells treated with BI-2536, an inhibitor of the mitotic kinase Plk1, showed a phenotype distinct from cells treated with SU6656, with pronounced bundling of interzonal microtubules in anaphase (Fig. 4.3 F; (Brennan et al., 2007). Under these conditions

(Methods), we did not observe a statistically significant increase in disorganized spindles as with SU6656 or monopolar spindles as had been previously reported (Lenart et al., 2007). These results suggest that SFK inhibition alters spindle phenotypes in a manner distinct from inhibition of other mitotic kinases indicating that the phenotype of cells treated with SU6656 is not due to off-target effects.

Distinct spindle phenotypes were observed in LLC-Pk1 cells transfected with either Eg5-Y211E-Em or Eg5-Y211F-Em mutants suggesting that the optimal properties of Eg5 are tuned by phosphorylation such that abnormal mitotic phenotypes can occur when Eg5 is either hyperphosphorylated or hypophosphorylated at this site. The simple model is that Eg5 phosphorylation at Y211 alters spindle phenotypes by inhibiting its motor activity, because of the inhibitory effects seen in Table 4.1 and the monopolar phenotype in cells expressing Eg5-Y211-E-Em (Goshima and Vale, 2003; Ma et al., 2010; Mayer et al., 1999; Skoufias et al., 2006a). Furthermore, the largely monopolar spindle phenotype of cells expressing the phosphomimetic Y211E mutant is consistent with the decrease in Eg5 motor activity that is observed when cells are treated with L5 inhibitors, which are thought to act by a similar mechanism (Maliga et al., 2002; Muretta et al., 2015). Finally, it is worth noting that in many systems, Eg5 plays an important role in centrosome separation (Tanenbaum et al., 2008; van Ree et al., 2016; Whalley et al., 2015) and the monopolar phenotype observed in cells expressing Eg5-Y211E-Em could be due to abnormal Eg5 activity during this earlier phase of mitosis.

It is less simple to speculate about how overactive Eg5 would cause the multipolar/disorganized spindle phenotype observed in the Eg5-Y211F-Em transfected LLC-Pk1 cells. One possibility is that excessive force from Eg5 in the spindle midzone

could lead to disorganized spindles. A second possibility is that phosphorylation of Eg5 Y211 could also modulate Eg5 localization, protein turnover rates, or its ability to bind MTs, as was observed for the yeast kinesin 5, Cin8p (Shapira and Gheber, 2016). Regardless of how the multipolar/disorganized spindle phenotype arises, its physiological relevance is reinforced by its similarity to the spindle phenotype observed in cells in which SFKs are inhibited, which has both been observed by other groups and is distinct from the phenotypes observed when other mitotic kinases are inhibited (Bain et al., 2007; Brennan et al., 2007; Nakayama et al., 2012).

Given that endogenous Eg5 is homotetrameric (Kapitein et al., 2005; Scholey et al., 2014; van den Wildenberg et al., 2008), it is likely that not all of the Eg5 motor heads in a homotetramer are phosphorylated. Eg5 motor heads are highly cooperative when assembled into dimers (Krzysiak and Gilbert, 2006; Krzysiak et al., 2008), with dimers having distinct kinetic properties from monomers (Cochran et al., 2006; Krzysiak and Gilbert, 2006). Additionally, recent structural studies of the Eg5 coiled-coil domain responsible for the assembly of Eg5 into homotetramers suggests that instead of being a dimer of dimers, each subunit in an Eg5 homotetramer directly contacts every other subunit in a highly intertwined and unique coiled-coil structure (Scholey et al., 2014). These data suggest that phosphorylation of even one motor head within the Eg5 homotetramer could alter the function of the molecule. There is also a substantial body of evidence that mitotic spindle establishment and maintenance involves a balance of forces (Brust-Mascher et al., 2009; Saunders et al., 1997; Tanenbaum et al., 2008), making it feasible that even small changes to Eg5 motor activity could disrupt this balance. In support of this possibility, we observed that endogenous Eg5 was only reduced to 50% of

wild-type levels in our experiments using LLC-Pk1 cells, so one can imagine that many Eg5 homotetramers in our experiments had both mutant and wild-type subunits. Despite this, nearly 90% of cells in those experiments had monopolar spindles (Fig. 4.3 A). The severity of this defect supports the view that either not all of the motors in a heterotetrameric motor are simultaneously modified, or that Eg5 undergoes a cycle of phosphorylation and dephosphorylation *in vivo*.

In summary, these experiments revealed a significant mitotic phenotype in LLC-Pk1 cells expressing Eg5 with phosphomimetic and non-phosphorylatable mutations at Y211, the same site that was shown to impact spindle assembly in *Drosophila* (Garcia et al., 2009). Y211 is a particularly interesting site because it is conserved in both insects and vertebrates, coinciding almost without exception with the presence of a –PXXP– SH3-targeting domain (Fig. 4.1 B, Fig. 4.4 D). Conversely, neither Y211 nor the -PXXP– motif is found in worms, which are viable with diminished levels of kinesin-5, suggesting that this organism has evolved alternative pathways for establishing bipolar spindles (Bishop et al., 2005).

Motor domain phosphorylation has also been described for the yeast kinesin-5, Cin8p (Avunie-Masala et al., 2011; Shapira and Gheber, 2016; Shapira et al., 2017). Only one of these sites, S337 *(H. sapiens* numbering) is in a region of the motor that is conserved in Eg5. Phosphorylation of each of these sites has unique effects on motor behavior including Cin8p microtubule binding, motor directionality, and velocity (Shapira and Gheber, 2016; Shapira et al., 2017). Although the precise locations of these modifications are not conserved from yeast to humans, one notable similarity amongst these modifications is that the changes to Cin8p motor behavior are primarily mediated

by electrostatic interactions, which we find to be a compelling hypothesis for the effects of Eg5 Y211 phosphorylation given the available structural data. Future experiments examining phosphorylation of kinesin-5 motors could illuminate the extent of their modifications and could reveal a potential mechanism by which kinesin-5s are differentially regulated to play similar, but non-identical, roles in varying cell types and species.

Our results support a growing body of data identifying phosphoregulatory mechanisms governing the activity of several different kinesin motors (for example: (Chee and Haase, 2010; DeBerg et al., 2013; Garcia et al., 2009). Previously identified Eg5 phosphoregulatory mechanisms target serine or threonine residues in the motor stalk and tail, and have been reported to affect Eg5 localization to the spindle or centrosome during mitosis (Blangy et al., 1995; Rapley et al., 2008). Our results showing phosphorylation of Eg5 in its motor domain at Y125, Y211, and Y231 suggest that in addition to altering motor localization, phosphoregulatory mechanisms can tune Eg5 enzymatic activity for optimal spindle morphology (Avunie-Masala et al., 2011; Garcia et al., 2009). Furthermore, our data suggest this post-translational modification could affect the efficacy of small molecule inhibitors that bind to L5, although further study is required to gauge whether this has any practical implications for use of Eg5 inhibitors as cancer therapy.

4.3 Materials and Methods

4.3.1 *In silico* prediction of phosphorylated residues in Eg5 and targeting kinases

There are several databases summarizing the results of large-scale proteomics experiments that provide evidence for the post-translational modification of specific residues in thousands of proteins. We searched PhosphositePlus (Hornbeck et al., 2015) and SysPTM (Li et al., 2009) for modifications entered for human Eg5 and narrowed the list of modifications down to tyrosine phosphorylations. We also did a manual search of PubMed articles for entries presenting phosphoproteomics experiments that included human Eg5 in their results. These searches generated a list of putative tyrosine phosphorylation sites in Eg5 (summarized in Fig. 4.4 B).

To generate hypotheses regarding possible kinases targeting human Eg5, we entered its full sequence as found in the UniProt database (accession number P52732, (UniProt, 2015) into the search engine found in the Scansite3 kinase predictor site (Obenauer et al., 2003). We used the "medium stringency" setting, which returns kinases for which the queried protein sequence is in the top percentile of sequences in the vertebrate subset of SWISS-PROT matching the optimal targeting motif (Obenauer et al., 2003). This search revealed three SFKs as possible kinases targeting the Y211 location. It also revealed a –PXXP– SH3 targeting site.

4.3.2 Cloning

Mutagenesis of the Eg5-367 monomer construct has been described previously (Larson et al., 2010). Briefly, Eg5-367 constructs for bacterial expression include the first 367 amino acids of *H. sapiens* Eg5 immediately followed by a C-terminal 6X-histidine

tag in a pRSET plasmid. KLP61F-364 constructs include the first 364 amino acids of the *Drosophila* kinesin-5, KLP61F, similarly followed by a 6X-histidine tag. Phosphomimetic (Y->E) and non-phosphorylatable (Y->F) point mutations were made using Quikchange site-directed mutagenesis (Agilent Technologies, Santa Clara, CA), as were enzymatically inactive mutations (E270A in Eg5-367 and E266A in KLP61F). To generate an Eg5-367 mutant lacking the -PXXP- SH3-targeting motif in its MT-binding domain, site-directed mutagenesis was used to replace residues ^{305}RTPH$_{308}$ with the homologous residues in *H. sapiens* kinesin-1 heavy chain (GSTY). This removes the initial proline from the SH3 targeting motif. The resulting motor can still hydrolyze ATP and bind MTs, albeit at reduced affinity (Table 4.1).

For expression in mammalian cells, we replaced the C-terminal 6X-histidine tag of Eg5-367 constructs with a 10-residue Myc tag (EQKLISEEDL). Myc-tagged Eg5-367 constructs were then cloned into the pcDNA3 vector (gift of Dr. Cara Gottardi, Northwestern University) between the Xho1 and HindIII restriction sites using Phusion polymerase (New England Biolabs, Ipswich, MA). All constructs were verified by sequencing. A mammalian c-Src construct in the pCMV-SPORT6 mammalian expression plasmid was a kind gift from Dr. Thomas Smithgall, University of Pittsburgh. This construct was mutated using Quikchange site-directed mutagenesis to generate a constitutively active c-Src construct (Y527F). This constitutively active construct was then further mutated to render it resistant to treatment with A-419259 (T338M, (Meyn and Smithgall, 2009). All c-Src construct numbering refers to the structure of human c-Src (PDB: 1FMK).

The Eg5-Emerald wild-type (Eg5-WT-Em) construct consisted of full-length human Eg5 fused to pmEmerald with an 18 amino acid linker; expression is under the control of a pCMV promoter. This construct was used to express fluorescent Eg5 in LLC-Pk1 cells, was a gift from the late Dr. Michael Davidson Florida State University and was made siRNA resistant using PCR site-directed mutagenesis (Forward primer: GTCACAAAAGCAATGTGGAAACCTAACTGAAGATCTCAAGACTATAAAGCAG ACCC; reverse primer: CAAAGTTCCTGGGAATGGGTCTGCTTTATAGTCTTGAGATCTTCAGTTAGGTT TCC) and verified by sequencing. Each mutant was then made in this backbone using PCR site-directed mutagenesis and verified by sequencing.

4.3.3 Protein Expression and Purification

Expression and purification of Eg5-367 constructs has been described previously (Larson et al., 2010). Briefly, 6x-His-tagged Eg5-367 and KLP61F-364 constructs were transformed into *E. coli* BL21-CodonPlus(DE3)-RP cells for expression. Cells were grown in TPM media (2% tryptone, 1.5% yeast extract, 137 mM NaCl, 14 mM Na_2HPO_4) with in 50 μg/mL carbenicillin and 34 μg/mL chloramphenicol at 37 ° C while shaking at 200 rpm until cells reached an OD_{600} between 0.6 and 1.0. Plasmid expression was induced through the addition of 0.125 mM IPTG. Cells were allowed to express at 18 ° C overnight. 2 L cultures were then harvested by centrifugation (6,300 rpm for 10 min at 4 ° C) and re-suspended in 20 mL Eg5 lysis buffer (10 mM HEPES, 2 mM $MgCl_2$, 1 mM EGTA, 5% sucrose, 0.02% polyoxyethylenesorbitan monolaurate (TWEEN-20), 10 μM ATP, leupeptin (1 μg/mL), aprotinin (1 μg/mL), pepstatin (1 μg/mL), and 100

μM PMSF, pH 8). Cells were lysed by sonication and the clarified lysate was batch-bound with pre-equlibrated nickel-nitrilotriacetic acid resin (Qiagen, Valencia, CA) for 2 h at 4 ° C. The resin was washed with nickel wash buffer (10 mM HEPES, 2 mM $MgCl_2$, 1 mM EGTA, 5% sucrose, 0.02% TWEEN-20, 10 μM ATP, 300 mM NaCl, and 20 mM imidazole, pH 6) and bound protein eluted in 5 mLs using nickel elution buffer (10 mM HEPES, 2 mM $MgCl_2$, 1 mM EGTA, 5% sucrose, 0.02% TWEEN-20, 10 μM ATP, 300 mM NaCl, and 400 mM imidazole, pH 6). Peak fractions were collected and diluted 20-fold in Buffer A (10 mM HEPES, 2 mM $MgCl_2$, 1 mM EGTA, 5% sucrose, 0.02% TWEEN-20, 10 μM ATP, 1 mM DTT pH 6) to decrease the ionic strength of the buffer. Diluted fractions were then purified further on a 5 mL HiTrap S-Sepharose cation exchange column (GE Healthcare, Little Chalfont, UK). Protein was eluted using a linear 0.05-1 M NaCl gradient. Peak fractions were identified by SDS-PAGE and pooled. After adding an additional 15% sucrose, protein was flash-frozen in liquid nitrogen and stored at -80 ° C until use.

4.3.4 *In vitro* kinase assay

E. coli-purified Eg5-367 E270A and KLP61F-364 E266A proteins were first dialyzed against Src kinase assay buffer (10 mM HEPES pH 6.8, 2 mM $MgCl_2$, 1 mM EGTA, 2.0 mM DTT, 10% glycerol, 0.02% TWEEN-20). Each reaction contained 3 μM Eg5 protein, [γ^{32}P]-ATP (Perkin-Elmer) to 50 nCi acitivity per reaction, and 200 μM ATP. Src kinase (Invitrogen, Carlsbad, CA) was diluted to a concentration of 2 μM in assay buffer with 0.2 mg/mL BSA (Sigma-Aldrich, St. Louis, MO), and 2 μL of this solution was added to each 20 μL reaction. Reactions were incubated at 30 º C for the

indicated reaction times, quenched with SDS sample buffer and run on an SDS-PAGE gels using the formulation of Laemmli (Laemmli, 1970). Gels were dried and exposed to film for 30 min.

Wee1 kinase assays were performed identically except for the buffer used. A Wee1 kinase assay buffer based on conditions cited by Garcia et al. (Garcia et al., 2009) was used instead (50 mM HEPES ph 6.8, 15 mM $MgCl_2$, 1 mM EGTA, 2 mM DTT, 10% glycerol).

4.3.5 Coupled-enzyme ATPase assay

MTs were purified from porcine brains according to published protocol (Mitchison and Kirschner, 1984). A subset were labeled with tetramethylrhodamine (as described in (Hyman et al., 1991a). For use in coupled-enzyme ATPase assays, MTs were prepared exactly as described in (Woehlke et al., 1997). ATPase assays were performed as described previously, with 10-60 nM Eg5 protein (Huang and Hackney, 1994; Woehlke et al., 1997). Briefly, reactions were conducted in ATPase assay buffer (10 mM HEPES, 2 mM $MgCl_2$, 1 mM EGTA, 5% sucrose, 50 mM KCl, 500 nM ATP). Eg5-367 protein and MTs were incubated with a coupled NADH oxidation system (0.3 μM phosphoenolpyruvate, 0.5 μM NADH, pyruvate kinase (11 U/mL), and lactate dehydrogenase (10 U/mL)). We calculated the decrease in absorbance at 340 nm over time to determine the ATPase rate. ATPase rates were determined at MT concentrations from 60 nM - 4 μM, and data were fit to a Michaelis-Menten shown below ($R^2 > 0.8$) with k_{cat} and $K_{0.5,\ MTs}$ as the only two fit parameters using KaleidaGraph software (Synergy Software, Reading, PA). Errors shown are errors in fit parameters.

$$v = \frac{k_{cat}[tubulin]}{K_{0.5_{MTs}} + [tubulin]}$$

4.3.6 Motility assay

For use in motility assays, a mixture of tetramethylrhodamine-labeled tubulin (Cytoskeleton, Inc., Denver, CO) and unlabeled tubulin was combined 1:1 with a 2X polymerization mix (80 mM Pipes buffer, 1 mM $MgCl_2$, 1 mM EGTA, 2 mM GTP, 20% DMSO, pH 6.8) and incubated at 37 ° C for 45 min. Paclitaxel (50 μM) was then added to stabilize MTs. For motility assays flow chambers were created using glass coverslips, microscopy slides, and double-sided tape. Anti-His H8 antibody (ab18184, Abcam, Cambridge, MA) in motility buffer (80 mM PIPES, pH 6.8, 2 mM $MgCl_2$, 1 mM EGTA, 0.2 mg/mL BSA, 150 mM sucrose and 1 mM ATP) was incubated in the flow chamber for two minutes. The flow chamber was then washed three times with motility buffer. Next, the flow chamber was incubated with motility buffer containing Eg5-367 proteins for two minutes, before being washed three times with motility buffer. Finally, motility buffer containing an oxygen scavenging system (glucose oxidase (0.432 mg/mL), catalase (0.072 mg/mL), glucose (45 mM), and β-mercaptoethanol (61 mM), an ATP regenerating system (2 mM creatine phosphate and 810 U/mL creatine phosphate), and tetramethlyrhodamine-labeled polymerized MTs stabilized with GTP (1 mM) and paclitaxel (100 μM) was flowed into the cell, which was then sealed with vacuum grease. MT sliding was visualized on a Nikon TE-2000 E microscope fitted with a X60 objective (N. A. 1.4) using epifluorescence. Images were captured using a Photometrics CoolSnap EZ camera (1392 x 1040 imaging pixels, 6.45 x 6.45 μm/pixel) and Metamorph software. The concentration of MTs and Eg5-367 construct was adjusted to promote sliding

populations suitable for tracking and quantification. For Eg5-367, Eg5-367 non-phosphorylatable, and Eg5-367 GSTY mutants, movies were 30 minutes long with a 20 second interval between frames. For Eg5-367 DL5 and Eg5-367 phosphomimetic mutants, movies were one hour long with a 40 second interval between frames to accommodate slower sliding velocities while minimizing photobleaching of MTs. We reported the mean non-zero sliding velocity calculated in the following manner. We tracked the ends of individual fluorescent MTs using the ImageJ plug-in MTrackJ. This plug-in calculates a step velocity based on the difference in location between consecutive frames in a movie. For each movie we tracked 3-7 MTs for a total of ≥ 190 step velocity measurements per slide. The non-zero mean velocity and standard deviation of these measurements for each individual slide were calculated using Microsoft Excel. For each Eg5-367 we calculated the weighted average and standard deviation for all step velocity measurements from three different movies to generate the final average velocity and standard deviation reported in Table 4.1.

4.3.7 Transient Transfection and Nucleofection of Mammalian Cell Lines

HEK293T cells, the kind gift from Dr. Cara Gottardi, Northwestern University, were cultured in 100 mm dishes containing DMEM medium (Corning Life Sciences, Tewksbury, MA) supplemented with 10% fetal bovine serum (FBS, Atlanta Biologicals, Flowery Branch, GA) and penicillin/streptomycin (200 U/mL, Life Technologies, Carlsbad, CA) in 5% carbon dioxide (CO_2) at 37 ° C. LLC-Pk1 cells were cultured in 1:1 Ham's F-10 medium and Opti-MEM (Life Technologies, Carlsbad, CA) supplemented with 7.5% FBS and 1X antibiotic/antimycotic solution (final concentrations 100 U/mL

penicillin, 0.1 mg/mL streptomycin, 0.25 μg/mL amphotericin B; Sigma-Aldrich, St. Louis, MO) at 37 ° C and 5% CO_2.

To transfect HEK293T cells, 100 mm plates at 70-80% confluence were transfected with 2 μg of DNA using the Effectene transfection reagent (Qiagen, Redwood City, CA), and allowed to express for 24 h.

LLC-Pk1 cells (parental or expressing mCherry- αTubulin) were transfected using an Amaxa nucleofector (Lonza, Portsmouth, NH) using program X-001 and Mirus nucleofection reagent (Mirus Bio LLC, Madison, WI) according to the manufacturers recommendations. siRNA used to target endogenous Eg5 (CUGAAGACCUGAAGACAAU) was obtained from Dharmacon (GE Healthcare Life Sciences, Pittsburgh, PA). Following nucleofection, cells were plated on #1.5 coverslips or Mattek glass bottom dishes (Mattek Corporation, Ashland, MA). Cells were used at 72 hours following nucleofection.

4.3.8 Inhibitors

For treatment of cells with the SFK inhibitor A-419259 (Sigma Aldrich, St. Louis, MO), the protocol developed and verified by the Smithgall lab was followed (Meyn and Smithgall, 2009). Specifically, A-419259 was dissolved in water (100 μM stock solution), aliquoted, and stored at -20 ° C. Twenty-four hours prior to harvest, cell culture media was aspirated from plates and carefully replaced with warmed media containing A-419259 (1 μM final concentration). Cells incubated at 37 ° C and 5% CO_2 until harvest. In cases where cells were both transiently transfected and treated with A-419259, the SFK inhibitor was added to cell media during the transfection procedure.

Stock solutions of SU6656 and BI-2536 were prepared in DMSO, stored at -20°C and diluted into culture medium before use. SU6656 was used at a final concentration of 500 nM and BI-2536 was used at 2 μM. Each was incubated on cells for 15-30 min prior to fixation.

4.3.9 Immunoprecipitation and 2-color Western Blot

Before harvesting, mammalian cells were first treated with pervanadate to inhibit phosphatase activity. Briefly, hydrogen peroxide (1.7%) was added to PBS containing 5 mM sodium orthovanadate to convert it to pervanadate, after which exposure to light was limited. Next, 0.5 mL of this solution was added to warmed DMEM to generate a final media concentration of 0.25 mM pervanadate. Existing media was then aspirated off each plate of cells and gently replaced with DMEM containing pervanadate. Cells were then incubated at 37 ° C and 5% CO_2 for 30 minutes. Next, cells were dislodged from the plate with a cell scraper and pelleted at 1000 x *g* for 5 minutes. The media was then aspirated off and pellets were re-suspended in PBS containing calcium (0.9 mM) and magnesium (0.49 mM) and washed 3 times. Finally, cells were re-suspended in 1% Triton lysis buffer (50 mM Tris, pH 7.5, 150 mM NaCl, 5 mM EDTA, 5% glycerol, 1% Triton X-100, plus COmplete protease and PhosStop phosphatase inhibitor tablets (Roche, Mannheim, Germany)) and incubated on ice for one hour. Total protein concentration of lysate samples was determined using a standard Bradford assay. All samples were normalized to the same protein concentration.

To immunoprecipitate endogenous Eg5, 5 μL of the polyclonal rabbit anti-Eg5 antibody NB500-181 (Novus Biologicals, Littleton, CO) was added to 2.0 mg total

protein lysate in the case of HEK293T lysates or 2.5 mg total protein lysate in the case of LLC-Pk1 lysates and incubated while rotating for 2 h at 4 ° C. To create IgG isotype controls, 1 μL of rabbit IgG (EMD Millipore, Billerica, MA) was added to 2.0 mg of total protein lysate and incubated similarly. Then, 60 μL of pre-equilibrated 50% Pierce Protein A agarose resin slurry (ThermoFisher Scientific, Rockford, IL) was added to each sample, which were then incubated while rotating for another 2 h at 4 ° C. To immunoprecipitate transfected myc-tagged Eg5-367 constructs, 25 μL of pre-equilibrated goat anti-myc beads, epitope EQKLISEEDL (Bethyl, Montgomery, TX), were tumbled with 2.0 mg of cell lysate for 3 h at 4 ° C. After 3 washes with 1% Triton lysis buffer and one wash with 0.1% Triton lysis buffer (50 mM Tris, pH 7.5, 150 mM NaCl, 5 mM EDTA, 5% glycerol, 0.1% Triton X-100, plus COmplete protease and PhosStop (Roche, Mannheim, Germany) inhibitor tablets), beads were re-suspended in 30 μL of 2X SDS-PAGE sample buffer (200 mM Tris-Cl, 0. 130 mM SDS, 33 mM DTT, 3 mM bromophenol blue, 20% glycerol, pH 6.8), boiled for 20 minutes, and run on a 6% SDS-PAGE gel overnight. For loading controls and verification of transfection, prior to immunoprecipitation we retained 2.5% of each 2.0 mg total protein lysate sample, to which we added an equal volume of hot 6X SDS-PAGE sample buffer (300 mM Tris-Cl, 0.4 M SDS, 0.1 M DTT, 9 mM bromophenol blue, and 60% glycerol). Each input sample was then boiled for 20 min and run on a 9% SDS-PAGE gel overnight.

After transfer to nitrocellulose (0.45 μm, Thermo Fisher Scientific, Waltham, MA), and blocking with 5% non-fat dehydrated milk in PBS at room temperature for one hour and washing three times with TBS containing 0.1% TWEEN-20 (TBS-T), we probed with primary antibodies in 5% BSA in TBS while rocking at 4 ° C overnight. For

detection of endogenous Eg5 we used 1:5000 polyclonal rabbit anti-Eg5 NB500-181 antibody (Novus Biologicals, Littleton, CO). For detection of myc-tagged Eg5 constructs we used 1:5000 rabbit anti-myc ab9106 antibody (Abcam, Cambridge, MA). To probe for pTyr we used 1:200 mouse anti-pTyr PY20 antibody (sc-508, Santa Cruz Biotechnology, Dallas, TX). To detect β-catenin and β-tubulin as loading controls, we used 1:250 mouse anti-β-catenin BD160154 antibody (BD Biosciences, San Jose, CA) and 1:5000 mouse anti-β-tubulin AA2 antibody (Sigma-Aldrich, St. Louis, MO), respectively. To probe for c-Src, we used 1:200 rabbit anti-c-Src SRC2 antibody (sc-18, Santa Cruz, Dallas, TX). After briefly washing blots three times with TBS containing 0.1% TWEEN-20, we incubated them in secondary antibodies diluted in 5% non-fat dehydrated milk in TBS at room temperature for one hour while rocking. For detection of all rabbit antibodies, we used a 1:5000 dilution of the donkey anti-rabbit IRDye 680RD fluorescent antibody (LI-COR, Lincoln, NE). For detection of all mouse antibodies, except for the anti-pTyr PY20 antibody, we used a 1:5000 dilution of the donkey anti-mouse IRDye 800CW (LI-COR, Lincoln, NE). The pTyr antibody signal was below the minimum detection limit of fluorescent secondary antibodies. Instead, we used a 1:5000 dilution of a goat anti-mouse IgG-HRP conjugate secondary antibody (Bio-Rad, Hercules, CA) for detection by chemiluminescence, which amplifies the signal. After incubation in secondary antibodies, blots were washed three times with TBS-T. Blots exposed only to fluorescent secondary antibodies were then dried for 20 min sandwiched between paper towels in a drawer. Blots exposed to the HRP-conjugate secondary antibody were instead developed for 20 min using the Pierce ECL2 Western Blotting substrate (Thermo Fisher Scientific, Rockford, IL) and imaged while wet. All

blots were imaged on a LI-COR Odyssey Fc imaging system (Lincoln, NE). Fluorescent antibody exposure times were 2 min; chemiluminescent detection occurred over 10 min. Entire images were contrast-adjusted using LI-COR Image Studio software without altering gamma settings before being exported to Adobe Illustrator for preparation for publication.

4.3.10 Phosphatase Assay

To verify that signal from the anti-pTyr antibody was specific to phosphorylated protein and not due to non-specific binding, we submitted our immunoprecipitated endogenous Eg5 to a lambda protein phosphatase assay according to the commercial protocol that came with the lambda protein phosphatase used (New England Biolabs, Ipswich, MA). Briefly, we immunoprecipitated Eg5 from 4.0 mg of HEK293T cell lysate by doubling reagents in the preceding protocol. After incubation with Pierce Protein A agarose resin (Thermo Fisher Scientific, Rockford, IL), we washed the beads 3 times with 1% Triton lysis buffer lacking protease and phosphatase inhibitor tablets, and once with 0.1% Triton lysis buffer lacking protease and phosphatase inhibitors. After the final wash the beads were re-suspended in an equal volume of 0.1% Triton lysis buffer lacking inhibitors, divided into two separate and equal samples. Both samples were spun down briefly in a tabletop microcentrifuge and the supernatants removed by aspiration. The resin in one sample was re-suspended in lambda protein phosphatase assay buffer (50 mM Hepes, 100 nM NaCl, 2 mM DTT, 0.01% Brij 35, 1 mM $MnCl_2$) containing lambda protein phosphatase (8000 U/mL). The resin in the other sample was re-suspended in lambda protein phosphatase buffer without the enzyme as a negative

control. Both samples were incubated at 30 ° C for an hour while agitating. Lambda protein phosphatase reactions were quenched by the addition of 50 μL of 2X SDS-PAGE sample buffer, boiled for 20 min, and run on an SDS-PAGE gel overnight. They were blotted for endogenous Eg5 and pTyr as described above.

4.3.11 Mammalian Cell Fixation and Immunofluorescence

LLC-Pk1 cells were rinsed twice with room temperature PBS lacking calcium and magnesium and were then fixed for 10 minutes in 2% paraformaldehyde, 0.25% glutaraldehyde, and 0.5% Triton X 100, made fresh daily in PBS lacking calcium and magnesium. Fixed cells were rinsed in PBS containing 0.02% TWEEN-20 and 0.02% sodium azide (PBS-Tw-Az), treated with sodium borohydride (10mg/10mL H_2O) for 10 minutes and then rehydrated in PBS-Tw-Az. The following antibodies were used: Phospho Aurora-A/B/C (Cell Signaling Technology, Danvers, MA); tubulin, DM1α mouse anti-tubulin (Sigma-Aldrich) or YL1/2 rat anti-tubulin (Accurate Chemical and Scientific Corporation, Westbury, NY) and appropriate secondary antibodies as previously described (Ma et al., 2011). Primary antibodies were mixed with 2% BSA in PBS-Tw-Az to block non-specific binding and used at the following final dilutions: Phosoho Aurora-A/B/C 1:1,000, DM1α and YL1/2 1:100; cells were incubated in primary antibodies for 1 hour at 37°C. Stained cells were mounted on glass slides using DAPI Fluomount G (Southern Biotech, Birmingham, AL) to stain DNA.

4.3.12 Immunofluorescence Microscopy/Imaging

To quantify mitotic phenotypes of fixed cells, a Nikon Eclipse Ti with an X-Cite series 120Q excitation light source, and a 100 X, 1.3 N.A., objective lens, was used. Images of fixed cells were acquired using a CSU-10 Yokogawa spinning-disk confocal scan head on a Nikon TE300 as previously described (Tulu et al., 2003). Transfected cells (identified by the Eg5-Emerald signal) were classified by spindle morphology based on microtubule staining as bipole, multipole, monopole, or disorganized. Disorganized spindles included spindles with extra foci, fragmented poles, short spindles, no pole, and bent spindles. For live cell imaging, a Nikon Ti-E microscope with a CSU-X1 Yokogawa spinning-disk confocal scan head (PerkinElmer, Wellesley, MA), an Andor iXon+ electron-multiplying charge-coupled device camera (Andor), and a 100×/1.4 NA objective lens was used. For live-cell imaging, exposures were adjusted without saturating the camera's pixels; typical exposures were 50–800 ms.

Table 4.1 Effects of phosphomimetic and non-phosphorylatable mutations on Eg5 motor characteristics and STLC binding.

Construct	Velocity (nm/s)	k_{cat} (s^{-1})	$K_{0.5}$(MT) (μM)	K_D - STLC (nm)	N (STLC)
WT	11.7 ± 3.4	7.01 ± 0.15	0.073 ± 0.008	86±21	1.07
DL5	4.2 ± 1.3	2.09 ± 0.07	0.181 ± 0.023	--	--
GSTY	12.3 ± 3.2	7.60 ± 0.38	0.261 ± 0.047	--	--
Y125E	4.9 ± 1.2	6.47 ± 0.25	0.128 ± 0.022	540±150	0.95
Y211E	4.4 ± 1.2	2.95 ± 0.15	0.336 ± 0.053	1600±250	0.74
Y231E	11.0 ± 3.0	8.68 ± 0.28	0.231 ± 0.024	304±32	0.89
Y125F	12.5 ± 3.5	5.42 ± 0.11	0.63 ± 0.008	42±18	1.03
Y211F	12.5 ± 3.4	4.94 ± 0.07	0.089 ± 0.009	45±6.0	0.62
Y231F	14.9 ± 3.8	7.33 ± 0.25	0.086 ± 0.017	55±19	1.09

Steady-state ATPase rates and MT sliding velocities of Eg5 phosphomimetic (E) and non-phosphorylatable (F) mutants were measured and compared to those of Eg5-367-WT and Eg5-367-DL5 mutants using standard *in vitro* assays (Methods). Dissociation constants of the L5 inhibitor STLC to Eg5-367 phosphomimetic and non-phosphorylatable mutants (K_D) was calculated from ITC titrations. Errors in K_D were estimated based on the nonlinear least-squares fits to raw ITC data. Stoichiometries (N) show some variability reflecting protein concentration determination, but are generally consistent with single-site binding.

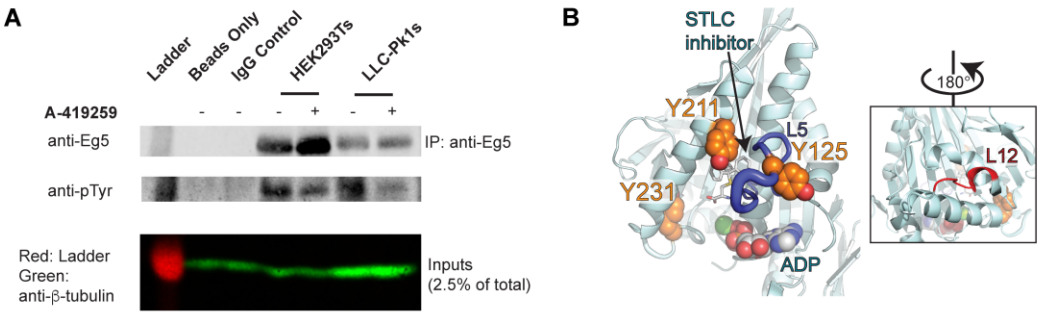

Species	Y125	Y211	Y231	PXXP
H. sapiens	SPNEEYTWEE----DPLAG	TVHNKDEVYQILEKGA	TAATLMNAYSSRSH	TALVER-TPHVPYRESKL
S. scrofa	SPNEEYTWEE----DPLAG	TVHNKNEVYQILEKGA	TAATLMNAYSSRSH	TALVER-TPHVPYRESKL
M. musculus	SPNEVYTWEE----DPLAG	TVHNKDEVYQILEKGA	TAATLMNAYSSRSH	TALVER-TPHIPYRESKL
G. gallus	SPNEEYTWEE----DPLAG	TVHNKNEVYQILERGA	TAATYMNAYSSRSH	SALVER-APHIPYRESKL
X. laevis	SSDEEFTWEQ----DPLAG	SVHNKDEVYQILERGA	TASTLMNAYSSRSH	TALVER-APHIPYRESKL
D. melanogaster	TAELKSSWED----DSDIG	PVHSKDDVYKLLEKGK	TATTLMNAQSSRSH	TALVDR-APHVPYRESKL
A. vitripennis	N-DPTLHWQA----DSPAG	TVHNKSEVYKILEKGS	TAATLMNAHSSRSH	TALVER-APHIPYRESKL
C. elegans	TD--AKSSTD----DPTTG	PVRNRSDVFKLLQLGA	TAATLMNMHSSRSH	RLLTTN-GQHIPYRESKL
T. canis	DPNGSYSWKD----DPHMG	AVRERDEVYELLRRGA	TAATWLNSTSSRSH	KALTSG-AGHIPYRESKL
A. queenslandica	SPQGALSWEE----DPLAG	TVHSKNEVYAILERGS	TAATLMNASSSRSH	TALVEK-CPHIPYRESKL
D. discoideum	KK--------------NPG	IVLSVEHVLSLISAGE	VGSTSYNLQSSRSH	SKLSEKDTGYIPYRDSKL
S. cerevisiae Kip1	NILGDVQSTDNLLLGEHAG	FINSAHEGLNLLMQGS	VAATKCNDLSSRSH	NALVDH-SNHIPYRESKL
S. cerevisiae Cin8	KL---YNGEL----SDAAG	HITNAMEGLNLLQKGL	VASTKMNDFSSRSH	NALVDK-SGHIPFRESKL

Figure 4.1 Human Eg5 is phosphorylated on tyrosine residues. (A) Two-color Western blot showing endogenous Eg5 immunoprecipitated from HEK293T or LLC-Pk1 cell lysates, with each channel displayed separately in black and white. A-419259 was added as indicated; the lower panel shows a β-tubulin loading control (green). (B) The structure of Eg5 bound to S-trityl-L-cysteine (STLC) is marked with tyrosines Y125, Y211, and Y231 (orange space fill, PDB: 3KEN). A predicted SH3 binding site in the MT-binding site of the Eg5 motor domain is shown in the inset. L5 is shown in dark blue; Loop 12 within the MT binding domain is shown in red. (C) Sequence alignment comparing the putative phosphorylation sites and the –PXXP– SH3 targeting domain. Putative phosphorylated tyrosines and the –PXXP– SH3 targeting motifs are shown in red. The accession numbers for each protein are listed in Fig. 4.4 C.

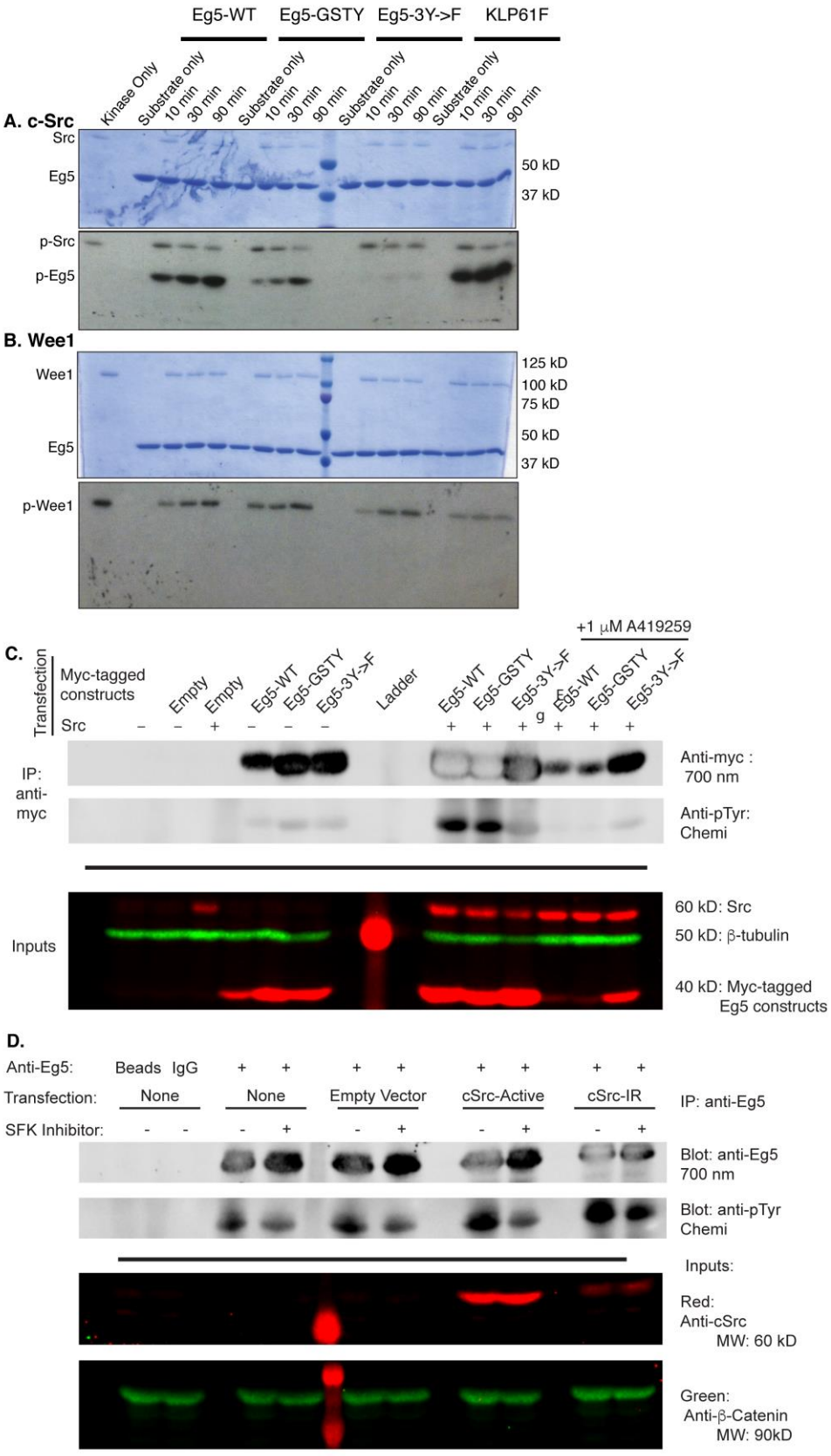
Eg5-WT
Eg5-GSTY
Eg5-3Y->F
KLP61F
Kinase Only
Substrate only
10 min
30 min
90 min
A. c-Src
Src
Eg5
50 kD
37 kD
p-Src
p-Eg5
B. Wee1
Wee1
125 kD
100 kD
75 kD
50 kD
37 kD
p-Wee1
+1 μM A419259
C.
Transfection
Myc-tagged constructs
Empty
Eg5-WT
Eg5-GSTY
Eg5-3Y->F
Ladder
Src
IP: anti-myc
Anti-myc : 700 nm
Anti-pTyr: Chemi
Inputs
60 kD: Src
50 kD: β-tubulin
40 kD: Myc-tagged Eg5 constructs
D.
Anti-Eg5:
Beads
IgG
Transfection:
None
Empty Vector
cSrc-Active
cSrc-IR
IP: anti-Eg5
SFK Inhibitor:
Blot: anti-Eg5 700 nm
Blot: anti-pTyr Chemi
Inputs:
Red: Anti-cSrc MW: 60 kD
Green: Anti-β-Catenin MW: 90kD

Figure 4.2 SFK dependent phosphorylation of Eg5 *in vitro* and in mammalian cells. Kinesin-5 constructs (denoted across the top) were incubated with human c-Src (A) or human Wee1 kinase (B) and radiolabeled ATP for the times indicated. Reactions were quenched and run on an SDS-PAGE (top) that was then dried and exposed to film (bottom). Position of c-Src, Eg5, and Wee1 marked on the left side. (C) Immunoprecipitation of Eg5 from HEK293T cells co-transfected with myc-tagged Eg5 motor head and c-Src constructs; A-419259 added as indicated. Western blot stained using anti-myc and anti-pTyr antibodies which here are displayed separately in black and white. The lower panel shows inputs and β-tubulin level as a loading control. (D) Endogenous Eg5 was immunoprecipitated from HEK293T cells transfected with the indicated constructs; A-419259 was added as indicated. pTyr was detected using a two-color Western blot. Each channel is displayed separately in black and white. Transfection efficacy was verified by detection of c-Src in the lysates from transfected cells. β-catenin level is shown as a loading control.

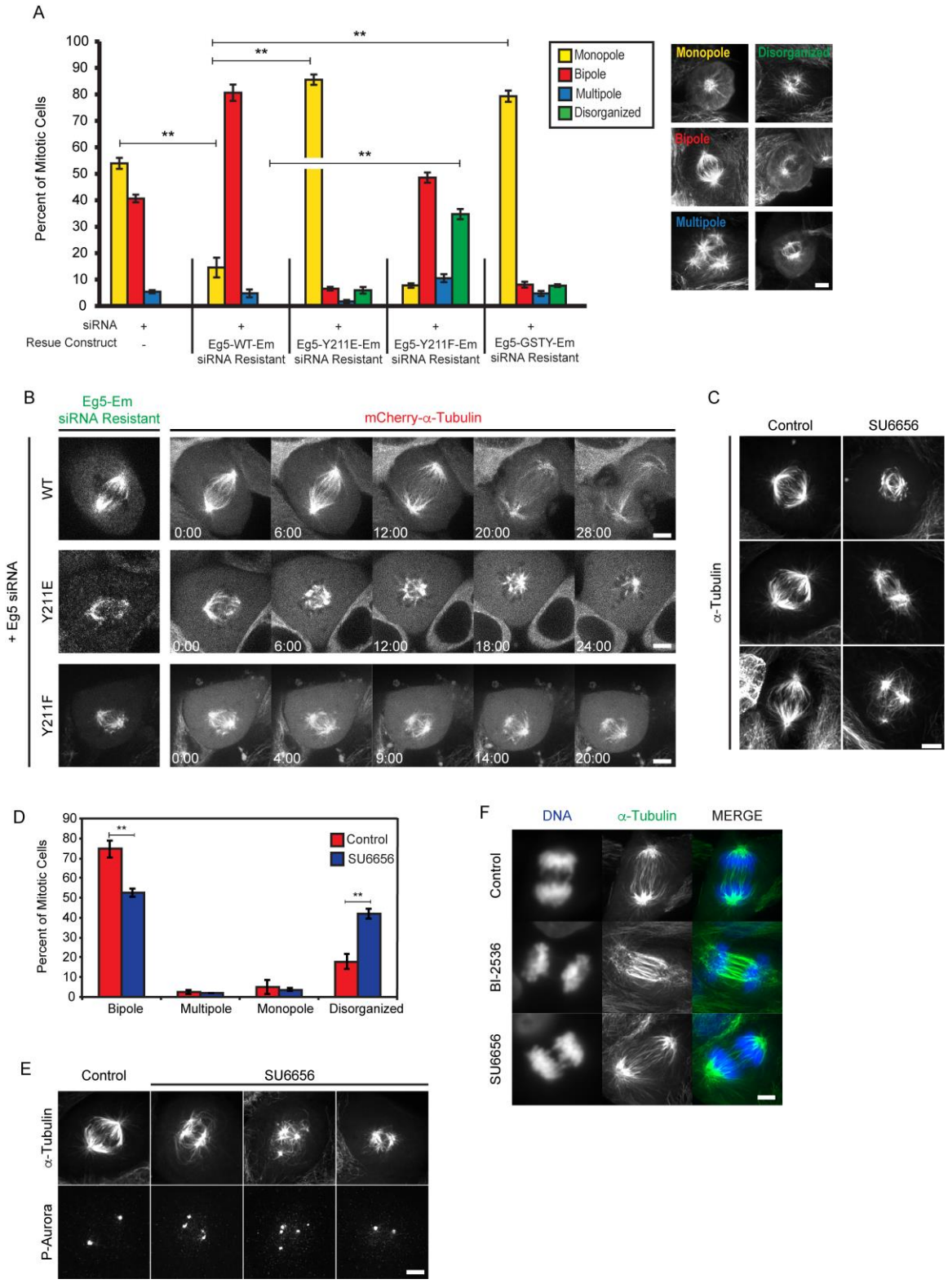

Figure 4.3 Mitotic spindle defects in cells expressing phosphomimetic and non-phosphorylatable mutants of Eg5. (A) Percent of mitotic phenotypes in LLC-Pk1 cells transfected with siRNA targeting endogenous Eg5 alone or co-transfected with an siRNA

resistant Eg5 Emerald construct (WT, Y211E, Y211F, GSTY). Monopole (yellow), bipole (red), muitipole (blue), disorganized (green). Examples of each phenotype are shown on right. (B) Time-lapse imaging of LLC-Pk1 cells expressing mCherry-α-tubulin (right panels) co-transfected with Eg5 siRNA and siRNA resistant Eg5 Emerald constructs (WT, Y211E, and Y211F left panels). (C) Immunofluorescence staining for MTs in control (left) and SU6656-treated (right) parental LLC-Pk1 cells. (D) Quantification of mitotic spindle phenotypes shown in C. (E) Immunofluorescence staining for MTs (top) and phospho-Aurora (bottom) for control and SU6656 treated cells. (F) Immunofluorescence staining of α-tubulin in anaphase LLC-Pk1 cells: control (top), BI-2536 (middle), SU6656 (bottom). ** = $p \leq 0.01$. Scale bars in A, B, C, E, F = 5 μm. Time in B (min:sec). Error Bars = St Dev.

A

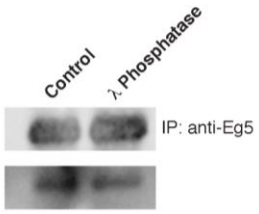

B

Site	Region	Species	Reference
Y125	Motor head	*H. sapiens*, *M. musculus*	Cell Signaling Technology, (Iliuk et al., 2010; Luo et al., 2008)
Y211	Motor head	*H. sapiens*	Cell Signaling Technology
Y231	Motor head	*H. sapiens*	Cell Signaling Technology, (Han et al., 2010)
Y399	BASS domain	*H. sapiens*, *M. musculus*	Cell Signaling Technology, (Sharma et al., 2014)
Y480	BASS domain	*H. sapiens*	Cell Signaling Technology
Y932	Tail domain	*H. sapiens*	Cell Signaling Technology
Y934	Tail domain	*H. sapiens*	Cell Signaling Technology

C

Species	UniProt Accession Numbers
H. sapiens	P52732
S. scrofa	F1SC89
M. musculus	Q6P9P6
G. gallus	F1NXA1
X. laevis	Q91783
D. melanogaster	P46863
A. vitripennis	K7J300
C. elegans	G5EGL7
T. canis	A0A0B2VHZ4
A. queenslandica	I1GB25
D. discoideum	Q6S001
S. cerevisiae Kip1	P28742
S. cerevisiae Cin8	P27895

D

Kinesin	Species	Accession Numbers	PXXP Domain
1	*H. sapiens*	P33176	NINKSLSALGNVISALAEG-------S--TYVPYRDSKMTRILQDSLGGNCRTTI
1	*C. elegans*	P34540	NINKSLTALGIVISALAEG-------T-KSHVPYRDSKLTRILQESLGGNSRTTV
2	*H. sapiens*	Q9Y496	KINLSLSTLGNVISALVDG-------KS-THVPYRNSKLTRLLQDSLGGNSKTMM
2	*X. laevis*	Q98TI1	KINLSLSTLGNVISALVDG-------KS-THVPYRNSKLTRLLQDSLGGNSKTMM
3	*H. sapiens*	Q15058	SINKSLLTLGKVISALSEQAN-----QRSVFIPYRESVLTWLLKESLGGNSKTAM
3	*X. tropicalis*	F7EHP6	SINKSLLTLGKVISALSEMSEV----KKRSFIPYRDSLLTWLLRESLGGNSKTAM
5	*H. sapiens*	P52732	NINQSLLTLGRVITALVER--------T-PHVPYRESKLTRILQDSLGGRTRTSI
5	*S. scrufa*	F1SC89	NINQSLLTLGRVITALVER--------T-PHVPYRESKLTRILQDSLGGRTRTSI
5	*D. melanogaster*	P46863	NINQSLLTLGRVITALVDR--------A-PHVPYRESKLTRLLQESLGGRTKTSI
5	*X. laevis*	Q91783	NINQSLLTLGRVITALVER--------A-PHIPYRESKLTRILQDSLGGRTKTSI
6	*H. sapiens*	Q02241	NINQSLMTLRTCMDVLRENQMYGTN----KMVPYRDSKLTHLFKNYFDGEGKVRM
6	*D. melanogaster*	O62528	NINNSLMTLRTCLEYLRENQLAASNGLAPKKVPYRDSKITHMFKNYFDGEGQVSM
7	*H. sapiens*	Q02224	NINRSLFILGQVIKKLSDG-------QVGGFINYRDSKLTRILQNSLGGNAKTRI
7	*X. laevis*	O42263	NINRSLFILGQVIKKLSDG-------QAGGFINYRDSKLTRILQNSLGGNAKTVI

E

CONSTRUCT	Expression Vector	Tag	Residues	Y125	Y211	Y231	PXXP
EG5-367 E270A	pRSET	C-term 6X His	1-367	SPNEEYTWEEDPLAG	TVHNKDEVYQILEKGA	TAATLMNAYSSRSH	TALVERTPHVPYRESKL
EG5-367 GSTY E270A	pRSET	C-term 6X His	1-367	SPNEEYTWEEDPLAG	TVHNKDEVYQILEKGA	TAATLMNAYSSRSH	TALVEGSTYVPYRESKL
EG5-367-3Y->F E270A	pRSET	C-term 6X His	1-367	SPNEEFTWEEDPLAG	TVHNKDEVFQILEKGA	TAATLMNAFSSRSH	TALVERTPHVPYRESKL
EG5-367-2Y->F E270A	pRSET	C-term 6X His	1-367	SPNEEYTWEEDPLAG	TVHNKDEVFQILEKGA	TAATLMNAFSSRSH	TALVERTPHVPYRESKL
Eg5-367myc	pcDNA3	C-term Myc	1-367	SPNEEYTWEEDPLAG	TVHNKDEVYQILEKGA	TAATLMNAYSSRSH	TALVERTPHVPYRESKL
Eg5-367myc-GSTY	pcDNA3	C-term Myc	1-367	SPNEEYTWEEDPLAG	TVHNKDEVYQILEKGA	TAATLMNAYSSRSH	TALVEGSTYVPYRESKL
Eg5-367myc-3Y->F	pcDNA3	C-term Myc	1-367	SPNEEFTWEEDPLAG	TVHNKDEVFQILEKGA	TAATLMNAFSSRSH	TALVERTPHVPYRESKL
Eg5-367	pRSET	C-term 6X His	1-367	SPNEEYTWEEDPLAG	TVHNKDEVYQILEKGA	TAATLMNAYSSRSH	TALVERTPHVPYRESKL
Eg5-367 DL5	pRSET	C-term 6X His	1-367	SPNEE-------LAG	TVHNKDEVYQILEKGA	TAATLMNAYSSRSH	TALVERTPHVPYRESKL
Eg5-367 GSTY	pRSET	C-term 6X His	1-367	SPNEEYTWEEDPLAG	TVHNKDEVYQILEKGA	TAATLMNAYSSRSH	TALVEGSTYVPYRESKL
EG5-367-Y125E	pRSET	C-term 6X His	1-367	SPNEEETWEEDPLAG	TVHNKDEVYQILEKGA	TAATLMNAYSSRSH	TALVERTPHVPYRESKL
EG5-367-Y211E	pRSET	C-term 6X His	1-367	SPNEEYTWEEDPLAG	TVHNKDEVEQILEKGA	TAATLMNAYSSRSH	TALVERTPHVPYRESKL
EG5-367-Y231E	pRSET	C-term 6X His	1-367	SPNEEYTWEEDPLAG	TVHNKDEVYQILEKGA	TAATLMNAESSRSH	TALVERTPHVPYRESKL
EG5-367-Y125F	pRSET	C-term 6X His	1-367	SPNEEFTWEEDPLAG	TVHNKDEVYQILEKGA	TAATLMNAYSSRSH	TALVERTPHVPYRESKL
EG5-367-Y211F	pRSET	C-term 6X His	1-367	SPNEEYTWEEDPLAG	TVHNKDEVFQILEKGA	TAATLMNAYSSRSH	TALVERTPHVPYRESKL
EG5-367-Y231F	pRSET	C-term 6X His	1-367	SPNEEYTWEEDPLAG	TVHNKDEVYQILEKGA	TAATLMNAFSSRSH	TALVERTPHVPYRESKL
Eg5-WT-Em	Clontech	Emerald Green	1-1056	SPNEEYTWEEDPLAG	TVHNKDEVYQILEKGA	TAATLMNAYSSRSH	TALVERTPHVPYRESKL
Eg5-GSTY-Em	Clontech	Emerald Green	1-1056	SPNEEYTWEEDPLAG	TVHNKDEVYQILEKGA	TAATLMNAYSSRSH	TALVEGSTYVPYRESKL
Eg5-Y211E-Em	Clontech	Emerald Green	1-1056	SPNEEYTWEEDPLAG	TVHNKDEVEQILEKGA	TAATLMNAYSSRSH	TALVERTPHVPYRESKL
Eg5-Y211F-Em	Clontech	Emerald Green	1-1056	SPNEEYTWEEDPLAG	TVHNKDEVFQILEKGA	TAATLMNAYSSRSH	TALVERTPHVPYRESKL
Eg5-Y125E-Em	Clontech	Emerald Green	1-1056	SPNEEETWEEDPLAG	TVHNKDEVYQILEKGA	TAATLMNAYSSRSH	TALVERTPHVPYRESKL
Eg5-Y125F-Em	Clontech	Emerald Green	1-1056	SPNEEFTWEEDPLAG	TVHNKDEVYQILEKGA	TAATLMNAYSSRSH	TALVERTPHVPYRESKL
Eg5-Y125E,Y211E-Em	Clontech	Emerald Green	1-1056	SPNEEETWEEDPLAG	TVHNKDEVEQILEKGA	TAATLMNAYSSRSH	TALVERTPHVPYRESKL

F

Name	Vector	Tag	Mutations	Use
Klp61F E266A	pRSET	C-term 6X His tag	E266A	Bacterial expression, *in vitro* kinase assays
c-Src Active	pCMV-SPORT 6	(none)	Y527F	Mammalian expression, transfection experiments
c-Src IR	pCMV-SPORT 6	(none)	T338M, Y527F	Mammalian expression, transfection experiments

Figure 4.4 Eg5 is phosphorylated on a conserved tyrosine in its motor head. (A) A single immunoprecipitation reaction from HEK293Ts (3.5 mg total lysate) was divided in two. Half was incubated with λ-phosphatase (right); the other was incubated with phosphatase buffer alone (left). (B) Table summarizing Eg5 tyrosine phosphorylations as reported in databases collecting results from phosphoproteomics experiments, including PhosphositePlus (Hornbeck et al., 2015). (C) Table showing the UniProt Accession numbers used to generate the alignment of kinesin-5 family members in Figure 4.1 C. (D) Alignment of kinesins from families 1-7, highlighting the MT binding region. The –PXXP- SH3 targeting motif, when present, is highlighted in red. Residues that are identical across the alignment are marked in dark grey, while similar residues are marked in light grey. While there is extensive conservation of sequence in this region across kinesin family members, the PXXP motif is only seen in kinesin-5s of higher order organisms. (E) List of the sequence mutations made in Eg5 constructs and (F) other constructs for experiments using Eg5 mutants.

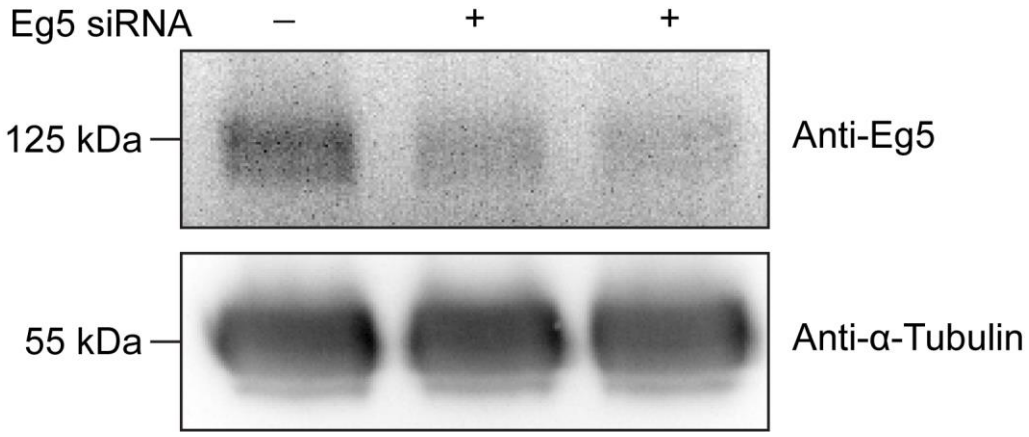

Figure 4.5 Eg5-targeting siRNA decreases endogenous Eg5 levels. Western blot showing the efficiency of Eg5 knockdown using siRNA in LLC-Pk1 cells. Treatment with siRNA led to an approximately 50% reduction in Eg5 signal as measured by densitometry.

4.4 References

Avunie-Masala, R., N. Movshovich, Y. Nissenkorn, A. Gerson-Gurwitz, V. Fridman, M. Koivomagi, M. Loog, M.A. Hoyt, A. Zaritsky, and L. Gheber. 2011. Phospho-regulation of kinesin-5 during anaphase spindle elongation. *Journal of cell science*. 124:873-878.

Bain, J., L. Plater, M. Elliott, N. Shpiro, C.J. Hastie, H. McLauchlan, I. Klevernic, J.S. Arthur, D.R. Alessi, and P. Cohen. 2007. The selectivity of protein kinase inhibitors: a further update. *The Biochemical journal*. 408:297-315.

Behnke-Parks, W.M., J. Vendome, B. Honig, Z. Maliga, C. Moores, and S.S. Rosenfeld. 2011. Loop L5 acts as a conformational latch in the mitotic kinesin Eg5. *The Journal of biological chemistry*. 286:5242-5253.

Bhatt, A.S., H. Erdjument-Bromage, P. Tempst, C.S. Craik, and M.M. Moasser. 2005. Adhesion signaling by a novel mitotic substrate of src kinases. *Oncogene*. 24:5333-5343.

Bishop, J.D., Z. Han, and J.M. Schumacher. 2005. The Caenorhabditis elegans Aurora B kinase AIR-2 phosphorylates and is required for the localization of a BimC kinesin to meiotic and mitotic spindles. *Molecular biology of the cell*. 16:742-756.

Blangy, A., L. Arnaud, and E.A. Nigg. 1997. Phosphorylation by p34cdc2 protein kinase regulates binding of the kinesin-related motor HsEg5 to the dynactin subunit p150. *The Journal of biological chemistry*. 272:19418-19424.

Blangy, A., H.A. Lane, P. d'Herin, M. Harper, M. Kress, and E.A. Nigg. 1995. Phosphorylation by p34cdc2 regulates spindle association of human Eg5, a kinesin-related motor essential for bipolar spindle formation in vivo. *Cell*. 83:1159-1169.

Brennan, I.M., U. Peters, T.M. Kapoor, and A.F. Straight. 2007. Polo-like kinase controls vertebrate spindle elongation and cytokinesis. *PloS one*. 2:e409.

Brust-Mascher, I., P. Sommi, D.K. Cheerambathur, and J.M. Scholey. 2009. Kinesin-5-dependent poleward flux and spindle length control in Drosophila embryo mitosis. *Molecular biology of the cell*. 20:1749-1762.

Calderwood, D.J., D.N. Johnston, R. Munschauer, and P. Rafferty. 2002. Pyrrolo[2,3-d]pyrimidines containing diverse N-7 substituents as potent inhibitors of Lck. *Bioorganic & Medicinal Chemistry Letters*. 12:1683-1686.

Caron, D., D.P. Byrne, P. Thebault, D. Soulet, C.R. Landry, P.A. Eyers, and S. Elowe. 2016. Mitotic phosphotyrosine network analysis reveals that tyrosine phosphorylation regulates Polo-like kinase 1 (PLK1). *Science signaling*. 9:rs14.

Chee, M.K., and S.B. Haase. 2010. B-cyclin/CDKs regulate mitotic spindle assembly by phosphorylating kinesins-5 in budding yeast. *PLoS genetics*. 6:e1000935.

Cochran, J.C., and S.P. Gilbert. 2005. ATPase mechanism of Eg5 in the absence of microtubules: insight into microtubule activation and allosteric inhibition by monastrol. *Biochemistry*. 44:16633-16648.

Cochran, J.C., T.C. Krzysiak, and S.P. Gilbert. 2006. Pathway of ATP hydrolysis by monomeric kinesin Eg5. *Biochemistry*. 45:12334-12344.

Cochran, J.C., C.A. Sontag, Z. Maliga, T.M. Kapoor, J.J. Correia, and S.P. Gilbert. 2004. Mechanistic analysis of the mitotic kinesin Eg5. *The Journal of biological chemistry*. 279:38861-38870.

David-Pfeuty, T., S. Bagrodia, and D. Shalloway. 1993. Differential localization patterns of myristoylated and nonmyristoylated c-Src proteins in interphase and mitotic c-Src overexpresser cells. *Journal of cell science*. 105 (Pt 3):613-628.

DeBerg, H.A., B.H. Blehm, J. Sheung, A.R. Thompson, C.S. Bookwalter, S.F. Torabi, T.A. Schroer, C.L. Berger, Y. Lu, K.M. Trybus, and P.R. Selvin. 2013. Motor domain phosphorylation modulates kinesin-1 transport. *The Journal of biological chemistry*. 288:32612-32621.

Enos, A.P., and N.R. Morris. 1990. Mutation of a gene that encodes a kinesin-like protein blocks nuclear division in A. nidulans. *Cell*. 60:1019-1027.

Falnikar, A., S. Tole, and P.W. Baas. 2011. Kinesin-5, a mitotic microtubule-associated motor protein, modulates neuronal migration. *Molecular biology of the cell*. 22:1561-1574.

Ferenz, N.P., A. Gable, and P. Wadsworth. 2010. Mitotic functions of kinesin-5. *Seminars in cell & developmental biology*. 21:255-259.

Fumagalli, S., N.F. Totty, J.J. Hsuan, and S.A. Courtneidge. 1994. A target for Src in mitosis. *Nature*. 368:871-874.

Gable, A., M. Qiu, J. Titus, S. Balchand, N.P. Ferenz, N. Ma, E.S. Collins, C. Fagerstrom, J.L. Ross, G. Yang, and P. Wadsworth. 2012. Dynamic reorganization of Eg5 in the mammalian spindle throughout mitosis requires dynein and TPX2. *Molecular biology of the cell*. 23:1254-1266.

Garcia, K., J. Stumpff, T. Duncan, and T.T. Su. 2009. Tyrosines in the kinesin-5 head domain are necessary for phosphorylation by Wee1 and for mitotic spindle integrity. *Current biology : CB*. 19:1670-1676.

Goshima, G., and R.D. Vale. 2003. The roles of microtubule-based motor proteins in mitosis: comprehensive RNAi analysis in the Drosophila S2 cell line. *The Journal of cell biology*. 162:1003-1016.

Hagan, I., and M. Yanagida. 1990. Novel potential mitotic motor protein encoded by the fission yeast cut7+ gene. *Nature*. 347:563-566.

Han, G., M. Ye, H. Liu, C. Song, D. Sun, Y. Wu, X. Jiang, R. Chen, C. Wang, L. Wang, and H. Zou. 2010. Phosphoproteome analysis of human liver tissue by long-gradient nanoflow LC coupled with multiple stage MS analysis. *Electrophoresis*. 31:1080-1089.

He, J., Z. Zhang, M. Ouyang, F. Yang, H. Hao, K.L. Lamb, J. Yang, Y. Yin, and W.H. Shen. 2016. PTEN regulates EG5 to control spindle architecture and chromosome congression during mitosis. *Nature communications*. 7:12355.

Hornbeck, P.V., B. Zhang, B. Murray, J.M. Kornhauser, V. Latham, and E. Skrzypek. 2015. PhosphoSitePlus, 2014: mutations, PTMs and recalibrations. *Nucleic acids research*. 43:D512-520.

Hoyt, M.A., L. He, K.K. Loo, and W.S. Saunders. 1992. Two Saccharomyces cerevisiae kinesin-related gene products required for mitotic spindle assembly. *The Journal of cell biology*. 118:109-120.

Huang, T.G., and D.D. Hackney. 1994. Drosophila kinesin minimal motor domain expressed in Escherichia coli. Purification and kinetic characterization. *The Journal of biological chemistry*. 269:16493-16501.

Hyman, A., D. Drechsel, D. Kellogg, S. Salser, K. Sawin, P. Steffen, L. Wordeman, and T. Mitchison. 1991. [39] Preparation of modified tubulins. *In* Methods in enzymology. Vol. Volume 196. Academic Press. 478-485.

Iliuk, A.B., V.A. Martin, B.M. Alicie, R.L. Geahlen, and W.A. Tao. 2010. In-depth analyses of kinase-dependent tyrosine phosphoproteomes based on metal ion-functionalized soluble nanopolymers. *Molecular & cellular proteomics : MCP*. 9:2162-2172.

Kaan, H.Y., V. Ulaganathan, D.D. Hackney, and F. Kozielski. 2009. An allosteric transition trapped in an intermediate state of a new kinesin-inhibitor complex. *The Biochemical journal*. 425:55-60.

Kapitein, L.C., E.J. Peterman, B.H. Kwok, J.H. Kim, T.M. Kapoor, and C.F. Schmidt. 2005. The bipolar mitotic kinesin Eg5 moves on both microtubules that it crosslinks. *Nature*. 435:114-118.

Kim, E.D., R. Buckley, S. Learman, J. Richard, C. Parke, D.K. Worthylake, E.J. Wojcik, R.A. Walker, and S. Kim. 2010. Allosteric drug discrimination is coupled to mechanochemical changes in the kinesin-5 motor core. *The Journal of biological chemistry*. 285:18650-18661.

Kim, L.C., L.X. Song, and E.B. Haura. 2009. Src kinases as therapeutic targets for cancer. *Nat Rev Clin Oncol*. 6:587-595.

Krzysiak, T.C., and S.P. Gilbert. 2006. Dimeric Eg5 maintains processivity through alternating-site catalysis with rate-limiting ATP hydrolysis. *The Journal of biological chemistry*. 281:39444-39454.

Krzysiak, T.C., M. Grabe, and S.P. Gilbert. 2008. Getting in sync with dimeric Eg5. Initiation and regulation of the processive run. *The Journal of biological chemistry*. 283:2078-2087.

Kuga, T., Y. Nakayama, M. Hoshino, Y. Higashiyama, Y. Obata, D. Matsuda, K. Kasahara, Y. Fukumoto, and N. Yamaguchi. 2007. Differential mitotic activation of endogenous c-Src, c-Yes, and Lyn in HeLa cells. *Arch Biochem Biophys*. 466:116-124.

Kull, F.J., E.P. Sablin, R. Lau, R.J. Fletterick, and R.D. Vale. 1996. Crystal structure of the kinesin motor domain reveals a structural similarity to myosin. *Nature*. 380:550-555.

Laemmli, U.K. 1970. Cleavage of structural proteins during the assembly of the head of bacteriophage T4. *Nature*. 227:680-685.

Larson, A.G., N. Naber, R. Cooke, E. Pate, and S.E. Rice. 2010. The conserved L5 loop establishes the pre-powerstroke conformation of the Kinesin-5 motor, eg5. *Biophys. J.* 98:2619-2627.

Lenart, P., M. Petronczki, M. Steegmaier, B. Di Fiore, J.J. Lipp, M. Hoffmann, W.J. Rettig, N. Kraut, and J.M. Peters. 2007. The small-molecule inhibitor BI 2536 reveals novel insights into mitotic roles of polo-like kinase 1. *Current biology : CB*. 17:304-315.

Levi, M., B. Maro, and R. Shalgi. 2010. Fyn kinase is involved in cleavage furrow ingression during meiosis and mitosis. *Reproduction*. 140:827-834.

Ley, S.C., M. Marsh, C.R. Bebbington, K. Proudfoot, and P. Jordan. 1994. Distinct intracellular localization of Lck and Fyn protein tyrosine kinases in human T lymphocytes. *The Journal of cell biology*. 125:639-649.

Li, H., X. Xing, G. Ding, Q. Li, C. Wang, L. Xie, R. Zeng, and Y. Li. 2009. SysPTM: a systematic resource for proteomic research on post-translational modifications. *Molecular & cellular proteomics : MCP*. 8:1839-1849.

Luo, W., R.J. Slebos, S. Hill, M. Li, J. Brabek, R. Amanchy, R. Chaerkady, A. Pandey, A.J. Ham, and S.K. Hanks. 2008. Global impact of oncogenic Src on a phosphotyrosine proteome. *J Proteome Res*. 7:3447-3460.

Ma, N., J. Titus, A. Gable, J.L. Ross, and P. Wadsworth. 2011. TPX2 regulates the localization and activity of Eg5 in the mammalian mitotic spindle. *The Journal of cell biology*. 195:87-98.

Ma, N., U.S. Tulu, N.P. Ferenz, C. Fagerstrom, A. Wilde, and P. Wadsworth. 2010. Poleward transport of TPX2 in the mammalian mitotic spindle requires dynein, Eg5, and microtubule flux. *Molecular biology of the cell*. 21:979-988.

Maliga, Z., T.M. Kapoor, and T.J. Mitchison. 2002. Evidence that monastrol is an allosteric inhibitor of the mitotic kinesin Eg5. *Chem Biol*. 9:989-996.

Maliga, Z., and T.J. Mitchison. 2006. Small-molecule and mutational analysis of allosteric Eg5 inhibition by monastrol. *BMC Chem Biol*. 6:2.

Maliga, Z., J. Xing, H. Cheung, L.J. Juszczak, J.M. Friedman, and S.S. Rosenfeld. 2006. A pathway of structural changes produced by monastrol binding to Eg5. *The Journal of biological chemistry*. 281:7977-7982.

Mayer, T.U., T.M. Kapoor, S.J. Haggarty, R.W. King, S.L. Schreiber, and T.J. Mitchison. 1999. Small molecule inhibitor of mitotic spindle bipolarity identified in a phenotype-based screen. *Science (New York, N.Y.)*. 286:971-974.

Meyn, M.A., 3rd, and T.E. Smithgall. 2009. Chemical genetics identifies c-Src as an activator of primitive ectoderm formation in murine embryonic stem cells. *Science signaling*. 2:ra64.

Mitchison, T., and M. Kirschner. 1984. Microtubule assembly nucleated by isolated centrosomes. *Nature*. 312:232-237.

Muretta, J.M., W.M. Behnke-Parks, J. Major, K.J. Petersen, A. Goulet, C.A. Moores, D.D. Thomas, and S.S. Rosenfeld. 2013. Loop L5 assumes three distinct orientations during the ATPase cycle of the mitotic kinesin Eg5: a transient and time-resolved fluorescence study. *The Journal of biological chemistry*. 288:34839-34849.

Muretta, J.M., Y. Jun, S.P. Gross, J. Major, D.D. Thomas, and S.S. Rosenfeld. 2015. The structural kinetics of switch-1 and the neck linker explain the functions of kinesin-1 and Eg5. *Proceedings of the National Academy of Sciences of the United States of America*. 112:E6606-6613.

Myers, K.A., and P.W. Baas. 2007. Kinesin-5 regulates the growth of the axon by acting as a brake on its microtubule array. *The Journal of cell biology*. 178:1081-1091.

Nadar, V.C., A. Ketschek, K.A. Myers, G. Gallo, and P.W. Baas. 2008. Kinesin-5 is essential for growth-cone turning. *Current biology : CB*. 18:1972-1977.

Nakayama, Y., Y. Matsui, Y. Takeda, M. Okamoto, K. Abe, Y. Fukumoto, and N. Yamaguchi. 2012. c-Src but not Fyn promotes proper spindle orientation in early prometaphase. *The Journal of biological chemistry*. 287:24905-24915.

Obenauer, J.C., L.C. Cantley, and M.B. Yaffe. 2003. Scansite 2.0: Proteome-wide prediction of cell signaling interactions using short sequence motifs. *Nucleic acids research*. 31:3635-3641.

Rapley, J., M. Nicolas, A. Groen, L. Regue, M.T. Bertran, C. Caelles, J. Avruch, and J. Roig. 2008. The NIMA-family kinase Nek6 phosphorylates the kinesin Eg5 at a novel site necessary for mitotic spindle formation. *Journal of cell science*. 121:3912-3921.

Sarli, V., and A. Giannis. 2008. Targeting the kinesin spindle protein: basic principles and clinical implications. *Clinical cancer research : an official journal of the American Association for Cancer Research*. 14:7583-7587.

Saunders, W., V. Lengyel, and M.A. Hoyt. 1997. Mitotic spindle function in Saccharomyces cerevisiae requires a balance between different types of kinesin-related motors. *Molecular biology of the cell*. 8:1025-1033.

Scholey, J.E., S. Nithianantham, J.M. Scholey, and J. Al-Bassam. 2014. Structural basis for the assembly of the mitotic motor Kinesin-5 into bipolar tetramers. *eLife*. 3:e02217.

Sen, B., and F.M. Johnson. 2011. Regulation of SRC family kinases in human cancers. *Journal of signal transduction*. 2011:865819.

Shapira, O., and L. Gheber. 2016. Motile properties of the bi-directional kinesin-5 Cin8 are affected by phosphorylation in its motor domain. *Scientific reports*. 6:25597.

Shapira, O., A. Goldstein, J. Al-Bassam, and L. Gheber. 2017. A potential physiological role for bi-directional motility and motor clustering of mitotic kinesin-5 Cin8 in yeast mitosis. *Journal of cell science*. 130:725-734.

Sharma, K., R.C. D'Souza, S. Tyanova, C. Schaab, J.R. Wisniewski, J. Cox, and M. Mann. 2014. Ultradeep human phosphoproteome reveals a distinct regulatory nature of Tyr and Ser/Thr-based signaling. *Cell reports*. 8:1583-1594.

Skoufias, D.A., S. DeBonis, Y. Saoudi, L. Lebeau, I. Crevel, R. Cross, R.H. Wade, D. Hackney, and F. Kozielski. 2006. S-trityl-L-cysteine is a reversible, tight binding inhibitor of the human kinesin Eg5 that specifically blocks mitotic progression. *J. Biol. Chem.* 281:17559-17569.

Smith, K.P., K.M. Gifford, J.S. Waitzman, and S.E. Rice. 2015. Survey of phosphorylation near drug binding sites in the Protein Data Bank (PDB) and their effects. *Proteins*. 83:25-36.

Tanenbaum, M.E., L. Macurek, N. Galjart, and R.H. Medema. 2008. Dynein, Lis1 and CLIP-170 counteract Eg5-dependent centrosome separation during bipolar spindle assembly. *The EMBO journal*. 27:3235-3245.

Tanenbaum, M.E., L. Macurek, A. Janssen, E.F. Geers, M. Alvarez-Fernandez, and R.H. Medema. 2009. Kif15 cooperates with eg5 to promote bipolar spindle assembly. *Current biology : CB*. 19:1703-1711.

Thomas, S.M., and J.S. Brugge. 1997. Cellular functions regulated by Src family kinases. *Annual review of cell and developmental biology*. 13:513-609.

UniProt, C. 2015. UniProt: a hub for protein information. *Nucleic acids research*. 43:D204-212.

Uzbekov, R., C. Prigent, and Y. Arlot-Bonnemains. 1999. Cell cycle analysis and synchronization of the Xenopus laevis XL2 cell line: study of the kinesin related protein XlEg5. *Microscopy research and technique*. 45:31-42.

van den Wildenberg, S.M., L. Tao, L.C. Kapitein, C.F. Schmidt, J.M. Scholey, and E.J. Peterman. 2008. The homotetrameric kinesin-5 KLP61F preferentially crosslinks microtubules into antiparallel orientations. *Current biology : CB*. 18:1860-1864.

van Ree, J.H., H.J. Nam, K.B. Jeganathan, A. Kanakkanthara, and J.M. van Deursen. 2016. Pten regulates spindle pole movement through Dlg1-mediated recruitment of Eg5 to centrosomes. *Nature cell biology*. 18:814-821.

Vanneste, D., M. Takagi, N. Imamoto, and I. Vernos. 2009. The role of Hklp2 in the stabilization and maintenance of spindle bipolarity. *Current biology : CB*. 19:1712-1717.

Venere, M., C. Horbinski, J.F. Crish, X. Jin, A. Vasanji, J. Major, A.C. Burrows, C. Chang, J. Prokop, Q. Wu, P.A. Sims, P. Canoll, M.K. Summers, S.S. Rosenfeld, and J.N. Rich. 2015. The mitotic kinesin KIF11 is a driver of invasion, proliferation, and self-renewal in glioblastoma. *Science translational medicine*. 7:304ra143.

Waitzman, J.S., A.G. Larson, J.C. Cochran, N. Naber, R. Cooke, F. Jon Kull, E. Pate, and S.E. Rice. 2011. The loop 5 element structurally and kinetically coordinates dimers of the human kinesin-5, Eg5. *Biophysical journal*. 101:2760-2769.

Waksman, G., D. Kominos, S.C. Robertson, N. Pant, D. Baltimore, R.B. Birge, D. Cowburn, H. Hanafusa, B.J. Mayer, M. Overduin, M.D. Resh, C.B. Rios, L. Silverman, and J. Kuriyan. 1992. Crystal structure of the phosphotyrosine recognition domain SH2 of v-src complexed with tyrosine-phosphorylated peptides. *Nature*. 358:646-653.

Wang, W., L. Chen, Y. Ding, J. Jin, and K. Liao. 2008. Centrosome separation driven by actin-microfilaments during mitosis is mediated by centrosome-associated tyrosine-phosphorylated cortactin. *Journal of cell science*. 121:1334-1343.

Whalley, H.J., A.P. Porter, Z. Diamantopoulou, G.R. White, E. Castaneda-Saucedo, and A. Malliri. 2015. Cdk1 phosphorylates the Rac activator Tiam1 to activate centrosomal Pak and promote mitotic spindle formation. *Nature communications*. 6:7437.

Wilson, M.B., S.J. Schreiner, H.J. Choi, J. Kamens, and T.E. Smithgall. 2002. Selective pyrrolo-pyrimidine inhibitors reveal a necessary role for Src family kinases in Bcr-Abl signal transduction and oncogenesis. *Oncogene*. 21:8075-8088.

Woehlke, G., A.K. Ruby, C.L. Hart, B. Ly, N. Hom-Booher, and R.D. Vale. 1997. Microtubule interaction site of the kinesin motor. *Cell*. 90:207-216.

Zaytsev, A.V., L.J. Sundin, K.F. DeLuca, E.L. Grishchuk, and J.G. DeLuca. 2014. Accurate phosphoregulation of kinetochore-microtubule affinity requires unconstrained molecular interactions. *The Journal of cell biology*. 206:45-59.

CHAPTER 5

PROTEIN TAGGING AT THE ENDOGENOUS LOCUS AS A TOOL FOR STUDYING MITOTIC PROTEIN DYNAMICS AND LEVELS

5.1 Introduction

Cell division is a carefully controlled, dynamic process, which ensures that genetic material is equally segregated between daughter cells. Mitosis requires precise spatial and temporal regulation of proteins to guarantee proper division. Understanding where and when these proteins localize and their local concentrations would help us gain insight into this basic, dynamic biological process.

Kinesin-5 is an essential motor protein that has been extensively studied (reviewed (Ferenz et al., 2010; Singh et al., 2018; Waitzman and Rice, 2014)). The human kinesin-5, HsEg5, is a homotetrameric, bipolar, protein that crosslinks parallel and antiparallel microtubules generating force between microtubules (Kapitein et al., 2005; Shimamoto et al., 2015). When these microtubules are antiparallel, outward forces are generated that antagonize inward forces caused by the minus-end directed activity of Dynein (Ferenz et al., 2009a; Mitchison et al., 2005; Sharp et al., 2000a; Tanenbaum et al., 2008). Cells depleted of Eg5 or treated with Eg5 specific inhibitors fail to establish bipolar mitotic spindles (Ferenz et al., 2010; Kapoor et al., 2000; Mayer et al., 1999). Despite decades of study, how Eg5 is regulated to achieve spindle bipolarity remains incompletely understood.

TPX2 is a multifunctional, microtubule associated protein first identified for its role in dynein-dependent targeting of the *Xenopus* kinesin-12, Xklp2, to spindle poles (Wittmann et al., 1998). During interphase, TPX2 resides in the nucleus due to importin-α/β binding to a nuclear localization signal. Following nuclear envelope breakdown, RanGTP binds importin-α/β releasing active TPX2 (Gruss et al., 2001; Gruss and Vernos, 2004; Schatz et al., 2003). Reduction in TPX2 by siRNA results in short bipolar or multipolar spindles that fail to progress through mitosis due to the essential roles TPX2 plays in spindle formation (Garrett et al., 2002; Gruss et al., 2002). The N-terminus of TPX2 activates and targets the mitotic kinase Aurora A to spindle microtubules, which then phosphorylates TPX2 contributing to spindle flux (Fu et al., 2015b; Kufer et al., 2002). TPX2 also nucleates microtubules around chromosomes, stabilizes microtubules, regulates motor proteins, and is involved in microtubule branch formation *in vitro* (Alfaro-Aco et al., 2017; Drechsler et al., 2014; Mann et al., 2017; Petry et al., 2013; Reid et al., 2016; Tulu et al., 2006; Vanneste et al., 2009).

TPX2 has been reported to show a distribution on the spindle that overlaps with Eg5 (Ma et al., 2011). The C-terminal 37 amino acids of TPX2 facilitate localization of both Eg5 *in vivo* and inhibit motor walking on microtubules *in vitro* (Balchand et al., 2015; Eckerdt et al., 2008; Ma et al., 2011; Ma et al., 2010). In cells, active Eg5 is needed on microtubules to separate centrosomes and form a bipolar spindle (Kashina et al., 1997). Eg5 also plays a role on interpolar microtubules in anaphase to facilitate spindle elongation (Scholey et al., 2016), suggesting that TPX2 may not globally inhibit Eg5.

Identifying when and where these proteins localize to specific spindle regions may provide clues as to where Eg5 is actively sliding microtubules and generating forces

and where TPX2 regulates its activity *in vivo*. Knowing the relative levels of these proteins will also provide insight into how TPX2 is able to perform all of its mitotic functions. Further, Eg5 has been shown *in vitro* to produce both pushing and braking forces that scale with motor number and microtubule length (Shimamoto et al., 2015) but how this relates *in vivo* remains unclear. Quantification of protein concentrarion in mammalian cells may help address these questions.

We therefore wanted a reliable system for protein quantification *in vivo*. In yeast, fluorescent protein tagging at endogenous loci has allowed researchers to ask questions about protein copy numbers and stoichiometry both globally and locally (Dhatchinamoorthy et al., 2017; Joglekar et al., 2006; Lawrimore et al., 2011; Wu and Pollard, 2005). Although some labs have attempted to quantify proteins in mammalian cells, protein overexpression was used (Johnston et al., 2010; Suzuki et al., 2015).

Recent advances in genetic engineering in mammalian cells have made it possible to tag proteins at the endogenous locus (Dambournet et al., 2014; Mali et al., 2013; Ran et al., 2013). With these approaches, it has also come to light that our understanding of dynamic processes may be incomplete or incorrect due to the technical limitations of previously used methods (Dambournet et al., 2014). For example, when the distribution of clathrin tagged at the endogenous locus was compared to the same protein expressed from a plasmid, differences in both the abundance and distribution were observed (Doyon et al., 2011).

To understand how pervasive this situation might be we tagged TPX2 and Eg5 using CRISPR/Cas9 and examined the distribution along the spindle throughout mitosis. The results obtained with CRISPR tagging differ from either expression from a BAC

(Gable et al., 2012) or via antibody staining, suggesting that novel insight can be gained by tagging proteins at the endogenous locus. Further, through quantitative imaging we found that TPX2 and Eg5 display distinct patterns of localization throughout mitosis; TPX2 is absent in areas where Eg5 activity is required. These results not only further strengthen the evidence that endogenous tagging may provide new understanding of dynamic processes, such as mitosis, but also be used for protein quantification by fluorescence *in vivo*.

5.2 Results

5.2.1 Knock-sideways is functional and rapidly moves motor proteins

Determining when proteins are specifically needed in mitosis requires a method to control protein localization and function with better temporal control than siRNA. Cells use compensatory pathways when proteins are depleted by methods such as siRNA; it can take days to reach desired depletion levels and other pathways can mask the effect of protein loss (Wordeman et al., 2016). Small molecule inhibitors provide temporal control that allows for rapid inactivation, however, only a small percentage of proteins have specific inhibitors. Alternately, researchers can inject single cells with antibodies that specifically target a protein rendering it inactive, though this also has its disadvantages (i.e. low number and time consuming). Recently, several novel approaches have been developed to inactivate proteins with improved temporal resolution. For example, proteins can be tagged with an Auxin-inducible degron, which induces rapid degradation by the proteasome following addition of Auxin or, Rapamycin-induced dimerization in

which fusion proteins with dimerization tags are used (Holland et al., 2012; Robinson et al., 2010; Wordeman et al., 2016).

We decided to adapt the "knock-sideways" approach for our system. To establish the functionality of knock-sideways, we chose to re-localize Eg5. There are specific small molecule inhibitors of Eg5 (STLC/Monastrol), which prevent ATP hydrolysis and ultimately the ability to bind microtubules (Kapoor et al., 2000; Mayer et al., 1999). When Eg5 is not bound to microtubules early in mitosis, outward forces cannot be generated resulting in spindles collapsing into monopoles. Therefore, if we knock Eg5 sideways, then we would expect to see monopolar spindles indicating that we can re-localize proteins to produce physiologically relevant phenotypes.

We therefore generated an LLC-Pk1 cell line expressing an siRNA resistant Eg5-FKBP-GFP and mCherry-Tubulin (Fig. 5.1A; Methods). To these cells we co-nucleofected siRNA, to knock down endogenous Eg5, and the FRB "trap" (LDR-FRB-BFP) (Wordeman et al., 2016). Cells containing Eg5-FKBP-GFP, mCherry-Tubulin, and FRB-BFP were bipolar in the absence of Rapamycin (Fig. 5.1B). Upon addition of 200nM Rapamycin for ~30 min, Eg5-FKBP-GFP re-localized to the membrane and spindles collapsed into monopoles (Fig. 5.1B) and this was specific to cells expressing both the trap and Eg5; cells with no FRB-BFP remained bipolar even in the presence of Rapamycin (Fig. 5.1B).

These results not only highlighted the functionality of Knock-sideways but how quickly it could produce a phenotype. We therefore wanted to determine how fast re-localization occurs. For this, we used a CRISPR modified cell line where we C-terminally tagged Dynein Heavy Chain (DHC) with FKBP-GFP (Fig. 5.1C; methods).

We chose Dynein (DHC) because it is expressed and functional in both interphase and mitosis (reviewed (Roberts et al., 2013)) allowing us to observe its movement in any cell that was expressing both the FKBP and FRB. We nucleofected the FRB-BFP membrane targeted trap and added the Rapamycin during time-lapse image acquisition. Within 2-3 minutes, the diffusive GFP observed in the cytoplasm of interphase cells began to re-localize to the membrane (Fig. 5.1D). Taken together, these results indicate that knock-sideways has physiological functionality and provides high temporal control. Due to the success of our knock-sideways initial experiments, we decided to tag other mitotic proteins at the endogenous locus using CRISPR/Cas9 but unfortunately only yielded heterozygotes (see section xxx; Discussion) and thus prohibited further knock-sideways experiments.

5.2.2 Generating CRISPR cells for protein localization

In order to generate mammalian cells expressing proteins that were fluorescently tagged at the endogenous locus, we added a C-terminal EGFP tag using CRISPR/Cas9 in HeLa cells (Methods; Fig. 5.2A; Fig. 5.3A). To do this a cassette containing the coding sequence for EGFP and a selectable marker was inserted downstream of each gene. After introduction of Cas9 and the repair cassette by nucleofection, only those cells that had undergone homologous recombination survive in antibiotic containing medium (Methods). Genotyping of clonal populations revealed that approximately half of all selected clones (6/10 Eg5 and 2/5 TPX2) were modified; of the clones that were genotyped (3 and 2 Eg5 and TPX2 respectively), all were heterozygous, with one allele tagged with the EGFP and the other wild-type (Fig. 5.3A, B). Western Blotting of total

cell extracts of cell clones, using Eg5 or TPX2 specific antibodies also verified genotypes (Fig. 5.3C, D). Quantification of Western blots showed that Eg5 clones expressed ~50% (55 ± 3.7%) EGFP tagged and ~50% (44.9 ± 3.7%) untagged protein. In contrast, TPX2 clones expressed ~20% (20.7 ± 2.4%) tagged vs. ~80% (79.3 ± 2.4%) untagged protein. Because we used HeLa cells for tagging and these cells are known to have irregular karyotypes (Landry et al., 2013; Macville et al., 1999) we wanted to ensure that expression in our TPX2 tagged cells was stable over time. In order to test this, we passaged the cells for >30 passages and compared the protein expression levels to the earlier passage number (Fig. 5.3C). No difference in the expression levels was observed indicating that this clone was stable over the period of our analysis (see Discussion). Finally, both the TPX2 and Eg5 CRISPR modified cells display mitotic morphology indistinguishable from the parental HeLa cells (Fig. 5.3E) and progressed through mitosis without any abnormalities, suggesting that the tag does not interfere with mitosis in these cells. In summary, this approach is a straightforward method to generate clonal cell populations with fluorescent tags at the endogenous locus. Because large numbers of cells are present following selection, testing additional clones is likely to yield homozygous lines. For the present experiments, having a fluorescent tag at both alleles is not required, so the heterozygous cells were used for the following experiments.

5.2.3 TPX2 but not Eg5 is enriched relative to microtubules at spindle poles

The CRISPR modified cells were used to quantify protein distribution throughout mitosis. This is important because knowing the distribution and relative levels of proteins in the mitotic spindle can provide information about the mechanisms by which

the proteins might interact and function. In previous work, enrichment of mitotic proteins, including Eg5 and TPX2, at spindle poles has been reported; however, the extent of enrichment, and if a given protein is enriched relative to microtubules, which are also more condensed at spindle poles, has not been established.

To measure protein distribution along the spindle axis, cells were arrested in metaphase using MG132 and Z-stacks of metaphase cells were acquired using spinning disc confocal microscopy (Methods). The distribution of Eg5 and TPX2 was measured using line scans along the pole-to-pole axis and additionally by quantifying fluorescence in selected regions: near the pole, in front of kinetochores and at the spindle midzone (Methods; Fig. 5.2). The results show that each protein is enriched at spindle poles relative to the midzone, consistent with earlier work. TPX2 was nearly 2-fold more enriched at poles compared to Eg5 (5 ± 1.12X vs. 2.6 ± 0.63X respectively) in cells with and without microtubule labels (Fig. 5.2D, Fig. 5.6A). When the level of each tagged protein was compared near the pole and just in front of kinetochores, however, there was a more similar enrichment for Eg5 and TPX2 (1.27 ± 0.22X vs. 1.48 ± 0.2X respectively) however they were still significantly different ($p=0.01$) (Fig. 5.6B). In summary, these results demonstrate that Eg5 and TPX2 have distinct distributions on the spindle, suggesting independent mechanisms for localization.

To determine if Eg5 and TPX2 were enriched relative to microtubules, we additionally imaged microtubules in the CRISPR cells. This was done in two different ways. First, Eg5-EGFP cells were transfected with mCherry tubulin, selected, and sorted using flow cytometry. The second way microtubules were labeled was using SiR Tubulin (Methods) (Hueschen et al., 2017) under conditions that had no detectable effect on

mitotic spindle morphology. In either case, similar ratios of tubulin at the pole compared to the midzone (2.3X for both) were obtained, and thus data from both approaches were averaged. When the enrichment level of each protein was compared to that of tubulin, the results show that Eg5 is not significantly enriched at spindle poles relative to microtubules, with a ratio of ~1 (1.2 ± 0.36X). In contrast, TPX2 was ~2 fold (2.2 ± 0.41X) enriched relative to microtubules. When the levels of Eg5 and TPX2 were compared to the microtubules near the pole and just in front of kinetochores, Eg5 was not enriched relative to microtubules while TPX2 was still slightly enriched (1.00 ± 0.13X, Eg5; 1.28 ± 0.16X, TPX2) (Fig. 5.4B).

As a control for our analysis method, cells expressing CRISPR tagged HURP were used. Unlike Eg5 and TPX2, HURP has been shown to be enriched towards kinetochores not poles (Koffa et al., 2006; Sillje et al., 2006). HURP indeed shows a distinct distribution from Eg5 and TPX2, and quantification shows that it is not enriched at the poles either alone or relative to tubulin (Fig. 5.2 B, C, D).

Because these data suggest that Eg5 and TPX2 are distributed differently along a metaphase spindle we were curious what their relative protein levels were on the spindle. On average, there was ~4 fold (3.9X) more TPX2 on a metaphase spindle than Eg5 (Fig. 5.2E), and this relationship was constant throughout all stages of mitosis (Fig. 5.8A). Additionally, by measuring the total cellular fluorescence and spindle-associated fluorescence for both Eg5 and TPX2, the fraction of each protein that is spindle associated can be determined. The data show that on average only a fraction of the total fluorescence (19.8% Eg5 and 33.9% TPX2) was associated with the spindle, regardless of mitotic stage (Fig. 5.8B, C).

5.2.4 Immunofluorescence quantification of metaphase spindles

Next we wished to compare the distribution of Eg5-EGFP and TPX2-EGFP obtained using CRISPR tagged cells with the distribution obtained using conventional immunofluorescence. To do this, parental HeLa cells were arrested at metaphase using MG132, fixed and stained for microtubules and either TPX2 or Eg5 and Z-stacks of metaphase cells were acquired using spinning disc confocal microscopy as with the live cells. Analysis was performed identically to the live cells (Fig. 5.6). In the case of TPX2, protein distribution on the spindle was similar to that obtained using the CRISPR EGFP tagged cells, although there is increased spindle-to-spindle variability using immunofluorescence (Fig. 5.6 A, B, C). In the case of Eg5, however, the results obtained with immunofluorescence suggest that Eg5 is concentrated relative to microtubules at spindle poles (1.76 ± 0.55X) which was not observed using CRISPR tagging (Fig. 5.6 C, D). The results obtained from the fixed and stained cells are more similar to cells overexpressing Eg5 (Gable et al., 2012). We then wondered if these differences might be a result of the method used and therefore looked for differences in spindles between the 2 techniques. On average spindles were significantly shorter (9.96 ± 0.87 μm; CRISPR vs. 5.91 ± 0.98 μm; IF) and they were shorter in Z (Fig. 5.4C). These differences might be attributed to the differences we observe between the two methods.

5.2.5 Redistribution of Eg5 and TPX2 are distinct in anaphase

Next, we quantified the dynamics and distribution of Eg5 and TPX2 as cells progressed through mitosis using time lapse imaging of cells expressing either Eg5-EGFP

or TPX2-EGFP. Cells were observed starting at anaphase onset when fluorescence of both proteins appears to decrease in the spindle midzone (Fig. 5.7). Analysis of the fluorescence intensity within the spindle midzone as anaphase progresses revealed that Eg5 redistributes to the midzone before TPX2 (Fig. 5.7 B, D). In fact, TPX2 remains accumulated at spindle poles throughout anaphase and showed only minimal redistribution to the midzone compared to Eg5 (Fig. 5.7C). This distinct distribution further suggested that Eg5 and TPX2 have different regulation and function in anaphase.

5.2.6 Eg5 but not TPX2 is found on overlapping microtubules

Eg5 generates outward force on overlapping antiparallel microtubules (Kapitein et al., 2005; Shimamoto et al., 2015), and this action is thought to be critical to maintain spindle length and bipolarity (Ferenz et al., 2009a). *In vitro*, TPX2 regulates Eg5 activity by acting as a brake, causing motors to slow on microtubules (Balchand et al., 2015). Because both proteins localize to spindle microtubules, the data suggest that Eg5's activity would be inhibited by TPX2 on spindle microtubules, preventing the generation of outward forces.

To understand how TPX2 regulates Eg5, the distribution of Eg5 and TPX2 in the region of the spindle where overlapping microtubules are present was examined (Mastronarde et al., 1993; McIntosh and Landis, 1971; Polak et al., 2017). To do this we took advantage of cells with spindles oriented perpendicular (90°) to the coverslip surface. We acquired Z-stacks of these perpendicular spindles and asked if Eg5 and/or TPX2 co-localized with microtubules in the mid-region of the spindle (between sets of K-fibers) (Fig. 5.8A). As expected, discrete puncta of microtubules in both metaphase and

anaphase cells (Fig. 5.8 B, C, Fig. 5.9) were detected in the 1.32 μm region in the spindle midplane. These microtubule puncta were generally organized in a circle consistent with the distribution of chromosomes on the periphery of the spindle at metaphase (Magidson et al., 2011). Z-planes away from the midplane contained microtubule bundles that were considerably brighter, consistent with kinetochore fibers which contain on average 17 microtubules (Simunic and Tolic, 2016; Tolic, 2017; Wendell et al., 1993).

Imaging of Eg5-EGFP CRISPR modified cells revealed that Eg5-EGFP was also present in the mid-region of both metaphase and early anaphase spindles (Fig. 5.8 B, C, Fig. 5.9 A, B) and further that these Eg5 puncta were present in a distribution that overlapped with the microtubule distribution (Fig. 5.8 B, C, Fig. 5.9 A, B). In the midplane of TPX2-EGFP CRISPR modified cells, however, fluorescent puncta above background fluorescence levels were rare for both metaphase and later anaphase cells. Moreover, TPX2 puncta that could be detected did not match the microtubule distribution except at the cell periphery (Fig. 5.8 B, C, Fig. 5.9 A, B). These few visible puncta at the cell periphery are likely part of long microtubules originating from the poles or K-fibers where TPX2 and Eg5 were both detected (Fig. 5.8 B, C). These results suggest that TPX2 is not significantly localized to regions of microtubule overlap. This result supports the hypothesis that Eg5 is active on overlapping antiparallel microtubules in the midzone and is not subject to inhibition by TPX2 in this location.

5.2.7 Absolute Protein Concentrations using Quantitative Fluorescence Microscopy

One of the advantages of endogenous tagging is that we can address relative protein accumulation as well as measure protein concentration both locally and globally *in vivo* (Wu and Pollard, 2005).

A major function of Eg5 is to drive centrosome separation during prophase; consistent with this function, Eg5 is detected at the centrosome (Blangy et al., 1995; Eibes et al., 2017; Gable et al., 2012; Rapley et al., 2008). Z-stacks of prophase Eg5-EGFP CRISPR modified cells were collected using spinning disc confocal microscopy and fluorescence of the whole cell vs. the centrosomes was determined (methods). For centrosome measurements, we chose an area ~2 μm (2.08 μm) in diameter centered on each centrosome (Area = 3.4 μm^2) with a height between 2-5 μm based on the number of z-steps needed to encompass all the centrosome fluorescence. This volume was similar in dimensions to the size of the total functioning centrosome which includes centrioles, and pericentriolar material (Alieva and Uzbekov, 2016). On average, the fluorescence of the centrosome, as defined here, is only ~2% (2.25 ± 1.18%) of the total cell fluorescence. We therefore determined the relative accumulation at the centrosomes and compared it to the entire cell by calculating their fluorescence per area (μm^2) (Fig. 5.5D). On centrosomes, Eg5 is ~7.5X (7.6 ± 1.94X) concentrated relative to the whole cell (Fig. 5.5D).

We then determined the local concentration of Eg5 at the centrosome. For this, we used cells with a known number of GFP molecules in a defined structure. We therefore imaged HeLa cells stably expressing Hec1-EGFP using identical conditions as our CRISPR modified cells. Knowing that there are 244 Hec1-EGFP molecules per kinetochore (Suzuki et al., 2015) we were able to measure the average total fluorescence

for Hec1-EGFP spots and convert fluorescence intensities to number of molecules (Fig. 5.10 A, B). We found that the concentration of Eg5 at a prophase centrosome to be ~4 μM (4.08 ± 1.93 μM) (Fig. 5.10C; methods). This is significantly concentrated compared to the whole cell Eg5 concentration of ~2 μM (1.97 ± 0.45 μM) (Fig. 5.10C). Similar calculations can be performed for other sub-regions of the mitotic cell to gain insight into local concentrations of mitotic proteins.

TPX2 is also detected at prophase centrosomes in animal cells (Eibes et al., 2017; Ma et al., 2011) and at the nuclear periphery in plant cells. Recent work shows that this pool of TPX2 contributes to Eg5 localization to prophase centrosomes (Eibes et al., 2017). However, given the bright nuclear signal of TPX2, which typically overlaps the centrosome signal, the enrichment of TPX2 at prophase centrosomes was not measured.

Regulation of Eg5 is only one of the many functions of TPX2 in mitosis and therefore one would expect that it is more abundant than Eg5 but this has never been quantified. Using our Hec1-EGFP standard, and the volume of an average HeLa cell (methods) we determined that TPX2 is significantly more concentrated in mitosis compared to Eg5 (3.14 μM vs. 1.97 μM respectively).

Finally, we asked how much Eg5 and TPX2 were on the spindle itself. We therefore measured the relative local accumulation of TPX2 and Eg5 on the spindle by comparing their respective fluorescence intensities (Figure 5.11). On average, there is ~3.5X more TPX2 than Eg5 on the spindle (Figure 5.11A). However, our live cell data suggest that the localization of these proteins change throughout mitosis. Therefore, we measured the relative local accumulation of TPX2 and Eg5 throughout mitosis and found that while Eg5 levels remain relatively constant early in mitosis (Figure 5.11 B,C), TPX2

is significantly higher early in mitosis compared to later stages (Figure 5.11 B,C) and remains significantly higher than Eg5 by the spindle poles. Taken together this suggests that there is spatial regulation of Eg5 by TPX2.

5.3 Discussion

5.3.1 Advantages and Disadvantages of CRISPR Tagging

Our data show that using CRISPR tagging provides insight into protein distribution in mitosis and that the values obtained differ from prior work using either BACs or immunofluorescence (Figures 5.2, 5.6) (Gable et al., 2012). These data highlight the differences in information gathered due to technical limitations. As others have argued, CRISPR and other endogenous tagging methods prevent overexpression artifacts (Dambournet et al., 2014; Doyon et al., 2011). More specifically, overexpression of TPX2 is a marker for many cancers as well as results in abnormal spindle phenotypes (Gruss et al., 2002; Neumayer et al., 2014). Additionally, because CRISPR modifications are permanent and specific, the chances of a plasmid integrating into unwanted places in the genome or being lost as cells divide is reduced.

Despite the value of using endogenous tagging, it may not be feasible to use this approach in all cases. For example, despite the fact that generating CRISPR tagged cells is becoming more straightforward, it is time consuming, and making cells with multiple tags could be limited by the availability of selectable markers. Additionally, examining the distribution of several different proteins following deletion, or deletion/replacement approaches would be more complicated. For example, many essential mitotic proteins were discovered using screens for defective phenotypes when they were absent or

inhibited (Goshima et al., 2007; Neumann et al., 2010; Zhu et al., 2005). For these and other essential proteins, CRISPR cannot be used for permanent knock-outs otherwise the cells would have irregularities that would ultimately affect their survival. Inducible knock-outs could be used as an alternative strategy to permanent deletion in a cell line (McKinley and Cheeseman, 2017); however, these too have their limitations. Therefore, testing the effects of specific perturbations regarding essential proteins would require a variety of different CRISPR lines with appropriate modifications.

In our experiments we used CRISPR modified cell lines that were heterozygotes (Fig. 5.3B). One drawback of this approach is the possibility that the tagged and untagged versions of the protein are not equivalent and thus not present in equal amounts in cellular structures. In addition, differential allele expression has been seen in human cells (Knight, 2004) and appears to be the case in our CRISPR modified TPX2 clones (Fig. 5.3C) where the amount of tagged and untagged protein are not equivalent. We assumed that even though there appears to be differential allele expression that both the tagged and untagged versions were present in cellular structures without any bias. However, this assumption needs to be validated by additional experimentation.

Alternatively, having all copies of the protein tagged could also be deleterious due to potential interference by the tag, and this could impact cellular processes. Prior work in genetically tractable systems has shown that proteins with GFP tags can complement deletion of the endogenous protein suggesting that the tag has little or no effect on cells. However, there are cases where the tag can affect a cellular process. Perhaps the best example is tubulin, in which cells that express high levels of GFP-tubulin are not viable or have shortened spindles. In yeast, GFP-TUB1 tagged cells display normal dynamics

and growth but only if there is a mixture of tagged and untagged TUB1 (Maddox et al., 1999; Straight et al., 1997). The same is seen in mammalian cells where tubulin translation is regulated by the cytoplasmic level of tubulin (Yen et al., 1988); thus when tubulin is expressed from a plasmid, the total level of tubulin is regulated by the cell (Goodson et al., 2010; Rusan et al., 2001). These examples provide strong evidence that a tag can affect cellular processes and therefore limiting the amount may be necessary in some cases, supporting the use of heterozygotes. In order to test this hypothesis, homozygous CRISPR modified clones would need to be made, characterized and compared to heterozygotes.

5.3.2 TPX2 is not present at sites where Eg5 is acting

Using cells with tags at the endogenous locus, our results provide new insight into the regulation of Eg5 by TPX2. Prior work demonstrated that TPX2 reduces the motility of Eg5 on microtubules *in vitro* (Balchand et al., 2015; Ma et al., 2011). This result has been difficult to reconcile with the requirement for active Eg5 during spindle assembly and maintenance (Kapoor et al., 2000; Mayer et al., 1999; Sawin and Mitchison, 1995). Our results show that Eg5 is present on regions of the spindle where overlapping antiparallel microtubules are located, consistent with the active force generation at this location (Shimamoto et al., 2015). In contrast, TPX2 was barely detected above background in this region, even though the protein was 4X more enriched on the spindle than Eg5. Thus the data suggest at sites where Eg5 is active, TPX2 is not detectable.

Consistent with this idea comes from or prophase data. As mentioned, in most cells, kinesin-5 activity is required for bipolar spindle formation; therefore, it was not

surprising to find a high local concentration of Eg5 at spindle poles (Fig. 5.10C; Fig. 5.5D). Though TPX2 has been shown to localize to the centrosomes in prophase (Eibes et al., 2017; Ma et al., 2011) it is potentially not as concentrated or has a different distribution allowing Eg5 to accumulate and be active.

In contrast to these regions where we observed a difference in localization of these proteins, both TPX2 and Eg5 were prominently localized to the half spindle, between the kinetochores and spindle pole, consistent with numerous reports (Cheerambathur et al., 2008; Gable et al., 2012; Garrett et al., 2002; Gruss et al., 2002; Sawin et al., 1992; Sawin and Mitchison, 1995; Wittmann et al., 2000). By measuring the fluorescence of microtubules the data show that TPX2, but not Eg5 is enriched relative to microtubules near spindle poles. The relatively uniform distribution of Eg5 is somewhat unexpected, as other work has reported that it is enriched at spindle poles and further, Eg5 has been reported to be transported poleward by dynein (Gable et al., 2012; Uteng et al., 2008). In yeast, kinesin-5 family members move toward the minus ends, and accumulate in the region between kinetochores and spindle poles (Goldstein et al., 2017; Roostalu et al., 2011; Tytell and Sorger, 2006). Eg5 is highly dynamic with a short dwell time on microtubules (Gable et al., 2012). This rapid binding and unbinding behavior may counteract poleward transport or plus end directed motility, resulting in this even distribution.

5.3.3 *In vivo* quantification of Eg5 and TPX2 levels in mitosis

Eg5 and TPX2 are both cell cycle regulated with levels increasing in S and G2, remaining high in M, and dropping in G1 (Gruss et al., 2002; Uzbekov et al., 1999;

Venere et al., 2015). Previous work showed that Eg5 and TPX2 are specifically ubiquitinated and degraded by the anaphase-promoting complex as cells exit mitosis (Stewart and Fang, 2005; Venere et al., 2015). Our data show that the levels do not appear to significantly decrease as cells progress through mitosis, but rather remain constant even through late anaphase (Fig. 5.5 A, B, C). It is possible that the methods used account for these differences and because we are imaging single cells live we are better able to detect subtle differences that a bulk assay cannot.

The ability to observe single cells live provided us the ability to correlate fluorescence to protein amount (Wu and Pollard, 2005). Knowing the concentrations and stoichiometries of proteins helps provide insight into how biological processes form and change as well as form the basis for modeling. Given that TPX2 is a multifunctional microtubule associated protein it is perhaps not surprising that it is present at a ~4x higher relative level than Eg5 on the spindle and ~1.5x more concentrated as a whole (Fig. 5.2E, Fig. 5.10D). Additionally, the fraction of each EGFP tagged protein is not particularly high on the spindle (Fig. 5.5B), which was also not unexpected, given that these are dynamic proteins *in vivo* (Gable et al., 2012; Ma et al., 2010).

Mammalian cells are more complex than yeast making them more challenging to quantify. Additionally, unlike yeast which have a reliable, endogenously tagged EGFP standard for comparison (Joglekar et al., 2006; Lawrimore et al., 2011), the mammalian cell standard does not have an endogenous tag (Suzuki et al., 2015). Therefore, it is subject to potential cellular problems like those mentioned above (section 5.3.1). Despite these potential problems, determining the protein amount *in vivo* both locally and globally is needed in the mammalian field. Our cells are potentially an improvement on

the mammalian standard due to the endogenous tag. In the future, this technique could be useful not only for quantifying other mitotic proteins but for analyzing targeting mechanisms and asking how specific proteins change after perturbations.

5.4 Materials and Methods

5.4.1 Materials

All chemicals, unless otherwise specified, were purchased from Sigma-Aldrich.

5.4.2 CRISPR gene editing

EGFP or FKBP-EGFP tags were added to the C-terminus of human TPX2, Eg5, and HURP using methods described previously (Sheridan and Bentley, 2016; Stewart-Ornstein and Lahav, 2016). In brief, repair cassettes containing either EGFP or FKBP-EGFP linked to a cleavable peptide (T2A) followed by a selectable marker (Neomycin) were cloned and used for PCR reactions. Each also encoded for Glycine-Alanine linkers between proteins. Guide sequences were selected using the CRISPR design tool (http://crispr.mit.edu/) from the Zhang lab at MIT (Ran et al., 2013). The parameters used were: “other regions” and the human target genome (hg19). We then had the tool search for guides close to the C-terminus of the protein of interest (~100nt surrounding and including the stop codon). Top and bottom oligos were obtained for each guide (Table 5.1) with the bases 5’-CACC -3’added to the top oligo and 5’-AAAC-3’ added to the complement of the bottom oligo.

Table 5.1 Guide RNAs (PAM)

Target Protein	Guide RNAs 5'-3'
TPX2	TGCGGATACCGCCCGGCAAT(**GGG**)
Eg5	AGGTTGATCTGGGCTCGCAG(**AGG**)
HURP	ACTTTTTCACCTCTACAACC(**AGG**)

Guides were cloned into a Cas9 containing plasmid (PX459) obtained from Addgene (Cambridge, MA) (#62988) following methods previously outlined (Moyer and Holland, 2015). Briefly, top and bottom oligos were annealed and then phosphorylated by T4 PNK (NEB, Ipswich, MA). Guides were then cloned into PX459 that was cut using BbsI (NEB, Ipswich, MA) and ligated using T4 ligase (NEB Ipswich, MA). Guide-Cas9 containing plamids were then sequenced using the U6 promotor primer (Ran et al., 2013) and purified using either endotoxin free mini-preps or midi-preps according to manufacturer protocol (Promega, Madison, WI).

Repair cassettes were amplified using primers designed to be homologous to the C-terminal genomic DNA surrounding the STOP codon (Table 5.2). In all cases, the guide target sequence was mutated to prevent Cas9 from recognizing the repair cassette and described previously (Moyer and Holland, 2015).

Table 5.2 Oligonucleotides Used

Protein	Repair Cassette PCR Primers 5'-3'
TPX2 F	GTACCAGGGTCTGGAGATAAAGTCAAGTGACCAGCCTCTGACTGTGCCTGTATCTCCCAAATTCTCCACTCGATTCCACTGC**GGAGCTGGTGCAGGCG**
TPX2 R	**CTATCGCCTTCTTGACGAGTTCTTC**TAAACTCAGCTGTGAGCTGCGGATACCGCCCGGCAATGCGACCTGCTCTTAACCTCAAACCTAGGACCGTCTTG
Eg5 F	CACTGGAGAGGTCTAAAGTGGAAGAAACTACAGAGCACTTGGTTACAAAGAGCAGATTACCACTCCGTGCGCAGATTAACCTT**GGAGCTGGTGCAGGCG**
Eg5 R	**CTATCGCCTTCTTGACGAGTTCTTC**TAATTCACTTGGGGGTTGGCAATTTTATTTTTAAAGAAAACTTAAAAATAAAACCTGAAACCCCAGAACTTGAGC
HURP F	GACATCAAGAACATGCCAGACACATTTCTTTTGGTGGTAACCTGATTACTTTTTCTCCTCTTCAGCCTGGTGAATTT**GGAGCTGGTGCAGGCG**
HURP R	**CTATCGCCTTCTTGACGAGTTCTTC**TGAATTTAAAAATAAATCCAAACATTTTCCTTCATATTATCAATGCTTATATATTCCTTAGACTATTGAAATTT
Protein	**Genomic DNA PCR Primers 5'-3'**
TPX2 F	GTGACTGGGACCTGTAAAACTC
TPX2 R	CTACCCGTGCCTGAGAAAG
Eg5 F	GAAGGCATTTGGCGCTAC
Eg5 R	CTTGAGCCCAGGAGTTTG
GFP R	CTACAACAGCCACAACGTC
Primer	**Knock-Sideways, Gibson Assembly Primers 5'-3'**
Eg5 F	CTTATGGCCATGGAGGCCCGAATTCGGATGGCGTCGCAGCCAAATTC
Eg5 R	CGCCTGCACCAGCTCCAAGGTTGATCTGGGCTCG
Cassette F	CGAGCCCAGATCAACCTTGGAGCTGGTGCAGGCG
Cassette R	CATGTCTGGATCCCCGCGGCCGCTCAGAAGAACTCGTCAAGAAGGC
Protein	**siRNA 5'-3'**
Eg5	CUGAAGACCUGAAGACAAU

Cells were grown in DMEM medium (ThermoFisher Scientific) with 10% Fetal bovine serum (FBS, Atlanta Biologicals, Flowery Branch, GA) and 0.5X

antibiotic/antimycotic solution (final concentrations 50 U/mL penicillin, 0.05 mg/mL streptomycin, 0.125 ug/mL amphotericin B; Sigma-Aldrich, St. Louis, MO) at 37 °C and 5% carbon dioxide (CO_2). For long term storage cells were frozen in DMEM medium with 5% FBS and 0.5X antibiotic/antimycotic solution and held at -80°C for 1-2 days before moving to liquid nitrogen.

Parental HeLa Cells were nucleofected using an Amaxa Nucleofector (Lonza, Portsmouth, NH) program I-013 and Mirus nucleofection reagent (Mirus Bio LLC, Madison, WI) according to the manufacturers recommendations. Plasmids and Repair cassettes were used at ratio of 1:1 at a concentration of 1 μg DNA each. Following nucleofection, cells were grown in regular growth media in 100mm dishes for 48-72 Hrs and then 0.2g/L Neomycin/G418 (InvivoGen, San Diego, CA) selection media was added. Media was then changed daily for 10-14 days and then colonies of green, CRISPR positive, cells were picked using cloning rings and returned to regular media for further screening and experiments.

5.4.3 Genotyping

Genomic DNA was isolated from clonal CRISPR tagged cells using the DNeasy Blood and Tissue Kit (Qiagen, Valencia, CA) according to manufacturers recommendations. DNA was then amplified by PCR using genomic primers (Table 5.2) targeting the C-terminus of each protein, the GFP tag, and downstream of the Stop codon (Fig. 5.3). KOD polymerase (MilliporeSigma, St. Louis, MO) was used to amplify 2 μL of isolated genomic DNA in a 20 μL reaction for 35 cycles. Extension times were varied based on primer combinations and products were analyzed using 1% agarose gel

electrophoresis. PCR Products of clones that produced bands of expected sizes were purified using a PrepEase DNA clean-up kit (USB Corporation, Cleveland, OH) and sequenced to verify proper integration of the tag.

5.4.4 Western Blotting and Quantification

Cell extracts of clonal CRISPR tagged cells were prepared by adding 1X SDS Sample buffer to cells grown to confluency in 35 mm dishes. Samples were boiled for 5 minutes and run on either an 8 or 10% SDS polyacrylamide gels using the formulation of Laemmli (Laemmli, 1970). Gels were transferred onto Amersham Hybond-P membrane (GE Healthcare, Waukesha, WI). Blots were probed with Eg5, TPX2 or Hec1 antibodies (Novus Biologicals, Littleton, CO) used at 1:1000 (Eg5 and TPX2) and 1:200 (Hec1) for 1 h at room temperature in 5% non-fat dry milk dissolved in Tris buffered saline containing 0.02% Tween-20 (TBS-Tween). Blots were then probed using goat anti-rabbit HRP conjugated secondary antibody (Eg5 and TPX2) and goat anti-mouse HRP conjugated secondary antibody (Hec1) (Jackson Immunoresearch Laboratories, Inc.) (1:5000) for 1 hr at room temperature in 5% non-fat dry milk dissolved in TBS-Tween and blots were imaged using chemiluminescence.

To quantify the levels of tagged and untagged protein in each sample from clonal cell populations, densitometry was used (Fiji). The total protein level was determined by adding the total fluorescence in each lane. The amount of tagged and untagged protein was calculated as a percentage of this total amount.

5.4.5 Knock-Sideways (Rapamycin-induced Dimerization)

Proteins were tagged on the C-terminus with an FKBP and an EGFP tag in either a plasmid (Eg5) or at the endogenous locus (DHC; see CRISPR gene editing methods). Cloning Eg5, FKBP, and EGFP into a Clonetech Laboratories (Mountain View, CA) expression vector (pCMV-Myc) was done using Gibson Assembly. Cloning was designed to mimic the endogenous tag in CRISPR modified cells (CRISPR gene editing methods) including a 10AA (Gly-Ala) linker between the C-terminus of Eg5 and FKBP. Eg5 and FKBP-EGFP-T2A-Neomycin cassette were amplified by PCR (Table 5.2). The Eg5 was made resistant to siRNA as described previously (Bickel et al., 2017).

The siRNA resistant pCMV-Myc-Eg5-FKBP-EGFP construct was nucleofected into mCherry-Tubulin expressing LLC-Pk1 cells as previously described (Bickel et al., 2017). With the help of Dr. Amy Burnside, GFP and mCherry positive cells were sorted by flow cytometry. These cells were then maintained as described previously (Bickel et al., 2017). Cells were then co-nucleofected with Eg5 siRNA (Table 5.2) obtained from Dharmacon (GE Healthcare Life Sciences, Pittsburgh, PA) and a membrane targeted FRB-BFP construct that was provided by Dr. Linda Wordeman and used previously for knock-sideways experiment (Wordeman et al., 2016). For knock-sideways experiments with DHC-FKBP-EGFP CRISPR modified HeLa cells, only the FRB-BFP construct was nucleofected as described above (CRISPR gene editing methods). Following nucleofection, cells were plated on mattek dishes and imaged ~24 hrs later.

5.4.6 Cell Fixation and Immunofluorescence

HeLa cells were rinsed twice with room temperature PBS lacking calcium and magnesium and were then fixed for 10 minutes in 3.2% paraformaldehyde, 0.1%

glutaraldehyde, and 0.5% Triton X 100, made fresh daily in PBS lacking calcium and magnesium. Fixed cells were rinsed in PBS containing 0.02% TWEEN-20 and 0.02% sodium azide (PBS-Tw-Az), treated with sodium borohydride (10mg/10mL H_2O) for 10 minutes and then rehydrated in PBS-Tw-Az.

The following antibodies were used: tubulin, DM1α mouse anti-tubulin (Sigma-Aldrich) or YL1/2 rat anti-tubulin (Accurate Chemical and Scientific Corporation, Westbury, NY), Eg5 rabbit polyclonal (Novus Biologicals, Littleton, CO), TPX2 rabbit polyclonal (Novus Biologicals, Littleton, CO) and appropriate secondary antibodies as previously described (Avunie-Masala et al., 2011). Primary antibodies were mixed with 2% BSA in PBS-Tw-Az to block non-specific binding and used at the following final dilutions: Eg5 and TPX2 1:1,000, DM1α and YL1/2 1:100; cells were incubated in primary antibodies for 1 hour at 37°C. Stained cells were mounted on glass slides using DAPI Fluomount G (Southern Biotech, Birmingham, AL) to stain DNA.

5.4.7 Microscopy

1-2 days prior to imaging, cells were plated on Mattek glass bottom dishes (Mattek Corporation, Ashland, MA). Before imaging, cells were transferred to imaging (non CO_2) media lacking phenol red (Collins et al., 2014) and maintained on the microscope in an Okolab UNO (Burlingame, CA) environmental chamber set to 37°C.

For z-stacks, cells were imaged on a Nikon Ti-E microscope with a CSU-X1 Yokogawa spinning-disk confocal scan head (PerkinElmer, Wellesley, MA), an Andor iXon+ electron-multiplying charge-coupled device camera (Andor), and a 100×/1.4 NA objective lens. Z-step size was set at 0.33 μm to optimize signal collected but not

oversample. Z-steps were taken relative to the bottom of the cell for a total Z-stack of 25 μm (77 steps) for live cells and 20 μm (62 steps) for fixed cells. In order to ensure cells did not photobleach prior to imaging, mitotics were identified using Phase Contrast and the focus was dropped below the cell before imaging began.

Laser powers and exposures were chosen to ensure that the sum of the fluorescent signal would not be saturated. For cells expressing EGFP tags, images were acquired using a 488nm laser at 20% power and 750 msec exposure. For cells also expressing mCherry tags (Tubulin) images were taken using a 561 laser at 32% power with 500ms exposure. For cells with far-red tags (SiR Tubulin, DRAQ5), images were acquired using a 640 laser at 20% power and 750 msec exposure. When 2 colors were imaged, each color was acquired before moving up in z. In the case of DRAQ5 (DNA marker), a single image was acquired following the 488 z-stack of the corresponding cell.

Timelapse images were acquired using a CSU-10 Yokogawa spinning-disk confocal scan head on a Nikon TE300 as previously described (Tulu et al., 2003). Images were acquired every minute with an exposure of 1000 msec and 4x4 binning.

To quantify mitotic phenotypes of fixed cells, a Nikon Eclipse Ti with an X-Cite series 120Q excitation light source, and a 100 X, 1.3 N.A., objective lens, was used. Mitotic phenotypes were classified by spindle morphology based on microtubule staining as bipole, multipole, monopole, or disorganized. Disorganized spindles included spindles with extra foci, fragmented poles, short spindles, no pole, and bent spindles.

For knock-sideways experiments, a Nikon A1R point scanning confocal microscopy with 60X/1.4 NA objective was used. Cells expressing the membrane bound FRB-BFP “trap” were found using epifluorescence and a Violet excitation block BFP

filter. Eg5-FKBP-GFP, mCherry Tubulin expressing LLC-Pk1 cells were then imaged for GFP and mCherry to determine spindle phenotypes following Rapamycin treatment. For time-lapse imaging of DHC-FKBP-GFP CRISPR modified HeLa cells, only the GFP signal was acquired and cell positions were marked using XY positioning in NIS elements.

5.4.8 Image Analysis

Analysis was performed in Fiji (Image J) (Schindelin et al., 2012). Sum intensity projections of z-stacks were created for single or double colors. For whole cell Fluorescence Intensity, images were background subtracted using a region of the same size from a z-stack of parental HeLa cells imaged using identical conditions. For background-corrected fluorescence intensity on the spindle, a region within a region background subtraction was used. This was done by manually drawing a region around the spindle and then a concentric larger region around the spindle, encompassing the spindle and surrounding cytoplasm. Then using the formulas: Background signal = (Integrated Fluorescence Intensity $_{\text{big area}}$ − Integrated Fluorescence Intensity $_{\text{small area}}$)/(Area $_{\text{big}}$ − Area $_{\text{small}}$). Total Intensity = Integrated Fluorescence Intensity $_{\text{small area}}$ − (Background signal × Area $_{\text{small}}$) (Ye et al., 2015), fluorescence intensity was calculated. Cells were grouped according to cell stage (identified using DRAQ5 to label DNA). In order to account for untagged protein in the cell, following background subtraction, fluorescence values were adjusted based on the amount of tagged and untagged protein determined to be in the clonal population (Fig. 5.3).

For local accumulation, the fluorescence of the whole cell was measured by drawing a freehand shape around the cell and then background subtracted using the region within a region method described above. The total fluorescence was then divided by the area, which resulted in the total fluorescence per unit area (μm^2). A smaller region was drawn around the centrosome within the cell and the same region was used for background subtraction. This total fluorescence was also divided by the area, which resulted in the total fluorescence per unit area (μm^2). Finally, the ratio of the fluorescence per area of the centrosome to the fluorescence per area of the whole cell was calculated.

For absolute levels, Hec1-EGFP expressing HeLa cells were imaged under the same conditions as the CRISPR modified Eg5 and TPX2 cells and served as a standard. Using a subset of the acquired z-slices that included all the fluorescence present in the kinetochores, circles were drawn around single kinetochores in a sum projection image, background subtracted and adjusted for untagged protein to determine the total fluorescence intensity. There are 244 molecules of Hec1 at the kinetochore (Suzuki et al., 2015). Therefore, the number of molecules of either Eg5 or TPX2 could be calculated using a ratio comparing their fluorescence to Hec1. To further determine the concentrations of each, number of molecules was converted to Molarity using an approximate volume of a HeLa cell (3000 μm^3) (Puck et al., 1956; Zhao et al., 2008) and/or the volume of a cylinder that contained all of the centrosome fluorescence.

For relative levels, boxes of 5 x 5 pixels were drawn on the GFP Sum intensity projections; measured areas include the spindle pole, the spindle midzone, and a background area outside the spindle but in the cytoplasm. Boxes were drawn in the corresponding places on the Tubulin (mCherry or SiR) sum projection using the ROI

manager. Integrated Fluorescence Intensity was measured and background subtracted. Ratios were then made between regions (pole:midzone) in each color and then a ratio of the ratio was taken to compare the GFP-tagged proteins to Tubulin.

These images were also used for line scans. Using the line tool, a line was drawn from pole-to-pole with a width of 50 pixels and 100 pixels for background subtraction. All of the spindle lengths were then normalized to the smallest spindle length and the fluorescence intensities were normalized to 1 to account for the difference in intensity between fluorescent channels.

Line scans were also used to determine the dynamics of TPX2 and Eg5. Lines were drawn both perpendicular to and through the pole-to-pole axis of the spindle (through the spindle midzone) and at each time interval. The fluorescence intensities were normalized to 1 to account for differences in expression and corresponding fluorescence between Eg5 and TPX2-EGFP.

5.4.9 Live Cell Labeling and Inhibitors

SiR tubulin (Cytoskeleton, Denver, CO), used at a concentration of 50 nM in combination with 10 μM Verapamil, was added between 30-90 min prior to imaging. MG132 was used at a concentration of 10 μM for 90 minutes. In experiments with both MG132 and SiR Tubulin, they were added to cells at the same time and both were washed out after 90 min by transferring cells to non-CO_2 media for imaging. DRAQ5 (Thermo Fisher Scientific) was used at 1 μM and was added to cells just before imaging (~1-5 min). For knock-sideways, 200nM Rapamycin was added to imaging media.

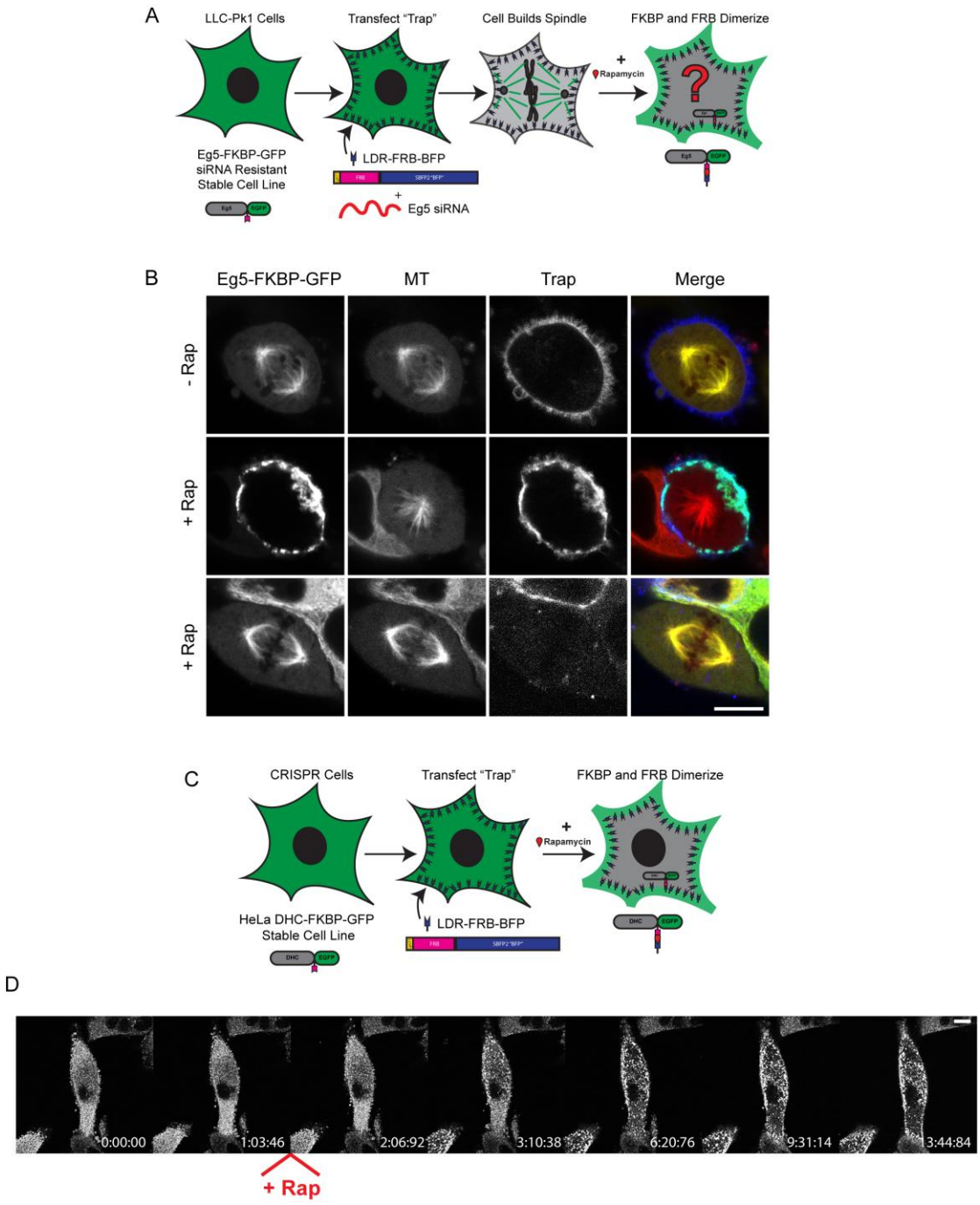

Figure 5.1 Rapamycin re-localizes Eg5 producing monopolar spindles and re-localizes Dynein to membranes in minutes. (A) Diagram of Knock-sideways method in LLC-Pk1 cells expressing siRNA-resistant Eg5-FKBP-GFP. (B) Images of Eg5-FKBP-GFP (green), Microtubules (red), Membrane targeted FRB-BFP (Trap; Blue) in cells with and without 200nM Rapamycin after 30 minutes. (C) Diagram of Knock-sideways in HeLa DHC-FKBP-GFP CRISPR modified cells. (D) Time-lapse images of DHC-FKBP-GFP before and after addition of 200nM Rapamycin. Time in min:sec:msec. Marker bar = 10 μm.

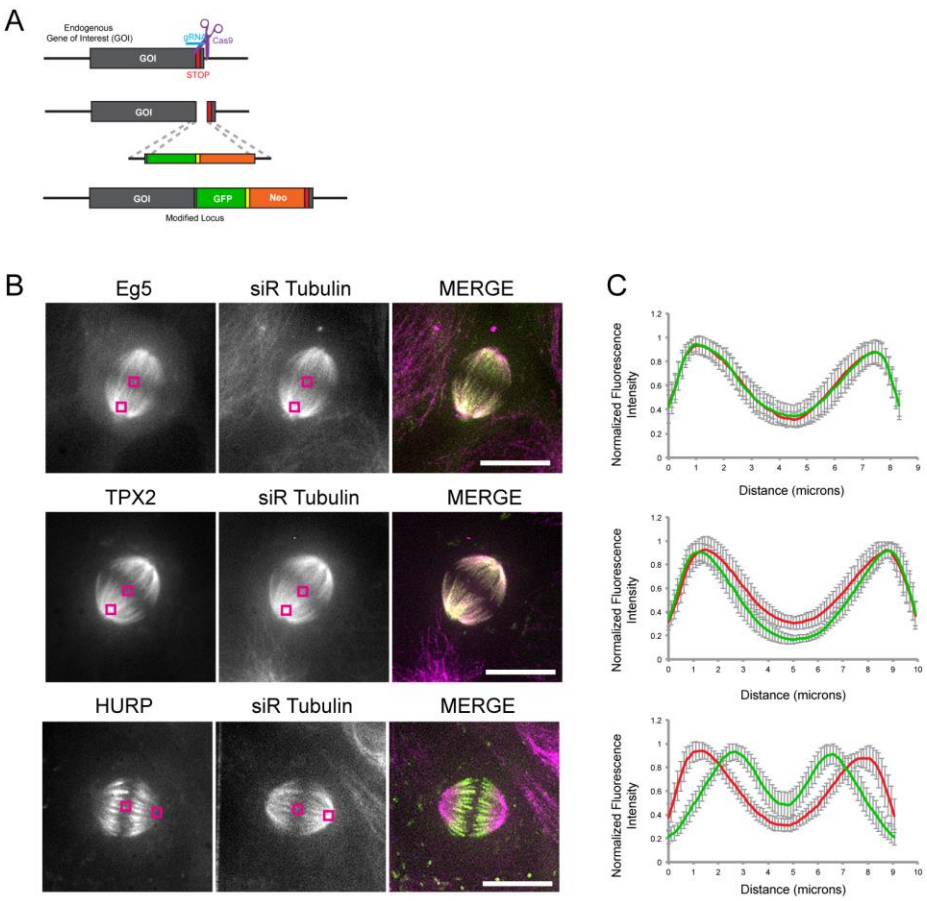
A
Endogenous Gene of Interest (GOI)
gRNA
Cas9
GOI
STOP
GOI
GOI
GFP
Neo
Modified Locus
B
Eg5
siR Tubulin
MERGE
TPX2
siR Tubulin
MERGE
HURP
siR Tubulin
MERGE
C
Normalized Fluorescence Intensity
Distance (microns)
Normalized Fluorescence Intensity
Distance (microns)
Normalized Fluorescence Intensity
Distance (microns)
D
Ratio of Integrated Fluorescence Spindle Pole:Midzone
****
****
Eg5
Tubulin
Eg5:Tubulin
TPX2
Tubulin
TPX2:Tubulin
HURP
Tubulin
HURP:Tubulin
Eg5
TPX2
HURP
E
Total Fluorescence Intensity (A.U.) on the Spindle (x100000)
****
Eg5
TPX2

Figure 5.2 Eg5 and TPX2 are concentrated at spindle poles in metaphase, but only TPX2 is concentrated relative to microtubules. (A) Diagram of CRISPR strategy. (B) Sum intensity projections of endogenous GFP-tagged proteins: Eg5 (top), TPX2 (middle) and HURP (bottom) in live cells arrested at metaphase using MG132. Cells were either expressing mCherry-Tubulin or labeled with 50nM SiR Tubulin ~30 min prior to imaging to stain microtubules. (C) Line scans of spindles; GFP-tagged protein (green) and tubulin (red) (see methods). (D) Ratio of spindle poles:midzone for each GFP-tagged protein (green) and tubulin (red); the ratio of poles:midzone of each protein:tubulin (yellow). (E) Relative, background subtracted (methods) Total Fluorescence Intensity for Eg5 (blue) and TPX2 (red) on a spindle in a cell arrested at metaphase using MG132. Amounts were adjusted to account for untagged protein. Error bars = St Dev. Marker bar = 10 μm. ****$p \leq 0.0001$. n= 8 each.

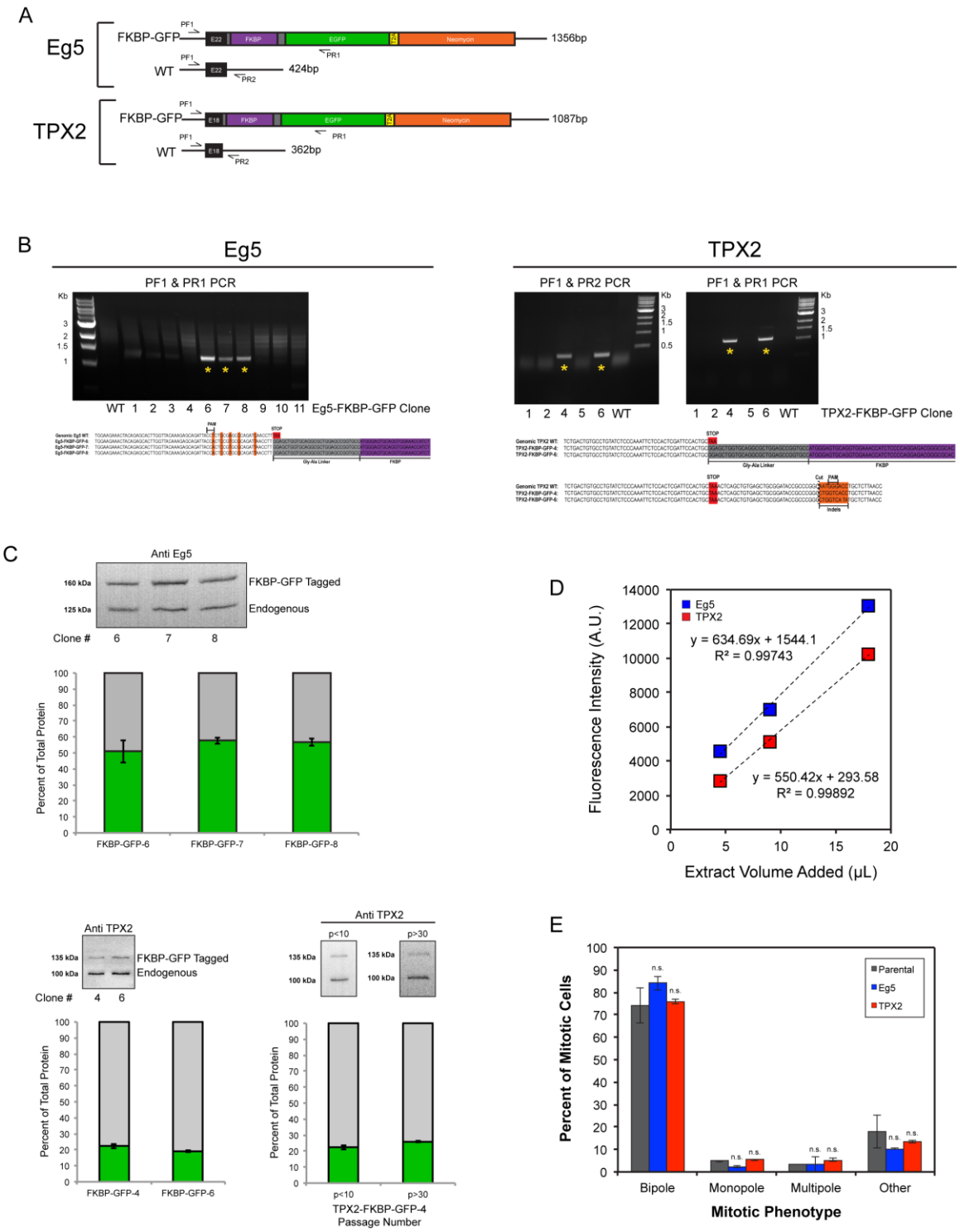

Figure 5.3 Generation and characterization of CRISPR cell lines. (A) Schematic diagram of DNA modified by CRISPR (top) and unmodified (lower) for Eg5 (top) and TPX2 (lower). (B) Genotyping of Eg5 (left) and TPX2 (right) CRISPR cell clones showing fragment size from genomic DNA and sequence analysis; yellow stars show

bands of correct size and the clones that were sequenced. (C) Quantification of EGFP-tagged and untagged proteins for Eg5 (top) and TPX2 (bottom) clones by Western Blot; quantification of blots shown below. Additional TPX2 blot showing tagged and untagged protein levels remain constant as passage number increases (bottom right) (D) Quantification of band intensity for Eg5 (blue) and TPX2 (red) from titration western blots. Linear trend lines, equations, and R^2 shown. (E) Eg5 (blue) and TPX2 (red) CRISPR modified cells display normal mitotic phenotypes compared to parental HeLa cells (gray).

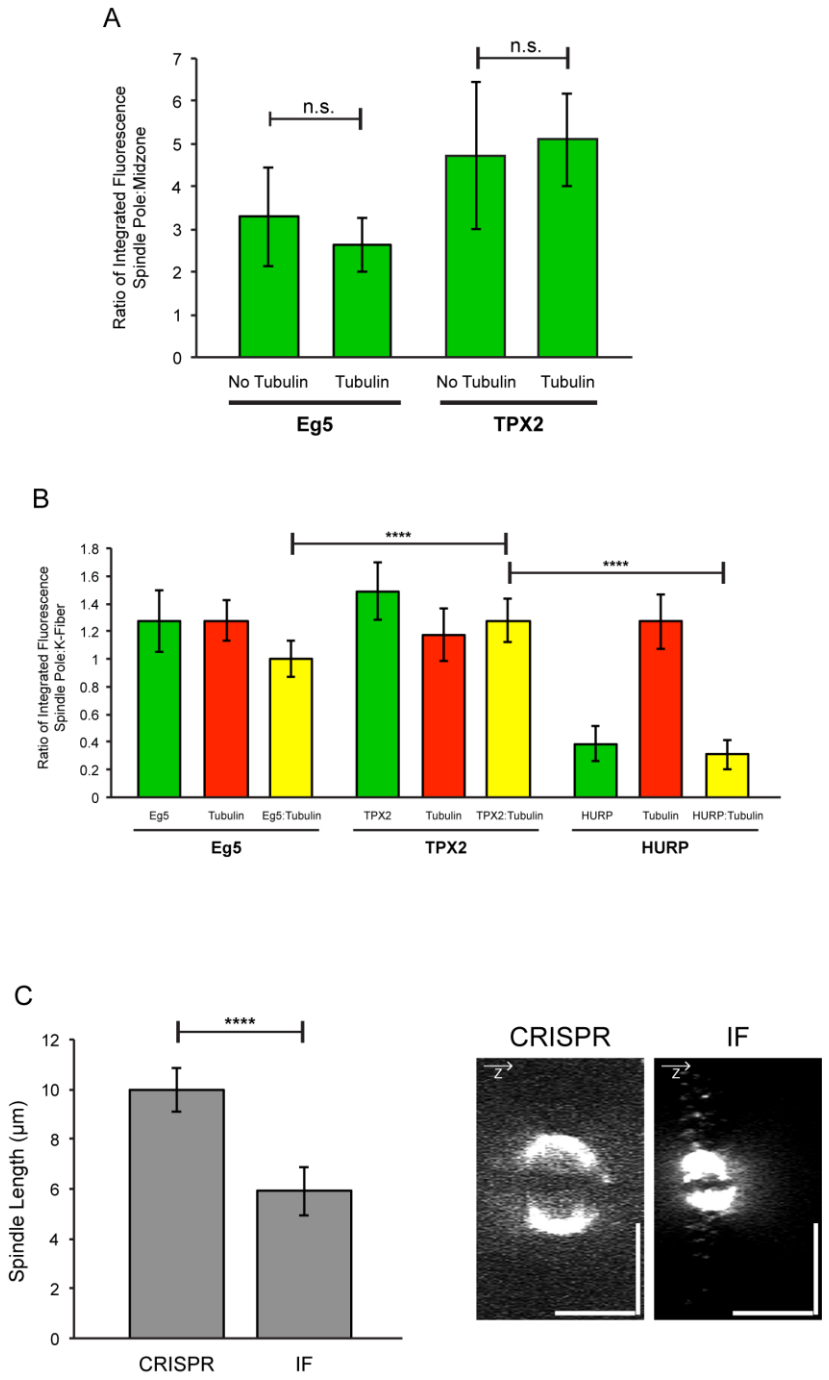

Figure 5.4 Only TPX2 is enriched relative to microtubules along K-fibers (A) Eg5-EGFP and TPX2-EGFP are enriched to the same extent at poles relative to the midzone in cells with and without Tubulin labeling. (B) Ratio of spindle poles:K-fiber for each GFP-tagged protein (green) and tubulin (red); the ratio of poles:K-fiber of each protein:tubulin (yellow). (C) Fixation for immunofluorescence results in spindle shrinking. Bar graph of length from pole-pole for live CRISPR cells compared to Immuofluorescence (left). Example images of Z distance from live CRISPR cells and Immunofluorescence (right). Error bars = St Dev. ****$p \leq 0.0001$.

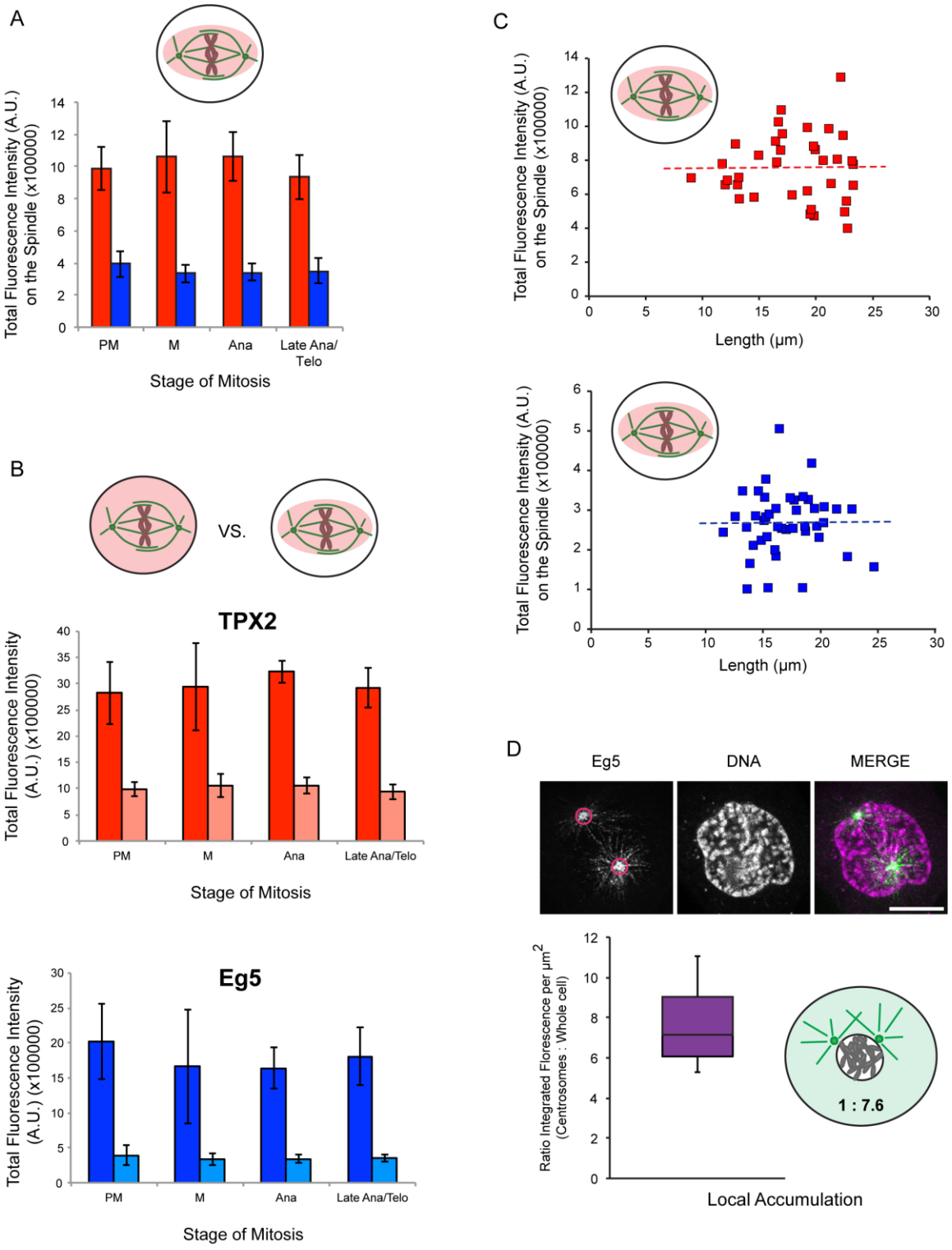

Figure 5.5 Relative amounts of Eg5 and TPX2 throughout mitosis. (A) Comparison of Eg5 (blue) and TPX2 (red) total Fluorescence levels on the spindle through mitosis. (B) Total Fluorescence Levels of TPX2 (top) and Eg5 (bottom) of the whole cell (dark colors) relative to the spindle (light colors) through mitosis; stages were identified using

DRAQ5. (C) As length increases the total fluorescence of TPX2 (red, top) and Eg5 (blue, bottom) on the spindle remain constant. Diagrams in A, B and C show region of the cell (whole cell or spindle) that was used for measuring fluorescence; all images were background subtracted. (D) Relative local concentration of Centrosomes vs. Whole cell. Box plot of the ratio of the Integrated Fluorescence Intensity per unit area. *Whiskers* define the range, *boxes* encompass the 25th to 75th quartiles, and *lines* depict the medians. Diagram representing Eg5 fluorescence distribution in a Prophase cell (right). Note that on average Eg5 is ~7.6X concentrated on centrosomes relative to the whole cell. Marker bars = 10 μm. Error Bars = St Dev.

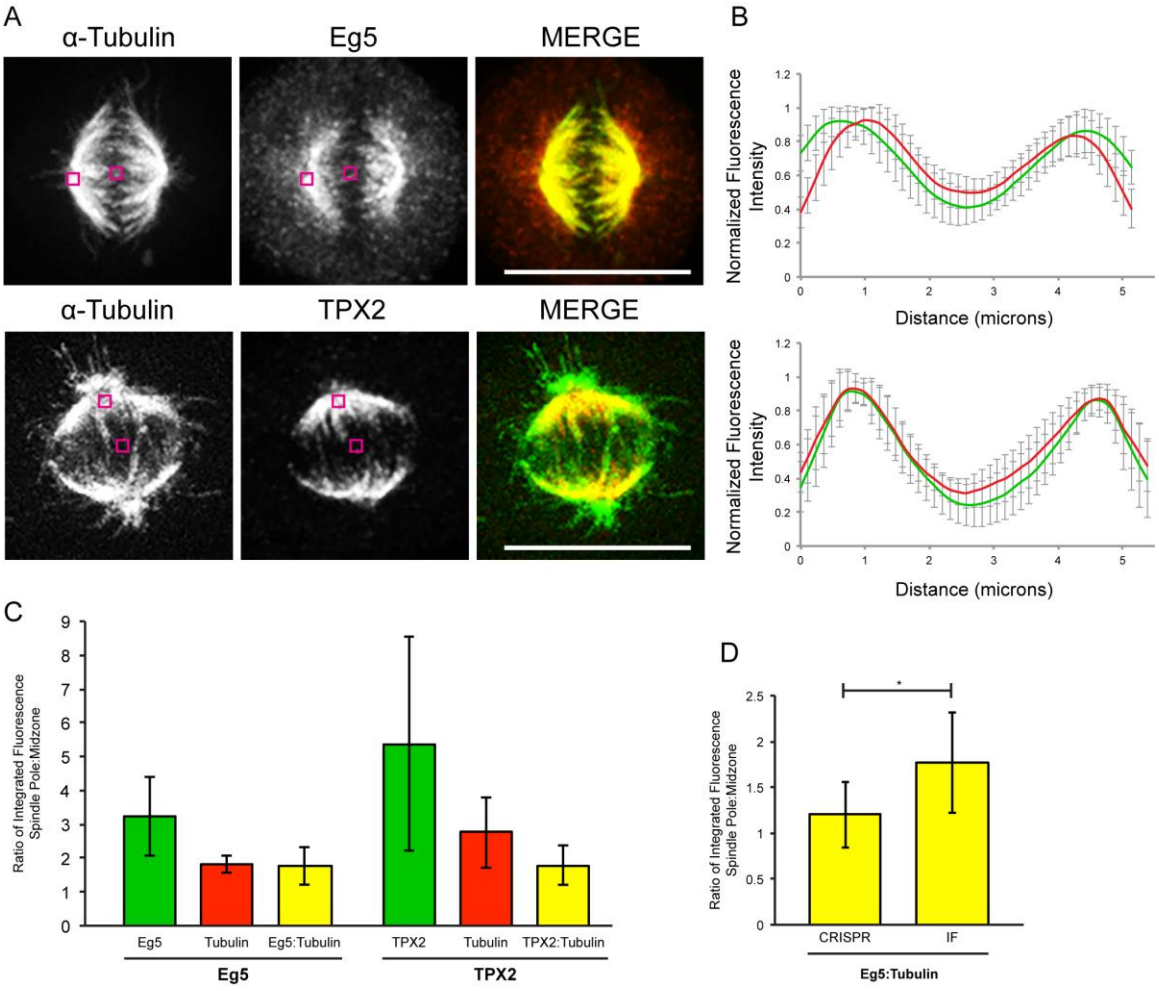

Figure 5.6 Immunofluorescence and CRISPR quantification differ. (A) Sum Intensity Projections of Parental cells arrested at metaphase using MG132, fixed and stained for α-Tubulin (green) and either Eg5 (top) or TPX2 (bottom) (red). (B) Line scans of immuno-stained spindles; Eg5 (top) a TPX2 (bottom) (green) and tubulin (red). (C) Ratio of spindle poles:midzone for Eg5 and TPX2 (green) and tubulin (red); the ratio of poles:midzone of Eg5/TPX2:Tubulin (yellow). (D) Comparison of the ratio of poles:midzone of Eg5:Tubulin for CRISPR and Immunofluorescently labeled cells. Error bars = St Dev. Marker bar = 10 μm. *p≤0.05 (p=0.025). n=8 Eg5, n=6 TPX2.

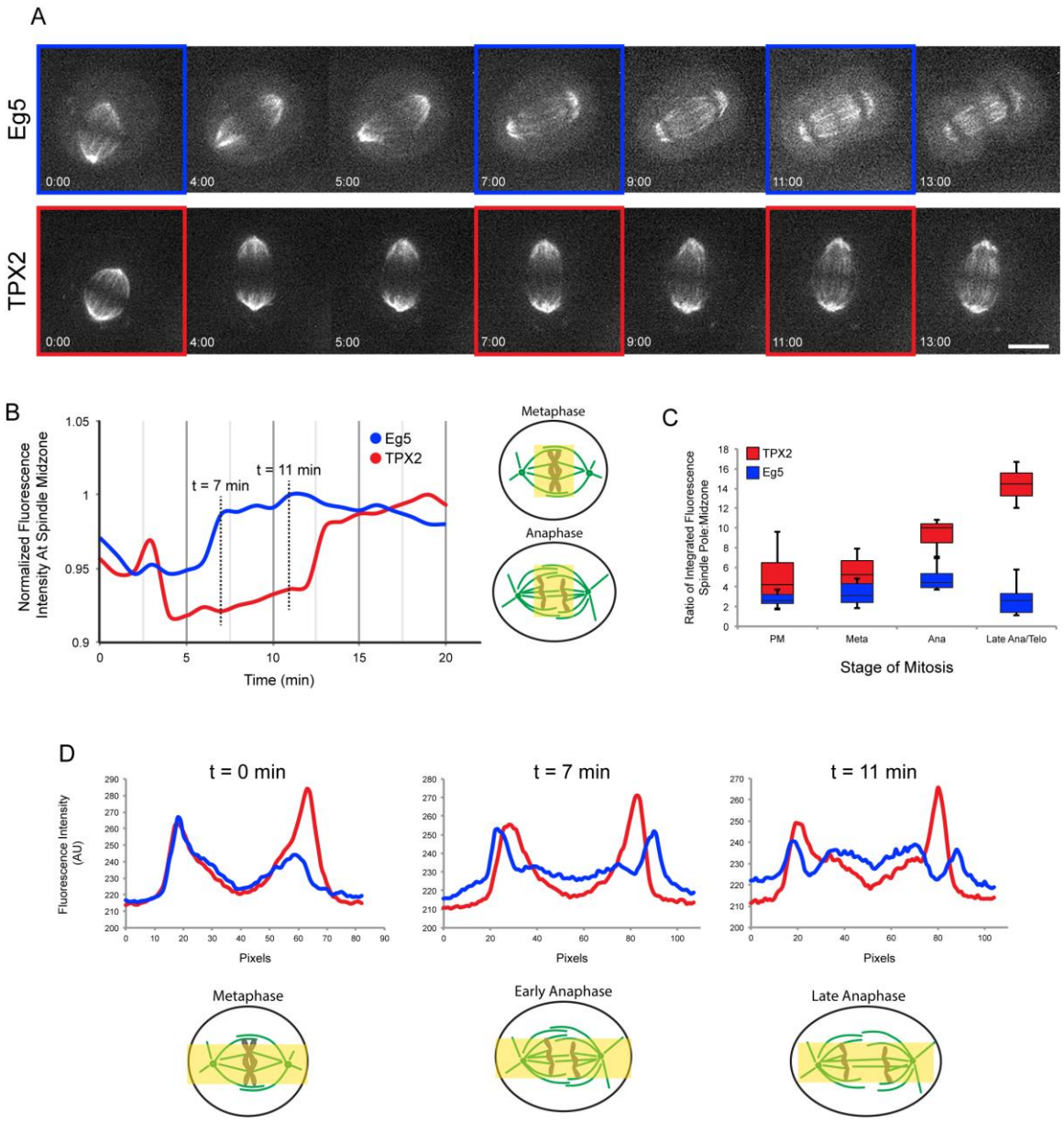

Figure 5.7 Distinct distribution of Eg5 and TPX2 throughout mitosis. (A) Time-lapse images of Eg5 and TPX2 from metaphase (0:00) through anaphase. (B) Schematic diagram and representative line scans perpendicular to pole-to-pole axis of Eg5 (blue) and TPX2 (red). Vertical lines indicate when protein begins to repopulate the midzone. (C) Box plot of spindle poles:midzone ratios for Eg5 (blue) and TPX2 (red) through different stages of mitosis. *Whiskers* define the range, *boxes* encompass the 25th to 75th quartiles, and *lines* depict the medians. (D) Line scans through the pole-to-pole spindle axis at indicated timepoints for Eg5 (blue) and TPX2 (red); schematic diagram of spindles. Note that Eg5 accumulates on interzonal microtubules before TPX2. Time in min:sec. Marker bar = 10 μm.

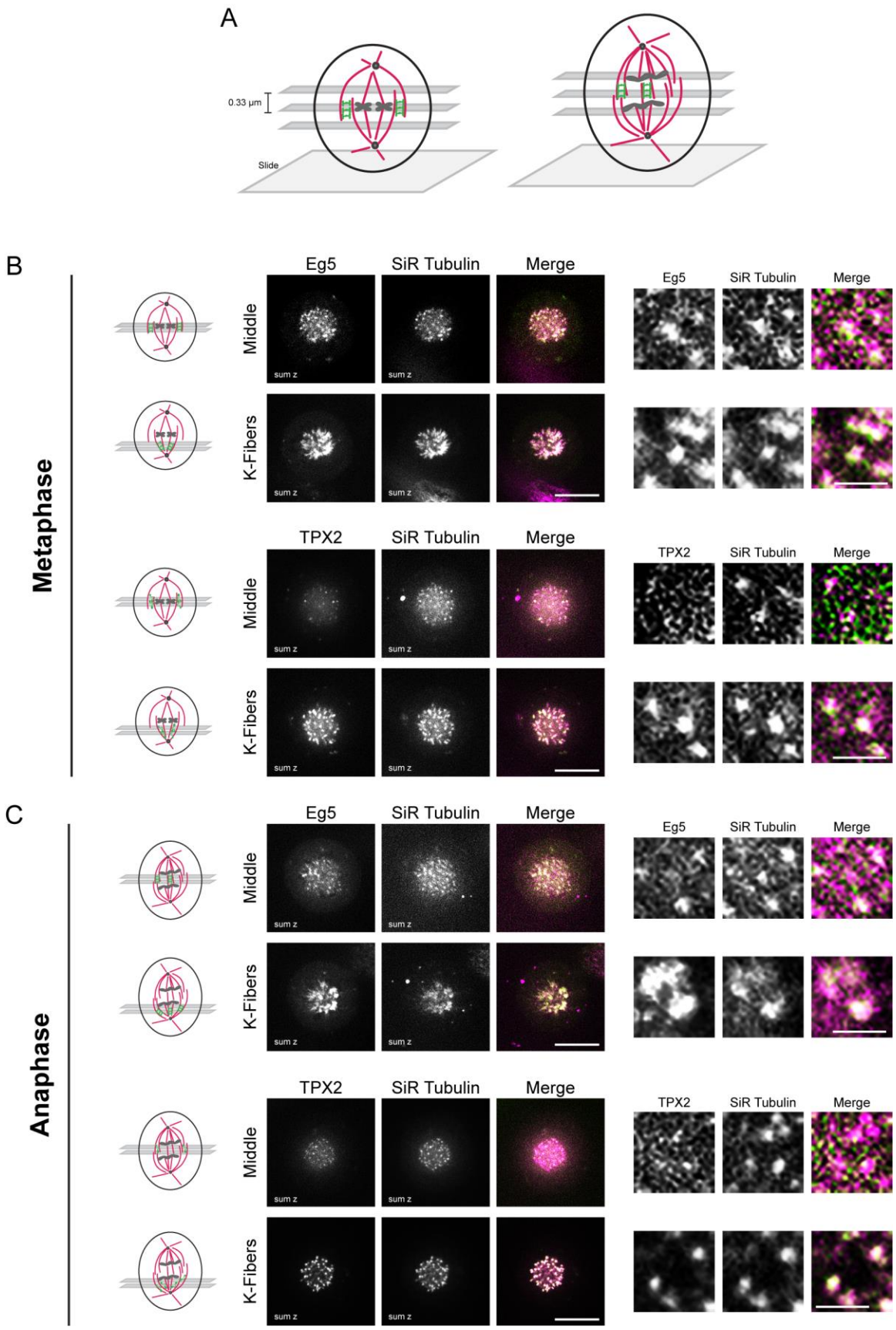
A
0.33 µm
Slide
B
Metaphase
Eg5
SiR Tubulin
Merge
Middle
K-Fibers
sum z
TPX2
C
Anaphase

Figure 5.8 Eg5, but not TPX2, localizes to the spindle midzone in metaphase and anaphase. (A) Schematic diagram of image acquisition and images of slices (0.33 μm) through metaphase (left) and anaphase (right) spindles oriented at 90° relative to the coverslip surface. (B) Sum projections of 1.32 μm total through the midzone (top) and kinetochore fibers (bottom) of metaphase spindles in CRISPR modified cells. Top rows Eg5, lower rows TPX2. SiR Tubulin was used as a microtubule marker. Right images show zoomed in area in the middle of the spindle. Schematic diagrams (left) show where sum projections were made. (C) Anaphase cells, imaged as in A. Top rows Eg5, lower rows TPX2. Marker bars = 10 μm and 2 μm (zoom).

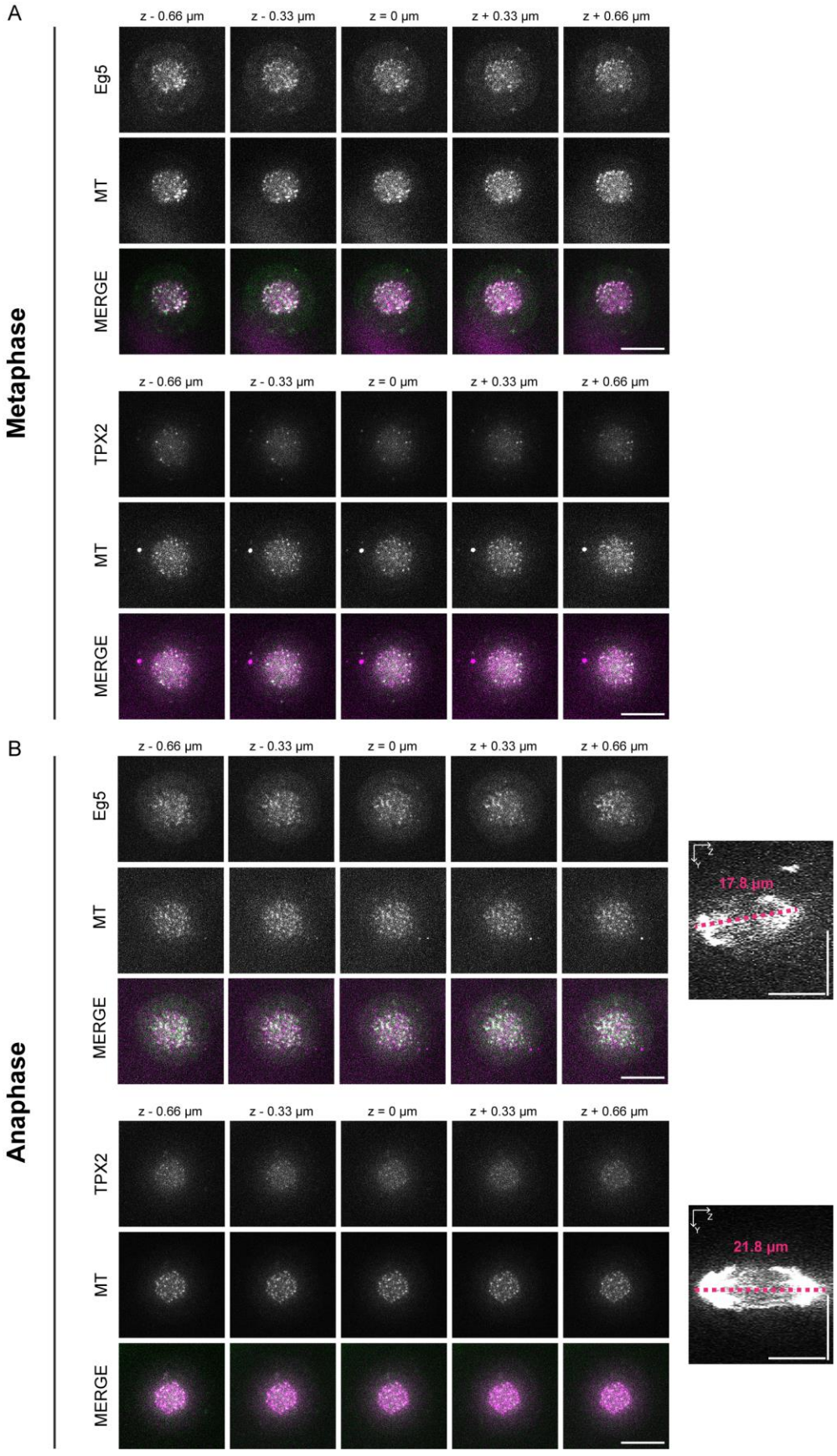
A
Metaphase
z - 0.66 µm
z - 0.33 µm
z = 0 µm
z + 0.33 µm
z + 0.66 µm
Eg5
MT
MERGE
TPX2
MT
MERGE
B
Anaphase
Eg5
MT
MERGE
17.8 µm
TPX2
MT
MERGE
21.8 µm

Figure 5.9 Eg5 is enriched in the spindle midzone relative to TPX2 at metaphase and anaphase. (A) Series of Z-slices through the middle of MG132 arrested metaphase spindles in GFP-tagged CRISPR cells oriented 90° from the surface of the coverslip; Eg5 (top) and TPX2 (bottom). Tubulin was stained using SiR Tubulin (methods). (B) Series of Z-slices through the middle of Anaphase cells imaged as in A. YZ images (right) show microtubules and length of spndle. Z-slices = 0.33μm. Marker bar = 10 μm.

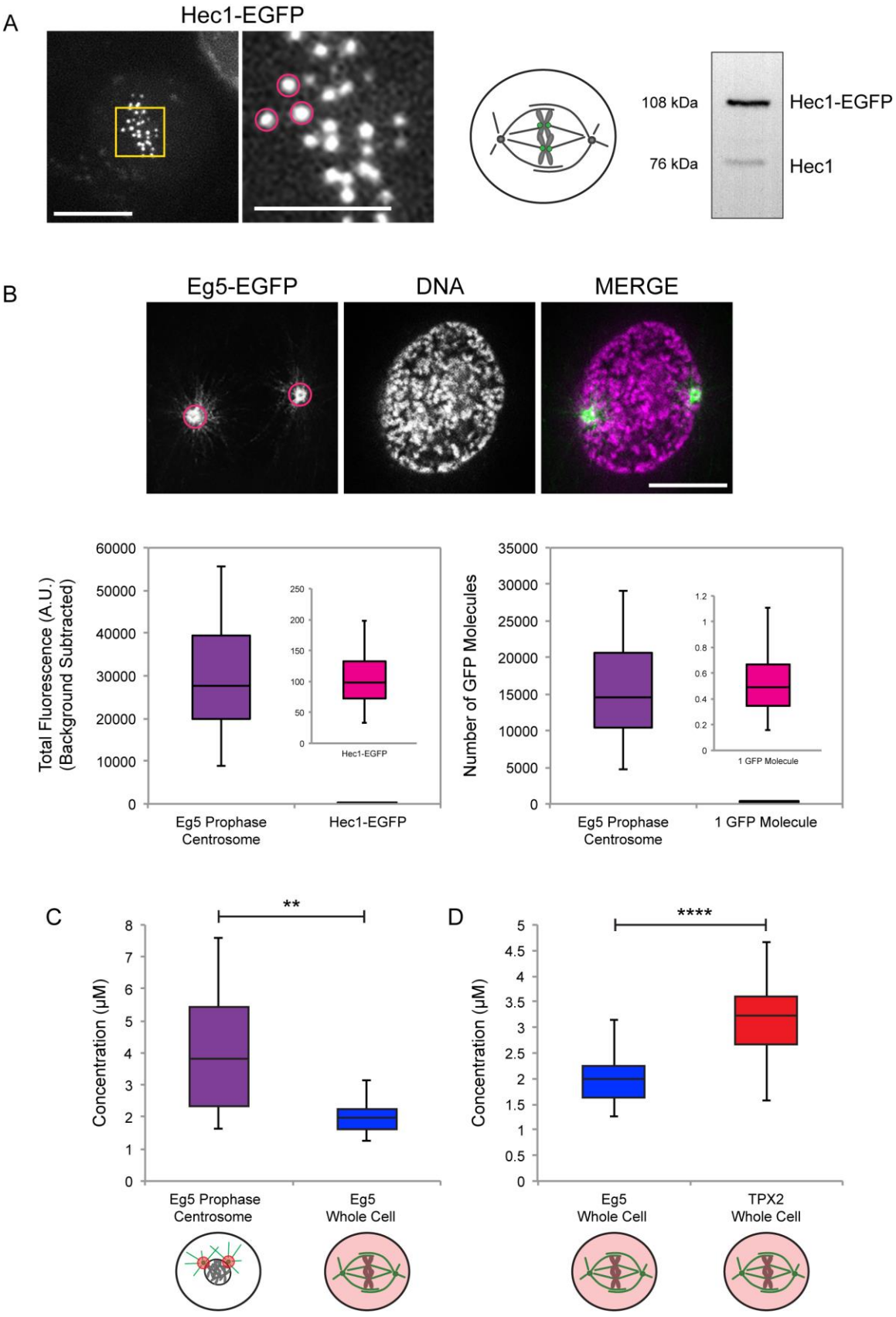
A
Hec1-EGFP
108 kDa
76 kDa
Hec1-EGFP
Hec1
B
Eg5-EGFP
DNA
MERGE
Total Fluorescence (A.U.)
(Background Subtracted)
60000
50000
40000
30000
20000
10000
0
250
200
150
100
50
0
Hec1-EGFP
Eg5 Prophase
Centrosome
Hec1-EGFP
Number of GFP Molecules
35000
30000
25000
20000
15000
10000
5000
0
1.2
1
0.8
0.6
0.4
0.2
0
1 GFP Molecule
Eg5 Prophase
Centrosome
1 GFP Molecule
C
**
Concentration (μM)
8
7
6
5
4
3
2
1
0
Eg5 Prophase
Centrosome
Eg5
Whole Cell
D
****
Concentration (μM)
5
4.5
4
3.5
3
2.5
2
1.5
1
0.5
0
Eg5
Whole Cell
TPX2
Whole Cell

Figure 5.10 *In vivo* concentration of Eg5 and TPX2. (A) Sum projection image of Hec1-EGFP expressing cell using a subset of planes from a z-stack (left); cartoon shows location of Hec1 spots in a spindle. Western Blot showing expression level of GFP tagged vs. untagged Hec1 in cells (right). (B) Box plot of total fluorescence of Eg5 at the prophase centrosome (purple) compared to Hec1-EGFP (pink); left. Box plot of the number of GFP molecules of Eg5 at the prophase centrosome (purple) compared to 1 GFP molecule (pink), calculated based on 244 Hec1 molecules in a kinetochore (Suzuki et al., 2015); right. (C) Box plot of the Eg5 concentration (μM) at the prophase centrosome (purple) vs. the whole cell (blue). (D) Box plot of the whole cell concentrations (μM) of Eg5 (blue) and TPX2 (red). *Whiskers* define the range, *boxes* encompass the 25th to 75th quartiles, and *lines* depict the medians. Marker bar in A = 10 μm. ****$p \leq 0.0001$.

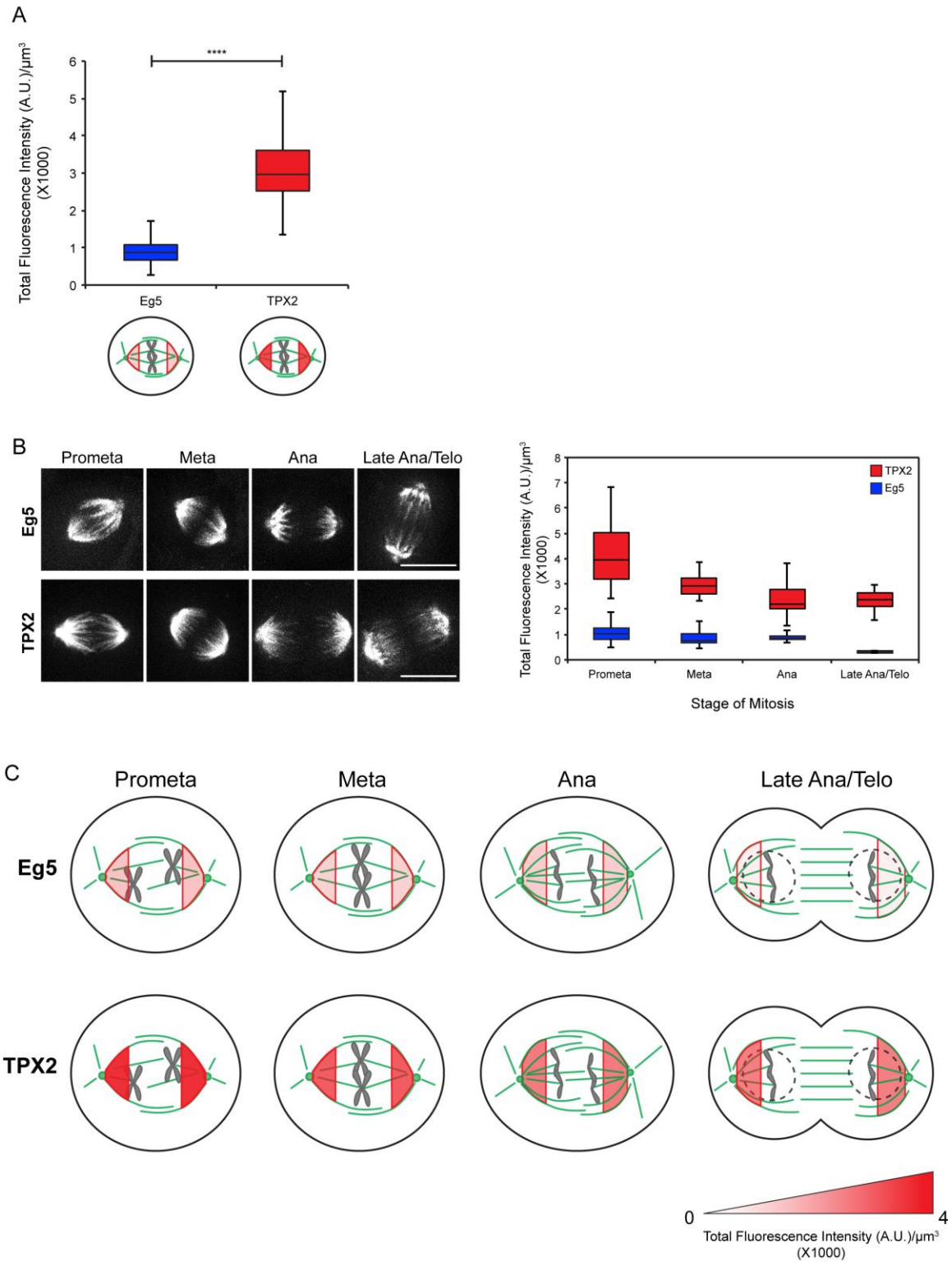

Figure 5.11 Relative amounts of Eg5 and TPX2 on the mitotic spindle. (A) Average, background subtracted (methods) Total Fluorescence Intensity per µm^3 for Eg5 (blue) and TPX2 (red) on a spindle close to the pole. (B) Max projection examples of Eg5 and TPX2 EGFP cells at different stages of mitosis (left); Quantification of the relative,

background subtracted Total Fluorescence intensity per μm^3 for Eg5 (blue) and TPX2 (red) on a spindle close to the pole at different mitotic stages (right). (C) Cartoon demonstrating the change in relative fluorescence on the spindle as mitosis progresses. The scale is shown bottom right. Amounts were adjusted to account for untagged protein. Marker bar in B = 10 μm. ****$p \leq 0.0001$.

BIBLIOGRAPHY

Acar, S., D.B. Carlson, M.S. Budamagunta, V. Yarov-Yarovoy, J.J. Correia, M.R. Ninonuevo, W. Jia, L. Tao, J.A. Leary, J.C. Voss, J.E. Evans, and J.M. Scholey. 2013. The bipolar assembly domain of the mitotic motor kinesin-5. *Nature communications*. 4:1343.

Akhmanova, A., and M.O. Steinmetz. 2008. Tracking the ends: a dynamic protein network controls the fate of microtubule tips. *Nature reviews. Molecular cell biology*. 9:309-322.

Akhmanova, A., and M.O. Steinmetz. 2010. Microtubule +TIPs at a glance. *Journal of cell science*. 123:3415-3419.

Alfaro-Aco, R., A. Thawani, and S. Petry. 2017. Structural analysis of the role of TPX2 in branching microtubule nucleation. *The Journal of cell biology*. 216:983-997.

Alieva, I.B., and R.E. Uzbekov. 2016. Where are the limits of the centrosome? *Bioarchitecture*. 6:47-52.

Avunie-Masala, R., N. Movshovich, Y. Nissenkorn, A. Gerson-Gurwitz, V. Fridman, M. Koivomagi, M. Loog, M.A. Hoyt, A. Zaritsky, and L. Gheber. 2011. Phospho-regulation of kinesin-5 during anaphase spindle elongation. *Journal of cell science*. 124:873-878.

Bain, J., L. Plater, M. Elliott, N. Shpiro, C.J. Hastie, H. McLauchlan, I. Klevernic, J.S. Arthur, D.R. Alessi, and P. Cohen. 2007. The selectivity of protein kinase inhibitors: a further update. *The Biochemical journal*. 408:297-315.

Balchand, S.K., B.J. Mann, J. Titus, J.L. Ross, and P. Wadsworth. 2015. TPX2 Inhibits Eg5 by Interactions with Both Motor and Microtubule. *The Journal of biological chemistry*. 290:17367-17379.

Bannigan, A., W.R. Scheible, W. Lukowitz, C. Fagerstrom, P. Wadsworth, C. Somerville, and T.I. Baskin. 2007. A conserved role for kinesin-5 in plant mitosis. *Journal of cell science*. 120:2819-2827.

Barlan, K., W. Lu, and V.I. Gelfand. 2013. The microtubule-binding protein ensconsin is an essential cofactor of kinesin-1. *Curr. Biol.* 23:317-322.

Bayliss, R., T. Sardon, I. Vernos, and E. Conti. 2003. Structural basis of Aurora A activation by TPX2 at the mitotic spindle. *Mol. Cell*. 12:851-862.

Behnke-Parks, W.M., J. Vendome, B. Honig, Z. Maliga, C. Moores, and S.S. Rosenfeld. 2011. Loop L5 acts as a conformational latch in the mitotic kinesin Eg5. *The Journal of biological chemistry*. 286:5242-5253.

Bell, K.M., H.K. Cha, C.V. Sindelar, and J.C. Cochran. 2017. The yeast kinesin-5 Cin8 interacts with the microtubule in a noncanonical manner. *The Journal of biological chemistry*. 292:14680-14694.

Bertran, M.T., S. Sdelci, L. Regue, J. Avruch, C. Caelles, and J. Roig. 2011. Nek9 is a Plk1-activated kinase that controls early centrosome separation through Nek6/7 and Eg5. *The EMBO journal*. 30:2634-2647.

Bhatt, A.S., H. Erdjument-Bromage, P. Tempst, C.S. Craik, and M.M. Moasser. 2005. Adhesion signaling by a novel mitotic substrate of src kinases. *Oncogene*. 24:5333-5343.

Bickel, K.G., B.J. Mann, J.S. Waitzman, T.A. Poor, S.E. Rice, and P. Wadsworth. 2017. Src family kinase phosphorylation of the motor domain of the human kinesin-5, Eg5. *Cytoskeleton (Hoboken, N.J.)*.

Bishop, J.D., Z. Han, and J.M. Schumacher. 2005. The Caenorhabditis elegans Aurora B kinase AIR-2 phosphorylates and is required for the localization of a BimC kinesin to meiotic and mitotic spindles. *Molecular biology of the cell*. 16:742-756.

Blackwell, R., C. Edelmaier, O. Sweezy-Schindler, A. Lamson, Z.R. Gergely, E. O'Toole, A. Crapo, L.E. Hough, J.R. McIntosh, M.A. Glaser, and M.D. Betterton. 2017. Physical determinants of bipolar mitotic spindle assembly and stability in fission yeast. *Science advances*. 3:e1601603.

Blangy, A., L. Arnaud, and E.A. Nigg. 1997. Phosphorylation by p34cdc2 protein kinase regulates binding of the kinesin-related motor HsEg5 to the dynactin subunit p150. *The Journal of biological chemistry*. 272:19418-19424.

Blangy, A., H.A. Lane, P. d'Herin, M. Harper, M. Kress, and E.A. Nigg. 1995. Phosphorylation by p34cdc2 regulates spindle association of human Eg5, a kinesin-related motor essential for bipolar spindle formation in vivo. *Cell*. 83:1159-1169.

Brennan, I.M., U. Peters, T.M. Kapoor, and A.F. Straight. 2007. Polo-like kinase controls vertebrate spindle elongation and cytokinesis. *PloS one*. 2:e409.

Britto, M., A. Goulet, S. Rizvi, O. von Loeffelholz, C.A. Moores, and R.A. Cross. 2016. Schizosaccharomyces pombe kinesin-5 switches direction using a steric blocking mechanism. *Proceedings of the National Academy of Sciences of the United States of America*. 113:E7483-e7489.

Brouhard, G.J., J.H. Stear, T.L. Noetzel, J. Al-Bassam, K. Kinoshita, S.C. Harrison, J. Howard, and A.A. Hyman. 2008. XMAP215 is a processive microtubule polymerase. *Cell*. 132:79-88.

Brunet, S., T. Sardon, T. Zimmerman, T. Wittman, R. Pepperkok, E. Karsenti, and I. Vernos. 2004. Characterization of the TPX2 domains involved in microtubule nucleation and spindle assembly in Xenopus egg extracts. *Mol. Biol. Cell*. 15:5318-5328.

Brust-Mascher, I., P. Sommi, D.K. Cheerambathur, and J.M. Scholey. 2009. Kinesin-5-dependent poleward flux and spindle length control in Drosophila embryo mitosis. *Molecular biology of the cell*. 20:1749-1762.

Cahu, J., A. Olichon, C. Hentrich, H. Schek, J. Drinjakovic, C. Zhang, A. Doherty-Kirby, G. Lajoie, and T. Surrey. 2008. Phosphorylation by Cdk1 increases the binding of Eg5 to microtubules in vitro and in Xenopus egg extract spindles. *PloS one*. 3:e3936.

Cai, D., D.P. McEwen, J.R. Martens, E. Meyhofer, and K.J. Verhey. 2009. Single molecule imaging reveals differences in microtubule track selection between kinesin motors. *PLOS Bio*. 7:e1000216.

Cai, D., K.J. Verhey, and E. Meyhofer. 2007. Tracking single kinesin molecules in the cytoplasm of mammalian cells. *Biophysical journal*. 92:4137-4144.

Calderwood, D.J., D.N. Johnston, R. Munschauer, and P. Rafferty. 2002. Pyrrolo[2,3-d]pyrimidines containing diverse N-7 substituents as potent inhibitors of Lck. *Bioorganic & Medicinal Chemistry Letters*. 12:1683-1686.

Cameron, L.A., G. Yang, D. Cimini, J.C. Canman, O. Kisurina-Evgenieva, A. Khodjakov, G. Danuser, and E.D. Salmon. 2006. Kinesin 5-independent poleward flux of kinetochore microtubules in PtK1 cells. *The Journal of cell biology*. 173:173-179.

Caron, D., D.P. Byrne, P. Thebault, D. Soulet, C.R. Landry, P.A. Eyers, and S. Elowe. 2016. Mitotic phosphotyrosine network analysis reveals that tyrosine phosphorylation regulates Polo-like kinase 1 (PLK1). *Science signaling*. 9:rs14.

Chee, M.K., and S.B. Haase. 2010. B-cyclin/CDKs regulate mitotic spindle assembly by phosphorylating kinesins-5 in budding yeast. *PLoS genetics*. 6:e1000935.

Cheerambathur, D.K., I. Brust-Mascher, G. Civelekoglu-Scholey, and J.M. Scholey. 2008. Dynamic partitioning of mitotic kinesin-5 cross-linkers between microtubule-bound and freely diffusing states. *The Journal of cell biology*. 182:429-436.

Cheeseman, I.M., and A. Desai. 2005. A combined approach for the localization and tandem affinity purification of protein complexes from metazoans. *Sci. STKE*:p11.

Chen, Y., and W.O. Hancock. 2015. Kinesin-5 is a microtubule polymerase. *Nature communications*. 6:8160.

Cochran, J.C., and S.P. Gilbert. 2005. ATPase mechanism of Eg5 in the absence of microtubules: insight into microtubule activation and allosteric inhibition by monastrol. *Biochemistry*. 44:16633-16648.

Cochran, J.C., T.C. Krzysiak, and S.P. Gilbert. 2006. Pathway of ATP hydrolysis by monomeric kinesin Eg5. *Biochemistry*. 45:12334-12344.

Cochran, J.C., C.A. Sontag, Z. Maliga, T.M. Kapoor, J.J. Correia, and S.P. Gilbert. 2004. Mechanistic analysis of the mitotic kinesin Eg5. *The Journal of biological chemistry*. 279:38861-38870.

Collins, E., B.J. Mann, and P. Wadsworth. 2014. Eg5 restricts anaphase B spindle elongation in mammalian cells. *Cytoskeleton (Hoboken, N.J.)*. 71:136-144.

Dambournet, D., S.H. Hong, A. Grassart, and D.G. Drubin. 2014. Tagging endogenous loci for live-cell fluorescence imaging and molecule counting using ZFNs, TALENs, and Cas9. *Methods in enzymology*. 546:139-160.

David-Pfeuty, T., S. Bagrodia, and D. Shalloway. 1993. Differential localization patterns of myristoylated and nonmyristoylated c-Src proteins in interphase and mitotic c-Src overexpresser cells. *Journal of cell science*. 105 (Pt 3):613-628.

Day, R.N., and M.W. Davidson. 2009. The fluorescent protein palette: tools for cellular imaging. *Chem Soc Rev*. 38:2887-2921.

DeBerg, H.A., B.H. Blehm, J. Sheung, A.R. Thompson, C.S. Bookwalter, S.F. Torabi, T.A. Schroer, C.L. Berger, Y. Lu, K.M. Trybus, and P.R. Selvin. 2013. Motor domain phosphorylation modulates kinesin-1 transport. *The Journal of biological chemistry*. 288:32612-32621.

DeBonis, S., D.A. Skoufias, L. Lebeau, R. Lopez, G. Robin, R.L. Margolis, R.H. Wade, and F. Kozielski. 2004. In vitro screening for inhibitors of the human mitotic kinesin Eg5 with antimitotic and antitumor activities. *Mol. Cancer Ther.* 3:1079-1090.

Dhatchinamoorthy, K., M. Shivaraju, J.J. Lange, B. Rubinstein, J.R. Unruh, B.D. Slaughter, and J.L. Gerton. 2017. Structural plasticity of the living kinetochore. *The Journal of cell biology*. 216:3551-3570.

Ding, R., K.L. McDonald, and J.R. McIntosh. 1993. Three-dimensional reconstruction and analysis of mitotic spindles from the yeast, Schizosaccharomyces pombe. *The Journal of cell biology*. 120:141-151.

Dixit, R., J.L. Ross, Y.E. Goldman, and E.L. Holzbaur. 2008. Differential regulation of dynein and kinesin motor proteins by Tau. *Science (New York, N.Y.)*. 319:1086-1089.

Doyon, J.B., B. Zeitler, J. Cheng, A.T. Cheng, J.M. Cherone, Y. Santiago, A.H. Lee, T.D. Vo, Y. Doyon, J.C. Miller, D.E. Paschon, L. Zhang, E.J. Rebar, P.D. Gregory, F.D. Urnov, and D.G. Drubin. 2011. Rapid and efficient clathrin-mediated endocytosis revealed in genome-edited mammalian cells. *Nature cell biology*. 13:331-337.

Drechsler, H., and A.D. McAinsh. 2016. Kinesin-12 motors cooperate to suppress microtubule catastrophes and drive the formation of parallel microtubule bundles. *Proceedings of the National Academy of Sciences of the United States of America*. 113:E1635-1644.

Drechsler, H., T. McHugh, M.R. Singleton, N.J. Carter, and A.D. McAinsh. 2014. The Kinesin-12 Kif15 is a processive track-switching tetramer. *eLife*. 3:e01724.

Dreschler, H., and A.D. McAinsh. 2016. Kinesin-12 motors cooperate to suppress microtubule catastrophes and drive the formation of parallel microtubule bundles. *Proc. Nat'l. Acad. Sci. USA*. 113:E1635-E1644.

Drummond, D.R., and I.M. Hagan. 1998. Mutations in the bimC box of Cut7 indicate divergence of regulation within the bimC family of kinesin related proteins. *Journal of cell science*. 111 (Pt 7):853-865.

Eckerdt, F., P.A. Eyers, A.L. Lewellyn, C. Prigent, and J.L. Maller. 2008. Spindle pole regulation by a discrete Eg5-interacting domain in TPX2. *Current biology : CB*. 18:519-525.

Edamatsu, M. 2014. Bidirectional motility of the fission yeast kinesin-5, Cut7. *Biochemical and biophysical research communications*. 446:231-234.

Eibes, S., N. Gallisa-Sune, M. Rosas-Salvans, P. Martinez-Delgado, I. Vernos, and J. Roig. 2017. Nek9 Phosphorylation Defines a New Role for TPX2 in Eg5-Dependent Centrosome Separation before Nuclear Envelope Breakdown. *Current biology : CB*.

Enos, A.P., and N.R. Morris. 1990. Mutation of a gene that encodes a kinesin-like protein blocks nuclear division in A. nidulans. *Cell*. 60:1019-1027.

Eyers, P.A., and J.L. Maller. 2004. Regulation of Xenopus Aurora A activation by TPX2. *J. Biol. Chem.* 279:9008-9015.

Fallesen, T., J. Roostalu, C. Duellberg, G. Pruessner, and T. Surrey. 2017. Ensembles of Bidirectional Kinesin Cin8 Produce Additive Forces in Both Directions of Movement. *Biophysical journal*. 113:2055-2067.

Falnikar, A., S. Tole, and P.W. Baas. 2011. Kinesin-5, a mitotic microtubule-associated motor protein, modulates neuronal migration. *Molecular biology of the cell*. 22:1561-1574.

Ferenz, N., R. Paul, C. Fagerstrom, A. Mogilner, and P. Wadsworth. 2009a. Dynein antagonizes Eg5 by crosslinking and sliding antiparallel microtubules. *Curr. Biol.* 19:1833-1838.

Ferenz, N.P., A. Gable, and P. Wadsworth. 2010. Mitotic functions of kinesin-5. *Seminars in cell & developmental biology*. 21:255-259.

Ferenz, N.P., R. Paul, C. Fagerstrom, A. Mogilner, and P. Wadsworth. 2009b. Dynein antagonizes eg5 by crosslinking and sliding antiparallel microtubules. *Current biology : CB*. 19:1833-1838.

Fridman, V., A. Gerson-Gurwitz, O. Shapira, N. Movshovich, S. Lakamper, C.F. Schmidt, and L. Gheber. 2013. Kinesin-5 Kip1 is a bi-directional motor that stabilizes microtubules and tracks their plus-ends in vivo. *Journal of cell science*. 126:4147-4159.

Fry, A.M., R. Bayliss, and J. Roig. 2017. Mitotic Regulation by NEK Kinase Networks. *Frontiers in cell and developmental biology*. 5:102.

Fu, J., M. Bian, G. Xin, Z. Deng, J. Luo, X. Guo, H. Chen, Y. Wang, Q. Jiang, and C. Zhang. 2015a. TPX2 phosphorylation maintains metaphase spindle length by regulating microtubule flux. *J. Cell Biol.* 210:373-383.

Fu, J., M. Bian, G. Xin, Z. Deng, J. Luo, X. Guo, H. Chen, Y. Wang, Q. Jiang, and C. Zhang. 2015b. TPX2 phosphorylation maintains metaphase spindle length by regulating microtubule flux. *The Journal of cell biology*. 210:373-383.

Fumagalli, S., N.F. Totty, J.J. Hsuan, and S.A. Courtneidge. 1994. A target for Src in mitosis. *Nature*. 368:871-874.

Gable, A., M. Qiu, J. Titus, S. Balchand, N.P. Ferenz, N. Ma, E.S. Collins, C. Fagerstrom, J.L. Ross, G. Yang, and P. Wadsworth. 2012. Dynamic reorganization of Eg5 in the mammalian spindle throughout mitosis requires dynein and TPX2. *Molecular biology of the cell*. 23:1254-1266.

Garcia, K., J. Stumpff, T. Duncan, and T.T. Su. 2009. Tyrosines in the kinesin-5 head domain are necessary for phosphorylation by Wee1 and for mitotic spindle integrity. *Current biology : CB*. 19:1670-1676.

Gardner, M.K., D.C. Bouck, L.V. Paliulis, J.B. Meehl, E.T. O'Toole, J. Haase, A. Soubry, A.P. Joglekar, M. Winey, E.D. Salmon, K. Bloom, and D.J. Odde. 2008. Chromosome congression by Kinesin-5 motor-mediated disassembly of longer kinetochore microtubules. *Cell*. 135:894-906.

Garrett, S., K. Auer, D.A. Compton, and T. Kapoor. 2002. hTPX2 is required for normal spindle morphology and centrosome integrity during vertebrate cell division. *Curr. Biol.* 12:2055-2059.

Gerson-Gurwitz, A., C. Thiede, N. Movshovich, V. Fridman, M. Podolskaya, T. Danieli, S. Lakamper, D.R. Klopfenstein, C.F. Schmidt, and L. Gheber. 2011. Directionality of individual kinesin-5 Cin8 motors is modulated by loop 8, ionic strength and microtubule geometry. *The EMBO journal*. 30:4942-4954.

Giet, R., R. Uzbekov, F. Cubizolles, K. Le Guellec, and C. Prigent. 1999. The Xenopus laevis aurora-related protein kinase pEg2 associates with and phosphorylates the kinesin-related protein XlEg5. *The Journal of biological chemistry*. 274:15005-15013.

Goldstein, A., N. Siegler, D. Goldman, H. Judah, E. Valk, M. Koivomagi, M. Loog, and L. Gheber. 2017. Three Cdk1 sites in the kinesin-5 Cin8 catalytic domain coordinate motor localization and activity during anaphase. *Cellular and molecular life sciences : CMLS*.

Goodson, H.V., J.S. Dzurisin, and P. Wadsworth. 2010. Methods for expressing and analyzing GFP-tubulin and GFP-microtubule-associated proteins. *Cold Spring Harbor protocols*. 2010:pdb.top85.

Gordon, D.M., and D.M. Roof. 1999. The kinesin-related protein Kip1p of Saccharomyces cerevisiae is bipolar. *The Journal of biological chemistry*. 274:28779-28786.

Goshima, G., and R.D. Vale. 2003. The roles of microtubule-based motor proteins in mitosis: comprehensive RNAi analysis in the Drosophila S2 cell line. *The Journal of cell biology*. 162:1003-1016.

Goshima, G., and R.D. Vale. 2005. Cell cycle-dependent dynamics and regulation of mitotic kinesins in Drosophila S2 cells. *Molecular biology of the cell*. 16:3896-3907.

Goshima, G., R. Wollman, S.S. Goodwin, N. Zhang, J.M. Scholey, R.D. Vale, and N. Stuurman. 2007. Genes required for mitotic spindle assembly in Drosophila S2 cells. *Science (New York, N.Y.)*. 316:417-421.

Groen, A.C., D. Needleman, C. Brangwynne, C. Gradinaru, B. Fowler, R. Mazitschek, and T.J. Mitchison. 2008. A novel small-molecule inhibitor reveals a possible role of kinesin-5 in anastral spindle-pole assembly. *J. Cell Sci.* 121:2293-2300.

Gruss, O.J., R.E. Carazo-Salas, C.A. Schatz, G. Guarguaglini, J. Kast, M. Wilm, N. Le Bot, I. Vernos, E. Karsenti, and I.W. Mattaj. 2001. Ran induces spindle assembly by reversing the inhibitory effect of importin alpha on TPX2 activity. *Cell*. 104:83-93.

Gruss, O.J., and I. Vernos. 2004. The mechanism of spindle assembly: functions of Ran and its target TPX2. *J. Cell Biol.* 166:949-955.

Gruss, O.J., M. Wittmann, H. Yokoyama, R. Pepperkok, T. Kufer, H. Sillje, E. Karsenti, I.W. Mattaj, and I. Vernos. 2002. Chromosome-induced microtubule assembly mediated by TPX2 is required for spindle formation in HeLa cells. *Nature cell biology*. 4:871-879.

Hagan, I., and M. Yanagida. 1990. Novel potential mitotic motor protein encoded by the fission yeast cut7+ gene. *Nature*. 347:563-566.

Han, G., M. Ye, H. Liu, C. Song, D. Sun, Y. Wu, X. Jiang, R. Chen, C. Wang, L. Wang, and H. Zou. 2010. Phosphoproteome analysis of human liver tissue by long-gradient nanoflow LC coupled with multiple stage MS analysis. *Electrophoresis*. 31:1080-1089.

He, J., Z. Zhang, M. Ouyang, F. Yang, H. Hao, K.L. Lamb, J. Yang, Y. Yin, and W.H. Shen. 2016. PTEN regulates EG5 to control spindle architecture and chromosome congression during mitosis. *Nature communications*. 7:12355.

Heck, M.M., A. Pereira, P. Pesavento, Y. Yannoni, A.C. Spradling, and L.S. Goldstein. 1993. The kinesin-like protein KLP61F is essential for mitosis in Drosophila. *The Journal of cell biology*. 123:665-679.

Helenius, J., G.J. Brouhard, Y. Kalaidzidis, S. Diez, and J. Howard. 2006. The depolymerizing kinesin MCAK uses lattice diffusion to rapidly target microtubule ends. *Nature*. 441:115-119.

Hildebrandt, E.R., L. Gheber, T. Kingsbury, and M.A. Hoyt. 2006. Homotetrameric form of Cin8p, a Saccharomyces cerevisiae kinesin-5 motor, is essential for its in vivo function. *The Journal of biological chemistry*. 281:26004-26013.

Hinrichs, M.H., A. Jalal, B. Brenner, E. Mandelkow, S. Kumar, and T. Scholz. 2012. Tau protein diffuses along the microtubule lattice. *J. Biol. Chem.* 287:38559-38568.

Holland, A.J., D. Fachinetti, J.S. Han, and D.W. Cleveland. 2012. Inducible, reversible system for the rapid and complete degradation of proteins in mammalian cells. *Proceedings of the National Academy of Sciences of the United States of America*. 109:E3350-3357.

Honnappa, S., S.M. Gouveia, A. Weisbrich, F.F. Damberger, N.S. Bhavesh, H. Jawhari, I. Grigoriev, F.J. van Rijssel, R.M. Buey, A. Lawera, I. Jelesarov, F.K. Winkler, K. Wuthrich, A. Akhmanova, and M.O. Steinmetz. 2009. An EB1-binding motif acts as a microtubule tip localization signal. *Cell*. 138:366-376.

Hornbeck, P.V., B. Zhang, B. Murray, J.M. Kornhauser, V. Latham, and E. Skrzypek. 2015. PhosphoSitePlus, 2014: mutations, PTMs and recalibrations. *Nucleic acids research*. 43:D512-520.

Hoyt, M.A. 1994. Cellular roles of kinesin and related proteins. *Current opinion in cell biology*. 6:63-68.

Hoyt, M.A., L. He, K.K. Loo, and W.S. Saunders. 1992. Two Saccharomyces cerevisiae kinesin-related gene products required for mitotic spindle assembly. *The Journal of cell biology*. 118:109-120.

Hu, C.K., M. Coughlin, C.M. Field, and T.J. Mitchison. 2011. KIF4 regulates midzone length during cytokinesis. *Current biology : CB*. 21:815-824.

Huang, T.G., and D.D. Hackney. 1994. Drosophila kinesin minimal motor domain expressed in Escherichia coli. Purification and kinetic characterization. *The Journal of biological chemistry*. 269:16493-16501.

Hueschen, C.L., S.J. Kenny, K. Xu, and S. Dumont. 2017. NuMA recruits dynein activity to microtubule minus-ends at mitosis. *eLife*. 6.

Hyman, A., D. Drechsel, D. Kellogg, S. Salser, K. Sawin, P. Steffen, L. Wordeman, and T. Mitchison. 1991a. [39] Preparation of modified tubulins. *In* Methods in enzymology. Vol. Volume 196. Academic Press. 478-485.

Hyman, A., D. Drechsel, D. Kellogg, S. Salser, K. Sawin, L. Wordeman, and T. Mitchison. 1991b. Preparation of modified tubulins. *Meth. Enzymol.* 196:478-485.

Iliuk, A.B., V.A. Martin, B.M. Alicie, R.L. Geahlen, and W.A. Tao. 2010. In-depth analyses of kinase-dependent tyrosine phosphoproteomes based on metal ion-functionalized soluble nanopolymers. *Molecular & cellular proteomics : MCP*. 9:2162-2172.

Illenberger, S., G. Drewes, B. Trinczek, J. Biernat, H.E. Meyer, J.B. Olmsted, E.-M. Mandelkow, and E. Mandelkow. 1996. Phosphorylation of microtubule-associated proteins MAP2 and MAP4 by the protein kinase p110mark. *J. Biol. Chem.* 271:10834-10843.

Joglekar, A.P., D.C. Bouck, J.N. Molk, K.S. Bloom, and E.D. Salmon. 2006. Molecular architecture of a kinetochore-microtubule attachment site. *Nature cell biology*. 8:581-585.

Johnston, K., A. Joglekar, T. Hori, A. Suzuki, T. Fukagawa, and E.D. Salmon. 2010. Vertebrate kinetochore protein architecture: protein copy number. *The Journal of cell biology*. 189:937-943.

Kaan, H.Y., V. Ulaganathan, D.D. Hackney, and F. Kozielski. 2009. An allosteric transition trapped in an intermediate state of a new kinesin-inhibitor complex. *The Biochemical journal*. 425:55-60.

Kahn, O.I., V. Sharma, C. Gonzalez-Billault, and P.W. Baas. 2015. Effects of kinesin-5 inhibition on dendritic architecture and microtubule organization. *Molecular biology of the cell*. 26:66-77.

Kalab, P., A. Pralle, E.Y. Isacoff, and K. Weis. 2006. Analysis of a RanGTP-regulated gradient in mitotic somatic cells. *Nature*. 440:697-701.

Kapitein, L.C., B.H. Kwok, J.S. Weinger, C.F. Schmidt, T.M. Kapoor, and E.J. Peterman. 2008. Microtubule cross-linking triggers the directional motility of kinesin-5. *The Journal of cell biology*. 182:421-428.

Kapitein, L.C., E.J. Peterman, B.H. Kwok, J.H. Kim, T.M. Kapoor, and C.F. Schmidt. 2005. The bipolar mitotic kinesin Eg5 moves on both microtubules that it crosslinks. *Nature*. 435:114-118.

Kapoor, T.M., T.U. Mayer, M.L. Coughlin, and T.J. Mitchison. 2000. Probing spindle assembly mechanisms with monastrol, a small molecule inhibitor of the mitotic kinesin, Eg5. *The Journal of cell biology*. 150:975-988.

Kashina, A.S., G.C. Rogers, and J.M. Scholey. 1997. The bimC family of kinesins: essential bipolar mitotic motors driving centrosome separation. *Biochimica et biophysica acta*. 1357:257-271.

Kim, E.D., R. Buckley, S. Learman, J. Richard, C. Parke, D.K. Worthylake, E.J. Wojcik, R.A. Walker, and S. Kim. 2010. Allosteric drug discrimination is coupled to mechanochemical changes in the kinesin-5 motor core. *The Journal of biological chemistry*. 285:18650-18661.

Kim, L.C., L.X. Song, and E.B. Haura. 2009. Src kinases as therapeutic targets for cancer. *Nat Rev Clin Oncol*. 6:587-595.

Knight, J.C. 2004. Allele-specific gene expression uncovered. *Trends in genetics : TIG*. 20:113-116.

Koffa, M.D., C.M. Casanova, R. Santarella, T. Kocher, M. Wilm, and I.W. Mattaj. 2006. HURP is part of a Ran-dependent complex involved in spindle formation. *Current biology : CB*. 16:743-754.

Korneev, M.J., S. Lakamper, and C.F. Schmidt. 2007. Load-dependent release limits the processive stepping fo the tetrameric Eg5 motor. *Eur. Biophys. J.* 36:675-681.

Krzysiak, T.C., and S.P. Gilbert. 2006. Dimeric Eg5 maintains processivity through alternating-site catalysis with rate-limiting ATP hydrolysis. *The Journal of biological chemistry*. 281:39444-39454.

Krzysiak, T.C., M. Grabe, and S.P. Gilbert. 2008. Getting in sync with dimeric Eg5. Initiation and regulation of the processive run. *The Journal of biological chemistry*. 283:2078-2087.

Kufer, T.A., H.H.W. Sillje, R. Korner, O.J. Gruss, P. Meraldi, and E.A. Nigg. 2002. Human TPX2 is required for targeting Aurora-A kinase to the spindle. *J. Cell Bio.* 158:617-623.

Kuga, T., Y. Nakayama, M. Hoshino, Y. Higashiyama, Y. Obata, D. Matsuda, K. Kasahara, Y. Fukumoto, and N. Yamaguchi. 2007. Differential mitotic activation of endogenous c-Src, c-Yes, and Lyn in HeLa cells. *Arch Biochem Biophys*. 466:116-124.

Kull, F.J., E.P. Sablin, R. Lau, R.J. Fletterick, and R.D. Vale. 1996. Crystal structure of the kinesin motor domain reveals a structural similarity to myosin. *Nature*. 380:550-555.

Kwok, B.H., L.C. Kapitein, J.H. Kim, E.J. Peterman, C.F. Schmidt, and T.M. Kapoor. 2006. Allosteric inhibition of kinesin-5 modulates its processive directional motility. *Nature chemical biology*. 2:480-485.

Laemmli, U.K. 1970. Cleavage of structural proteins during the assembly of the head of bacteriophage T4. *Nature*. 227:680-685.

Landry, J.J., P.T. Pyl, T. Rausch, T. Zichner, M.M. Tekkedil, A.M. Stutz, A. Jauch, R.S. Aiyar, G. Pau, N. Delhomme, J. Gagneur, J.O. Korbel, W. Huber, and L.M. Steinmetz. 2013. The genomic and transcriptomic landscape of a HeLa cell line. *G3 (Bethesda, Md.)*. 3:1213-1224.

Larson, A.G., N. Naber, R. Cooke, E. Pate, and S.E. Rice. 2010. The conserved L5 loop establishes the pre-powerstroke conformation of the kinesin-5 motor, Eg5. *Biophysical journal*. 98:2619-2627.

Lawrimore, J., K.S. Bloom, and E.D. Salmon. 2011. Point centromeres contain more than a single centromere-specific Cse4 (CENP-A) nucleosome. *The Journal of cell biology*. 195:573-582.

Lenart, P., M. Petronczki, M. Steegmaier, B. Di Fiore, J.J. Lipp, M. Hoffmann, W.J. Rettig, N. Kraut, and J.M. Peters. 2007. The small-molecule inhibitor BI 2536 reveals novel insights into mitotic roles of polo-like kinase 1. *Current biology : CB*. 17:304-315.

Levi, M., B. Maro, and R. Shalgi. 2010. Fyn kinase is involved in cleavage furrow ingression during meiosis and mitosis. *Reproduction*. 140:827-834.

Ley, S.C., M. Marsh, C.R. Bebbington, K. Proudfoot, and P. Jordan. 1994. Distinct intracellular localization of Lck and Fyn protein tyrosine kinases in human T lymphocytes. *The Journal of cell biology*. 125:639-649.

Li, C., Y. Zhang, Q. Yang, F. Ye, S.Y. Sun, E.S. Chen, and Y.C. Liou. 2016. NuSAP modulates the dynamics of kinetochore microtubules by attenuating MCAK depolymerization activity. *Scientific reports*. 6.

Li, H., X. Xing, G. Ding, Q. Li, C. Wang, L. Xie, R. Zeng, and Y. Li. 2009. SysPTM: a systematic resource for proteomic research on post-translational modifications. *Molecular & cellular proteomics : MCP*. 8:1839-1849.

Liu, Y., Z. Zhang, H. Liang, X. Zhao, L. Liang, G. Wang, J. Yang, Y. Jin, M.A. McNutt, and Y. Yin. 2017. Protein Phosphatase 2A (PP2A) Regulates EG5 to Control Mitotic Progression. *Scientific reports*. 7:1630.

Lowry, O.H., N.J. Rosenbrough, A.L. Farr, and R.J. Randall. 1951. Protein measurement with the Folin phenol reagent. *J. Biol. Chem.* 193:265-275.

Luo, W., R.J. Slebos, S. Hill, M. Li, J. Brabek, R. Amanchy, R. Chaerkady, A. Pandey, A.J. Ham, and S.K. Hanks. 2008. Global impact of oncogenic Src on a phosphotyrosine proteome. *J Proteome Res*. 7:3447-3460.

Ma, N., J. Titus, A. Gable, J.L. Ross, and P. Wadsworth. 2011. TPX2 regulates the localization and activity of Eg5 in the mammalian mitotic spindle. *The Journal of cell biology*. 195:87-98.

Ma, N., U.S. Tulu, N.P. Ferenz, C. Fagerstrom, A. Wilde, and P. Wadsworth. 2010. Poleward transport of TPX2 in the mammalian mitotic spindle requires dynein, Eg5, and microtubule flux. *Molecular biology of the cell*. 21:979-988.

Macville, M., E. Schrock, H. Padilla-Nash, C. Keck, B.M. Ghadimi, D. Zimonjic, N. Popescu, and T. Ried. 1999. Comprehensive and definitive molecular cytogenetic characterization of HeLa cells by spectral karyotyping. *Cancer research*. 59:141-150.

Maddox, P., E. Chin, A. Mallavarapu, E. Yeh, E.D. Salmon, and K. Bloom. 1999. Microtubule dynamics from mating through the first zygotic division in the budding yeast Saccharomyces cerevisiae. *The Journal of cell biology*. 144:977-987.

Magidson, V., C.B. O'Connell, J. Loncarek, R. Paul, A. Mogilner, and A. Khodjakov. 2011. The spatial arrangement of chromosomes during prometaphase facilitates spindle assembly. *Cell*. 146:555-567.

Mali, P., L. Yang, K.M. Esvelt, J. Aach, M. Guell, J.E. DiCarlo, J.E. Norville, and G.M. Church. 2013. RNA-guided human genome engineering via Cas9. *Science (New York, N.Y.)*. 339:823-826.

Maliga, Z., T.M. Kapoor, and T.J. Mitchison. 2002. Evidence that monastrol is an allosteric inhibitor of the mitotic kinesin Eg5. *Chem Biol*. 9:989-996.

Maliga, Z., and T.J. Mitchison. 2006. Small-molecule and mutational analysis of allosteric Eg5 inhibition by monastrol. *BMC Chem Biol*. 6:2.

Maliga, Z., J. Xing, H. Cheung, L.J. Juszczak, J.M. Friedman, and S.S. Rosenfeld. 2006. A pathway of structural changes produced by monastrol binding to Eg5. *The Journal of biological chemistry*. 281:7977-7982.

Mann, B.J., S.K. Balchand, and P. Wadsworth. 2017. Regulation of Kif15 localization and motility by the C-terminus of TPX2 and microtubule dynamics. *Molecular biology of the cell*. 28:65-75.

Markus, S.M., K.A. Kalutkiewicz, and W.-L. Lee. 2012. She1-mediated inhibition of dynein motility along astral microtubules promotes polarized spindle movements. *Current biology : CB*. 22:1-10.

Mastronarde, D.N., K.L. McDonald, R. Ding, and J.R. McIntosh. 1993. Interpolar spindle microtubules in PTK cells. *The Journal of cell biology*. 123:1475-1489.

Mayer, T.U., T.M. Kapoor, S.J. Haggarty, R.W. King, S.L. Schreiber, and T.J. Mitchison. 1999. Small molecule inhibitor of mitotic spindle bipolarity identified in a phenotype-based screen. *Science (New York, N.Y.)*. 286:971-974.

McIntosh, J.R., and S.C. Landis. 1971. The distribution of spindle microtubules during mitosis in cultured human cells. *The Journal of cell biology*. 49:468-497.

McIntosh, J.R., M.I. Molodtsov, and F.I. Ataullakhanov. 2012. Biophysics of mitosis. *Quarterly reviews of biophysics*. 45:147-207.

McKinley, K.L., and I.M. Cheeseman. 2017. Large-Scale Analysis of CRISPR/Cas9 Cell-Cycle Knockouts Reveals the Diversity of p53-Dependent Responses to Cell-Cycle Defects. *Developmental cell*. 40:405-420.e402.

Meunier, S., and I. Vernos. 2016. Acentrosomal microtubule assembly in mitosis: the where, when and how. *Trends in Cell Biol.* 26:80-87.

Meyn, M.A., 3rd, and T.E. Smithgall. 2009. Chemical genetics identifies c-Src as an activator of primitive ectoderm formation in murine embryonic stem cells. *Science signaling*. 2:ra64.

Miki, H., Y. Okada, and N. Hirokawa. 2005. Analysis of the kinesin superfamily: insights into structure and function. *Trends in cell biology*. 15:467-476.

Mitchison, T., and M. Kirschner. 1984. Microtubule assembly nucleated by isolated centrosomes. *Nature*. 312:232-237.

Mitchison, T.J., P. Maddox, J. Gaetz, A. Groen, M. Shirasu, A. Desai, E.D. Salmon, and T.M. Kapoor. 2005. Roles of polymerization dynamics, opposed motors, and a tensile element in governing the length of Xenopus extract meiotic spindles. *Molecular biology of the cell*. 16:3064-3076.

Moyer, T.C., and A.J. Holland. 2015. Generation of a conditional analog-sensitive kinase in human cells using CRISPR/Cas9-mediated genome engineering. *Methods in cell biology*. 129:19-36.

Muretta, J.M., W.M. Behnke-Parks, J. Major, K.J. Petersen, A. Goulet, C.A. Moores, D.D. Thomas, and S.S. Rosenfeld. 2013. Loop L5 assumes three distinct orientations during the ATPase cycle of the mitotic kinesin Eg5: a transient and time-resolved fluorescence study. *The Journal of biological chemistry*. 288:34839-34849.

Muretta, J.M., Y. Jun, S.P. Gross, J. Major, D.D. Thomas, and S.S. Rosenfeld. 2015. The structural kinetics of switch-1 and the neck linker explain the functions of kinesin-1 and Eg5. *Proceedings of the National Academy of Sciences of the United States of America*. 112:E6606-6613.

Muretta, J.M., B.J.N. Reddy, G. Scarabelli, A.F. Thompson, S. Jariwala, J. Major, M. Venere, J.N. Rich, B. Willard, D.D. Thomas, J. Stumpff, B.J. Grant, S.P. Gross, and S.S. Rosenfeld. 2018. A posttranslational modification of the mitotic kinesin Eg5 that enhances its mechanochemical coupling and alters its mitotic function. *Proceedings of the National Academy of Sciences of the United States of America*. 115:E1779-e1788.

Myers, K.A., and P.W. Baas. 2007. Kinesin-5 regulates the growth of the axon by acting as a brake on its microtubule array. *The Journal of cell biology*. 178:1081-1091.

Nadar, V.C., A. Ketschek, K.A. Myers, G. Gallo, and P.W. Baas. 2008. Kinesin-5 is essential for growth-cone turning. *Current biology : CB*. 18:1972-1977.

Nakayama, Y., Y. Matsui, Y. Takeda, M. Okamoto, K. Abe, Y. Fukumoto, and N. Yamaguchi. 2012. c-Src but not Fyn promotes proper spindle orientation in early prometaphase. *The Journal of biological chemistry*. 287:24905-24915.

Neumann, B., T. Walter, J.K. Heriche, J. Bulkescher, H. Erfle, C. Conrad, P. Rogers, I. Poser, M. Held, U. Liebel, C. Cetin, F. Sieckmann, G. Pau, R. Kabbe, A. Wunsche, V. Satagopam, M.H. Schmitz, C. Chapuis, D.W. Gerlich, R. Schneider, R. Eils, W. Huber, J.M. Peters, A.A. Hyman, R. Durbin, R. Pepperkok, and J. Ellenberg. 2010. Phenotypic profiling of the human genome by time-lapse microscopy reveals cell division genes. *Nature*. 464:721-727.

Neumayer, G., C. Belzil, O.J. Gruss, and M.D. Nguyen. 2014. TPX2: of spindle assembly, DNA damage response, and cancer. *Cellular and molecular life sciences : CMLS*. 71:3027-3047.

Nousiainen, M., H.H.W. Sillje, G. Sauer, E.A. Nigg, and R. Korner. 2006. Phosphoproteome analysis of the human mitotic spindle. *Proc. Nat'l. Acad. Sci. USA*. 103:5391-5396.

O'Connell, C.B., J. Loncarek, P. Kalab, and A. Khodjakov. 2009. Relative contributions of chromatin and kinetochores to mitotic spindle assembly. *J. Cell Biol.* 187:43-51.

Obenauer, J.C., L.C. Cantley, and M.B. Yaffe. 2003. Scansite 2.0: Proteome-wide prediction of cell signaling interactions using short sequence motifs. *Nucleic acids research*. 31:3635-3641.

Paschal, B.M., R.A. Obar, and R.B. Vallee. 1989. Interaction of brain cytoplasmic dynein and MAP2 with a common sequence at the C terminus of tubulin. *Nature*. 342:569-572.

Petry, S., A.C. Groen, K. Ishihara, T.J. Mitchison, and R.D. Vale. 2013. Branching microtubule nucleation in Xenopus egg extracts mediated by augmin and TPX2. *Cell*. 152:768-777.

Piehl, M., U.S. Tulu, P. Wadsworth, and L. Cassimeris. 2004. Centrosome maturation: measurement of microtubule nucleation throughout the cell cycle using GFP tagged EB1. *Proc. Natl. Acad. Sci. USA*. 101:1584-1588.

Polak, B., P. Risteski, S. Lesjak, and I.M. Tolic. 2017. PRC1-labeled microtubule bundles and kinetochore pairs show one-to-one association in metaphase. *EMBO reports*. 18:217-230.

Puck, T.T., P.I. Marcus, and S.J. Cieciura. 1956. Clonal growth of mammalian cells in vitro; growth characteristics of colonies from single HeLa cells with and without a feeder layer. *The Journal of experimental medicine*. 103:273-283.

Raaijmakers, J.A., R.G. van Heesbeen, J.L. Meaders, E.F. Geers, B. Fernandez-Garcia, R.H. Medema, and M.E. Tanenbaum. 2012. Nuclear envelope-associated dynein drives prophase centrosome separation and enables Eg5-independent bipolar spindle formation. *EMBO J.*

Ran, F.A., P.D. Hsu, J. Wright, V. Agarwala, D.A. Scott, and F. Zhang. 2013. Genome engineering using the CRISPR-Cas9 system. *Nature protocols*. 8:2281-2308.

Rapley, J., M. Nicolas, A. Groen, L. Regue, M.T. Bertran, C. Caelles, J. Avruch, and J. Roig. 2008. The NIMA-family kinase Nek6 phosphorylates the kinesin Eg5 at a novel site necessary for mitotic spindle formation. *Journal of cell science*. 121:3912-3921.

Reid, T.A., B.M. Schuster, B.J. Mann, S.K. Balchand, M. Plooster, M. McClellan, C.E. Coombes, P. Wadsworth, and M.K. Gardner. 2016. Suppression of microtubule assembly kinetics by the mitotic protein TPX2. *J. Cell Sci.* 129:1319-1328.

Rincon, S.A., A. Lamson, R. Blackwell, V. Syrovatkina, V. Fraisier, A. Paoletti, M.D. Betterton, and P.T. Tran. 2017. Kinesin-5-independent mitotic spindle assembly requires the antiparallel microtubule crosslinker Ase1 in fission yeast. *Nature communications*. 8:15286.

Roberts, A.J., T. Kon, P.J. Knight, K. Sutoh, and S.A. Burgess. 2013. Functions and mechanics of dynein motor proteins. *Nature reviews. Molecular cell biology*. 14:713-726.

Robinson, M.S., D.A. Sahlender, and S.D. Foster. 2010. Rapid inactivation of proteins by rapamycin-induced rerouting to mitochondria. *Developmental cell*. 18:324-331.

Roostalu, J., N.I. Cade, and T. Surrey. 2015. Complementary activities of TPX2 and chTOG constitute an efficient importin-rregulated microtubule nucleation module. *Nat. Cell Biol.* 17:1422-1437.

Roostalu, J., C. Hentrich, P. Bieling, I.A. Telley, E. Schiebel, and T. Surrey. 2011. Directional switching of the kinesin Cin8 through motor coupling. *Science (New York, N.Y.)*. 332:94-99.

Roostalu, J., E. Schiebel, and A. Khmelinskii. 2010. Cell cycle control of spindle elongation. *Cell cycle (Georgetown, Tex.)*. 9:1084-1090.

Rozelle, D.K., S.D. Hansen, and K.B. Kaplan. 2011. Chromosome passenger complexes control anaphase duration and spindle elongation via a kinesin-5 brake. *The Journal of cell biology*. 193:285-294.

Rusan, N.M., C.J. Fagerstrom, A.M. Yvon, and P. Wadsworth. 2001. Cell cycle-dependent changes in microtubule dynamics in living cells expressing green fluorescent protein-alpha tubulin. *Molecular biology of the cell*. 12:971-980.

Sarli, V., and A. Giannis. 2008. Targeting the kinesin spindle protein: basic principles and clinical implications. *Clinical cancer research : an official journal of the American Association for Cancer Research*. 14:7583-7587.

Saunders, A.M., J. Powers, S. Strome, and W.M. Saxton. 2007. Kinesin-5 acts as a brake in anaphase spindle elongation. *Current biology : CB*. 17:R453-454.

Saunders, W., V. Lengyel, and M.A. Hoyt. 1997. Mitotic spindle function in Saccharomyces cerevisiae requires a balance between different types of kinesin-related motors. *Molecular biology of the cell*. 8:1025-1033.

Saunders, W.S., and M.A. Hoyt. 1992. Kinesin-related proteins required for structural integrity of the mitotic spindle. *Cell*. 70:451-458.

Sawin, K.E., K. LeGuellec, M. Philippe, and T.J. Mitchison. 1992. Mitotic spindle organization by a plus-end-directed microtubule motor. *Nature*. 359:540-543.

Sawin, K.E., and T.J. Mitchison. 1995. Mutations in the kinesin-like protein Eg5 disrupting localization to the mitotic spindle. *Proceedings of the National Academy of Sciences of the United States of America*. 92:4289-4293.

Schatz, C.A., R. Santarella, A. Hoenger, E. Karsenti, I.W. Mattaj, O.J. Gruss, and R.E. Carazo-Salas. 2003. Importin alpha-regulated nucleation of microtubules by TPX2. *The EMBO journal*. 22:2060-2070.

Schindelin, J., I. Arganda-Carreras, E. Frise, V. Kaynig, M. Longair, T. Pietzsch, S. Preibisch, C. Rueden, S. Saalfeld, B. Schmid, J.Y. Tinevez, D.J. White, V. Hartenstein, K. Eliceiri, P. Tomancak, and A. Cardona. 2012. Fiji: an open-source platform for biological-image analysis. *Nature methods*. 9:676-682.

Scholey, J.E., S. Nithianantham, J.M. Scholey, and J. Al-Bassam. 2014. Structural basis for the assembly of the mitotic motor Kinesin-5 into bipolar tetramers. *eLife*. 3:e02217.

Scholey, J.M., G. Civelekoglu-Scholey, and I. Brust-Mascher. 2016. Anaphase B. *Biology*. 5.

Sen, B., and F.M. Johnson. 2011. Regulation of SRC family kinases in human cancers. *Journal of signal transduction*. 2011:865819.

Shapira, O., and L. Gheber. 2016. Motile properties of the bi-directional kinesin-5 Cin8 are affected by phosphorylation in its motor domain. *Scientific reports*. 6:25597.

Shapira, O., A. Goldstein, J. Al-Bassam, and L. Gheber. 2017. A potential physiological role for bi-directional motility and motor clustering of mitotic kinesin-5 Cin8 in yeast mitosis. *Journal of cell science*. 130:725-734.

Sharma, K., R.C. D'Souza, S. Tyanova, C. Schaab, J.R. Wisniewski, J. Cox, and M. Mann. 2014. Ultradeep human phosphoproteome reveals a distinct regulatory nature of Tyr and Ser/Thr-based signaling. *Cell reports*. 8:1583-1594.

Sharp, D.J., H.M. Brown, M. Kwon, G.C. Rogers, G. Holland, and J.M. Scholey. 2000a. Functional coordination of three mitotic motors in Drosophila embryos. *Molecular biology of the cell*. 11:241-253.

Sharp, D.J., K.L. McDonald, H.M. Brown, H.J. Matthies, C. Walczak, R.D. Vale, T.J. Mitchison, and J.M. Scholey. 1999a. The bipolar kinesin, KLP61F, cross-links microtubules within interpolar microtubule bundles of Drosophila embryonic mitotic spindles. *The Journal of cell biology*. 144:125-138.

Sharp, D.J., G.C. Rogers, and J.M. Scholey. 2000b. Microtubule motors in mitosis. *Nature*. 407:41-47.

Sharp, D.J., K.R. Yu, J.C. Sisson, W. Sullivan, and J.M. Scholey. 1999b. Antagonistic microtubule-sliding motors position mitotic centrosomes in Drosophila early embryos. *Nature cell biology*. 1:51-54.

She, Z.Y., and W.X. Yang. 2017. Molecular mechanisms of kinesin-14 motors in spindle assembly and chromosome segregation. *Journal of cell science*. 130:2097-2110.

Sheridan, R.M., and D.L. Bentley. 2016. Selectable one-step PCR-mediated integration of a degron for rapid depletion of endogenous human proteins. *BioTechniques*. 60:69-74.

Shimamoto, Y., S. Forth, and T.M. Kapoor. 2015. Measuring Pushing and Braking Forces Generated by Ensembles of Kinesin-5 Crosslinking Two Microtubules. *Developmental cell*. 34:669-681.

Sillje, H.H., S. Nagel, R. Korner, and E.A. Nigg. 2006. HURP is a Ran-importin beta-regulated protein that stabilizes kinetochore microtubules in the vicinity of chromosomes. *Current biology : CB*. 16:731-742.

Simunic, J., and I.M. Tolic. 2016. Mitotic Spindle Assembly: Building the Bridge between Sister K-Fibers. *Trends in biochemical sciences*. 41:824-833.

Singh, S.K., H. Pandey, J. Al-Bassam, and L. Gheber. 2018. Bidirectional motility of kinesin-5 motor proteins: structural determinants, cumulative functions and physiological roles. *Cellular and molecular life sciences : CMLS*.

Skoufias, D.A., S. DeBonis, Y. Saoudi, L. Lebeau, I. Crevel, R. Cross, R.H. Wade, D. Hackney, and F. Kozielski. 2006a. S-trityl-L-cysteine is a reversible, tight binding inhibitor of the human kinesin Eg5 that specifically blocks mitotic progression. *J. Biol. Chem.* 281:17559-17569.

Skoufias, D.A., S. DeBonis, Y. Saoudi, L. Lebeau, I. Crevel, R. Cross, R.H. Wade, D. Hackney, and F. Kozielski. 2006b. S-trityl-L-cysteine is a reversible, tight binding inhibitor of the human kinesin Eg5 that specifically blocks mitotic progression. *J. Biol. Chem.* 281:17559-17569.

Smith, K.P., K.M. Gifford, J.S. Waitzman, and S.E. Rice. 2015. Survey of phosphorylation near drug binding sites in the Protein Data Bank (PDB) and their effects. *Proteins*. 83:25-36.

Stewart, S., and G. Fang. 2005. Anaphase-promoting complex/cyclosome controls the stability of TPX2 during mitotic exit. *Molecular and cellular biology*. 25:10516-10527.

Stewart-Ornstein, J., and G. Lahav. 2016. Dynamics of CDKN1A in Single Cells Defined by an Endogenous Fluorescent Tagging Toolkit. *Cell reports*. 14:1800-1811.

Straight, A.F., W.F. Marshall, J.W. Sedat, and A.W. Murray. 1997. Mitosis in living budding yeast: anaphase A but no metaphase plate. *Science (New York, N.Y.)*. 277:574-578.

Straight, A.F., J.W. Sedat, and A.W. Murray. 1998. Time-lapse microscopy reveals unique roles for kinesins during anaphase in budding yeast. *The Journal of cell biology*. 143:687-694.

Sturgill, E.G., D.K. Das, Y. Takizawa, Y. Shin, S.E. Collier, M.D. Ohi, W. Hwang, M.J. Lang, and R. Ohi. 2014. Kinesin-12 Kif15 targets kinetochore fibers through an intrinsic two-step mechanism. *Current biology : CB*. 24:2307-2313.

Sturgill, E.G., S.R. Norris, Y. Guo, and R. Ohi. 2016. Kinesin-5 inhibitor resistance is driven by kinesin-12. *The Journal of cell biology*. 213:213-227.

Sturgill, E.G., and R. Ohi. 2013. Kinesin-12 differentially affects spindle assembly depending on its microtubule substrate. *Current biology : CB*. 23:1280-1290.

Sung, H.-H., I.A. Telley, P. Papadaki, A. Ephrussi, T. Surrey, and P. Rorth. 2008. Drosophila Ensconsin promotes productive recruitment of kinesin-1 to microtubules. *Devel. Cell*. 15:866-876.

Suzuki, A., B.L. Badger, and E.D. Salmon. 2015. A quantitative description of Ndc80 complex linkage to human kinetochores. *Nature communications*. 6:8161.

Tanenbaum, M.E., L. Macurek, N. Galjart, and R.H. Medema. 2008. Dynein, Lis1 and CLIP-170 counteract Eg5-dependent centrosome separation during bipolar spindle assembly. *The EMBO journal*. 27:3235-3245.

Tanenbaum, M.E., L. Macurek, A. Janssen, E.F. Geers, M. Alvarez-Fernandez, and R.H. Medema. 2009. Kif15 cooperates with eg5 to promote bipolar spindle assembly. *Current biology : CB*. 19:1703-1711.

Thiede, C., V. Fridman, A. Gerson-Gurwitz, L. Gheber, and C.F. Schmidt. 2012. Regulation of bi-directional movement of single kinesin-5 Cin8 molecules. *Bioarchitecture*. 2:70-74.

Thomas, S.M., and J.S. Brugge. 1997. Cellular functions regulated by Src family kinases. *Annual review of cell and developmental biology*. 13:513-609.

Thorn, K.S., J.A. Ubersax, and R.D. Vale. 2000. Engineering the processive run length of the kinesin motor. *The Journal of cell biology*. 151:1093-1100.

Tikhonenko, I., D.K. Nag, N. Martin, and M.P. Koonce. 2008. Kinesin-5 is not essential for mitotic spindle elongation in Dictyostelium. *Cell motility and the cytoskeleton*. 65:853-862.

Tolic, I.M. 2017. Mitotic spindle: kinetochore fibers hold on tight to interpolar bundles. *European biophysics journal : EBJ*.

Toso, A., J.R. Winter, A.J. Garrod, A.C. Amaro, P. Meraldi, and A.D. McAinsh. 2009. Kinetochore-generated pushing forces separate centrosomes during bipolar spindle assembly. *J. Cell Biol.* 184:365-372.

Tulu, U.S., C. Fagerstrom, N.P. Ferenz, and P. Wadsworth. 2006. Molecular requirements for kinetochore-associated microtubule formation in mammalian cells. *Curr. Biol.* 16:536-541.

Tulu, U.S., N. Rusan, and P. Wadsworth. 2003. Peripheral, non-centrosome-associated microtubules contribute to spindle formation in centrosome containing cells. *Curr. Biol.* 13:1894-1899.

Tytell, J.D., and P.K. Sorger. 2006. Analysis of kinesin motor function at budding yeast kinetochores. *The Journal of cell biology*. 172:861-874.

UniProt, C. 2015. UniProt: a hub for protein information. *Nucleic acids research*. 43:D204-212.

Uteng, M., C. Hentrich, K. Miura, P. Bieling, and T. Surrey. 2008. Poleward transport of Eg5 by dynein-dynactin in Xenopus laevis egg extract spindles. *The Journal of cell biology*. 182:715-726.

Uzbekov, R., C. Prigent, and Y. Arlot-Bonnemains. 1999. Cell cycle analysis and synchronization of the Xenopus laevis XL2 cell line: study of the kinesin related protein XlEg5. *Microscopy research and technique*. 45:31-42.

Valentine, M.T., P.M. Fordyce, T.C. Krzysiak, S.P. Gilbert, and S.M. Block. 2006. Individual dimers of the mitotic kinesin motor Eg5 step processively and support substantial loads in vitro. *Nature cell biology*. 8:470-476.

Valentine, M.T., and S.P. Gilbert. 2007. To step or not to step? How biochemistry and mechanics influence processivity in Kinesin and Eg5. *Current opinion in cell biology*. 19:75-81.

van den Wildenberg, S.M., L. Tao, L.C. Kapitein, C.F. Schmidt, J.M. Scholey, and E.J. Peterman. 2008. The homotetrameric kinesin-5 KLP61F preferentially crosslinks microtubules into antiparallel orientations. *Current biology : CB*. 18:1860-1864.

van Heesbeen, R.G., M.E. Tanenbaum, and R.H. Medema. 2014. Balanced activity of three mitotic motors is required for bipolar spindle assembly and chromosome segregation. *Cell reports*. 8:948-956.

van Ree, J.H., H.J. Nam, K.B. Jeganathan, A. Kanakkanthara, and J.M. van Deursen. 2016. Pten regulates spindle pole movement through Dlg1-mediated recruitment of Eg5 to centrosomes. *Nature cell biology*. 18:814-821.

vanHeesbeen, R.G., J.A. Raaijmakers, M.E. Tanenbaum, V.A. Halim, D. Lelieveld, C. Lieftink, A.J. Heck, D.A. Egan, and R.H. Medema. 2016. Aurora A, MCAK, and Kif18b promote Eg5-independent spindle formation. *Chromosoma*. 125:1-14.

Vanneste, D., M. Takagi, N. Imamoto, and I. Vernos. 2009. The role of Hklp2 in the stabilization and maintenance of spindle bipolarity. *Current biology : CB*. 19:1712-1717.

Venere, M., C. Horbinski, J.F. Crish, X. Jin, A. Vasanji, J. Major, A.C. Burrows, C. Chang, J. Prokop, Q. Wu, P.A. Sims, P. Canoll, M.K. Summers, S.S. Rosenfeld, and J.N. Rich. 2015. The mitotic kinesin KIF11 is a driver of invasion, proliferation, and self-renewal in glioblastoma. *Science translational medicine*. 7:304ra143.

Verhey, K.J., N. Kaul, and V. Soppina. 2011. Kinesin assembly and movement in cells. *Annu. Rev. Biophys.* 40:267-288.

Waitzman, J.S., A.G. Larson, J.C. Cochran, N. Naber, R. Cooke, F. Jon Kull, E. Pate, and S.E. Rice. 2011. The loop 5 element structurally and kinetically coordinates dimers of the human kinesin-5, Eg5. *Biophysical journal*. 101:2760-2769.

Waitzman, J.S., and S.E. Rice. 2014. Mechanism and regulation of kinesin-5, an essential motor for the mitotic spindle. *Biology of the cell*. 106:1-12.

Waksman, G., D. Kominos, S.C. Robertson, N. Pant, D. Baltimore, R.B. Birge, D. Cowburn, H. Hanafusa, B.J. Mayer, M. Overduin, M.D. Resh, C.B. Rios, L. Silverman, and J. Kuriyan. 1992. Crystal structure of the phosphotyrosine recognition domain SH2 of v-src complexed with tyrosine-phosphorylated peptides. *Nature*. 358:646-653.

Walczak, C.E., and R. Heald. 2008. Mechanisms of mitotic spindle assembly and function. *Int. Rev. Cytol.* 265:111-158.

Wang, W., L. Chen, Y. Ding, J. Jin, and K. Liao. 2008. Centrosome separation driven by actin-microfilaments during mitosis is mediated by centrosome-associated tyrosine-phosphorylated cortactin. *Journal of cell science*. 121:1334-1343.

Wang, Z., and M.P. Sheetz. 2000. The C-terminus of tubulin increases cytoplasmic dynein and kinesin processivity. *Biophys. J.* 78:1955-1964.

Weinger, J.S., M. Qiu, G. Yang, and T.M. Kapoor. 2011. A nonmotor microtubule binding site in kinesin-5 is required for filament crosslinking and sliding. *Current biology : CB.* 21:154-160.

Welburn, J.P.I., and I.M. Cheeseman. 2012. The microtubule-binding protein Cep170 promotes the targeting of the kinesin-13 depolymerase Kif2b to the mitotic spindle. *Molecular biology of the cell*. 23:4786-4796.

Wendell, K.L., L. Wilson, and M.A. Jordan. 1993. Mitotic block in HeLa cells by vinblastine: ultrastructural changes in kinetochore-microtubule attachment and in centrosomes. *Journal of cell science*. 104 (Pt 2):261-274.

Whalley, H.J., A.P. Porter, Z. Diamantopoulou, G.R. White, E. Castaneda-Saucedo, and A. Malliri. 2015. Cdk1 phosphorylates the Rac activator Tiam1 to activate centrosomal Pak and promote mitotic spindle formation. *Nature communications*. 6:7437.

Wignall, S.M., and A.M. Villeneuve. 2009. Lateral microtubule bundles promote chromosome alignment during acentrosomal oocyte meiosis. *Nat Cell Bio*. 11:839-844.

Wilson, M.B., S.J. Schreiner, H.J. Choi, J. Kamens, and T.E. Smithgall. 2002. Selective pyrrolo-pyrimidine inhibitors reveal a necessary role for Src family kinases in Bcr-Abl signal transduction and oncogenesis. *Oncogene*. 21:8075-8088.

Winey, M., C.L. Mamay, E.T. O'Toole, D.N. Mastronarde, T.H. Giddings, Jr., K.L. McDonald, and J.R. McIntosh. 1995. Three-dimensional ultrastructural analysis of the Saccharomyces cerevisiae mitotic spindle. *The Journal of cell biology*. 129:1601-1615.

Wittmann, T., H. Boleti, C. Antony, E. Karsenti, and I. Vernos. 1998. Localization of the kinesin-like protein Xklp2 to spindle poles requires a leucine zipper, a microtubule-associated protein, and dynein. *The Journal of cell biology*. 143:673-685.

Wittmann, T., M. Wilm, E. Karsenti, and I. Vernos. 2000. TPX2, a novel Xenopus MAP involved in spindle pole organization. *J. Cell Biol.* 149:1405-1418.

Woehlke, G., A.K. Ruby, C.L. Hart, B. Ly, N. Hom-Booher, and R.D. Vale. 1997. Microtubule interaction site of the kinesin motor. *Cell*. 90:207-216.

Wolff, I.D., M.V. Tran, T.J. Mullen, A.M. Villeneuve, and S.M. Wignall. 2016. Assembly of Caenorhabditis elegans acentrosomal spindles occurs without evident microtubule-organizing centers and requires microtubule sorting by KLP-18/kinesin-12 and MESP-1. *Molecular biology of the cell*. 27:3122-3131.

Wordeman, L., J. Decarreau, J.J. Vicente, and M. Wagenbach. 2016. Divergent microtubule assembly rates after short- versus long-term loss of end-modulating kinesins. *Molecular biology of the cell*. 27:1300-1309.

Wu, J.Q., and T.D. Pollard. 2005. Counting cytokinesis proteins globally and locally in fission yeast. *Science (New York, N.Y.)*. 310:310-314.

Ye, A.A., J. Deretic, C.M. Hoel, A.W. Hinman, D. Cimini, J.P. Welburn, and T.J. Maresca. 2015. Aurora A Kinase Contributes to a Pole-Based Error Correction Pathway. *Current biology : CB*. 25:1842-1851.

Yen, T.J., P.S. Machlin, and D.W. Cleveland. 1988. Autoregulated instability of beta-tubulin mRNAs by recognition of the nascent amino terminus of beta-tubulin. *Nature*. 334:580-585.

Yvon, A.C., P. Wadsworth, and M.A. Jordan. 1999. Taxol suppresses dynamics of individual microtubules in living human tumor cells. *Molec. Biol. Cell*. 10:947-959.

Zaytsev, A.V., L.J. Sundin, K.F. DeLuca, E.L. Grishchuk, and J.G. DeLuca. 2014. Accurate phosphoregulation of kinetochore-microtubule affinity requires unconstrained molecular interactions. *The Journal of cell biology*. 206:45-59.

Zhao, L., C.D. Kroenke, J. Song, D. Piwnica-Worms, J.J. Ackerman, and J.J. Neil. 2008. Intracellular water-specific MR of microbead-adherent cells: the HeLa cell intracellular water exchange lifetime. *NMR in biomedicine*. 21:159-164.

Zhu, C., J. Zhao, M. Bibikova, J.D. Leverson, E. Bossy-Wetzel, J.B. Fan, R.T. Abraham, and W. Jiang. 2005. Functional analysis of human microtubule-based motor proteins, the kinesins and dyneins, in mitosis/cytokinesis using RNA interference. *Molecular biology of the cell*. 16:3187-3199.